Miguel Araújo Maia

Xanthene as a privileged scaffold in medicinal chemistry – synthesis and biological applications

U.PORTO
FACULDADE DE FARMÁCIA
UNIVERSIDADE DO PORTO

Porto, 2022

Xanthene as a privileged scaffold in medicinal chemistry – synthesis and biological applications

Miguel Araújo Maia

Tese do 3º Ciclo de Estudos Conducente ao grau de Doutoramento em Ciências Farmacêuticas, na especialidade de Química Farmacêutica e Medicinal

PhD thesis of the 3rd Cycle of Studies in Pharmaceutical Sciences on the Specialty of Pharmaceutical and Medicinal Chemistry

Trabalho realizado sob a orientação de

Elaborated under supervision of

Professora Doutora Maria Emília Silva Pereira da Sousa

Professor Doutor Patrício Manuel Vieira Araújo Soares da Silva

Doutor László Erno Kiss

Outubro 2022

This work was developed in the Laboratory of Organic and Pharmaceutical Chemistry, Department of Chemistry, Faculty of Pharmacy, University of Porto, Portugal, and in the School of Chemistry, University College Dublin, Dublin, Ireland.

This research was supported by national funds through FCT - Foundation for Science and Technology within the scope of UIDB/04423/2020 and UIDP/04423/2020 (Group of Natural Products and Medicinal Chemistry) and CIIMAR (Interdisciplinary Centre of Marine and Environmental Research, University of Porto, Portugal) worked as host institution. This research was developed under the projects PTDC/SAU-PUB/28736/2017, EXPL/CTA-AMB/0810/2021, and PTDC/CTA-AMB/0853/2021, co-financed by COMPETE 2020, Portugal 2020 and the European Union through the ERDF, and by FCT through national funds. The candidate performed this work with a doctoral fellowship (SFRH/BD/146211/2019) supported by FCT, Portugal.

Author:

Miguel Araújo Maia

PhD Thesis in Pharmaceutical and Medicinal Chemistry

Title: Xanthene as a privileged scaffold in medicinal chemistry – synthesis and biological applications

Publication date: October 2024

Supervisor:

Professora Doutora Maria Emília da Silva Pereira de Sousa
(Associate Professor, Faculty of Pharmacy, University of Porto)

Co-supervisors:

Professor Doutor Patrício Manuel Vieira Araújo Soares da Silva
(Full Professor, Faculty of Medicine, University of Porto)

László Erno Kiss
(Medicinal Chemistry Manager at BIAL - PORTELA & C. ª, S.A)

Faculty of Pharmacy, University of Porto, 31st October 2022

Author's Declaration

Under the terms of "Decreto-Lei no 216/92, de 13 Outubro", is hereby declared that the author afforded a major contribution to the conceptual design and technical execution of the work, interpretation of the results, and manuscript preparation of the original articles included in this thesis.

Under the term of the "Decreto-Lei no 216/92, de 13 Outubro", it is hereby declared that the following original articles/communication were prepared in the scope of this thesis.

SCIENTIFIC PRODUCTION

PUBLICATIONS

Patent

Provisional patent application No. 118521, submitted on 17/02/2023.

Publications in peer-reviewed scientific journals

Maia M, Sousa E. BACE.1 and γ-secretase as therapeutic targets for Alzheimer's disease. Pharmaceuticals. 2019;12(1):41 doi: https://doi.org/10.3390/ph12010041.

Maia M, Resende DISP, Durães F, Pinto MMM, Sousa E. Xanthenes in Medicinal Chemistry – Synthetic strategies and biological activities. European Journal of Medicinal Chemistry. 2021;210:113085. doi: https://doi.org/10.1016/j.ejmech.2020.113085.

Maia M, Durães F, Resende DISP, Durães F, Szemerédi N, Gales L, Pinto MMM, Spengler G, Sousa E. Towards new tricyclic derivatives targeting bacterial resistance mechanisms. Submitted to Drugs and Drug Candidates 2022.

COMMUNICATIONS (*presenting author)

Miguel Maia*, Andreia Palmeira, Diana Resende, László Kiss, Emília Sousa. In silico studies towards new BACE-1 inhibitors, poster communication at XXVI National Meeting of the Portuguese Chemical Society (SPQ), Porto, Portugal, 24-26 July 2019;

Miguel Maia*, Andreia Palmeira, Diana Resende, Luís Gales, László Kiss, Emília Sousa. "Towards new BACE1 inhibitors: in silico studies and synthesis", poster communication at 13th National Organic Chemistry Meeting - 6th National Medicinal Chemistry Meeting, 13ENQO-6ENQT, Aveiro, Portugal, 15 - 17 of January 2020;

Miguel Maia*, Andreia Palmeira, Diana Resende, Luís Gales, Emília Sousa. “Towards new BACE1 inhibitors: in silico studies and synthesis”, poster communication at Blue Think Conference – Share Science, Spread Knowledge, Interdisciplinary Centre of Marine and Environmental Research (CIIMAR), Matosinhos, Portugal, 17th Sept. 2020;

Miguel Maia*, Andreia Palmeira, Diana Resende, Luís Gales, Madalena Pinto, Emília Sousa. “Design and synthesis of novel xanthenes derivatives”, poster communication at 6th International Electronic Conference on Medicinal Chemistry, Pharmaceuticals, Multidisciplinary Digital Publishing Institute (MDPI), 01-30 Nov. 2020;

Miguel Maia*, Fernando Durães, Diana Resende, Nikoletta Szemerédi, Luís Gales, Madalena Pinto, Gabriella Spengler, Emília Sousa. "Xanthene derivatives against mechanisms of bacterial resistance", poster communication at HIPS Symposium 2021, Helmholtz Institute for Pharmaceutical Research Saarland, May 20, 2021;

Miguel Maia*, Fernando Durães, Diana Resende, Nikoletta Szemerédi, Luís Gales, Madalena Pinto, Gabriella Spengler, Emília Sousa. "Towards new agents against mechanisms of bacterial resistance", poster communication at RICT 2021 - 56th International Conference on Medicinal Chemistry, virtual event, France, July 8, 2021.

Table of Contents

Agradecimentos xiv

Abstract xvi

Keywords xvii

Resumo xix

Palavras-chave xx

List of figures xxii

Abbreviations and acronyms xxix

Outline of the thesis xxxii

Chapter 1. – Introduction 1

1.1. Xanthenes 5
1.1.1. Synthesis 6
1.1.1.1. Synthesis of 9*H*-xanthene derivatives 6
1.1.1.2. Functionalization of 9*H*-xanthene derivatives 8
1.1.1.3. Synthesis of 9-hydroxyxanthene 10
1.1.1.4. Synthesis of 9-hydroxyxanthene derivatives 10
1.1.1.5. Synthesis of xanthene-9-carboxylic acid 12
1.1.1.6. Synthesis of xanthene-9-carboxylic acid derivatives 13
1.1.1.7. Synthesis of 9-alkyl xanthene derivatives 14
1.1.1.8. Functionalization of 9-alkyl xanthene derivatives 16
1.1.2. Biological activities of xanthenes 17
1.1.2.1. Neuroprotection 17
1.1.2.1.1. BACE1 inhibitors 17
1.1.2.1.2. mGluR1 enhancers 19
1.1.2.1.3. Antitumor activity 21
1.1.2.2. Antimicrobial activity 25
1.1.2.2.1. Antifungal and antibacterial activities 25
1.1.2.2.2. Antiviral activity 27
1.1.2.2.3. Antiparasitic activity 28
1.1.2.3. Anti-inflammatory and analgesic activities 31
1.1.2.4. Antidiabetic activity 33
1.1.2.5. Antioxidant activity 34
1.1.2.6. Antipsychotic activity 36

1.2. Aims of the thesis and work plan 43

Chapter 2. – Synthesis and biological activity of 9-hydroxyxanthene derivatives 45

2.1. Introduction 48

2.2. Synthesis of 9-xanthenyl derivatives 49

2.3. Biological activity results and discussion 50
2.3.1. Minimum inhibitory concentration (MIC) 50
2.3.2. QS inhibition 51
2.3.3. Biofilm formation inhibition 52
2.3.4. Efflux pump inhibition 52

2.4. Conclusion 58

2.5. Experimental 58
2.5.1. Chemical synthesis and characterization 58
2.5.2. Biological assays and docking studies 62

Chapter 3. – Synthesis and biological activity of xanthene-9-carboxylic acid derivatives 67

3.1. Introduction 68
3.1.1. Alzheimer's disease 68
3.1.2. The amyloid hypothesis of AD 68
3.1.3. Amyloid targeting strategies 69
3.1.3.1. Inhibition of BACE1 69
3.1.2. P-glycoprotein and amyloid- β export 70

3.2. Synthesis of xanthene-9-carboxylic acid derivatives 71
3.2.1. Aromatic halogenation 71
3.2.2. Amide coupling 72
3.2.3. Amide reduction 78
3.2.4. Suzuki-Miyaura coupling 79

3.3 Biological activity results and discussion 80
3.3.1. Cytotoxicity 80
3.3.2. Modulation of P-gp 86
3.3.3. Neuroprotective effects against iron (III)-induced cytotoxicity 89
3.3.4. CNS penetration: *in vitro* parallel artificial membrane permeability assay (PAMPA)-BBB. 97

3.4. Conclusion 101

3.5. Experimental 101
3.5.1. Chemical synthesis and characterization 101
3.5.1.2. Synthesis, purification, and structural characterization 103
3.5.2. Biological assays 121
3.5.2.1. Cytotoxicity, modulation of P-gp and FeNTA 121
3.5.2.2. CNS penetration: in vitro parallel artificial membrane permeability assay (PAMPA)-BBB. 125

Chapter 4 - Synthesis and biological activity of benzhydryl derivatives 127

4.1. Introduction 128
4.1.1. Trypanosoma brucei and Human African Trypanosomiasis 128

4.2. Synthesis of diphenylacetic acid derivatives 129
4.2.1. Synthesis of benzhydryl carbamates 130
4.2.2. Synthesis of benzhydryl ureas 131

4.3. Flow *versus* batch assessment 133

4.4. Biological activity results and discussion 136
4.4.1. Activity against *Trypanosoma brucei* 136

4.5. Conclusion 140

4.6. Experimental data 140
4.6.1. Chemical synthesis and characterization 140
4.6.1.1. General information 140
4.6.1.2. Synthesis, purification and structural characterization 141
4.6.2. Biological assays 153
4.6.2.1. Activity against *Trypanosoma brucei* 153

Chapter 5 – General conclusions 155

Chapter 6 – References 162

Annex I - HPLC and NMR spectra and electrospray ESI data 180

Annex II - Chemical structures of the investigated compounds 262

Dedicated to my parents

“In this great future

You can’t forget your past”

Bob Marley

Agradecimentos

Em primeiro lugar, gostaria de expressar a minha imensa gratidão à minha orientadora, Professora Emília Sousa. Pela paixão em química medicinal e pelo ensino. Por não ter hesitado em embarcar nesta jornada e por todo o tempo e apoio investido em mim ao longo do doutoramento. Pela persistência, motivação e orientação. Por ter tido sempre em consideração o meu percurso profissional.

Gostaria também de agradecer ao meu co-orientador, Doutor László Kiss, pelos valiosos contributos na definição do plano de trabalhos e discussão dos resultados.

Ao Professor Patrício Soares da Silva, pela disponibilidade em integrar a equipa de coorientação.

À Professora Renata Silva e à Mestre Rita Monteiro pelo extenso trabalho de avaliação dos compostos sintetizados nos ensaios de citotoxicidade e neuroprotecção.

Ao Professor Marcus Baumann e a todo o grupo de investigação pelo acolhimento e amizade no meu período *Erasmus* na *School of Chemistry, University College Dublin*.

À Doutora Sara Cravo e à Doutora Diana Resende por todos os contributos e discussões científicas e à Gisela Adriano e Liliana Teixeira pelo apoio técnico e pela boa disposição constante.

Ao Fernando Durães pela realização dos ensaios de atividade antibacteriana e antiparasitária e por todo o apoio durante todo o percurso.

À Daniela Loureiro pelo conhecimento partilhado e à Márcia Martins pela dedicação e leitura atenta desta tese.

A todos os colegas de laboratório e Professores do LQOF pelos bons momentos e cooperação durante estes anos.

Ao Miguel Santos, Margarida Castro e Pedro Figueiredo, pela amizade de uma vida.

Aos meus pais, irmã, tias e avós, a quem devo tudo o que sou.

A ti, Mariana, por tudo, todos os dias.

Abstract

Xanthenes are a special class of oxygen-incorporating tricyclic compounds. Structurally related to xanthones, the presence of different substituents in position 9 strongly influences their physical and chemical properties, as well as their biological applications. Several methodologies have been employed to obtain 9*H*-xanthene, 9-hydroxyxanthene (xanthydrol) and xanthene-9-carboxylic acid, as well as respective derivatives, from simple starting materials or through modification of related structures. Xanthene derivatives have shown ability to act as neuroprotectors, antitumor, antimicrobial, among others, proving the versatility of this nucleus for different biological applications.

This work reports the synthesis of 36 compounds, xanthene and benzhydryl derivatives, from which 24 were synthetized for the first time. Diverse modifications were performed to obtain the reported compounds, particularly, amide coupling, amide reduction, aromatic halogenation, Suzuki coupling, and Curtius rearrangement.

The first set of compounds arise from the conjugation of xanthydrol with sulfamerazine, sulfamethazine, sulfacetamide, and aniline. These compounds were evaluated regarding their minimum inhibitory concentration on Gram-positive and Gram-negative strains, efflux pump inhibition activity, influence on biofilm formation, and quorum-sensing inhibition. Despite no activity was found on inhibiting bacterial growth, the compounds obtained, particularly the xanthene sulfonamide derivatives **MM17** and **MM18**, showed interesting preliminary results regarding their impact on different mechanisms of bacterial resistance.

A series of xanthene-9-carboxylic acid derivatives were obtained employing distinctive synthetic procedures: aromatic halogenation, amide coupling, amide reduction, and Suzuki coupling. Twenty different compounds were obtained, with different substituents in the position 9 of the xanthene and at positions 2,7 of the aromatic rings. Fourteen compounds showed to be activators of P-glycoprotein, a key transporter for the elimination of the amyloid beta peptide, whose abnormal accumulation is linked with neurotoxicity and development of Alzheimer's disease. Compound **MM42C** provided the best result, showing an increase in P-glycoprotein activity of 58% and 76% at the concentration of 10 μM and 25 μM, respectively. All the 14 compounds showed to be permeant to blood-brain barrier, 8 in an *in vitro* assay and the remain compounds by *in silico* predictions. Additionally, eleven compounds showed to provide protection against iron-induced cytotoxicity, another potential strategy for neuroprotection.

Diphenylacetic acid was used as starting material for the synthesis of benzhydryl carbamate and urea derivatives through a continuous flow, diphenylphosphoryl azide - mediated Curtius rearrangement procedure. Twelve compounds were easily obtained through the conjugation of diphenylacetic acid with different alcohols and amines as nucleophiles. These compounds were tested against *T. brucei*, the parasite responsible for the Human African Trypanosomiasis, also known as sleeping sickness. Compound **MM99** showed to be the most promising compound, with an IC_{50} = 1.1 µM and a SI (IC_{50} (HeLa cells) / IC_{50} (T. brucei) =181.4. Additionally, this compound also showed to be tolerated at the cumulative dose of 150 mg/kg in an *in vivo* study.

The work presented in this thesis aims to contribute to the discovery of suitable synthetic routs to easily obtain novel xanthene and benzhydryl derivatives with biological activity, hopefully leading to a compound with clinical relevance.

Keywords

Xanthene derivatives; benzhydryl derivatives; multi-drug resistance; neuroprotection; Alzheimer's disease; P-glycoprotein activation; Aβ clearance; iron-induced cytotoxicity; *Trypanosoma brucei*; amide coupling; amide reduction; aromatic halogenation; Suzuki coupling; Curtius rearrangement; Flow chemistry.

Resumo

Os xantenos são uma classe especial de compostos tricíclicos que incorporam oxigénio. Estruturalmente relacionados com as xantonas, a presença de diferentes substituintes na posição 9 influencia fortemente as suas propriedades físicas e químicas, bem como as suas aplicações biológicas. Diversas metodologias têm vindo a ser utilizadas para obter 9*H*-xanteno, 9-hidroxi-xanteno (xantidrol) e ácido xanteno-9-carboxílico, bem como os seus respetivos derivados, a partir de materiais de partida simples ou através da modificação de estruturas relacionadas. Os derivados de xanteno têm demonstrado capacidade de agir como neuroprotetores, antitumorais, antimicrobianos, entre outros, comprovando a versatilidade deste núcleo para diferentes aplicações biológicas.

Este trabalho relata a síntese de 36 compostos, derivados do xanteno e do núcleo benzidrílico, dos quais 24 foram sintetizados pela primeira vez. Foram realizadas diversas modificações para obter os compostos descritos, nomeadamente, acoplamento de amida, redução, halogenação aromática, acoplamento de Suzuki e rearranjo de Curtius.

A primeira série de compostos surge da conjugação do xantidrol com sulfamerazina, sulfametazina, sulfacetamida e anilina. Estes compostos foram avaliados em relação à sua concentração inibitória mínima em estirpes bacterianas Gram-positivo e Gram-negativo, atividade de inibição da bomba de efluxo, influência na formação de biofilme e inibição do *quorum sensing*. Apesar de não ter sido encontrada atividade na inibição do crescimento bacteriano, os compostos obtidos, particularmente os derivados xanteno-sulfonamida **MM17** e **MM18**, apresentaram resultados preliminares interessantes em relação ao seu impacto em diferentes mecanismos de resistência bacteriana.

Foi obtida uma série de derivados do ácido xanteno-9 carboxílico utilizando diversos procedimentos de síntese: halogenação aromática, acoplamento de amida, redução de amida e acoplamento de Suzuki. Foram obtidos 20 compostos diferentes, com diferentes substituintes na posição 9 do xanteno e também nas posições 2,7 dos anéis aromáticos. Catorze compostos mostraram ser ativadores da glicoproteína-P, um transportador chave para a eliminação do peptídeo beta-amiloide, cuja acumulação anormal está ligada a neurotoxicidade e ao desenvolvimento da doença de Alzheimer. O composto **MM42C** apresentou o resultado mais promissor, mostrando um aumento da atividade da glicoproteína-P de 58% e 76% na concentração de 10 μM e 25 μM, respetivamente. Todos os catorze compostos mostraram ser capazes de penetrar a barreira hematoencefálica, oito através de um ensaio *in vitro* e os restantes num ensaio preditivo *in silico*. Além disso,

onze compostos mostraram fornecer proteção contra citotoxicidade induzida pelo ferro, outra potencial estratégia para promover neuroproteção.

O ácido difenilacético foi utilizado como material de partida para a síntese de ureias e carbamatos benzidrílicos através de um procedimento de síntese em fluxo contínuo por rearranjo de Curtius mediado por difenilfosforil azida. Doze compostos foram obtidos através da conjugação de ácido difenilacético com diferentes álcoois e aminas como nucleófilos. Estes compostos foram testados contra *T. brucei*, o parasita responsável pela tripanossomíase africana (HAT), também conhecida como doença do sono. O composto **MM99** mostrou ser o composto mais promissor, com um IC_{50} = 1,1 μM e um SI (células HeLa) / IC_{50} (T. brucei) =181,4. Além disso, este composto também mostrou ser bem tolerado num estudo *in vivo*, onde foi estado numa dose cumulativa de 150 mg/kg.

O trabalho apresentado nesta tese pretende contribuir para o desenvolvimento de vias sintéticas adequadas para a obtenção de novos xantenos e benzidrilos com atividade biológica, na expectativa de conduzir à obtenção de um composto com relevância clínica.

Palavras-chave

Derivados de xanteno; derivados do ácido difenilacético; derivados benzidrílicos; resistência a múltiplos fármacos; neuroproteção; doença de Alzheimer; ativação da glicoproteína P; eliminação do Aβ; citotoxicidade induzida pelo ferro; *Trypanosoma brucei*; acoplamento amida; redução de amida; halogenação aromática, acoplamento Suzuki; rearranjo de Curtius; química de fluxo.

List of figures

Figure 1. Natural xanthenes. 5
Figure 2. Structures of 9*H*-xanthene (**7**), 9-hydroxyxanthene (xanthydrol, **8**), and xanthene-9-carboxylic acid (**9**)..... 6
Figure 3. Lead optimization and modulation of hERG activity in xanthene BACE1 inhibitors..... 19
Figure 4. (A) Interaction of fluorine atom and dihydropyran moiety of compound **66** with Trp76 with Arg128 in P2' of the catalytic pocket of BACE1, respectively. Copyright from [64]. (A') Co-crystal structure of rat CatD and inhibitor **66** (yellow). (A'') Co-crystal structure of human BACE1 and inhibitor **66**. (B) Co-crystal structure of human BACE1 (blue) + compound **67** (green) overlaid with CatD (pink). Copyright from [65]. 19
Figure 5. Structure-activity relationship analysis of 9H-xanthenes as potent, orally available mGlu1 receptor enhancers. 20
Figure 6. Structure-activity relationship analysis of cancer cell cytotoxicities for a series of substituted xanthenes **73**..... 21
Figure 7. Structure-activity relationship analysis of cancer cell cytotoxicity for two series of substituted xanthenes **74** and **75**..... 22
Figure 8. Structures and cytotoxicity of xanthenes **76-85**..... 24
Figure 9. Structures and cytotoxicity of rose bengal (**86**). 25
Figure 10. Xanthenes **5** and **6** with antimicrobial properties..... 25
Figure 11. *N*-Arylmethyl-4(xanthen-9-yl)anilines (**87a**-**d**) and structurally related *N*-arylmethylene-4-(xanthen-9-yl)anilines (**88a**-**d**). 26
Figure 12. Structure of compounds **89**-**94**..... 26
Figure 13. Diamines **95a** and **95b** and polymers **96**-**100** with potential antimicrobial activity..... 27
Figure 14. Structure-activity relationship analysis on the antiviral activity of xanthenes **101**..... 28
Figure 15. Xanthenes with antiviral activity. 28
Figure 16. Putative structure-activity relationship analysis on the TR inhibition of 9,9-dimethylxanthene derivatives **106**-**110**. 29
Figure 17. Structures and antimalarial activity of xanthenes **111**-**113**. 31
Figure 18. Structure-activity relationship analysis on the anti-inflammatory and analgesic activities of 9-aryl-9*H*-xanthene-3,6-diol derivatives **114a**-**114f**..... 31
Figure 19. Structure-activity relationship analysis on the anti-inflammatory and analgesic activities of spiro-xanthene-9',2-[1,3,4]thiadiazole derivatives **115a**-**115e**..... 32
Figure 20. Structures and activity on hCCR1 receptors of xanthenes **116-117**. 33
Figure 21. Xanthene derivatives with antidiabetic activity. 34
Figure 22. 9H-Xanthene-2,7-diols **119**-**123** with antioxidant activity..... 35
Figure 23. Benzo[kl]xanthene lignans **124** and **125** with antioxidant properties. 35
Figure 24. DPPH and ABTS radical scavenging activity compared with BHT (concentration of 250 µg mL^{-1}) of 14-aryl-14*H*-dibenzo[a,j]xanthene derivatives **126a**-**e**.. 36
Figure 25. Structure-activity relationship on the neuroleptic activity of xanthene derivatives **127-139**..... 37
Figure 26. Structure of xanthene (**140**) and sulfonamide (**141**) derivatives 49
Figure 27. ORTEP view of the crystal structure of xanthenyl sulfonamides **MM16** (A), **MM17** (B) and **MM18** (C) and **MM7** (D). 50
Figure 28. RFI curves of the tested compounds against *S. aureus* 272123. 54
Figure 29. RFI curves of the tested compounds against SE03. 54
Figure 30. Fluorescence studies of compound **MM16**..... 55

Figure 31. Fluorescence studies of compound **MM17**.....55
Figure 32. Fluorescence studies of compound **MM18**.....56
Figure 33. Compounds **MM7** and **MM16-18** in the binding site of the AcrB portion. Crystal structure of the AcrB portion obtained from the Protein Data Bank (PDB: 4DX5 [161])..... 57
Figure 34. Molecular visualization of compounds **MM16** (A and A'), **MM17** (B and B'), **MM18** (C and C'), and **MM7** (D) A in the AcrB portion of the AcrAB-TolC efflux system. Crystal structure of the AcrB portion obtained from the Protein Data Bank (PDB: 4DX5 [161]) 57
Figure 35. (1-Cyano-2-ethoxy-2-oxoethylidenaminooxy)-dimethylamino-morpholino-carbenium hexafluorophosphate (COMU, **146**). 73
Figure 36. Diethanolamine, N-boc-1,6-hexanediamine and BTFFH. 77
Figure 37. Chemical structures of neutral red outside lysosome, at physiological pH, and positive charged NR inside lysosome, at lower pH than physiological pH. 81
Figure 38. Cytotoxicity evaluation of compounds **MM7**, **MM29**, **MM30**, **MM32**, **MM36**, **MM42B**, **MM42C, MM43**, **MM46**, **MM48A**, **MM50**, **MM52** at concentrations of 5 µM, 10 µM, 25 µM and 50 µM with neutral red uptake assay. Results are expressed as mean + SD from five independent experiences, performed in triplicate. Statistical comparisons were made using One-way ANOVA followed by the Dunnett's multiple comparisons test [*p < 0.05; **p < 0.01*; versus* control cells (0 µM)]. In all cases, p values < 0.05 were considered significant. 82
Figure 39. Cytotoxicity evaluation of compounds **MM54**, **MM56**, **MM57A**, **MM57B**, **MM59B3**, **MM63B**, **MM68**, **MM73**, **MM74** at concentrations of 5 µM, 10 µM, 25 µM, and 50 µM with neutral red uptake assay. Results are expressed as mean + SD from five independent experiences, performed in triplicate. Statistical comparisons were made using One-way ANOVA followed by the Dunnett's multiple comparisons test [***p < 0.001; ****p < 0.0001 *versus* control cells (0 µM)]. In all cases, p values < 0.05 were considered significant. 83
Figure 40. Cytotoxicity evaluation of compounds **MM7**, **MM29**, **MM30**, **MM32**, **MM36**, **MM42B**, **MM43**, **MM46**, **MM48A**, **MM50**, **MM52** at concentrations of 5 µM, 10 µM, 25 µM, and 50 µM with MTT assay. Results are expressed as mean + SD from five independent experiences, performed in triplicate. Statistical comparisons were made using One-way ANOVA followed by the Dunnett's multiple comparisons test [**p < 0.01; ****p < 0.0001 *versus* control cells (0 µM)]. In all cases, p values < 0.05 were considered significant. ...84
Figure 41. Cytotoxicity evaluation of compounds **MM54**, **MM56**, **MM57A**, **MM57B**, **MM59B3**, **MM63B**, **MM68**, **MM73**, **MM74** at concentrations of 5 µM, 10 µM, 25 µM, and 50 µM with MTT assay. Results are expressed as mean + SD from five independent experiences, performed in triplicate. Statistical comparisons were made using One-way ANOVA followed by the Dunnett's multiple comparisons test [****p < 0.0001 *versus* control cells (0 µM)]. In all cases, p values < 0.05 were considered significant. 85
Figure 42. Modulation of P-gp activity by compounds **MM7B**, **MM29**, **MM30**, **MM32**, **MM36**, **MM42B**, **MM42C**, **MM43**, **MM46**, **MM50**, **MM52** and **MM52** at concentrations of 10 µM and 25 µM. Results are expressed as mean + SD from five independent experiences, performed in triplicate. Statistical comparisons were made using One-way ANOVA followed by the Dunnett's multiple comparisons test [*p < 0.05; **p < 0.01; ***p < 0.001; ****p < 0.0001 *versus* control cells (0 µM)]. In all cases, p values < 0.05 were considered significant. 87
Figure 43. Modulation of P-gp activity by compounds **MM56**, **MM59B3**, **MM63B** and **MM74** at concentrations of 10 µM and 25 µM. For compounds **MM57A**, **MM57B** and **MM48A** only the 10µM concentration was tested. Results are expressed as mean + SD from five independent experiences, performed in triplicate. Statistical comparisons were made using One-way ANOVA followed by the Dunnett's multiple comparisons test [*p <

0.05; ***p < 0.001; ****p < 0.0001 *versus* control cells (0 μM)]. In all cases, p values < 0.05 were considered significant. 88
Figure 44. FeNTA (500 and 1000 μM) cytotoxicity towards RA differentiated SH-SY5Y cells, in the presence or absence of the tested compounds **MM7B**, **MM29**, **MM30**, **MM32**, **MM36**, **MM42B**, **MM42C**, **MM43**(10 and 25 μM), evaluated by the neutral red uptake assay, 24 h after exposure. Results are presented as mean + SD from five independent experiments, performed in triplicate. Statistical comparisons were made using Two-way ANOVA, followed by the Tukey's multiple comparisons test (*p < 0.05; **p < 0.01; ***p < 0.001; ****p < 0.0001 *versus* FeNTA alone, at each FeNTA concentration)..... 91
Figure 45. FeNTA (500 and 1000 μM) cytotoxicity towards RA differentiated SH-SY5Y cells, in the presence or absence of the tested compounds **MM46**, **MM50**, **MM52**, **MM54**, **MM56**, **MM59B3**, **MM63B**, **MM74** (10 and 25 μM), evaluated by the neutral red uptake assay, 24 h after exposure. Results are presented as mean + SD from five independent experiments, performed in triplicate. Statistical comparisons were made using Two-way ANOVA, followed by the Tukey's multiple comparisons test (*p < 0.05; **p < 0.01; ***p < 0.001; ****p < 0.0001 *versus* FeNTA alone, at each FeNTA concentration)..... 92
Figure 46. FeNTA (500 and 1000 μM) cytotoxicity towards RA differentiated SH-SY5Y cells, in the presence or absence of the tested compounds **MM48A**, **MM57A** and **MM57B** (10 μM), evaluated by the neutral red uptake assay, 24 h after exposure. Results are presented as mean + SD from five independent experiments, performed in triplicate. Statistical comparisons were made using Two-way ANOVA, followed by the Tukey's multiple comparisons test (*p < 0.05; **p < 0.01; ***p < 0.001; ****p < 0.0001 *versus*. FeNTA alone, at each FeNTA concentration). 93
Figure 47. UV/Vis spectra of compounds **MM7B**, **MM29**, **MM32**, **MM36**, **MM42B**, **MM42C**, **MM43**, **MM48A**, **MM52**, **MM57B** and **MM74** in methanolic solution with 1 % of DMSO with sequential additions of $FeCl_3$. 96
Figure 48. Linear correlation between experimental and reported permeability of commercial drugs using the PAMPA-BBB assay. 99
Figure 49. Suramin (**146**). 128
Figure 50. Compound **147** and compound **148**. 128
Figure 51. Mebendazole (**149**). 129
Figure 52. Diphenylacetic acid (**150**)..... 129
Figure 53. Comparison of the MIC of compounds **MM32**, **MM56** and **MM68**..... 138
Figure 54. ^{1}H and ^{13}C NMR of compound **MM7**. 181
Figure 55. ^{1}H NMR (top, 300.13 MHz, DMSO-d_6) and ^{13}C NMR (bottom, 75.48 MHz, DMSO-d_6) for compound **MM16**. 182
Figure 56. ^{1}H and ^{13}C NMR of compound **MM17**. 183
Figure 57. ^{1}H and ^{13}C NMR of compound **MM18**. 184
Figure 58. Chromatogram (HPLC) of compound **MM7**. Purity (% a/a): 99.5%. 185
Figure 59. Chromatogram (HPLC) of compound **MM16**. Purity (% a/a): 99.2%. 185
Figure 60. Chromatogram (HPLC) of compound **MM17**. Purity (% a/a): 99.9%. 186
Figure 61. Chromatogram (HPLC) of compound **MM18**. Purity (% a/a): 99.9%. 186
Figure 62. ^{1}H NMR (top, 300.13 MHz, $CDCl_3$) and ^{13}C NMR (bottom, 75.48 MHz, $CDCl_3$) for compound **MM30**. 187
Figure 63. ORTEP view of the crystal structure of compound **MM30**. 188
Figure 64. Electrospray ESI data for compound **MM30**. 188
Figure 65. ^{1}H NMR (top, 300.13 MHz, $CDCl_3$) and ^{13}C NMR (bottom, 75.48 MHz, $CDCl_3$) for compound **MM32**. 189
Figure 66. ORTEP view of the crystal structure of compound **MM32**. 190
Figure 67. Electrospray ESI data for compound **MM32**. 190

Figure 68. ^{1}H NMR (top, 300.13 MHz, $CDCl_3$) and ^{13}C NMR (bottom, 75.48 MHz, $CDCl_3$) for compound **MM36**. 191
Figure 69. ORTEP view of the crystal structure of compound **MM36**. 192
Figure 70. Electrospray ESI data for compound **MM36**. 192
Figure 71. ^{1}H NMR (top, 300.13 MHz, $CDCl_3$) and ^{13}C NMR (bottom, 75.48 MHz, $CDCl_3$) for compound **MM42B**. 193
Figure 72. Electrospray ESI data for compound **MM42B**. 194
Figure 73.^{1}H NMR (top, 300.13 MHz, $CDCl_3$) and ^{13}C NMR (bottom, 75.48 MHz, $CDCl_3$) for compound **MM42C**. 195
Figure 74. Electrospray ESI data for compound **MM42C**. 196
Figure 75.^{1}H NMR (top, 300.13 MHz, DMSO-d_6) and ^{13}C NMR (bottom, 75.48 MHz, DMSO-d_6) for compound **MM43**. 197
Figure 76. Electrospray ESI data for compound **MM43**. 198
Figure 77.^{1}H NMR (top, 300.13 MHz, $CDCl_3$) and ^{13}C NMR (bottom, 75.48 MHz, $CDCl_3$) for compound **MM46**. 199
Figure 78. Electrospray ESI data for compound **MM46**. 200
Figure 79.^{1}H NMR (top, 300.13 MHz, $CDCl_3$) and ^{13}C NMR (bottom, 75.48 MHz, $CDCl_3$) for compound **MM48A**. 201
Figure 80. Electrospray ESI data for compound **MM48A**. 202
Figure 81.^{1}H NMR (top, 300.13 MHz, $CDCl_3$) and ^{13}C NMR (bottom, 75.48 MHz, $CDCl_3$) for compound **MM50**. 203
Figure 82. Electrospray ESI data for compound **MM50**. 204
Figure 83.^{1}H NMR (top, 300.13 MHz, DMSO-d_6) and ^{13}C NMR (bottom, 75.48 MHz, DMSO-d_6) for compound **MM52**. 205
Figure 84.^{1}H NMR (top, 300.13 MHz, DMSO-d_6) and ^{13}C NMR (bottom, 75.48 MHz, DMSO-d_6) for compound **MM54**. 206
Figure 85.^{1}H NMR (top, 300.13 MHz, $CDCl_3$) and ^{13}C NMR (bottom, 75.48 MHz, $CDCl_3$) for compound **MM56**. 207
Figure 86. Electrospray ESI data for compound **MM56**. 208
Figure 87.^{1}H NMR (top, 300.13 MHz, $CDCl_3$) and ^{13}C NMR (bottom, 75.48 MHz, $CDCl_3$) for compound **MM57A**. 209
Figure 88. Electrospray ESI data for compound **MM57A**. 210
Figure 89.^{1}H NMR (top, 300.13 MHz, $CDCl_3$) and ^{13}C NMR (bottom, 75.48 MHz, $CDCl_3$) for compound **MM57B**. 211
Figure 90. Electrospray ESI data for compound **MM57B**. 212
Figure 91.^{1}H NMR (top, 300.13 MHz, DMSO-d_6) and ^{13}C NMR (bottom, 75.48 MHz, DMSO-d_6) for compound **MM59B3**. 213
Figure 92. Electrospray ESI data for compound **MM59B3**. 214
Figure 93.^{1}H NMR (top, 300.13 MHz, Methanol-d_4) and ^{13}C NMR (bottom, 75.48 MHz, Methanol-d_4) for compound **MM63B**. 215
Figure 94. Electrospray ESI data for compound **MM63B**. 216
Figure 95.^{1}H NMR (top, 300.13 MHz, DMSO-d_6) and ^{13}C NMR (bottom, 75.48 MHz, DMSO-d_6) for compound **MM68**. 217
Figure 96. Electrospray ESI data for compound **MM68**. 218
Figure 97.^{1}H NMR (top, 300.13 MHz, DMSO-d_6) and ^{13}C NMR (bottom, 75.48 MHz, DMSO-d_6) for compound **MM73**. 219
Figure 98. Electrospray ESI data for compound **MM73**. 220
Figure 99.^{1}H NMR (top, 300.13 MHz, Acetone-d_6) and ^{13}C NMR (bottom, 75.48 MHz, Acetone-d_6) for compound **MM74**. 221
Figure 100. Electrospray ESI data for compound **MM74**. 222

Figure 101. ^{1}H NMR (top, 400 MHz, $CDCl_3$) and ^{13}C NMR (bottom, 101 MHz, $CDCl_3$) for compound **MM81**. 223
Figure 102. Electrospray ESI data for compound **MM81**. 224
Figure 103. ^{1}H NMR (top, 400 MHz, $CDCl_3$) and ^{13}C NMR (bottom, 101 MHz, $CDCl_3$) for compound **MM85**. 225
Figure 104. Electrospray ESI data for compound **MM85**. 226
Figure 105. ^{1}H NMR (top, 400 MHz, $CDCl_3$) and ^{13}C NMR (bottom, 101 MHz, $CDCl_3$) for compound **MM88**. 227
Figure 106. Electrospray ESI data for compound **MM88**. 228
Figure 107. ^{1}H NMR (top, 400 MHz, $CDCl_3$) and ^{13}C NMR (bottom, 101 MHz, $CDCl_3$) for compound **MM90**. 229
Figure 108. Electrospray ESI data for compound **MM90**. 230
Figure 109. ^{1}H NMR (top, 400 MHz, $CDCl_3$) and ^{13}C NMR (bottom, 101 MHz, $CDCl_3$) for compound **MM91**. 231
Figure 110. Electrospray ESI data for compound **MM91**. 232
Figure 111. ^{1}H NMR (top, 400 MHz, $CDCl_3$) and ^{13}C NMR (bottom, 101 MHz, $CDCl_3$) for compound **MM92**. 233
Figure 112. Electrospray ESI data for compound **MM92**. 234
Figure 113. ^{1}H NMR (top, 400 MHz, DMSO-d_6) and ^{13}C NMR (bottom, 101 MHz, DMSO-d_6) for compound **MM94**. 235
Figure 114. ^{1}H NMR (top, 400 MHz, $CDCl_3$) and ^{13}C NMR (bottom, 101 MHz, $CDCl_3$) for compound **MM95**. 236
Figure 115. Electrospray ESI data for compound **MM95**. 237
Figure 116. ^{1}H NMR (top, 400 MHz, DMSO-d_6) and ^{13}C NMR (bottom, 101 MHz, DMSO-d_6) for compound **MM96**. 238
Figure 117. ^{1}H NMR (top, 400 MHz, DMSO-d_6) and ^{13}C NMR (bottom, 101 MHz, DMSO-d_6) for compound **MM97**. 239
Figure 118. Electrospray ESI data for compound **MM97**. 240
Figure 119. ^{1}H NMR (top, 400 MHz, DMSO-d_6) and ^{13}C NMR (bottom, 101 MHz, DMSO-d_6) for compound **MM98**. 241
Figure 120. Electrospray ESI data for compound **MM98**. 242
Figure 121. ^{1}H NMR (top, 400 MHz, DMSO-d_6) and ^{13}C NMR (bottom, 101 MHz, DMSO-d_6) for compound **MM99**. 243
Figure 122. Electrospray ESI data for compound **MM99**. 244
Figure 123. Chromatogram (HPLC) of compound **MM29**. Purity (% a/a): 98.7%. 245
Figure 124. Chromatogram (HPLC) of compound **MM30**. Purity (% a/a): 98.7%. 245
Figure 125. Chromatogram (HPLC) of compound **MM32**. Purity (% a/a): 99.7%. 246
Figure 126. Chromatogram (HPLC) of compound **MM36**. Purity (% a/a): 99.5%. 246
Figure 127. Chromatogram (HPLC) of compound **MM42B**. Purity (% a/a): 91.8%. 247
Figure 128. Chromatogram (HPLC) of compound **MM42C**. Purity (% a/a): 87.6%. 247
Figure 129. Chromatogram (HPLC) of compound **MM43**. Purity (% a/a): 87.6%. 248
Figure 130. Chromatogram (HPLC) of compound **MM46**. Purity (% a/a): 99.7%. 248
Figure 131. Chromatogram (HPLC) of compound **MM48A**. Purity (% a/a): 98.6%. 249
Figure 132. Chromatogram (HPLC) of compound **MM50**. Purity (% a/a): 99.9%. 249
Figure 133. Chromatogram (HPLC) of compound **MM52**. Purity (% a/a): 100.0%..... 250
Figure 134. Chromatogram (HPLC) of compound **MM54**. Purity (% a/a): 97.0%. 250
Figure 135. Chromatogram (HPLC) of compound **MM56**. Purity (% a/a): 98.5%. 251
Figure 136. Chromatogram (HPLC) of compound **MM57A**. Purity (% a/a): 97.2%. 251
Figure 137. Chromatogram (HPLC) of compound **MM57B**. Purity (% a/a): 94.3%. 252
Figure 138. Chromatogram (HPLC) of compound **MM59B3**. Purity (% a/a): 99.1%. 252
Figure 139. Chromatogram (HPLC) of compound **MM63B**. Purity (% a/a): 84.2%. 253

Figure 140. Chromatogram (HPLC) of compound **MM68**. Purity (% a/a): 96.7%. 253
Figure 141. Chromatogram (HPLC) of compound **MM73**. Purity (% a/a): 69.12%..... 254
Figure 142. Chromatogram (HPLC) of compound **MM74**. Purity (% a/a): 98.8%. 254
Figure 143. Chromatogram (HPLC) of compound **MM81**. Purity (% a/a): 90.9%. Peak purity index: 99.9 %..... 255
Figure 144. Chromatogram (HPLC) of compound **MM85**. Purity (% a/a): 49.5% (degradation occurred under HPLC procedure). Peak purity index: 99,9. 255
Figure 145. Chromatogram (HPLC) of compound **MM88**. Purity (% a/a): 99.7%. Peak purity index: 99.9 %..... 256
Figure 146. Chromatogram (HPLC) of compound **MM90**. Purity (% a/a): 66.9% (degradation occurred under HPLC procedure). Peak purity index: 99.8 %..... 256
Figure 147. Chromatogram (HPLC) of compound **MM91**. Purity (% a/a): 85.9% (degradation occurred under HPLC procedure). Peak purity index: 99.8 %..... 257
Figure 148. Chromatogram (HPLC) of compound **MM92**. Purity (% a/a): 94.1%. Peak purity index: 99.9 %..... 257
Figure 149. Chromatogram (HPLC) of compound **MM94**. Purity (% a/a): 80.8%. Peak purity index: 99.8 %..... 258
Figure 150. Chromatogram (HPLC) of compound **MM95**. Purity (% a/a): 92.8%. Peak purity index: 99.9 %..... 258
Figure 151. Chromatogram (HPLC) of compound **MM96**. Purity (% a/a): 99.6%. Peak purity index: 93.01 %..... 259
Figure 152. Chromatogram (HPLC) of compound **MM97**. Purity (% a/a): 99.8%. Peak purity index: 99.7 %..... 259
Figure 153. Chromatogram (HPLC) of compound **MM98**. Purity (% a/a): 92.9%. Peak purity index: 99.x4 %..... 260
Figure 154. Chromatogram (HPLC) of compound **MM99**. Purity (% a/a): 91.3%. Peak purity index: 99.7 %..... 260

Abbreviations and acronyms

Aβ - Amyloid beta

ABC - ATP-binding cassette

ABTS - 2,2'-Azino-bis-3-ethylbenzothiazoline-6-sulfonic acid

AcOH – Acetic acid

AD - Alzheimer's disease

ADME - Absorption, distribution, metabolism, excretion

AHL - Acyl-homoserine lactones

APP - Amyloid precursor protein

ATP - Adenosine triphosphate

ATCC - American Type Culture Collection

BACE1 - β-Site amyloid precursor protein cleaving enzyme 1

BBB - Blood-brain barrier

$BH_3.Me_2S$ - Borane dimethyl sulfide complex

$BH_3.THF$ - Borane-tetrahydrofuran

$BmimBF_4$ - 1-Butyl-3-methylimidazolium tetrafluoroborate

CAN - Ceric ammonium nitrate

CCCP - Carbonyl cyanide 3-chlorophenylhydrazone

CCR1 - CC-type chemokine receptor 1

CDC - Cross-dehydrogenative coupling

CDI - Carbonyldiimidazole

CHO - Chinese hamster ovary

CLSI - Clinical and Laboratory Standard Institute

CNS - Central nervous system

CT-DNA - Calf thymus DNA

CV026 - *Chromobacterium violaceum* CV026

CYP450 - Cytochrome P450

DIEA - *N,N*-Diisopropylethylamine

DMF - *N*,*N*-Dimethylformamide

DMT's - Disease modifying therapies or treatments

DPPA - Diphenylphosphoryl azide

DPPH - 2,2-Diphenyl-1-picrylhydrazyl

EB - Ethidium bromide

ee – Enantiomeric excess

EtOAc – Ethyl acetate

EtOH - Ethanol

EPI - Efflux pump inhibition

ESBl - Extended-spectrum β-lactamase producer

EZF - *Sphingomonas paucimobilis* Ezf 10-17

FBS - Fetal bovine serum

Fc - Ferrocene

FDA - Food and Drug Administration

FI_{IA} - Fluorescence intensity (inhibition condition)

FI_{NA} - Fluorescence intensity (normal condition)

GR - Glucocorticoid receptor

HAT - Human african trypanosomiasis

hCCR1 - Human CC-type chemokine receptor 1

hERG - Human ether-a-go-go-related gene

hGR - Human glutathione reductase

HMBC - Heteronuclear multiple bond correlation

HSQC - Heteronuclear single quantum coherence

HPLC - High performance liquid chromatography

IC_{50} - Half maximal inhibitory concentration

K_{is} - Binding affinity to the enzyme-substrate complex

LDA - Lithium diisopropylamide

LOAD - Late-onset Alzheimer's disease

logP - logarithm (base 10) of the partition coefficient (P), which is defined as the ratio of the compound's organic (oil)-to-aqueous phase concentrations

MDR - Multidrug resistant

Me_3Al – Trimethylaluminum

mGluR - Metabotropic glutamate receptors

MIC - Minimum inhibitory concentration

MIP-1α - Macrophage inflammatory protein-1α

mp - Melting point

MRSA - Methicillin-resistant *Staphylococcus aureus*

MTT - (3-(4,5-Dimethylthiazol-2-yl)-2,5-diphenyltetrazolium bromide)

MW – Microwave

NBS - *N*-Bromosuccinimide

NCS - *N*-Chlorosuccinimide

OD - Optical density

ORTEP - Oak ridge thermal ellipsoid plot

PAMPA - Parallel artificial membrane permeability assay

PARP - Poly (ADP-ribose) polymerase

PD - Pharmacodynamic

P-gp - P-glycoprotein

PK - Pharmacokinetic

PP1 - Phosphatases 1

PP2 - Phosphatase-2A

QS - Quorum sensing

QTc - Corrected QT interval

RA - Retinoic Acid

RF - Relative fluorescence

RFI - Relative fluorescence index

RHO 123 - Rhodamine 123

ROS - Reactive oxygen species

rpm – Revolutions per minute

rt - Room temperature

SAR - Structure-activity relationship

SE03 - *Salmonella enterica* serovar Typhimurium SL1344

s-CDs - Carbon dots surface functionalized with – SO_3H groups

SI - Selectivity index

TCI - Tokyo Chemical Industry Co. Ltd

TFA - Trifluoroacetic acid

THF – Tetrahydrofuran

$TMSN_3$ - Trimethylsilyl azide

TR - Trypanothione reductase

TSB - Tryptic soy broth

UV - Ultraviolet

WHO - World Health Organization

w/o - Without

wt85 - Wild type 85

ZOS - Zosuquidar

Outline of the thesis

Chapter 1 – Introduction

In this chapter a theoretical background concerning the synthetic methodologies developed to obtain 9*H*-xanthene, 9-hydroxyxanthene and xanthene-9-carboxylic acid, as well as respective derivatives, from simple starting materials or through modification of related structures is presented. Biological and pharmacological activities of several derivatives are described.

This chapter was adapted from the review paper of Miguel Maia *et al* *. The review manuscript was written by Miguel Maia, Diana Resende and Fernando Durães, under the supervision of Emília Sousa. All co-authors contributed to the bibliographic search and revision of the manuscript.

Chapter 2 – Synthesis of 9-hydroxyxanthene derivatives and biological activity

Chapter 2 describes the synthesis and structural characterization of the 9-hydroxyxanthene derivatives, obtained from xanthydrol with sulfonamides and aniline. Results of biological activity against mechanisms of bacterial resistance are also presented.

This chapter was adapted from the original research work submitted to *Drugs and Drug Candidates* in October 2022.

Candidate contribution: synthesis and characterization of the 9-hydroxyxanthene derivatives and discussion of the results obtained in the biological activity assays; writing of the original manuscript. The docking studies and biological activity was performed by Fernando Durães and Nikoletta Szemerédi under the supervision of Gabriella Spengler, at Department of Medical Microbiology, Albert Szent-Györgyi Health Center and Faculty of Medicine, University of Szeged, Hungary. Single crystal X-ray diffraction was performed by Luís Gales at I3S – Instituto de Investigação e Inovação em Saúde, University of Porto, Portugal.

* Maia, M.; Resende, D. I. S. P.; Durães, F.; Pinto, M. M. M.; Sousa, E., Xanthenes in Medicinal Chemistry – Synthetic strategies and biological activities. European Journal of Medicinal Chemistry 2021, 210, 113085.

Chapter 3 – Synthesis of xanthene-9-carboxylic acid derivatives and biological activity

Chapter 3 describes the synthesis and structural characterization of derivatives of xanthene-9 carboxylic acid, namely xanthene-carboxamides, and further functionalization with aromatic halogenation and Suzuki coupling. This set of compounds was tested for anti-parasitic and neuroprotection activities.

The introduction to Alzheimer's disease and BACE1 inhibition was adapted from the review paper of Miguel Maia *et al* *. The review manuscript was written by Miguel Maia under the supervision of Emília Sousa

Candidate contribution: synthesis and structural characterization of the xanthene-9-carboxylic acid derivatives described; discussion of the results obtained in the biological activity assessment.

The biological activity was performed by 1) Ana Rita Monteiro under the supervision of Renata Silva and Fernando Remião, at Department of Biological Sciences, Laboratory of Toxicology, Faculty of Pharmacy, University of Porto (cytotoxicity, modulation of P-gp and iron (III)-induced cytotoxicity assays); 2) Ana Martínez *et col.*, at Center for Biological Research (CIB), Spanish National Research Council (CSIC), Madrid, Spain (PAMPA-BBB assay).

Chapter 4 – Synthesis of benzhydryl derivatives and biological activity

In this chapter, the synthesis and structural characterization of diphenyl acetic acid derivatives obtained through a continuous flow, Curtius rearrangement procedure is described. Several alcohols and amines were used as nucleophiles and a library of carbamate and urea derivatives was obtained. These compounds were tested for antiparasitic activity.

Candidate contribution: synthesis and structural characterization of the benzhydryl derivatives herein described; discussion of the results obtained in the biological activity assessment. The synthesis was performed at the Baumann Research Group, School of Chemistry of the University College Dublin, Dublin, Ireland. The biological activity assays was performed by Fernando Durães under the supervision of John Kelly and Amanda Fortes Francisco at London School of Hygiene & Tropical Medicine, London, UK.

* Maia, M. A.; Sousa, E., BACE-1 and γ-Secretase as Therapeutic Targets for Alzheimer's Disease. Pharmaceuticals 2019, 12 (1)

Chapter 5 – General discussion and conclusions

This chapter summarizes the main results obtained in this thesis regarding synthesis and biological activities and presents the main achievements and conclusions of this thesis.

Chapter 6 – References

The references of this thesis are presented in this chapter and follow the ACS style guide. The main databases/search engines used were ISI Web of Knowledge, Scopus, PubMed, Google Scholar, Espacenet and PATENTSCOPE.

Annex I – HPLC and NMR spectra and electrospray ESI data

This annex depicts HPLC, NMR and electrospray ESI data for each compound described in this thesis.

Annex II - Chemical structures of the investigated compounds

Annex II provides a resume of the chemical structures, molecular weight and name of the compounds synthetize in the present work.

Chapter 1. – Introduction

Adapted from Miguel Maia *et al* *.

* Maia, M.; Resende, D. I. S. P.; Durães, F.; Pinto, M. M. M.; Sousa, E., Xanthenes in Medicinal Chemistry – Synthetic strategies and biological activities. European Journal of Medicinal Chemistry 2021, 210, 113085.

Graphical Abstract

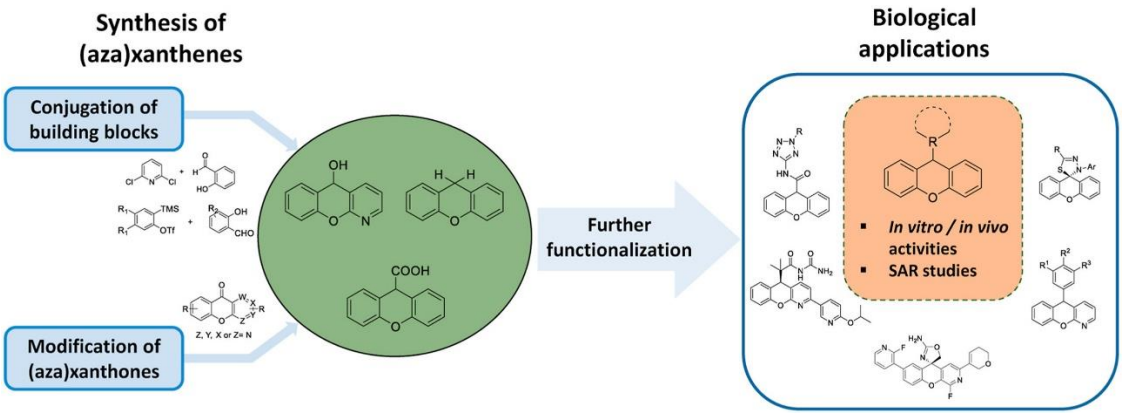

1.1. Xanthenes

Xanthenes are a special class of oxygen-incorporating tricyclic compounds characterized by a dibenzo[*b,e*]pyran nucleus. Despite their sparkly occurrence in nature, in the last decades there were some reports regarding their discovery from natural extracts: blumeaxanthene (**1**) has been isolated from *Blumea riparia* DC., a Chinese medicinal herb traditionally used to treat gynecological disorders [1], compounds **2**, **3**, and **4** were isolated from a marine mangrove endophytic fungus *Penicillium sp* and showed potential to be precursors of new biopesticides [2], and compounds **5** and **6** from foliar fungal endophytes of *Pinus strobus* exhibited antimicrobial activity [3].

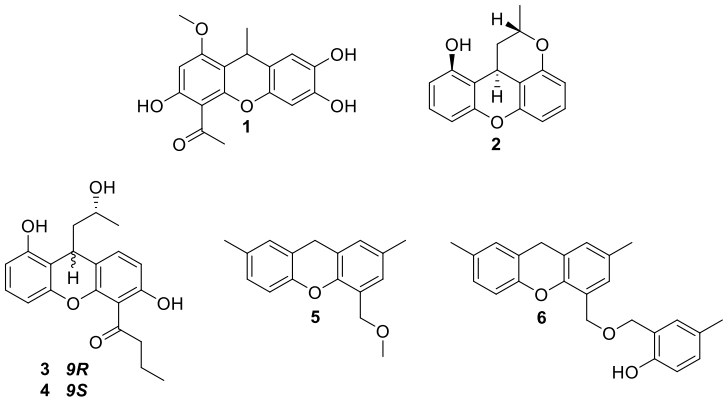

Figure 1. Natural xanthenes.

Most of the known xanthenes were obtained artificially, through cyclization processes of suitable building blocks or by modification of related structures, namely xanthones. The presence of different substituents in position 9 has a large impact on their physical and chemical properties, as well as their biological applications. 9*H*-Xanthene (**7**), 9-hydroxyxanthene (xanthydrol, **8**), xanthene-9-carboxylic acid (**9**) (**Figure 2**), and their respective derivatives have been reported to exhibit remarkable biological activities, namely neuroprotection, antiparasitic, cytotoxic, and antibacterial. These compounds have also been used as sensitizers in photodynamic therapy [4] and as dyes in food (rhodamine B, erythrosine) [5], industrial materials [6] and in the visualization of biomolecules as chemical probes [7].

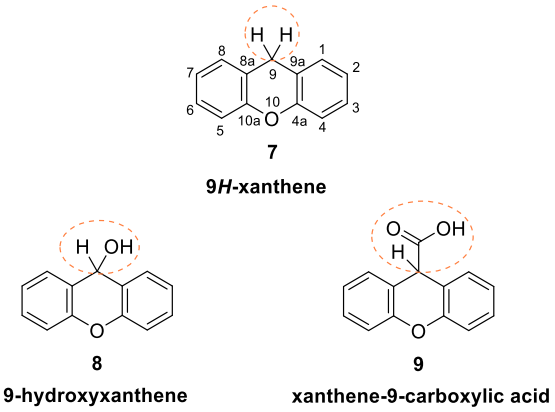

Figure 2. Structures of 9*H*-xanthene (**7**), 9-hydroxyxanthene (xanthydrol, **8**), and xanthene-9-carboxylic acid (**9**).

1.1.1. Synthesis

1.1.1.1. Synthesis of 9*H*-xanthene derivatives

Different strategies have been applied for the synthesis of 9*H*-xanthene, as depicted in Scheme 1. One of the first synthesis was reported by Sean *et al.* [8], where 3-hydroxyxanthene was obtained through the condensation of saligenin (**10**) with resorcinol (**11**) in the presence of $ZnCl_2$ (**Scheme 1**, Method A). Xanthene derivatives with alkyl substituents can be obtained through the condensation of alkylphenoxy-magnesium halides **12** with 2-hydroxyaryl-1-carboxyaldehyde diethylacetals **13** (**Scheme 1**, Method B) [9]. Firstly, **13** is obtained through a C-regiospecific attack of triethyl orthoformate at the phenolic system of **12**, which then reacts with another equivalent of **12** to form an ether intermediate. Consequent aromatic cyclization via xanthylium ion led to the obtention of several xanthene derivatives with alkyl substituents at positions 2 and 5 with 25-85 % yield. Böβ *et al*. [10] developed a more versatile method, allowing to obtain derivatives containing hydroxyl, alkyl, methoxyl, and halogen derivatives (**Scheme 1**, Method C). It consists on a condensation of different salicylaldehydes **15** and cyclohexanones **14** using $Sc(OTf)_3$ (scandium(III) trifluoromethanesulfonate) as a Lewis acid catalyst. The application of microwave radiation (MW) instead of conventional heating provided better results, up to 200 % increase in yield and applying shorter reaction times. Eight xanthene derivatives were obtained with 55-86 % yield with these conditions. Lastly, 9*H*-xanthenes can be obtained through the reduction of xanthone derivatives **16** (**Scheme 1**, Method D). Sousa *et al.* [11] explored the catalytic activity of several high-valent dioxidomolybdenum complexes for the direct deoxygenation of aryl ketones to aryl alkanes, and reported the use of $PhSiH_3$/$[Mo^{VI}Cl_2O_2(H_2O)_2]$ in toluene for the reduction of unsubstituted xanthone to xanthene with 98 % yield. Despite the excellent yield obtained, these reaction conditions were not applied to substituted

xanthones and no information is provided regarding its selectivity. Another method for the reduction of xanthones was reported by Vieira *et al*. [12], describing the reduction of several halogenated xanthones with borane dimethyl sulfide complex ($BH_3.Me_2S$). Despite no yields being provided, it suggests the use of this standard reducing agent as suitable for the reduction of substituted xanthones to the respective xanthenes.

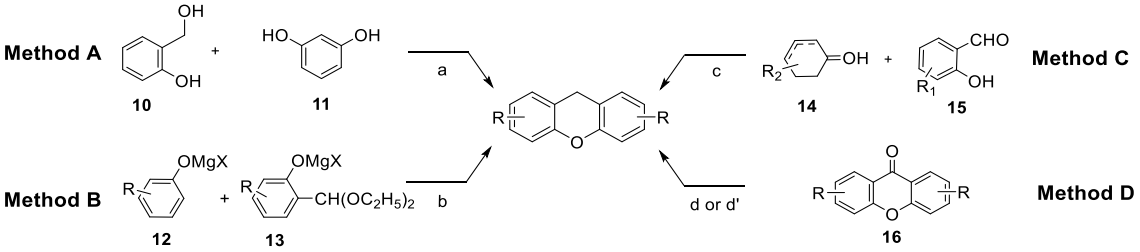

Reagents and conditions: (**a**) anhydrous $ZnCl_2$, , 2-3 h, 140-180 °C; (**b**) *s*- butoxymagnesium bromide, benzene, 10-12 h, reflux; (**c**) $Sc(OTf)_3$, chlorobenzene, MW (180 °C, 30 min) or reflux (conventional heating,18-44 h). (**d**) $PhSiH_3/[Mo^{VI}Cl_2O_2(H_2O)_2]$, toluene, 16 h, reflux; (**d'**) $BH_3.Me_2S$, THF, 2 h, 45 °C;

Scheme 1. Synthesis of 9*H*-xanthene derivatives.

Knight and Little [13] reported a synthetic methodology for the intramolecular trapping of benzynes by phenols and 4-iodo-5-methoxy-9*H*-xanthene (**24**) was successfully obtained (**Scheme 2**). Firstly, the dianionic species **18** is generated through the metalation of 1-(*tert*-butoxycarbonylamino)benzotriazole (**17**) with butyllithium in the presence of tetraglyme and $CeCl_3$ [14]. Subsequent condensation with 2-(*tert*-butyldimethylsilyloxy)-3-methoxybenzaldehyde (**19**) provided a good isolated yield of the *ortho*-substituted intermediate **20**. Cleavage of the *tert*-butyldimethylsilyl (TBDMS) group was readily achieved by treatment with hydrogen fluoride-pyridine complex to obtain the free phenol **21**, followed by reduction with hydrogen and 5% Pd/C (palladium on carbon) leading to the benzyl derivative **22.** Lastly, *N*-deprotection with trifluoroacetic acid (TFA) and benzyne generation using two equivalents of *N*-iodosuccinimide (NIS) [15] led to the reactive intermediate **23**, which undergo intramolecular cyclisation with incorporation of iodine, giving the iodoxanthene **24**, with an overall yield of 37 %.

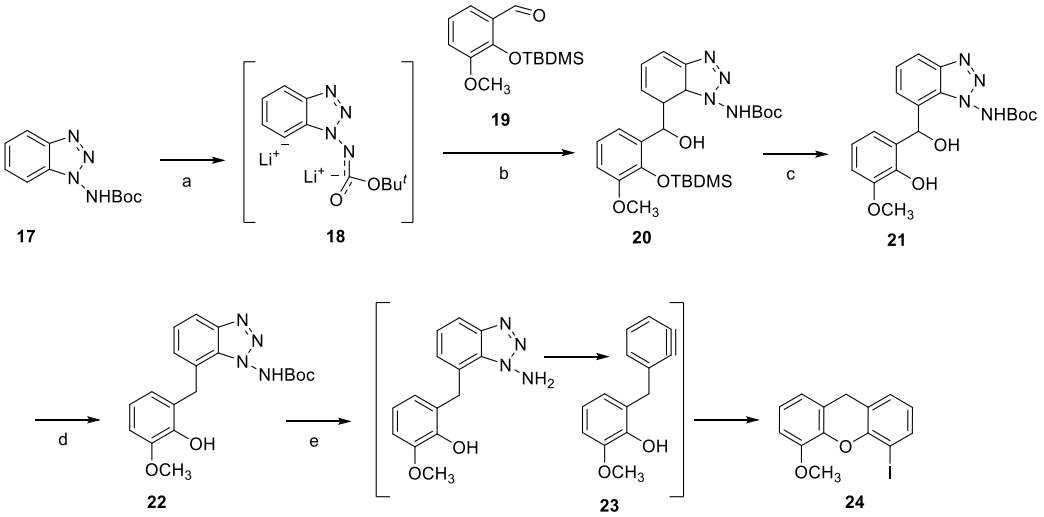

Reagents and conditions: (**a**) butyllithium, dry tetraglyme, $CeCl_3$, dry THF, 4 h, -70 °C to 0 °C; (**b**) **18** in dry THF (1 mL $mmol^{-1}$), 16 h, -78 °C to rt; (**c**) hydrogen fluoride-pyridine complex, dichloromethane, 48 h, rt; (**d**) H_2, 5 % Pd/C, methanol, 4 h, rt; (**e**) i) TFA, CH_2Cl_2, 0.5 h, rt, ii) NIS, CH_2Cl_2, 0.5 h, rt.

Scheme 2. Synthesis of 4-iodo-5-methoxy-9*H*-xanthene **24**.

1.1.1.2. Functionalization of 9*H*-xanthene derivatives

Functionalization of position 9 of xanthene has been performed through different techniques (**Scheme 3**). One methodology is by asymmetric conjugation of xanthene with aldehydes through an oxidative dehydrogenative α-alkylation process via benzylic C-H bond activation (**Scheme 3**, Method A) [16]. Oxygen was used as an inexpensive and environmental benign oxidant in conjugation with a MacMillan catalyst. This asymmetric transformation led to several xanthene derivatives **25** in moderate to good yields (48-77 %) with excellent enantiomeric excess (ee) values (81-92 %). For the conjugation of xanthene with *n*-alkoxyamides, Lin *et al*. [17] used an intermolecular electrochemical C(sp^3)-H/N-H cross-coupling method using ferrocene (Fc) as redox catalyst and eighteen *N*-alkoxy-*N*-(9*H*-xanthen-9-yl)-benzamides **26** were obtained with 70-77 % yields (**Scheme 3**, Method B). Electrochemical methodologies were also employed in the dehydrogenative coupling of xanthenes with azoles and imides (**Scheme 3**, Method C) [18, 19]. Pyrazoles, imidazoles, triazoles, tetrazoles, and benzimidazoles react smoothly with xanthene derivatives using these metal free coupling methodologies, affording the corresponding xanthen-9-amines **27** in 50-92 % yield.

Another methodology allows the one-pot azidation of xanthene to obtain xanthene 9-yl-triazoles (**Scheme 3**, Method D) [20]. This technique was developed for compounds in which a stable radical or carbocation can be generated, in which the azide unit of the C(sp^3)-N_3 species is promptly cleaved. Therefore, the *in situ* generation and trapping of the azide

would be essential when the target is difficult to handle during workup, purification, and following synthetic steps. The tandem reaction of 1) azidation of 9*H*-xanthene with trimethylsilyl azide ($TMSN_3$) and copper bromide as catalyst and 2) cycloaddition with different alkynes allows to obtain several xanthene-9-yl-triazoles **28**. The method showed a good steric and electronic functional group tolerance providing substituted products in good yields (up to 82 %). A more recent method reports the conjugation of xanthenes with ketones, 1,3-dicarbonyls, and arenes under mild reaction conditions using acidic carbon dots surface functionalized with $-SO_3H$ groups (s-CDs) as visible-light induced photocatalyst (**Scheme 3**, Method E) [21]. The s-CDs demonstrated dual catalytic properties that include photoactivation of benzylic $-CH_2$ groups in xanthene in the presence of O_2 resulting in the formation of the hydroperoxyl intermediate, followed by coupling of the nucleophiles catalyzed by acid surface functionalities. This cross-dehydrogenative coupling (CDC) methodology showed to be selective and efficient, allowing to obtain several xanthene derivatives **29** with 68-96 % yield. The easy synthesis of s-CDs, biocompatibility, recyclability, possibility of integrating catalytically active entities on the surface and inherent enzyme mimetic activities are pointed as benefic characteristics that made this catalyst a green alternative to metal catalysts for various multi-step organic synthesis.

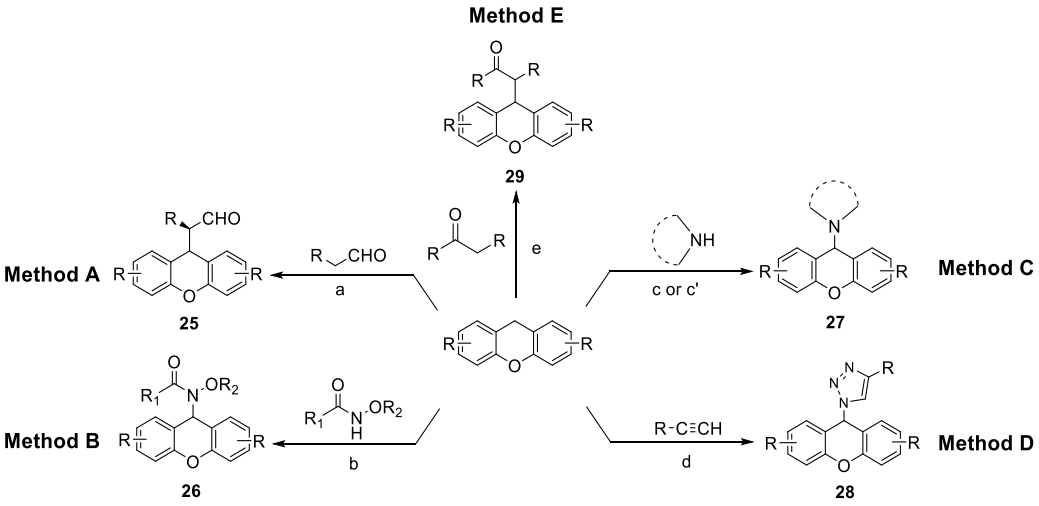

Reagents and conditions: (**a**) MacMillan catalyst ((*S*)-2,2,3-trimethyl-5-phenylimidazolidin-4-one trifluoroacetate salt), H_2O, CH_3NO_2, O_2 (1 atm), -5 to 5 °C, 96 h; (**b**) Fc, Na_2CO_3, carbon anode, carbon cathode, supporting electrolyte: $LiClO_4/CH_3CN:CH_2Cl_2$, (2:1), undivided cell, J=5 mA/cm^2, rt, 5.5 to 8 h; (**c**) MsOH, CH_3CN, carbon rod anode, platinum plate cathode, supporting electrolyte : $^nBu_4NBF_4$, constant current = 10 mA, air, rt, 2 h; (**c'**) CH_3CN, carbon cathode, nickel anode, supporting electrolyte: nBu_4NClO_4 (tetra-*n*-butylammonium tetrafluoroborate), undivided cell, constant current = 7 mA, air, 23 °C, 1.5 to 3 h; (**d**) i) CuBr, $TMSN_3$, TBHP, CH_3CN, 50 °C, 2 h; ii) R-acetylene, sodium ascorbate, DIPEA, *t*ert-butanol, 50 ° C, 4 to 24 h; (**e**) s-CD, 34 W blue LED lamp (hn = 425 nm), O_2, 25 °C, 3 to 12 h.

Scheme 3. Synthesis of 9*H*-xanthene derivatives.

1.1.1.3. Synthesis of 9-hydroxyxanthene

Xanthydrol can be obtained starting with the coupling reaction of 3-(dimethoxymethyl)phenol (**30**) with 2-bromobenzaldehyde (**31**) (**Scheme 4**, Method A) [22]. A diphenyl ether is obtained, which through intramolecular phenyl-carbonyl coupling reaction affords a xanthydrol derivative with a carbaldehyde in position 3 with 81 % yield. Another methodology to obtain xanthydrols consists in the reaction of *o*-trimethylsilylphenyl triflates **32** with salicylaldehydes **33** (**Scheme 4**, Method B) [23]. Using this one-step procedure under smooth conditions, several alkyl and methoxyl xanthydrol derivatives were obtained with 52-85 % yield. Later, the same authors reported a similar method for the synthesis of unsubstituted xanthydrol (**8**, **Scheme 4**, Method C) [24]. Two equivalents of *o*-trimethylsilylphenyl triflate (**34**) reacted with DMF to afford xanthydrol in 52 % yield. In both methods, CsF is used as catalyst and K_2CO_3 assures basic conditions to prevent disproportionation. Lastly, xanthydrol (**8**) can be obtained through the reduction of xanthones **35**. Older reports considered the use of toxic and unsafety conditions (Hg and metal Na) [25], but recently this reduction has been accomplished through a very simple procedure applying zinc and sodium hydroxide in reflux EtOH (ethanol) (**Scheme 4**, Method D) [26]. If no issues are predicted regarding the presence of other functional groups susceptible to reduction, this seems to be the most straightforward procedure for the synthesis of xanthydrol derivatives, considering the commercially availability and low price of xanthones.

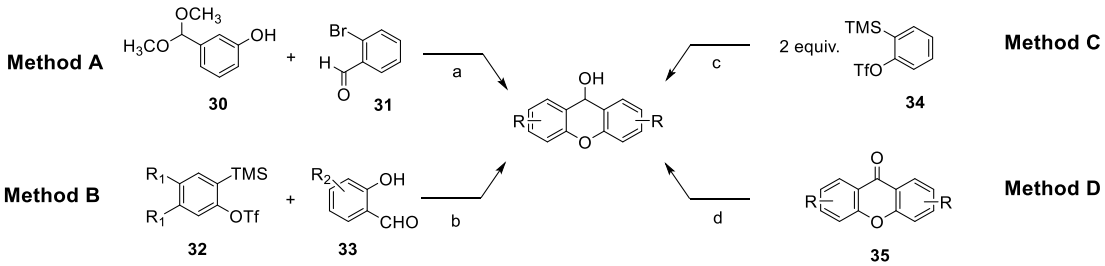

Reagents and conditions: (**a**) i) $(CuOTf)_2C_6H_6$, Cs_2CO_3, toluene, 110 °C,12 h, ii) HCl, rt, 3 h, iii) SmI_2/HMPA, THF, 0 °C, 0.5 h; (**b**) CsF, K_2CO_3, CH_3CN, rt, 6 to 15h; (**c**) CsF, DMF, K_2CO_3, CH_3CN, rt, 14 h; (**d**) Zn, NaOH, 96 % ethanol, 90 °C, 2 h.

Scheme 4. Synthesis of 9-hydroxyxanthenes.

1.1.1.4. Synthesis of 9-hydroxyxanthene derivatives

Since the report of the use of 9-hydroxyxanthene (xanthydrol, **8**) for the estimation of blood urea, its reactivity has been explored for the determination of different components in different matrices [27-31]. Additionally, it has been used for the synthesis of xanthene derivatives, taking advantage of its reactivity through the formation of the xanthylium ion,

readily formed in presence of an appropriate catalyst [32]. Nucleophilic attack by an electron pair through S_N1 reaction from a molecule of relatively high electron density leads to the substitution product **36** (**Scheme 5**, Method A). Acetic acid [32, 33], ceric ammonium nitrate (CAN) [34], ferric hydrogensulfate ($Fe(HSO_4)$) [35], and ionic liquid medium of 1-butyl-3-methylimidazolium tetrafluoroborate ($BmimBF_4$) [36] were reported as efficient catalysts for this transformation. A different methodology was developed by Xiau [37] to obtain chiral xanthene derivatives. He reported the use of cooperative systems of diarylprolinol silyl ether with CuCl, $IrCl_3$, or $InBr_3$ as Lewis acid catalysts to achieve the enantioselective intermolecular α-alkylation of aldehydes with alcohols (**Scheme 5**, Method B). Xanthydrol (**8**) was used as a model substrate and react with both linear and bulky aldehydes **37** to produce chiral xanthene derivatives **38** in high yields (63-96 %) and excellent enantioselectivities (90-99 % ee). Xanthydrol (**8**) was also explored as starting material to obtain six-membered lactams. Through a five-step methodology Carmen de la Fuente and Domínguez [26] reported the synthesis of the isoquinolinone **39** through the construction of the nitrogenated ring by electrophilic cyclization with an overall yield of 40 % (**Scheme 6**).

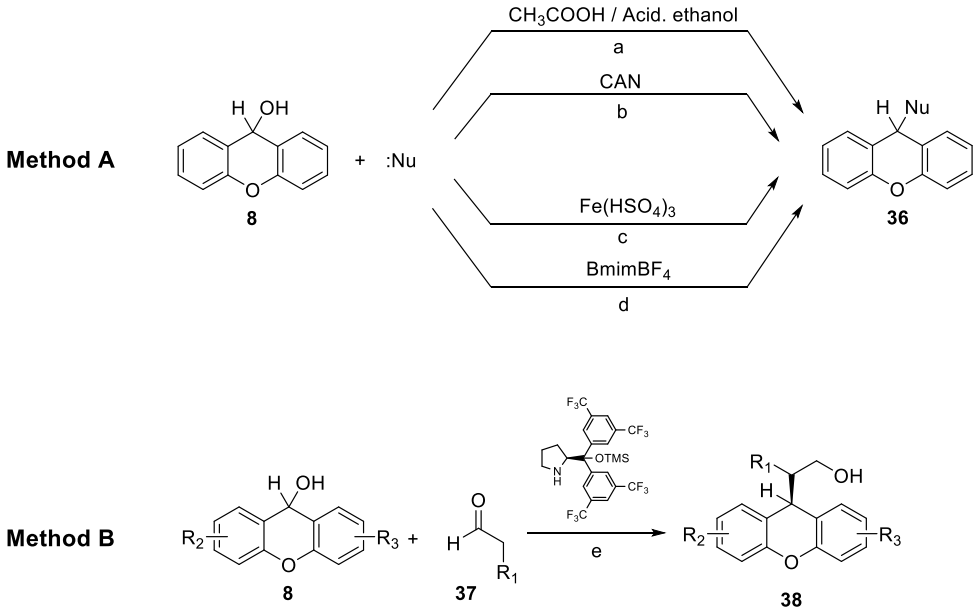

Reagents and conditions: (**a**) rt, 0.5 h; (**b**) methanol, rt, sonication, 0.5 to 3 h; (**c**) ethanol, reflux, 0.5 to 2 h; (**d**) rt, 24 h; (**e**) CuCl or $IrCl_3$, CH_2Cl_2, rt, 12 to 36 h.

Scheme 5. Synthesis of 9-hydroxyxanthene derivatives.

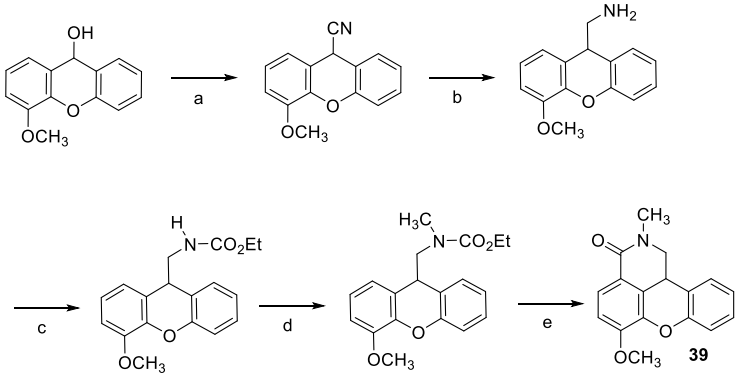

Reagents and conditions: (**a**) TMSCN, ZnI_2, CH_2Cl_2, 0 °C, 3 h; (**b**) $BH_3.Me_2S$, THF, reflux, 2 h; (**c**) i) Na_2CO_3, ethyl chloroformate, THF, rt, 1 h; (**d**) i) sodium hydride, DMF, 30 °C, 0.5 h, ii) methyl iodide, rt, 0.5 h; (**e**) TF_2O, DMAP, CH_2Cl_2, 0 °C, 4 h.

Scheme 6. Synthesis of isoquinolinone **39**.

1.1.1.5. Synthesis of xanthene-9-carboxylic acid

Xanthene-9-carboxylic acid (**9**) is another intermediate of considerable value in Medicinal Chemistry for the synthesis of bioactive compounds. In a protocol developed for the synthesis of the natural dibenzopyranazepine alkaloid (±)-clavizepine, Vázquez *et al*. [38] described the synthesis of the xanthene-9-carboxylic acid derivative **45** from simple and commercially available materials (**Scheme 7**). It starts with 3,4-dimethoxyphenylacetic acid (**40**), which was brominated and esterified to give **41**. This compound was subjected to an Ullmann condensation with catechol monobenzyl ether **42** under standard conditions to give the diphenyl ether **43** in 54 % yield. Subsequent bromination and intramolecular addition of the ester enolate afforded xanthene 9-carboxylate **44**. Lastly, through alkaline hydrolysis xanthene-9-carboxylic acid **45** was obtained.

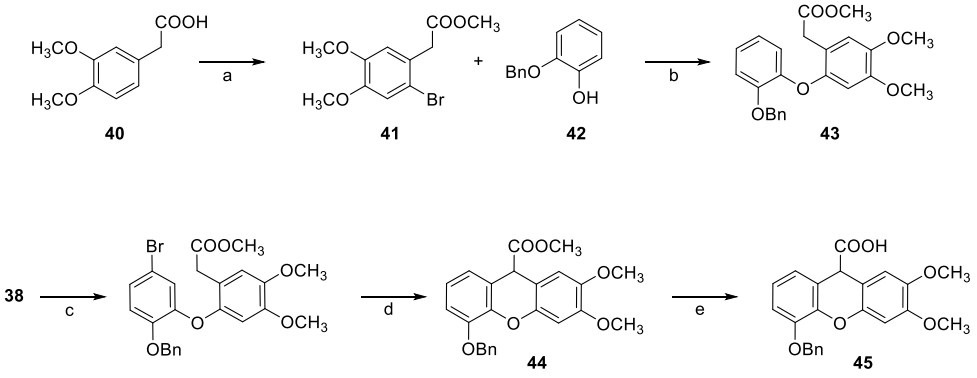

Reagents and conditions: (**a**) i) Br_2, AcOH, rt, 1 h, ii) methanol, H_2SO_4, rt, 2 h (**b**) Cu, CuO, K_2CO_3, pyridine, reflux, 10 h; (**c**) Br_2, NaOAc, AcOH, rt, 4 h; (**d**) i) LDA, THF, -78 °C, 45 min, ii) 3 h at 0 °C; (**e**) LiOH, THF, 80 °C, 3 h.

Scheme 7. Synthesis of xanthene-9-carboxylic acid **45**.

Xanthene-9-carboxylic acid (**9**) can also be obtained by modification of related structures (**Scheme 8**). Treatment of xanthydrol (**8**) with NaCN (sodium cyanide) and subsequent hydrolysis under alkaline conditions afforded xanthene-9-carboxylic acid (**9**) with 68 % yield (Scheme 7, Method A) [39]. Starting with xanthene derivatives, deprotonation with lithium diisopropylamide (LDA) and carboxylation with carbon dioxide afforded the corresponding carboxylic acids in moderate to good yields (45-87 %) (Scheme 7, Method B) [12, 40].

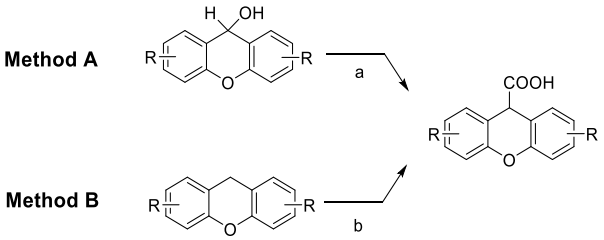

Reagents and conditions: (**a**) i) NaCN, glacial acetic acid, 100 °C, 24 h ii) 75% methanol, KOH, reflux, 24 h; (**b**) i) LDA, THF, -70 °C, ii) CO_2

Scheme 8. Synthesis of the xanthene-9-carboxylic acid from related structures.

1.1.1.6. Synthesis of xanthene-9-carboxylic acid derivatives

Modifications to xanthene-9-carboxylic acid (**9**) have also been explored to obtain biologically active substances through different techniques (**Scheme 9** and **Scheme 10**). Formation of amides is an usually explored methodology, employing coupling agents as carbonyldiimidazole (CDI) or through the formation of an acyl chloride and subsequent addition of the primary or secondary amine (**Scheme 9**, Method A) [41, 42]. Amide derivatives **46** obtained can be easily reduced to the correspondent amines **47** [42]. Formation of ester derivatives **48** through Fisher esterification was also explored [43] (**Scheme 9**, Method B), as well as further functionalization with the inclusion of a hydroxyl in position 9 to obtain derivatives **49** [44].

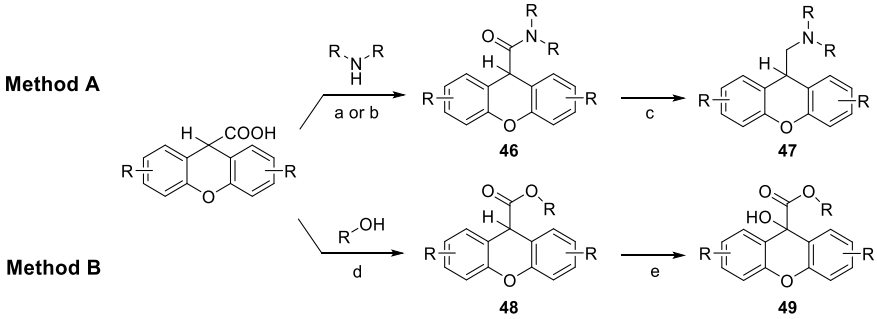

Reagents and conditions: (**a**) i) CDI, MeOTf, CH_3NO_2, 10 °C, 10 min; ii) 10 °C to rt, 15 h; (**b**) oxalyl chloride, DMF, CH_2Cl_2, reflux; (**c**) BH_3.THF, THF; (**d**) absolute dioxane, H_2SO_4, reflux, 24 h; (**e**) i) potassium *t*-butoxide, THF, 0 °C, ii) O_2, -10 to -5 °C, 2 h, iii) aqueous hydrochloric acid.

Scheme 9. Synthesis of xanthene-9-carboxylic acid derivatives.

A different xanthene derivative obtained from a xanthene-9-carboxylic acid was disclosed in an international patent regarding compounds for treatment of viral diseases [40]. As depicted in **Scheme 10**, reduction of the carboxylic acid **50** to an alcohol and subsequent chlorination allows to perform a cyclization with the deprotected hydroxy group at position 1 to obtain the tetracyclic compound **51**.

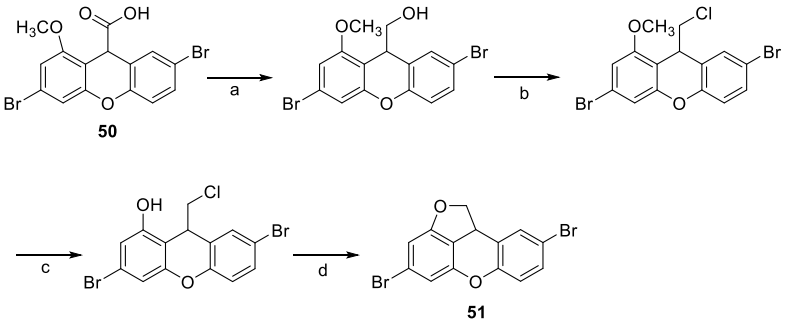

Reagents and conditions: (**a**) $BH_3.Me_2S$, THF, rt to reflux, 6 h; (**b**) $SOCl_2$, pyridine, THF, reflux, 8 h; (**c**) BBr_3, DCM, 0 °C, 24 h; (**d**) K_2CO_3, DMF, 80 °C, 15 h;

Scheme 10. Synthesis of tetracyclic compound **51**.

1.1.1.7. Synthesis of 9-alkyl xanthene derivatives

9-Alkyl derivatives can be obtained directly from the conjugation of building blocks employing distinct methodologies (**Scheme 11**). Several examples were efficiently prepared using $FeCl_3$ as catalyst under MW irradiation conditions, under a cascade benzylation-cyclization of phenols **53** with a variety of benzylating reagents **52** (**Scheme 11**, Method A) [45]. Twenty-two examples **54** were synthesized with this ecofriendly and low-cost protocol with 40-77 % yield. Another method to obtain 9-alkyl xanthenes consists of a

cascade nucleophilic addition-cyclic Michael addition process of arynes **55** and phenols **56** substituted with α,β-unsaturated groups at *ortho* positions (**Scheme 11**, Method B) [46]. This mechanism is performed in the presence of CsF and THF under reflux and several xanthene derivatives **57** were obtained in moderate to good yields. Similar reaction conditions were employed to obtain the exomethylene **60** reacting **58** with 2-hydroxyacetophenone (**59**) (**Scheme 11**, Method C) [23].

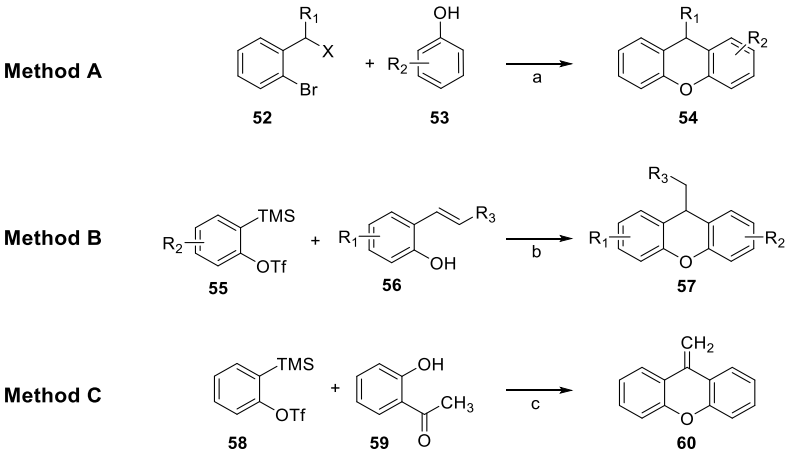

Reagents and conditions: (**a**) i) $FeCl_3$, MW, 50 °C, 10 min, ii) Cs_2CO_3, DMF, MW, 130 °C, 10 min; (**b**) CsF, THF, 66 °C, 36 h; (**c**) CsF, CH_3CN, rt, 15 h.

Scheme 11. Synthesis of 9-alkyl xanthenes.

9-Alkyl xanthenes can also be obtained from xanthone derivatives (**Scheme 12**). One strategy is the reaction of xanthones with Grignard reagents to obtain several different 9-alkyl xanthenols **61** (22 examples, 53-89 % yield) (**Scheme 12**, Method A) [47]. Exomethylenes **62** can be obtained through Peterson olefination of xanthones by treatment with trimethylsilylmethyllithium followed by acetyl chloride workup (**Scheme 12**, Method B) [48]. Methylation of xanthones with trimethylaluminum (Me_3Al) affords 9,9-dimethylxanthenes **63** (**Scheme 12**, Method C) [49] and coupling with propiophenone under McMurry reaction conditions affords compounds **64** (**Scheme 12**, Method D) [50].

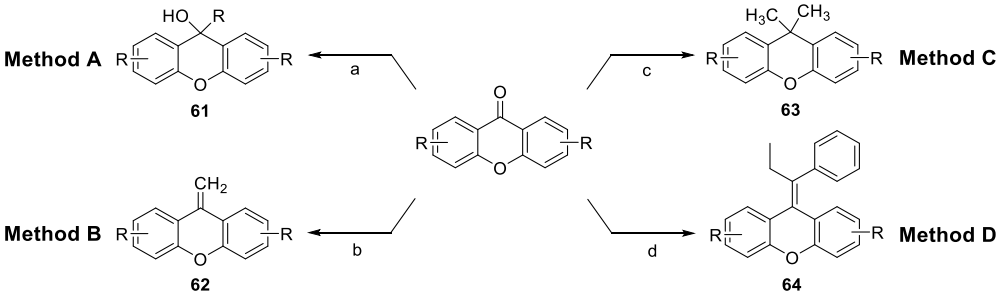

Reagents and conditions: (**a**) RMgBr, THF, -78 °C 1 h to rt 5 h; (**b**) i) trimethylsilylmethyllithium, THF, -78 °C, 0.5 h, ii) AcCl, rt, 3 h; (**c**) Me_3Al, toluene, 0 °C, 50 min, to rt 17 h; (**d**) propriophenone, $TiCl_4$, Zn, THF, -15 °C to reflux.

Scheme 12. Synthesis of 9-alkyl xanthenes from xanthone derivatives.

1.1.1.8. Functionalization of 9-alkyl xanthene derivatives

Further modifications are reported allowing increasing functionalization and drug-likeness of xanthene compounds (**Scheme 13**). Friedel-Crafts alkylation and bromination were reported to introduce functional groups in the aromatic rings, in positions 2, 7 and 4, 5, respectively (**Scheme 13**, Method A) [49, 51]. Another interesting modification was employed to introduce a fourth ring at position 9 (**Scheme 13**, Method B) [48]. Several exomethylenes treated with iodine isocyanate followed by ammonia allowed to obtain racemic mixtures of aminooxazoline xanthene derivatives.

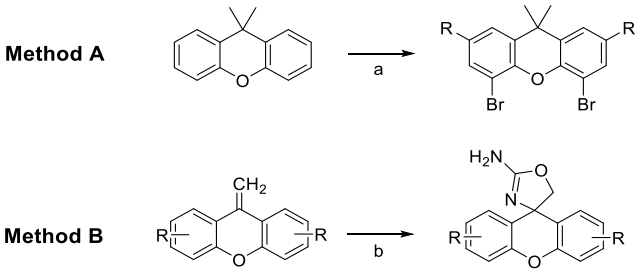

Reagents and conditions: (**a**) i) RCl, $FeCl_3$, CH_2Cl_2, 0 °C 50 min to rt 18 h, ii) CCl_4, Br_2, 0 °C 25 min to rt 26 h; (**b**) i) silver cyanate, iodine, diethyl ether, 40 min, rt, ii) NH_4OH, THF, rt, 15 h.

Scheme 13. Synthesis of 9-alkyl xanthenes derivatives.

1.1.2. Biological activities of xanthenes

1.1.2.1. Neuroprotection

Considering the worldwide prevalence of neurodegenerative diseases it is vital to find potent and safe compounds that comply with the rigid pre-requisites for a drug aimed for central nervous system (CNS) [52, 53]. Xanthene derivatives have been reported as neuroprotectors in *in vivo* studies [12, 54], and so the tricyclic core of (aza)xanthene showed to be suitable to obtain compounds that penetrate the blood brain barrier (BBB) and avoid P-glycoprotein (P-gp) efflux, and at the same time establish the appropriate interactions with a biological target.

1.1.2.1.1. BACE1 inhibitors

Epstein *et al*. [54] reported a series of small-molecule β-site amyloid precursor protein cleaving enzyme 1 (BACE1) inhibitors including a xanthene core with a spirocyclic aminooxazoline head group. The authors started with the lead xanthene **65** (**Figure 3**) which showed a good amyloid beta (Aβ) lowering activity in a rat pharmacodynamic model. However, it also revealed a low therapeutic window to corrected QT interval (QTc) prolongation, consistent with *in vitro* activity on the human ether-a-go-go gene (hERG) ion channel, which potentially lead to a fatal arrhythmia called *torsades de pointes* [55]. Introduction of polar groups is a common strategy to reduce compounds' affinity for hERG channel. However, it increases total polar surface area (TPSA), which is strongly correlated with an increased P-gp recognition [56]. Hence, a series of structure-activity relationship (SAR) studies were conducted in order to determine how to balance hERG, P-gp efflux, and BACE1 potency by identifying moieties of the molecule where polarity could be incorporated to minimize hERG activity without leading to a significant efflux or a potency decrease. This balance was accomplished by introducing polarity at the P2' site with a dihydropyran moiety and at the same time reducing the TPSA of the P3 group (**Figure 3**). The introduction of a fluorine in position 4 of the xanthene ring also improved BACE1 enzymatic and cellular potencies, attributed to a favorable hydrogen-bond interaction between the 4-fluor atom and the NH of Trp76 of BACE1 catalytic pocket (**Figure 4**, A). *In vivo* studies with inhibitor **66** showed a robust reduction of CNS Aβ40 levels (74 % and 75 % for CSF and brain, respectively) when orally administered in Dawley rats. It showed a bioavailability of 50 % and 43 % in rat and Cynomolgus monkey, respectively, and no significant effect on the QTc interval at a maximum dose of 12 mg/kg [57]. Nonetheless, compound **66** displayed retinal toxicity in rats [58], an off-target effect found in preclinical studies of others BACE1 inhibitors [59, 60]. This off-target effect has been related with the inhibition of cathepsin D (CatD), a structurally related aspartyl protease that plays an important role in phagolysosomal

processing in the retinal pigment epithelium (RPE) [61]. In order to improve the selectivity of compound **66** for BACE1 over CatD, Low et al. [62] followed a structure-based approach focusing on the differences of the S3 sub-pocket ($S3_{sp}$) of BACE1 *versus* the one on CatD. It was observed that the P3 group of compound **66** occupies the S3 pocket in CatD as well as in BACE1, but the protein surfaces revealed an opportunity to extend the P3 group deeper in the S3 pocket of BACE1, and potentially increase selectivity over CatD (**Figure 4,** A' and A''). Comparing the S3 regions of both proteases, it was observed a key difference between an alanine residue (Ala335) in BACE1 and the correspondingly larger and more polar Asp 318 residue in CatD. Hence, the strategy was to extend the P3 group of the inhibitor, balancing this modification with BACE1 inhibition potency and pharmacokinetic (PK) parameters. The introduction of a 5-chloropicolinamide at P3 led to compound **67**, showing high enzymatic BACE1 activity (IC_{50} = 0.62 nM) together with improved BACE1/CatD selectivity (770,000×). **Figure 4** (B) shows an X-ray co-crystal structure of **67** in BACE1 overlaid with CatD protein. It is observed the extension of the picolinamide moiety into the S3 and the chlorine in *para*-position establishing repulsive steric interactions with the Asp318 resulting in very high selectivity over CatD for this compound. To further evaluate the likelihood for retinal toxicity, a 4 day repeat dose toxicology study was conducted in male Sprague Dawley rats with compound **67** [62]. At high multiples (127×) over the exposure necessary for 50% Aβ40 reduction in the CSF no microscopic changes in the retina were observed for compound **67** after 4 days. Unfortunately, it was also found that compound **67** blocks hERG-mediated current *in vitro* (IC_{50} = 0.9 μM) and caused QTc prolongation in a dog cardiovascular model, leading to the discontinuation of its development.

Hicken *et al*. [63] reported in an international patent its own series of tricyclic compounds for BACE1 inhibition. Several spirocyclic hydroxanthene compounds possessing a pivalamide group in P3 were disclosed, with compound **68** showing a high inhibition potency for BACE1 (1.1 nM). Nonetheless, no information is provided regarding other *in vitro*/*in vivo* assays to conclude about compound's safety, namely off-target effects over hERG ion channel and CatD.

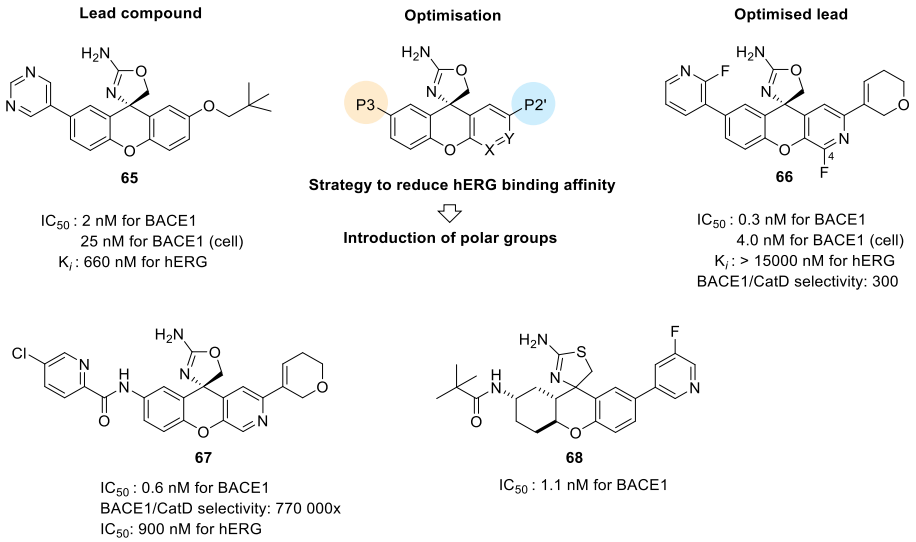

Figure 3. Lead optimization and modulation of hERG activity in xanthene BACE1 inhibitors.

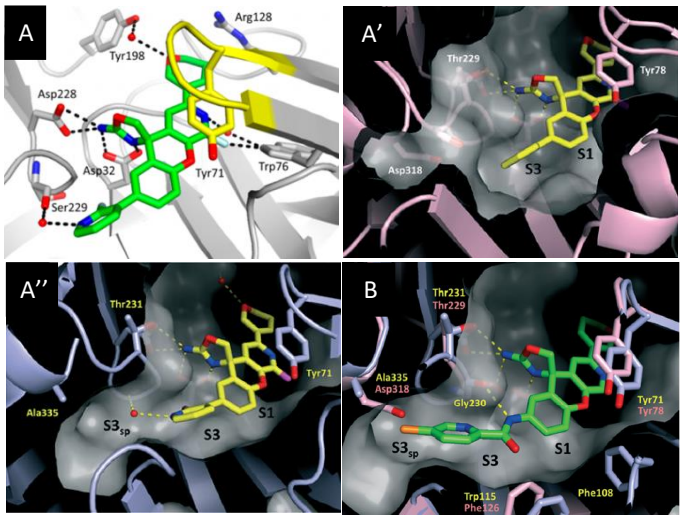

Figure 4. (A) Interaction of fluorine atom and dihydropyran moiety of compound **66** with Trp76 and with Arg128 in P2' of the catalytic pocket of BACE1, respectively. Copyright from [64]. (A') Co-crystal structure of rat CatD and inhibitor **66** (yellow). (A'') Co-crystal structure of human BACE1 and inhibitor **66**. (B) Co-crystal structure of human BACE1 (blue) + compound **67** (green) overlaid with CatD (pink). Copyright from [65].

1.1.2.1.2. mGluR1 enhancers

Metabotropic glutamate receptors (mGluR) belong to class C of G-protein coupled receptors and are activated by glutamate, the major excitatory amino acid neurotransmitter in the CNS [12]. One of the eight subtypes of G-protein coupled receptors are mGlu1, which stimulate phosphoinositide hydrolysis, leading to mobilization of intracellular calcium storage and an increase of the intracellular calcium concentration [12]. Vieira *et al*. reported four series of 9*H*-

xanthenes bearing carbonyl carbamate (**69**) [66], 1,2,4-oxadiazole (**70**) [41], tetrazole (**71**) [41], and 1,4-oxazole (**72**) [12] moieties, that behave as selective positive allosteric modulators (enhancers) of rat and human mGlu1 receptors (**Figure 5**). Initially, a random-screening using recombinant mGlu1 receptors expressed at very high levels led to the discovery of a 9*H*-xanthene-carbonyl carbamate series (**69**) of selective and potent positive allosteric modulators of mGlu1 receptors [66]. Based on these findings, a second and third series of compounds was screened to find two potent orally available mGluR1 enhancers bearing a 1,2,4-oxadiazole (R = CH_3) or a tetrazole moiety (R = CH_2CH_3) (**Figure 5**) [41]. Optimization of PK properties (clearance, half-life, and bioavailability) led to the replacement of the tetrazole moiety with the oxazole ring system, which resulted in compounds with similar activities [12]. However, metabolism of 1,2,4-oxadiazole derivative (R = CH_3) was found to take place on the methyl substituent of the oxadiazole ring as well as on positions 2 and 7 of the xanthene moiety. To reduce metabolic alterations on these positions, the synthesis of two series of trifluoromethyloxazole derivatives with improved metabolic stability and longer half-life were developed. Several derivatives with good activities at rat mGlu1 receptors were prepared and the compounds with the most promising *in vitro* profiles were selected for further PK evaluation, with some of them revealing to be suitable tools to further study the role of positive allosteric modulation of mGlu1 receptors *in vivo*. When compared with the unsubstituted trifluoromethyl-1,4-oxazole (R^1 = R^2 = H), additional fluorination of the xanthene moiety led in most cases to further reduction of the *in vitro* as well as the *in vivo* clearance values. The half-life of these compounds was also markedly increased. The volume of distribution was in the intermediate range, while brain penetration seemed to decrease for the fluoroxanthene derivatives (**Figure 5**).

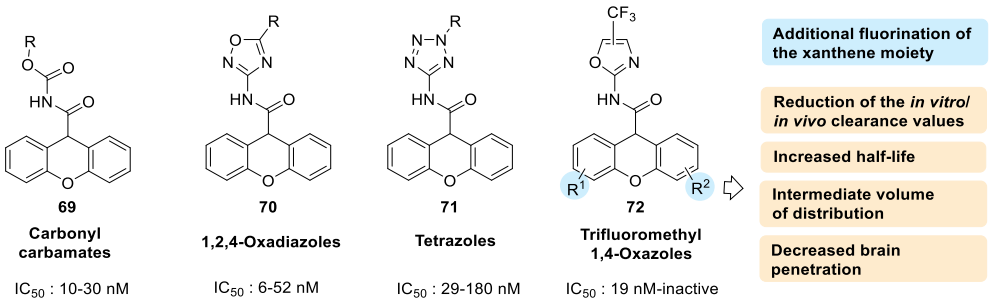

Figure 5. Structure-activity relationship analysis of 9H-xanthenes as potent, orally available mGlu1 receptor enhancers.

1.1.2.1.3. Antitumor activity

Several studies have been reported concerning the cytotoxicity of xanthene derivatives, mainly on human hepatocellular (HepG2, SK-HEP-1, SMMC-7721, BEL-7402) and breast (MCF7, MDA-MB-231) carcinoma cell lines. Other examples include prostate (DU-145), cervical (HeLa), colon (SW480), lung (A549), osteosarcoma (MG-63), and acute promyelocytic leukemia NB4 cells. In 2010, Giri *et al*. [47] reported a series of xanthenes (**73**) and evaluated their cytotoxic activity *in vitro* against three human cancer cell lines - DU-145, MCF-7, and HeLa. [*N*,*N*-Diethyl]-9-hydroxy-9-(3-methoxyphenyl)-9*H*-xanthene-3-carboxamide (**Figure 6**) exhibited interesting inhibitory cancer cell growth [half maximal inhibitory concentration (IC_{50}) = 36-50 µM] towards the three cancer cell lines. SAR studies suggested that a simple addition of a 3-methoxyl group to the 9-phenyl ring of 9-phenyl-xanthenol has a dramatic impact on activity. Additionally, replacement of the *N*-methylpiperazine with the diethylamine at R^2 position or the presence of a bulky phenyl or 3-methoxyphenyl substitution in both the chloro- and fluoro-series (R^1) also had a positive impact on the activity. Ultimately, derivatization of the hit compound (e.g., incorporation of a 7-fluoro substituent) may lead to additional gain in potency. Supplementary studies on the effect of the compounds on the catalytic activity of human topoisomerase II were developed, but no activity on the relaxation assays was detected.

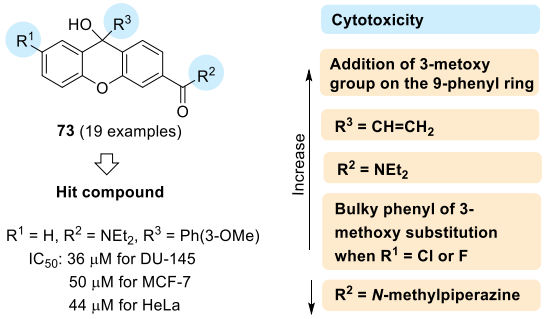

Figure 6. Structure-activity relationship analysis of cancer cell cytotoxicities for a series of substituted xanthenes **73**.

The *in vitro* antitumor activity of four series of *N*-substituted 14-aryl-14*H*-dibenzo[*a,j*]xanthene-3,11-dicarboxamide derivatives was evaluated on hepatocellular carcinoma cell lines (SK-HEP-1, Hep-G2, and SMMC-7221) and acute promyelocytic leukemia NB4 cells (**Figure 7**) [67]. Generally, the presence of side chains on the C-3 and C-11 was favourable for cytotoxicity since unsubstituted **74** did not shown significant antitumor activity (IC_{50} > 50 µM). Additionally, the nature of the carboxamide side chains in **75** exerted a strong effect, with the activity decreasing towards bulkier substituents. The easier

formation of a hydrogen bond between the N atom and the acceptor, when a smaller or polar substituent was used, showed to be beneficial to the antitumor activity. Regarding the nature of the substituent at the 14-phenyl group, derivatives presenting a substituent in the *para* position showed better activity than derivatives substituted in the *ortho* or *meta* positions. Compounds **75a** and **75b** exhibited significant inhibitory activity against NB4 cells with IC_{50} values of 0.52 μM and 0.76 μM, respectively, much lower than 5.31 μM of the positive control As_2O_3 [67].

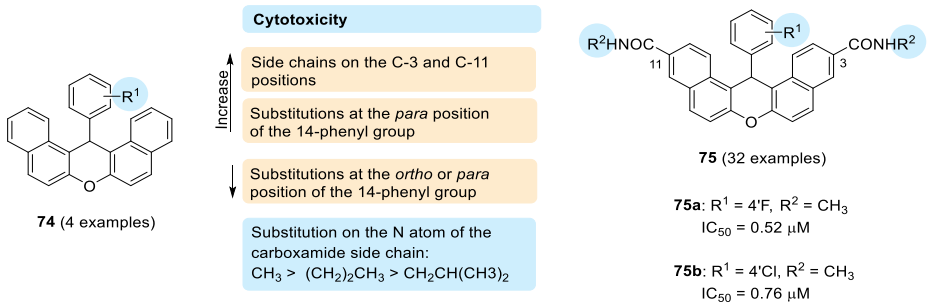

Figure 7. Structure-activity relationship analysis of cancer cell cytotoxicity for two series of substituted xanthenes **74** and **75**.

The antiproliferative activity of benzoxanthene lignans **76-82** was evaluated against two different cancer cell lines, SW480 (human colon carcinoma) and HepG2 (human hepatoblastoma) (**Figure 8**) [68]. Compounds bearing a phenylethyl group at positions 1 and 2 (**79** and **81**) revealed to be significantly more active than compounds with methyl ester groups at the same positions (**76** and **78**). Interestingly, the presence of methoxyl groups at the same positions dramatically decreased the cytostatic effect when compared to the hydroxylated congener.

In a study developed to evaluate the cytotoxicity and pro-apoptotic potential of tamoxifen-based derivatives, xanthene **83** revealed to be the most promising of the set, showing an activity profile comparable to that of tamoxifen (**Figure 8**) [50]. Besides affecting MCF-7 cell growth, further elucidation of the molecular basis of the pro-apoptotic behaviour on this cell line revealed that **83** induces mitochondria-mediated apoptosis through activation of poly (ADP-ribose) polymerase (PARP) cleavage. In order to predict the propensity of the cell to undergo apoptosis, Bax/Bcl-2 ratio was determined, and an increase was noticed suggesting their feasibility to circumvent cancer cells apoptosis deficiency by affecting tumour progression and aggressiveness. Additionally, the antitumor activity of **83** was attributed to the induction of apoptosis by modulation of Bim gene expression levels and

although **83** presented a more genotoxic profile than tamoxifen, further studies still need to be addressed, particularly on non-transformed cells [50].

Dibenzoxanthene compounds **84a-84d** were studied for their *in vitro* cytotoxicity and interactions with DNA [69]. The cell viability decreased with increasing concentrations of compounds **84a-84d**, showing a dose-dependent relation. Comparing the IC_{50} values obtained, compound **84b** appeared to be more active against BEL-7402, HeLa, and SKBR-3 cell lines (IC_{50} = 10.1 μM, 9.4 μM, and 6.2 μM, respectively), while compound **84a** presented the lowest IC_{50} against MG-63 cell line (IC_{50} = 20.1 μM). The presence of two bromine atoms in compound **84b** seems to be responsible for its increased cytotoxicity activity. DNA binding behaviours showed that these compounds interact with calf thymus DNA (CT-DNA) through an intercalative mode. However, it was found that its cytotoxicity is not consistent with their DNA-binding affinities, but instead seems to be more related with their logarithm (base 10) of the partition coefficient (P) (logP) values. Additionally, an analysis of the cell cycle status of BEL-7402 and SKBR-3 cells after treatment with compound **84a** and compounds **84b-d**, respectively, showed that the antiproliferative mechanism of these compounds was associated to a S phase arrest.

The cytotoxic effect of a synthetic polycyclic bridged–ring xanthene **85** against BEL-7402, HeLa, A549, and MG-63 cell lines was determined by MTT assays (**Figure 8**) [70]. Since **85** exhibited relatively high cytotoxicity against BEL-7402 cells, this cell line was used for further investigation on apoptosis, comet assay, reactive oxygen species (ROS), mitochondrial membrane potential, cell cycle arrest, and western blotting assay. The results indicated that xanthene **85** induces apoptotic insults to BEL-7402 cells via an intrinsic mitochondrion-caspase protease pathway.

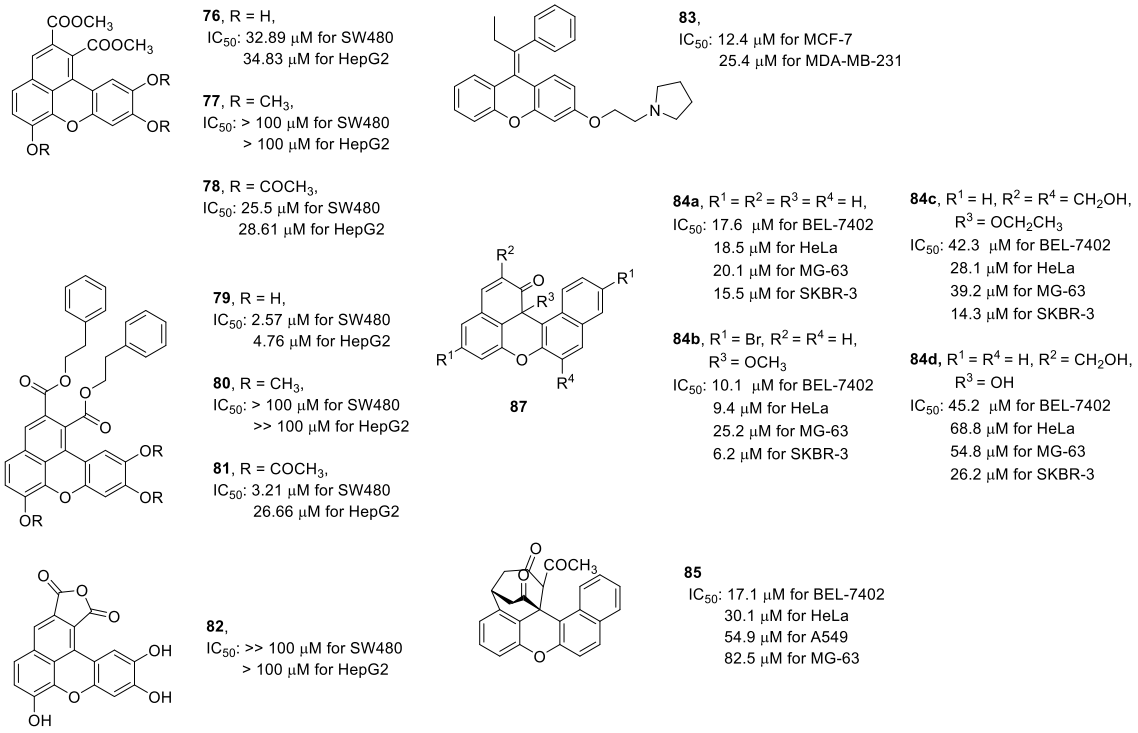

Figure 8. Structures and cytotoxicity of xanthenes **76-85**.

Among the xanthene derivatives with antitumor activity, the rose bengal disodium (**86**,**Figure 9**), a photosensitizing xanthene dye, is in the most advanced stage in clinical trials for the treatment of melanoma. Intralesional administration of PV-10 - a sterile, non-pyrogenic 10% solution of rose bengal - has been evaluated in a multi-center Phase II trial of 80 patients with Stage III and IV melanoma. PV-10 treatment produced a 51% overall response rate and 26% of complete response rate for target lesions and a complete response rate of 50% when all disease was injected [71]. A patent published in 2019 [72] disclosed the use of PV-10 for refractory pediatric solid tumors, and provided *in vitro* results of its ability to decrease cell viability in Ewing sarcoma, neuroblastoma, osteosarcoma, rhabdomyosarcoma, and normal fibroblast cell lines. PV-10 decreased cell viability in a concentration - dependent manner in all cell lines tested with IC_{50} values ranged from 45-108 μM, with a mean of 70 μM. One the other hand, IC_{50} values for the normal fibroblast cell lines and primary bone marrow samples were higher and ranged from 73-143 μM, with a mean of 104 μM. The platform *clinicaltrials.gov* [73] indicates three active recruiting clinical studies with PV-10, showing the current interest in PV-10 for future antitumor therapies, namely for liver and metastatic melanoma [74].

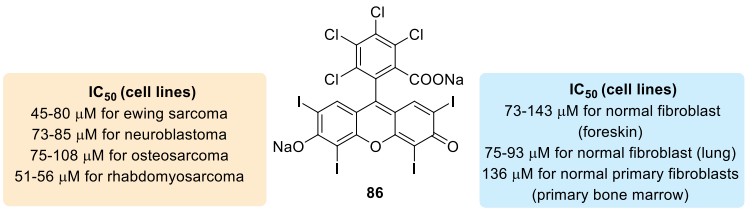

Figure 9. Structures and cytotoxicity of rose bengal (**86**).

1.1.2.2. Antimicrobial activity

1.1.2.2.1. Antifungal and antibacterial activities

In 2015, xanthenes **5** and **6** (**Figure 10**) were isolated from foliar fungal endophytes of *Pinus strobus* (eastern white pine) and tested for their antimicrobial activity [3]. Although none of the isolated compounds **5** and **6** demonstrated bioactivity against *Pseudomonas fluorescens* or *Saccharomyces cerevisiae* at concentrations up to 500 µM, they were able to significantly reduce the growth of *Microbotryum violaceum* at 50 µM. In addition, they exhibited significant activity against the Gram-positive bacterium *Bacillus subtilis* with a MIC of 25.4 µg/mL and 36.1 µg/mL, respectively (chloramphenicol as positive control, MIC = 68.7 µg/mL) [3].

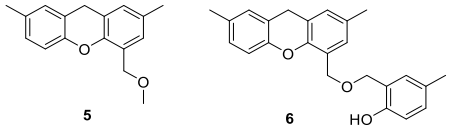

Figure 10. Xanthenes **5** and **6** with antimicrobial properties.

Yunnikova and Voronina [75] designed and synthesized a series of *N*-arylmethyl-4(xanthen-9-yl)anilines (**87a**-**d**) and structurally related *N*-arylmethylene-4-(xanthen-9-yl)anilines (**88a**-**d**), which were evaluated as potential antimicrobial agents. From their study, although the tested compounds showed no activity with respect to bacteria of the *Escherichia coli* group, even at a concentration of 1,000 µg/mL, **88c** exhibited a bacteriostatic affect with respect to *Staphylococcus aureus* (500 µg/mL) (**Figure 11**).

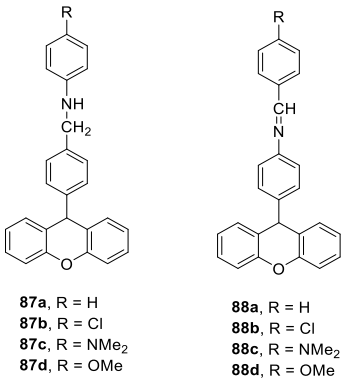

Figure 11. *N*-Arylmethyl-4(xanthen-9-yl)anilines (**87a**-**d**) and structurally related *N*-arylmethylene-4-(xanthen-9-yl)anilines (**88a**-**d**).

Since xanthene derivatives have displayed some antimicrobial activity, under the same conditions, the authors assessed this activity for isosteric 1-azaxanthene derivatives. Compounds containing primary and secondary amines linked to an azaxanthene scaffold were synthesized, and their antimicrobial activity investigated. In a first approach, one of the compounds (**89**, **Figure 12**) successfully inhibited the growth of the fungi *Candida albicans*, albeit at a high concentration range of 1,000 – 2,000 µg/mL but did not display antibacterial activity. On the other hand, two compounds (**90** and **91**, **Figure 12**) were able to prevent the growth of *S. aureus*, at the same concentration [76]. Imine derivatives of (aza)xanthenes were also synthesized and their antibacterial activity tested. It was shown that compound **92** (**Figure 12**) could inhibit the growth of *S. aureus* in a concentration of 1,000 µg/mL, and compounds **93** and **94** (**Figure 12**) displayed a bacteriostatic activity for the same microorganism at 500 µg/mL [33].

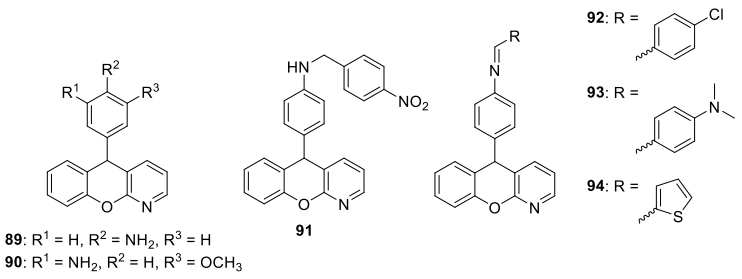

Figure 12. Structure of compounds **89**-**94**.

Amininasab *et al.* [77-80] reported studies on the antimicrobial activity and potential industrial applicability of four series of diamines and the corresponding polymers. Their two most recent works considered the synthesis of diamines **95a** and **95b** and their transformation into polymers **96**-**100** (**Figure 13**). Further antimicrobial evaluation against *Pseudomonas*

aeruginosa, *S. aureus*, *Aspergillus oryzae* and *A. niger* (fungi) disclosed good inhibition values (range of inhibition 7-16 mm), mainly attributed to the pyridine rings and xanthene pendent group, as well as the presence of electron-withdrawing groups in the dicarboxylic acid structure of synthesized polymers [79, 80]. Further studies on the solubility, thermal stability, and mechanical properties of polymers **96**-**100** revealed that they can be used industrially as alternative materials in a variety of applications, or even for hexavalent chromium ion adsorption in the form of a membrane.

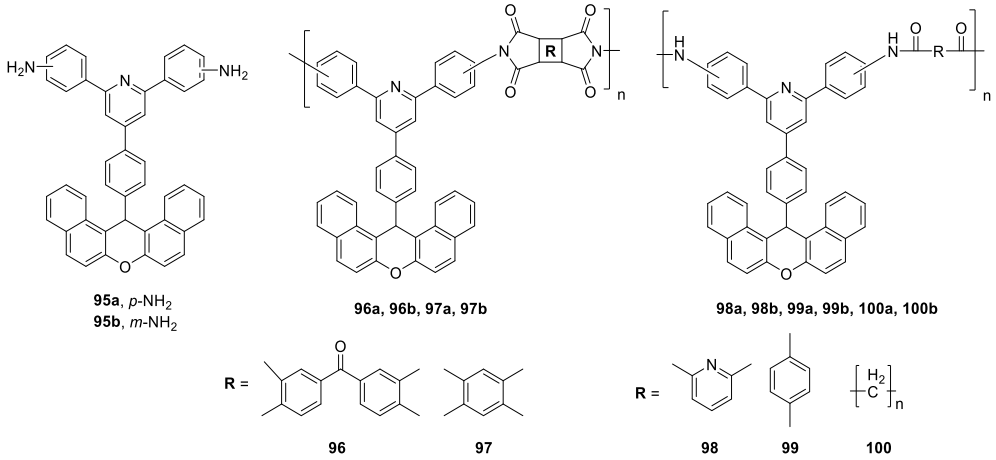

Figure 13. Diamines **95a** and **95b** and polymers **96**-**100** with potential antimicrobial activity.

1.1.2.2.2. Antiviral activity

Encephalomyocarditis (EMC) is a significant viral infection in many mammalian species that causes not only myocarditis and encephalitis, but also neurological disorders. Evaluation of a series of 2,7-bis(aminoacyl)xanthenes effectiveness in protecting mice against EMC virus infection revealed compound **101** (**Figure 14**) as a hit compound, and that an increase in length of the side chain and/or size of dialkylamino groups caused a decrease in oral activity, while the obtained survival time ratios after subcutaneous administration were higher in 2,7-bis(aminoacyl)xanthenes with higher molecular weight [81]. Compound **101** displayed the most prominent oral activity against EMC virus and evaluation against RNA arbovirus Semliki Forest virus (SFV) revealed that maximal antiviral activity was achieved when the administration was 4 hours (h) before virus inoculation. Additionally, compound **101** was effective in mice against a nonlethal challenge of vaccinia virus, a DNA virus. When given orally at a 250 mg/kg dose 24 and 28 h before infection, and again 24 and 48 h after infection, reduced the severity of virus-induced tail lesions by 31 %.

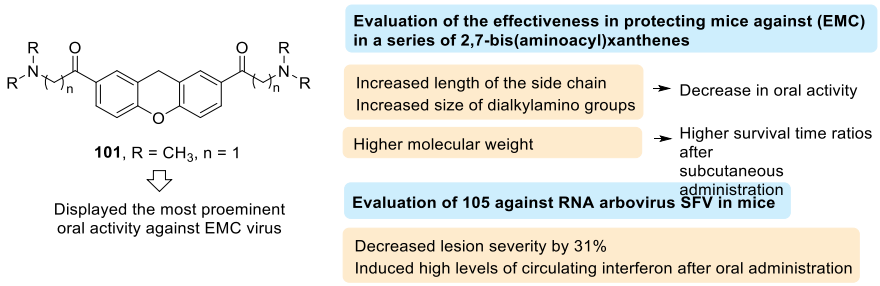

Figure 14. Structure-activity relationship analysis on the antiviral activity of xanthenes **101**.

Tobacco mosaic virus (TMV) is a pathogen able to reproduce and multiply in the host cells of the plant. It is known to infect nine plant families such as tobacco, tomato, pepper, cucumbers, and a number of ornamental flowers [82]. Ningnanmycin was used as a positive control in a study on the antiviral activity of a series of twelve arylxanthenes to inhibit the replication of TMV. The encouraging results with compounds **102**-**105** (**Figure 15**), revealing inhibition rates higher than 50 % and in the same range of the positive control, were attributed to the presence of electron-withdrawing groups in the 9-aryl moiety.

Rose bengal (**86**) was also evaluated for application as antiviral (virucidal agent) through photodynamic inactivation. Lenard *et al.* [83, 84] studied the virucidal activity (inactivation of infectivity) of rose bengal for Influenza, human immunodeficiency virus (HIV) and vesicular stomatitis virus (VSV) and reported IC_{50} values of 300, 50 and 8 nM, respectively, motivating further results for the application of this compound in the photodynamic inactivation of different products, namely biological samples as blood fractions.

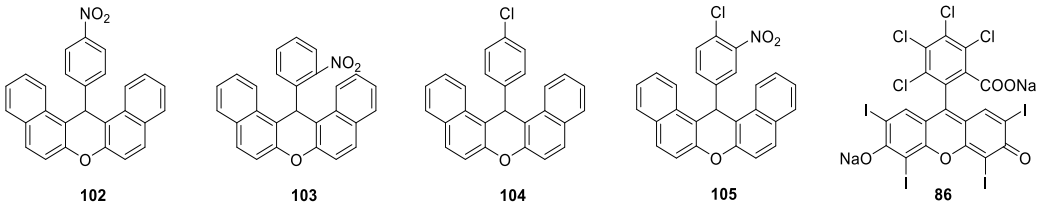

Figure 15. Xanthenes with antiviral activity.

1.1.2.2.3. Antiparasitic activity

Trypanothione reductase (TR) has long been investigated as a promising target for chemotherapeutic intervention in the causative agents of human African trypanosomiasis (*Trypanossoma brucei* spp), Chagas disease (*T. cruzi*), and leishmaniasis (*Leishmania* spp), through disruption of the natural redox defence systems of the respective parasitic

protozoa. Due to their resemblance to other tricyclic compounds already reported as competitive inhibitors of TR, 9,9-dimethylxanthene derivatives **106a-c** were evaluated against TR [85, 86]. SAR analysis indicated that weaker inhibitions are attributed to the presence of either one (**107b**) or no methylene spacer (**106a** and **106c**) between the tricyclic moiety and the secondary nitrogen atom. The functionalization of **108b** with sulphonamides (**108c**, **108d**) or ureas (**108e**-**g**) was revealed not to be beneficial towards activity. On the contrary, derivatives with two (**108a**, **108b**) or three (**07**) methylene spacer exhibited improved activity. Aryl amines **109a** and **109b**, and α,β-unsaturated amide **110** were the most promising derivatives and, therefore, their IC_{50} were determined [86], with **110** showing comparable activity to that of clomipramine. *In vitro* studies on the antiparasitic activity of **106a**-**c**, **107, 108a**, and **108b** against parasitic trypanosomes and leishmania disclosed derivative **106c** as being the most active against all three parasites (ED_{50} with values of 0.02, 0.48 and 0.55 μM, for *T. brucei*, *T. cruzi*, and *Leishmania donovani*, respectively). Additionally, **108b** showed a 5-6-fold increase in chloroquine (CQ) accumulation, against a 3.5-fold exhibited by the control verapamil, and sulfonamides **108c** and **108d** showed intrinsic antimalarial activity, comparable and superior to CQ in a CQ-sensitive (D10) and a CQ-resistant (K1) strain, respectively. These results are depicted in **Figure 16**.

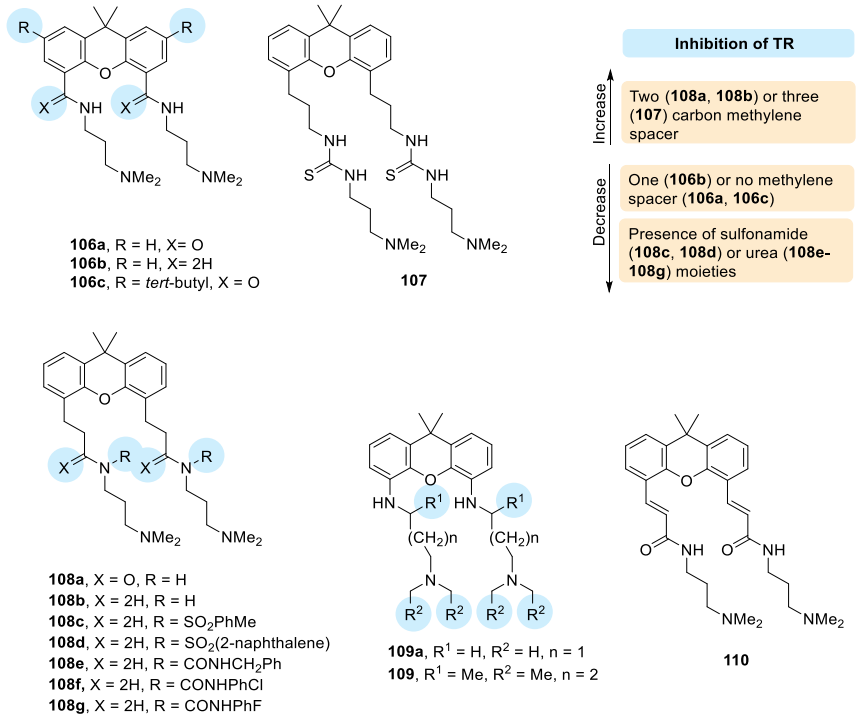

Figure 16. Putative structure-activity relationship analysis on the TR inhibition of 9,9-dimethylxanthene derivatives **106**-**110**.

Wu *et al*. [42] prepared a small series of 9*H*-xanthene derivatives and evaluated their intrinsic antimalarial activity against a CQ-sensitive (CQS) strain D10 and a CQ-resistant (CQR) strain of *Plasmodium falciparum*, along with their cytotoxicity. Among the series, compound **111** (**Figure 17**) showed relatively high intrinsic antimalarial activity; however, its mechanism of action may differ to that of CQ since it was observed in the CQR strain. Additionally, **111** showed the highest synergistic effect, with a response modification index of 0.36, and caused a four-fold increase in chloroquine accumulation in a resistant strain of *P. falciparum*. The highest selective therapeutic index obtained when **112** was tested against a mammalian cell line signifying a positive selectivity where the drug is more toxic to the malaria parasite than it is to the mammalian cells.

In another study on the antimalarial activity of xanthene derivatives with a dispiro-β-lactam moiety, good to excellent activities were obtained against CQ-resistant *P. falciparum* K14 strain, with the most promising compound (**112**, **Figure 17**) presenting a low toxicity up to 100 µM whatever the considered cells (HEL, VERO, or HeLa) [87]. Under the scope of the same study, compounds were also evaluated for their antimicrobial and antiviral activities, with no significant results**.**

As a result of the high metabolic rate of the rapidly multiplying parasite, large quantities of toxic redox-active by-products are generated. Hence, *P. falciparum* requires a highly efficient thiol metabolism to protect themself from intracellular ROS. This implies a highly susceptibility to oxidative stress, which can be explored as a promising therapeutic approach against malaria [88, 89]. The inhibition of human glutathione reductase (hGR) would lead to an increase of oxidative stress in human erythrocytes offering partial protection against the infection. In a study for the identification of hGR inhibitors, Savvides *et al*. [90] identified 6-hydroxy-3-oxo-3*H*-xanthene-9-propionic acid (**113**, **Figure 17**) as a noncompetitive inhibitor of human glutathione reductase (hGR). Crystallographic analysis revealed that compound **113** bound in the large cavity present at the hGR dimer interface where it does not overlap the glutathione binding site. Compound **113** showed an inhibition potency 16 times higher than dye 3,7-diamino-2,8-dimethyl-5-phenyl-phenazinium chloride (safranin), a previously reported noncompetitive inhibitor of hGR (binding affinity to the enzyme-substrate complex (K_{is}) (oxidized glutathione) = 27 µM and 453 µM, respectively). Further studies would be required to optimize this xanthene derivative and confirm its efficacy and safety against malaria.

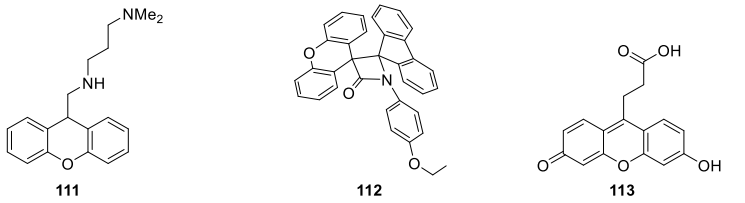

Figure 17. Structures and antimalarial activity of xanthenes **111**-**113**.

1.1.2.3. Anti-inflammatory and analgesic activities

The anti-inflammatory activity of 9-aryl-9*H*-xanthene-3,6-diol derivatives **114a**-**114f** (**Figure 18**) was assessed using the carrageenan-induced rat paw edema in mice along with estimation of gastric ulcerogenicity index [91]. Generally, a significant anti-inflammatory activity was observed at second phase (180-360 min) at 30, 60, and 90 mg/kg dose p.o. (*per os*), indicating that these compounds exhibit their effect through the prostaglandin mediated mechanism. Compounds **114e** and **114f** showed comparable activity to standard drugs. The ulcerogenic liabilities of compounds **114a**-**114f** were either absent or less than that of the standard drug indomethacin at all the graded doses. Further studies on the analgesic activity were developed using the acetic acid induced writhing test and the formalin induced model, with compounds **114a**, **114d**, **114e**, and **114f** exhibiting significant activity. The higher analgesic activity was presented by **114e** with percentage inhibition values of 64.50 % (100 mg/kg) and 67.14 % (150 mg/kg), higher than the control aspirin. In this study it was also disclosed that 9-aryl-9*H*-xanthene-3,6-diol derivatives (**114a-114f**) contain an active analgesic principle acting peripherally and not through CNS as shown by indomethacin and pentazocine [92].

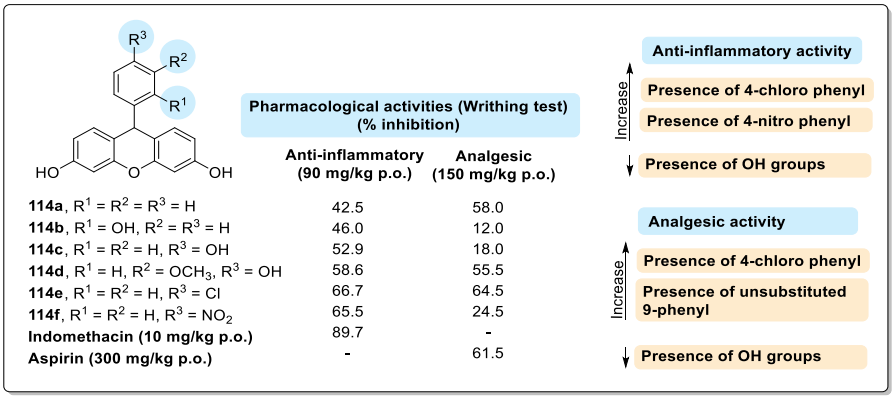

Figure 18. Structure-activity relationship analysis on the anti-inflammatory and analgesic activities of 9-aryl-9*H*-xanthene-3,6-diol derivatives **114a**-**114f**.

The carrageenan induced paw edema method was also the method of choice for the evaluation of the anti-inflammatory activity of a series of spiro-xanthene-9',2-(1,3,4)thiadiazole derivatives **115a**-**115e**, using an oral dose of 70 mg/kg body weight. Anti-inflammatory and analgesic activities of the test compounds were measured with respect to a control (placebo) and compared with respect to the standard drug, ibuprofen, in the same dosage (**Figure 19**) [92]. The tested derivatives exhibited significant activity when compared to the standard drug, ranging from 76-84 % after 4 h. The presence of a 4-nitrophenyl group at position 3 and acetyl group at position 5 showed the maximum activity (**115e**, 84 %), and substitution of the nitro group by a chlorine (**115d**) did not significantly affect the anti-inflammatory activity (82 %). On the other hand, a slightly decrease in the activity was observed when the nitro group is replaced by a hydrogen (**115b**) or a bromine (**115c**) (79 % and 76 %, respectively). Additionally, the analgesic activity was tested for derivatives that presented anti-inflammatory activity higher than 80 %. The best results were obtained with the presence of two phenyl groups (**115a**) or the presence of a 4-chlorophenyl group at the position 3 (**115d**). Further studies on the toxicity of these derivatives revealed that neither death nor other behavioral or toxicological changes were observed on rats up to a dose as high as 200 mg/kg [92].

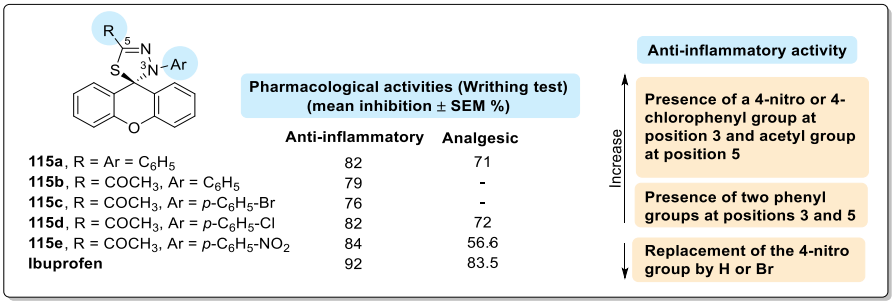

Figure 19. Structure-activity relationship analysis on the anti-inflammatory and analgesic activities of spiro-xanthene-9',2-(1,3,4)thiadiazole derivatives **115a**-**115e**.

Chemokines are proinflammatory molecules implicated in the recruitment and activation of leukocytes in various diseases. Among them, MIP-1α (macrophage inflammatory protein-1α) known as a ligand for CC-type chemokine receptor 1 (CCR1) receptors, may play an important role in chronic inflammatory diseases such as rheumatoid arthritis and multiple sclerosis [93]. In a work to elucidate the pathophysiological role of CCR1 receptors in murine models of disease, Naya *et al.* [94] identified xanthene-9-carboxamide **116a** with an IC_{50} value of 510 nM for human CCR1 (hCCR1) receptors as a lead compound. Optimization of **116a**

was initiated by substituting the *n*-pentyl group on the piperidine nitrogen with cycloalkyl or arylmethyl groups. Replacement with a cyclooctyl (**116b**) or a cyclohexyl (**116c**) group resulted in improvement of the binding affinities for hCCR1 receptors, especially in the case of **116b,** which showed approximately 3-fold higher binding affinity compared with **116a**. By contrast, replacement with cyclodecanyl (**116d**) and aromatic groups, namely benzyl (**116e**) and 2-naphthyl (**116f**), led to a substantial decrease in affinity. Afterwards, the tertiary pyridine nitrogen was replaced by a quaternary ammonium group, with compound **117a** showing an enhanced binding affinity (IC_{50} = 14 nM). Further modifications led to compound **117b**, where the quaternary ammonium group is linked to a 1-cyclooctenyl and an ethyl group (IC_{50} value of 2.0 nM). Finally, introduction of chlorine at positions 2 and 7 of the xanthene moiety further improved potency (IC_{50} = 1.2 nM, compound **117c**). These results are summarized in **Figure 20**.

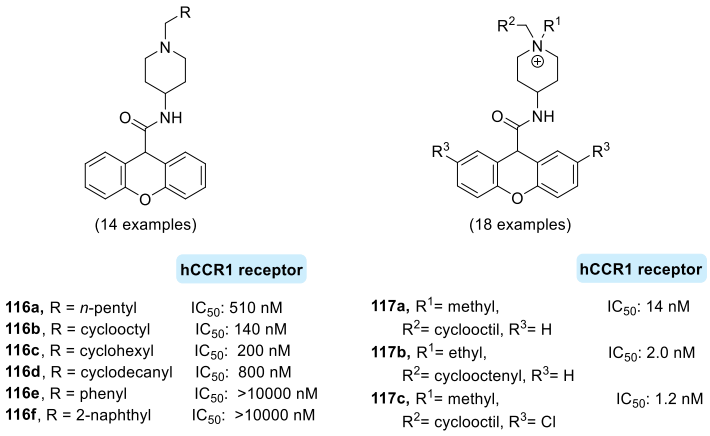

Figure 20. Structures and activity on hCCR1 receptors of xanthenes **116-117**.

1.1.2.4. Antidiabetic activity

Kwon *et al.* [95] explored *x*anthene derivatives **118a** and **118b** (**Figure 21**) as 5' adenosine monophosphate -activated protein kinase (AMPK) activators. AMPK is an is an energy-sensing enzyme whose activation elicits insulin-sensitizing effects, making it an ideal therapeutic target for type 2 diabetes [96]. Xanthene compounds were chosen due to the similarity with mangiferin, a xanthone secondary metabolite used as supplement to treat diabetes in Southeast Asia [97]. *In vitro* studies of compounds **118a-b** in L6 myotubes showed an EC_{50} value for the phosphorylation of AMPK of approximately 1.5 µM, about 6,000-fold less than metformin (EC_{50} = 10 mM). Additionally, *in vivo* studies in high-fat diet-induced diabetic mice showed that the administration of 3 mg/kg produced similar improvements in glucose tolerance to administration of 50 mg/kg of metformin; thus, the experimental

dosages of **118a** and **118b** were about 16-fold lower than metformin, motivating further studies for their exploitation as potential candidates for the treatment of type 2 diabetes mellitus.

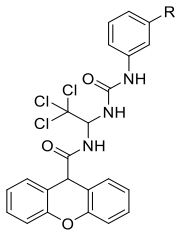

118a, $R^1 = NO_2$
118b, $R^1 = CN$

Figure 21. Xanthene derivatives with antidiabetic activity.

1.1.2.5. Antioxidant activity

Evaluation of the antioxidant activities of 9*H*-xanthene-2,7-diols **119a**–**e** (**Figure 22**), in the autoxidation of tetralin and linoleic acid, in a homogeneous solution and in an aqueous micelle dispersion [98, 99], showed that these act as hydrogen donors and suppress the oxidation of tetralin and linoleic acid. Following these results, the same authors assessed the antioxidant activities of the same compounds **119a-e**, **120b-c**, and **121b-c** upon the oxidation of soybean phosphatidylcholine liposomal membranes, induced by 2,2‘-azobis(2-amidinopropane) dihydrochloride and 2,2‘-azobis(2,4-dimethylvaleronitrile) [100]. The authors found that the referred activity depend not only on the initial hydrogen abstraction from the xanthene, but also on a second hydrogen abstraction from the residual phenolic group of the oxidation product. Further work concerning the introduction of butylated hydroxytoluene (BHT) or catechol into the 9-position of the 9*H*-xanthene-2,7-diols disclosed that **119e**, **122a-c**, and **123a-c** behaved as better chain breaking antioxidants for the autoxidation of tetralin than BHT and catechol [101].

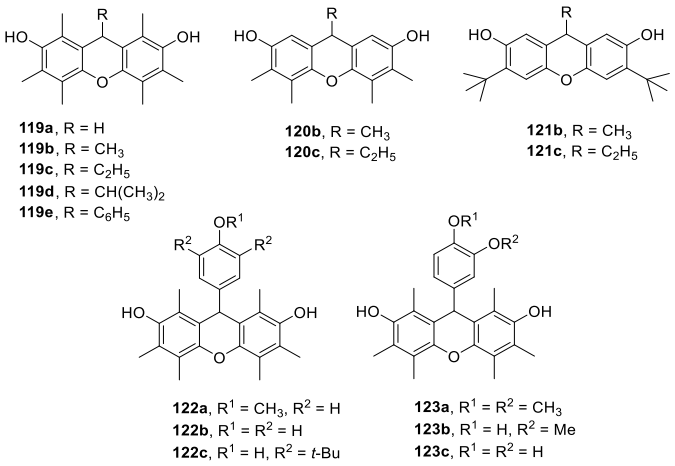

Figure 22. 9*H*-Xanthene-2,7-diols **119**-**123** with antioxidant activity.

In order to shed some light on the mechanism of action of benzo[kl]xanthene lignans **124** and **125** (**Figure 23**) as bio-antioxidants, their capacity to scavenge free radicals (antiradical activity) and to inhibit lipid oxidation processes was assessed by applying different methods: radical scavenging activity by 2,2-diphenyl-1-picrylhydrazyl (DPPH) rapid test, chain-breaking antioxidant activity, and quantum chemical calculations [102]. Compound **125** demonstrated the strongest activity in all methods applied. Concerning radical scavenging activity, DPPH• method gives information about the H-atom donating capacity of the studied compounds and some preliminary information about the possibility of using these compounds as antioxidants. Although **124** and **125** were found to be active as DPPH• scavengers, a strong influence was noticed when different reaction times and concentrations were tested. When compared with standard antioxidants DL-α-tocopherol (TOH), caffeic acid (CA) and BHT, the following order of maximum radical scavenging activity was disclosed: TOH (61.1 %) > CA (58.6 %) > **125** (28.1 %) > **124** (3.6 %) = BHT (3.6 %). Additionally, it was found that the catechol structure present in these compounds plays an important role in the chain-breaking antioxidant activity.

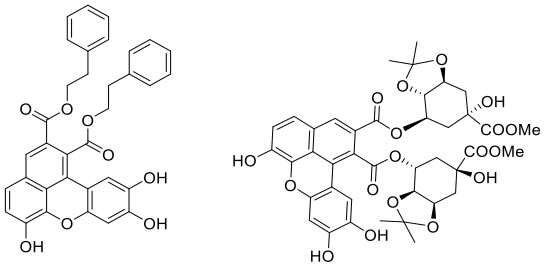

Figure 23. Benzo[kl]xanthene lignans **124** and **125** with antioxidant properties.

In a study developed by Ilangovan *et al*. [103] concerning the synthesis, DNA-binding study, and antioxidant activity of 14-aryl-14*H*-dibenzo[*a,j*]xanthene derivatives, it was found that **126a-e** (**Figure 24**) exhibited free radical scavenging activity against DPPH and 2,2'-azino-bis-3-ethylbenzothiazoline-6-sulfonic acid (ABTS) cationic radical. Substitution with 3-methoxyl and 4-hydroxyl in the phenyl ring was found to be beneficial to the antioxidant activity since among the five studied compounds, **126d** proved to be more effective inhibitor against both DPPH (86.78 %) as well as $ABTS^{+}$ (83.32 %). Furthermore, a SAR study exposed that the compounds substituted with free –OH group acted as better scavengers when compared to compounds with a protected –OH group.

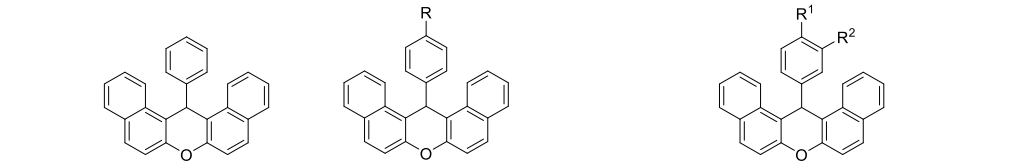

	126a	**126b**, R = OMe	**126c**, R = OH	**126d**, R^1 = OH, R^2 = OMe	**126e**, R^1 = OMe, R^2 = OMe
DPPH	31.05 %	47.13 %	53.08 %	86.78 %	52.64 %
ABTS	63.55 %	67.46 %	73.19 %	83.13 %	70.78 %

Figure 24. DPPH and ABTS radical scavenging activity compared with BHT (concentration of 250 µg mL^{-1}) of 14-aryl-14*H*-dibenzo[a,j]xanthene derivatives **126a**-**e**.

1.1.2.6. Antipsychotic activity

Antipsychotic (neuroleptic) activity can be associated with thioxanthenes, which are structurally related to phenothiazines, and act by suppressing the effect of dopamine in the brain in the treatment of schizophrenia. Other structurally related xanthenes have also been assessed for their antipsychotic activity, particularly chlorpromazine analogs of the diphenylmethane type [104]. Compounds **127**-**139** or the corresponding salts (HCl, 2HCl, citrate, maleate, or dimaleate) were investigated in several pharmacological tests with aminoalkyl derivative **136** (**Figure 25**) being nearly equipotent with chlorpromazine and, interestingly, xanthene **131** revealed to be even more potent than chlorpromazine in several animal tests in which many neuroleptic agents are active.

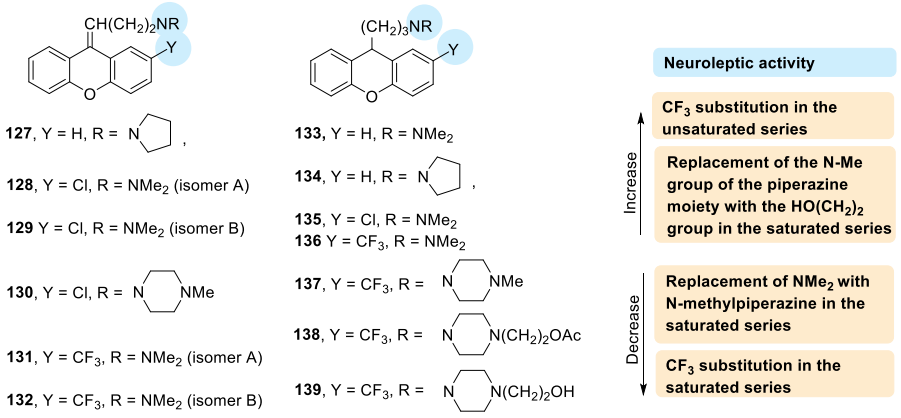

Figure 25. Structure-activity relationship on the neuroleptic activity of xanthene derivatives **127-139**.

1.1.3. Final remarks: highlights on synthesis and drug-like properties analysis

Xanthenes represent an important scaffold in Medicinal Chemistry and their synthesis and biological activity are being extensive explored. Concerning synthesis, one strategy commonly used is the one-step conjugation of simple building blocks, namely phenols, aldehydes, and benzynes intermediates, allowing to obtain the respective derivatives in good yields. However, these methodologies have a limited versatility, and few derivatives are obtained from each technique, being from a Medicinal Chemistry perspective an important limitation. A more straightforward and frequently used procedure to obtain xanthenes is starting from xanthones. Xanthone is a widely explored scaffold and several derivatives are commercially available at competitive prices. Further modification and functionalization of aromatic rings are also widely explored and described by several authors. Through standard and simple procedures, the carbonyl in position 9 in easily converted into different function groups, namely alkyl, alcohol, or carboxylic acid.

Further modifications in position 9 could be performed through diverse techniques. In what concerns to 9*H*-xanthene, the development of electrochemical procedures for the conjugation of xanthene with several nucleophiles are herein highlighted, considering their metal-free protocol and improved yields. Additionally, the recently disclosed methodology of cross-dehydrogenative coupling (CDC) employing acidic carbon dots surface as visible-light induced photocatalyst also represents a green methodology for the conjugation of xanthene's position 9 with ketones, 1,3-dicarbonyls and arenes. Considering xanthydrol, the simplest methodology used to obtain derivatives is taking advantage of its reactivity through the formation of the xanthylium ion, and reaction with several nucleophiles through S_N1 reaction. Among the catalysts described, the application of acetic acid and the ionic liquid of 1-butyl-3-methylimidazolium tetrafluoroborate ($BmimBF_4$) represents the greener approaches. Xanthene-9-carboxylic acid derivatives can be easily obtained by exploring the

reactivity of the carboxyl functional group. Application of coupling agents such as CDI, formation of acyl chlorides, or esterification under Fischer–Speier conditions showed to be appropriate to obtain the corresponding derivatives. Lastly, the synthesis of the lead aminooxazoline **65** from an exomethylene shows the potential of 9-alkyl xanthenes to obtain interesting compounds with drug-like properties. Of potential interest are also azaxanthones, whose bioisosteric introduction of a nitrogen atom confers a more drug-like scaffold to the compound. The syntheses described so far can vary, especially in the starting materials. The most used method is through the reduction of the respective azaxanthone, which can be achieved using metals. However, other methods that did not involve the synthesis of a xanthone intermediate were proposed, such as the use of Mannich bases as starting material, and the use of a pyridine derivative which, upon reaction with an aldehyde, originated a diaryl alcohol intermediate, ultimately leading to the desired azaxanthene.

Concerning the biological applications, the xanthene nucleus showed to be versatile and suitable towards obtaining compounds for different biological targets. As expected, the substitution pattern of the xanthene core will define the capability to interact with specific targets and lead to the respective pharmacological response. Additionally, another essential aspect to be considered is the drug-likeness of the compounds developed, which should present appropriate absorption, distribution, metabolism, excretion – toxicity (ADMET) properties to allow its progression from pre-clinical assessment to clinical evaluation. Therefore, a closer look regarding the drug-likeness of the most potent molecules in each biological activity described was performed in this review. To complement the information disclosed in the literature, their PK parameters were assessed herein employing the SwissADME platform [105]. Hence, a representative example of each series of compounds was analyzed with this *in silico* tool regarding their BBB permeation, P-gp efflux, Lipinski's rules violations, pan-assay interference compounds (PAINS) alerts, inhibition of cytochrome P450 (CYP450) (1A2, 2C19, 2C9, 2D6, 3A4) and estimated solubility (ESOL) class and considerations were performed in accordance with the information gathered. Thirty-two molecules were assessed, and detailed results are provided in **Table 1**. Among them, 9 were found to be BBB permeant and 11 indicated not to be substrates of P-gp efflux pump. Eighteen violate at least one Lipinski's rule and 28 violate at least one leadlikeness rule. Twenty-eight inhibit at least one of the CYP enzymes studied, wherein 19 inhibit CYP3A4, the most abundant isoform and responsible for the metabolization of approximately half of the drugs in the liver [106]. Eighteen compounds revealed high gastrointestinal absorption (GI) and 27 revealed a favorable bioavailability score (>0.55). Finally, compound **79** displayed PAINS alerts. Concerning synthetic accessibility, favorable results (scores ≤5) were obtained for all the lead compounds assessed, with the exception of compound **68** (score of 6). A common drawback of hit compounds, for instance **67**, **73**

85 and 115e, would be the presence of a stereogenic center on carbon 9, which would require extensive data proving the efficacy and safety of the racemic mixture or the application of asymmetric synthesis or enantiomeric purification and, at late-stage programs, tight quality control to assure enantiomeric purity at release and shelf life.

The xanthene derivatives reported as possessing antitumor activity, in general, present limitations regarding drug-likeness properties. A high number of aromatic rings with few functionalization are observed, making them highly lipophilic compounds with poor solubility in aqueous media. Several compounds do not comply with the Lipinski's rule of five (**75a**, **79**, **83**, **86** and compound **79** gave a PAINS alert. Nonetheless, although compound **86** (rose bengal) showed some unfavorable druglike properties such as being a P-gp substrate, which is accordance with previously described studies [107, 108], properties difficult to compute such as off-target toxicity were already assed experimentally, such selectivity for tumor cells over normal fibroblasts. Additionally, it was already assessed in clinical trials for treating melanoma and is expected to be involved in future studies, indicating no significant founds in term of toxicity and safety. Apart from rose bengal 86) and compound **83**, described as genotoxic, no information is provided regarding bioactive xanthenes selectivity and toxicity over healthy human cells. Xanthenes presented as possessing antioxidant activity present similar drawbacks, with highly lipophilic skeletons, violations to the Lipinski's rule of five (**122c**) and lack of information regarding their *in vivo* activity and safety. Regarding xanthenes with antimicrobial activity, we highlight compounds **101** and **111,** combining both efficacy with no violation to Lipinski's rules and were predicted as soluble in aqueous media (ESOL) [109]. Together with preliminary studies of oral bioavailability (compound **101**) and selective therapeutic index (compound **111**), these seem to be promising compounds for further improvement to lead compounds. Additionally, both are symmetric molecules and, therefore, do not display the limitations of the presence of a stereogenic center at position 9.

With anti-inflammatory and analgesic properties, the series of 9-aryl-9*H*-xanthene-3,6-diol derivatives **114a**-**114f** and the series of spiro-xanthene-9',2-(*1,3,4*)thiadiazole derivatives **115a**-**115e** are highlighted. These compounds do not present Lipinski's violations nor PAINS alerts, and *in vivo* studies showed efficacy comparable with golden standards with no safety issues in terms of ulcerogenic liabilities or toxicological changes in animal models. Compounds **118a** and **118b** showed similar results *in vivo* studies in high-fat diet-induced diabetic mice concerning glucose tolerance. However, the computation prediction analysis shower higher solubility and gastrointestinal absorption for compound **118b**, indicating a potential advantage of the compound over **118a** in what concerns to PK parameters. Regarding 9*H*-xanthene-carbonyl carbamates acting as mGlu1 enhancers, the series containing a tetrazole ring (**71**) represents the one with favorable PK properties already

characterized experimentally, namely oral availability, brain penetration, volume distribution, and half-life. Lastly, the xanthenes pointed out as neuroprotectors, despite the computational prediction indication of no BBB permeation and P-gp recognition, already showed optimized drug-likeness and PK properties in *in vivo* studies. The BACE1 inhibitor **66** was designed considering the necessity to avoid the hERG affinity (identified in the lead compound) but maintaining low TPSA to avoid P-gp recognition and efflux. The optimized lead compound **66** successfully complied with these specific requisites as confirmed with *in vivo* assays, which showed appropriate CNS penetration and no significant impact on the QTc interval, while maintaining its activity as potent BACE1 inhibitor. Nonetheless, a lack of selectivity over CatD impose further modifications. This drawback was successfully overcome with the design and synthesis of compound **67**; unluckily, safety concerns regarding hERG affinity were found again, enforcing new studies to correctly balance compound's affinity for BACE1 and off-targets.

Table 1. Pharmacokinetic properties prediction for a representative example of each series of compounds. Analysis performed with the SwissADME platform [105].

Compound	BBB permeant [a]	Pgp substrate [b]	CYP1A2 inhibitor [c]	CYP2C19 inhibitor [d]	CYP2C9 inhibitor [e]	CYP2D6 inhibitor [f]	CYP3A4 inhibitor [g]	Lipinski #violations [h]	Bioavailability Score [i]	PAINS #alerts [j]	Leadlikeness #violations [k]	MW [l]	TPSA [m]	Consensus Log P [n]	ESOL Class [o]	GI absorption [p]	Synthetic Accessibility [q]
66	No	Yes	Yes	Yes	Yes	No	Yes	0	0.55	0	1	448.42	91.85	3.43	Moderately soluble	High	5.12
67	No	Yes	No	Yes	Yes	Yes	Yes	0	0.55	0	1	489.91	120.95	2.66	Moderately soluble	High	5.12
68	No	Yes	No	Yes	No	Yes	Yes	0	0.55	0	2	468.59	114.90	3.73	Moderately soluble	High	5.61
72	No	Yes	Yes	Yes	Yes	Yes	Yes	0	0.55	0	2	360.29	64.36	3.68	Moderately soluble	High	3.54
73	Yes	Yes	No	Yes	Yes	Yes	Yes	0	0.55	0	2	403.47	59.00	4.03	Moderately soluble	High	3.80
75a	No	No	Yes	No	No	No	Yes	1	0.55	0	2	490.52	67.43	5.45	Poorly soluble	High	3.83
79	No	No	No	Yes	No	No	No	1	0.55	1	3	562.57	122.52	5.39	Poorly soluble	Low	4.37
83	No	Yes	Yes	No	No	Yes	No	1	0.55	0	2	411.54	21.70	5.75	Poorly soluble	High	3.82
85	Yes	No	No	Yes	Yes	No	Yes	0	0.55	0	1	382.41	60.44	3.67	Moderately soluble	High	4.79
86	No	Yes	No	No	No	No	No	2	0.17	0	2	1017.64	65.74	6.37	Insoluble	Low	3.82
88b	No	Yes	Yes	Yes	No	No	No	1	0.55	0	2	396.87	34.48	5.65	Poorly soluble	Low	3.79
88c	No	Yes	Yes	Yes	No	No	Yes	1	0.55	0	2	404.50	24.83	5.70	Poorly soluble	Low	3.97
101	Yes	No	No	Yes	Yes	Yes	Yes	0	0.55	0	0	338.40	49.85	2.71	Soluble	High	2.94
102	No	No	Yes	Yes	No	No	No	1	0.55	0	2	403.43	55.05	5.57	Poorly soluble	Low	3.65
108a	Yes	Yes	No	Yes	No	Yes	Yes	1	0.55	0	3	518.69	73.91	4.28	Moderately soluble	High	4.64
111	Yes	Yes	No	No	No	Yes	Yes	0	0.55	0	0	296.41	24.50	3.32	Soluble	High	3.46
112	No	No	Yes	Yes	Yes	No	No	2	0.17	0	2	507.58	38.77	6.32	Poorly soluble	Low	5.22
113	No	No	Yes	No	No	No	No	0	0.56	0	0	284.26	87.74	1.88	Soluble	High	3.15
114e	Yes	Yes	Yes	Yes	No	Yes	Yes	0	0.55	0	1	324.76	49.69	4.12	Moderately soluble	High	3.26
115e	No	No	Yes	Yes	Yes	No	Yes	0	0.55	0	2	417.44	113.02	3.44	Moderately soluble	High	4.72
117c	No	Yes	No	No	No	No	No	1	0.55	0	2	516.52	38.33	4.77	Poorly soluble	Low	4.44
118a	No	No	Yes	Yes	Yes	No	Yes	1	0.55	0	3	535.76	125.28	3.46	Poorly soluble	Low	4.37
118b	No	Yes	Yes	Yes	Yes	Yes	Yes	1	0.55	0	3	515.78	103.25	4.03	Moderately soluble	High	4.18
122	No	Yes	No	No	No	No	No	2	0.17	0	2	502.68	69.92	7.51	Poorly soluble	Low	5.00
126d	No	No	Yes	Yes	No	No	No	1	0.55	0	2	404.46	38.69	5.74	Poorly soluble	Low	3.86
131	No	No	Yes	Yes	No	Yes	No	1	0.55	0	1	333.35	12.47	4.81	Moderately soluble	Low	3.33

[a] Brain permeation. According to the yolk of the BOILED-Egg [110]; [b] Support vector machine algorithm (SVM)[111] built on 1033 molecules (training set) and tested o 415 molecules (test set); [c] SVM model built on 9145 molecules (training set) and tested on 3000 molecules (test set); [d] SVM model built on 9272 molecules (training set) and tested on 3000 molecules (test set); [e] SVM model built on 5940 molecules (training set) and tested on 2075 molecules (test set); [f] SVM model built on 3664 molecules (training set) and tested on 1068 molecules (test set); [g] SVM model built on 7518 molecules (training set) and tested on 2579 molecules (test set); [h] Implemented from [112]; [i] Probability of F > 10% in rat. Implemented from [113]; [j] Implemented from [114]; [k] Implemented from [115]; [l] Molecular weight. Calculated from [116]; [m] Topological polar surface area. Calculated from [117]; [n] Average of five predicted models: XLOGP3 [118], WLOGP [119], MLOGP [120, 121], SILICOS-IT [122]and iLOGP [123]; [o] Estimated aqueous solubility. Topological method implemented from [109]; [p] Gastrointestinal absorption. According to the white of the BOILED-Egg [110]; [q] From 1 (very easy) to 10 (very difficult). Calculation method developed by SwissADME [105].

1.2. Aims of the thesis and work plan

The main goal of this thesis was to obtain novel xanthene and benzhydryl derivatives with potential biological applications, namely as anti-infectious and neuroprotective agents.

The specific goals of this thesis were:

i) to synthesize structurally diverse xanthene and benzhydryl compounds using feasible synthetic methods with scale-up potential from affordable starting materials;

ii) to enhance the drug-likeness of the compounds by further functionalization;

iii) to evaluate the biological activity of the compounds obtained through diverse *in vitro* and *in vivo* assays, as potential anti-infectious (antibacterial and antiparasitic) and neuroprotective agents.

Chapter 2. – Synthesis and biological activity of 9-hydroxyxanthene derivatives

Original research work submitted to *Drugs and Drug Candidates* in October 2022

Candidate contribution: synthesis and structural characterization of the 9-hydroxyxanthene acid derivatives herein described; discussion of the results obtained in the biological activity assessment.

Graphical abstract:

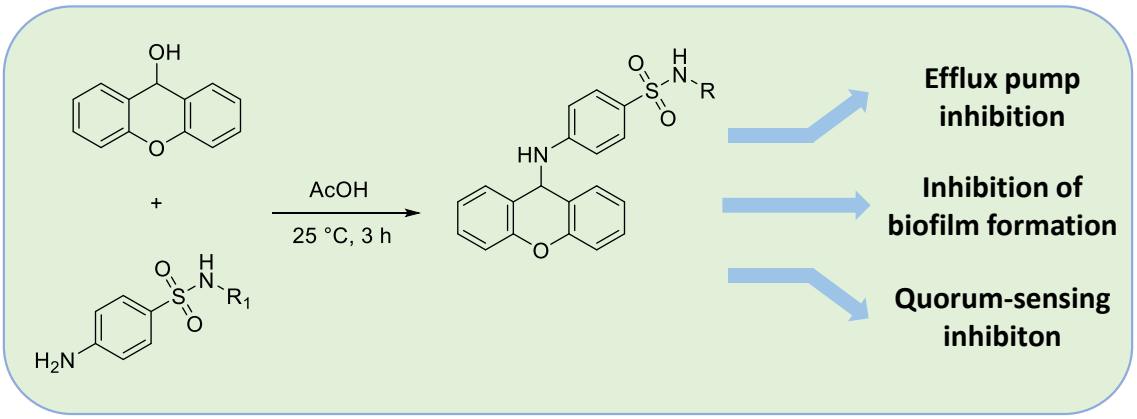

2.1. Introduction

Antimicrobial resistance has become a major threat to global health, enhanced by the decreasing effectiveness of antibacterial agents due to their wide use in both human and veterinary. Currently, multidrug resistant (MDR) bacteria in nosocomial and health-care-acquired infections are widespread and responsible for more than 700,000 deaths each year and growing to 10 million by 2050 [124-126]. Regarding the mechanisms of antimicrobial resistance in bacteria, the formation of biofilm plays a central role, allowing its survival even in the presence of antibiotics and other adverse environmental conditions. For instance, in the field of biomedical implants, a worldwide increasing clinical procedure, biofilms are responsible for the persistence of implant infections and are a source of bacterial dissemination to other body sites and eventually to systemic and fatal infections [127, 128]. One of the processes that regulates the formation of biofilms is quorum sensing (QS), a bacterial cell-cell communication process that involves the production, detection, and response to extracellular signaling molecules called autoinducers. The contribution of QS to biofilm formation, as well as bacteriocin production and virulence, reveals its importance to bacterial pathogenesis [129-131]. These phenomena are intrinsically connected to efflux pumps [132], whose overexpression contributes not only to the potentiation of these mechanisms, but also to increase transport of antibiotics and antiseptics outward the bacterial cell. In fact, efflux pumps can increase the efflux of QS molecules, such as acyl-homoserine lactones (AHL), as well as extracellular polymeric substances for biofilm formation, and regulate biofilm genes and promote bacterial aggregation [133]. Hence, the identification of new agents capable to overtaking these mechanisms of antimicrobial resistance would represent a novel and important strategy to fight multidrug resistance strains.

Xanthenes (**140**, **Figure 26**) are a class of oxygen-incorporating tricyclic compounds which have been explored for different biological applications, where the presence of different substituents in position 9 impacts their chemical properties and bioactivity [134]. Several studies have shown their potential as antibacterial agents, where xanthenes revealed moderate to good inhibition in Gram-positive and Gram-negative bacteria [33, 80, 135-138]. Additionally, the tricyclic nucleus of xanthenes possesses electronic and geometrical similarities with phenothiazines, thioxanthones and thioxanthenes, classes of compounds known for their activity in inhibiting biological processes responsible for antimicrobial resistance, namely QS [139, 140] and efflux pump activity [140-144] . Sulfonamides (**141**, **Figure 26**) represent another important class of therapeutic agents in medicine. After their discovery as potent antimicrobial agents for systemic infections in humans [145, 146], sulfonamides were further derivatized to find compounds with different biological

applications. This strategy led to the development of compounds with diuretic activity [147], hypoglycemic [148], anticonvulsant [149], anticancer [150] and antiviral [151]. Hence, in this work we focus on the synthesis of xanthene sulfonamide derivatives aiming to explore their activity against bacterial resistance mechanisms. The compounds obtained were fully characterized and evaluated regarding their minimum inhibitory concentration (MIC) on Gram-positive and Gram-negative strains, efflux pump inhibition (EPI) activity, influence on biofilm formation, and quorum-sensing (QS) inhibition.

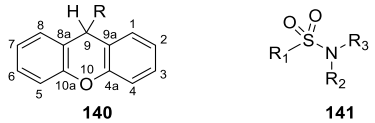

140 **141**

Figure 26. Structure of xanthene (**140**) and sulfonamide (**141**) derivatives

2.2. Synthesis of 9-xanthenyl derivatives

The desired 9-xanthenyl derivatives were obtained following a previously reported procedure describing the condensation of benzenoid sulfonamides with xanthydrol [152]. The solubilization of xanthydrol in glacial acetic acid allows the formation of the xanthylium ion. Then, the nucleophilic attack by an electron pair from a molecule of relatively high electron density leads to the substitution product (**Scheme 14**, A) [32]. The synthesis of a xanthene derivative possessing an aniline in position 9 (**MM7**) was also performed for structure-activity relationship purposes. When using an aniline nucleophile, due to the activating influence of the amine, the electrophilic aromatic substitution at the *para* position of the aromatic ring with the xanthenyl group was observed (**Scheme 14**, B) [153]. To the best of our knowledge, this is the first time that these compounds are fully characterized and explored against mechanisms of bacterial resistance. **Figure 27** depicts the Oak Ridge Thermal Ellipsoid Plot (ORTEP) view of the crystal structure of xanthenyl sulfonamides **MM16** (A), **MM17** (B) and **MM18** (C) and **MM7** (D). Further details regarding characterization data are provided in section ***2.5.*** *Experimental*.

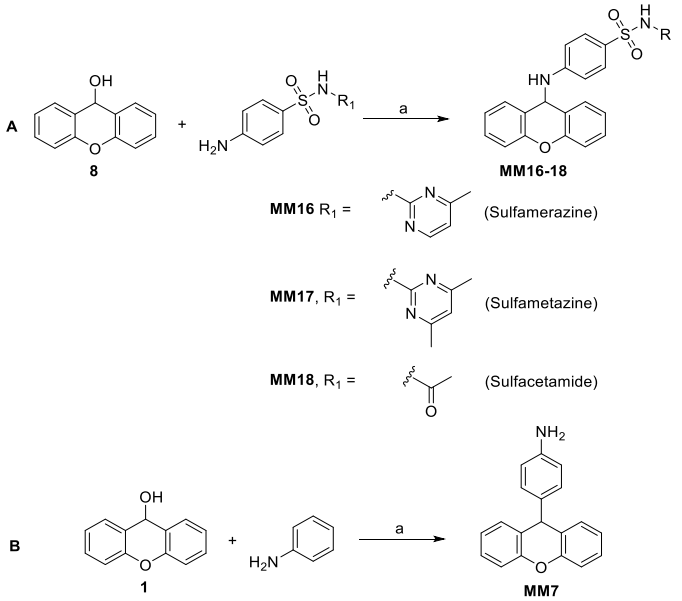

Scheme 14. Synthesis of 9-xanthenyl derivatives **MM7** and **MM16-18**.

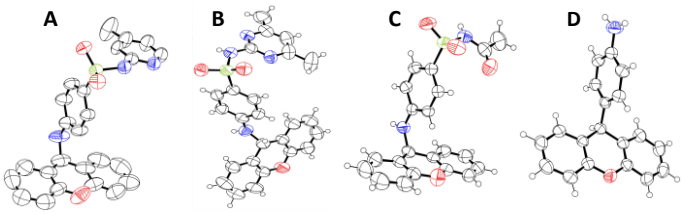

Figure 27. ORTEP view of the crystal structure of xanthenyl sulfonamides **MM16** (A), **MM17** (B) and **MM18** (C) and **MM7** (D).

2.3. Biological activity results and discussion

2.3.1. Minimum inhibitory concentration (MIC)

Firstly, compounds **MM7** and **MM16 – MM18** were evaluated for their antibacterial activity by assessing their minimum inhibitory concentration (MIC) on six different strains of bacteria. The broth microdilution method was used in a 96-well plate and the concentrations tested ranged from 64 µg/mL to 4 µg/mL. It was observed that none of the compounds present antibacterial activity, considering the concentration used and the strains tested. Sulfonamide drugs are important antimicrobial drugs with a broad spectrum of actions, effective against Gram-positive and certain Gram-negative bacteria, such as *Escherichia*

coli, *Klebsiella* sp., *Salmonella* sp., *Shigella* sp. and *Enterobacter* sp. strains. They act as bacteriostatic agents through the competitive inhibition of folic acid synthesis, which prevents the growth and reproduction of bacteria [154, 155]. Structure-activity relationship studies of sulfonamides showed that, in addition to the sulfonamide group attached directly to the benzene ring, the presence of the free aromatic NH_2 group in *the para* position is essential for the activity of sulfonamides [156]. Hence, despite possessing a sulfonamide moiety, the presence of the xanthenyl group in the amine of the sulfonamide drug should be responsible for the absence of bacteriostatic activity of compounds **MM16 – MM18**. Compound **MM7**, not structurally related to sulfonamides, also presents unsatisfactory antibacterial activity.

2.3.2. QS inhibition

The QS inhibitory effect of compounds **MM7** and **MM16 – MM18** was examined against three Gram-negative strains: *Sphingomonas paucimobilis* Ezf 10-17 (EZF) and the sensor *C. violaceum* CV026 (CV026) strains, *Chromobacterium violaceum* wild type 85 (wt85) and *Serratia marcescens* AS-1 [157]. The results are depicted in **Table 2**. It was observed that compounds **MM17** and **MM18** inhibited QS in EZF and sensor CV026 strain, showing a reduction of pigment production of 48 and 41 mm, respectively. Compounds **MM7** and **MM16** showed no activity as QS inhibitors. Previous works reported the QS inhibition activity of phenothiazines and related compounds, namely, promethazine, amitriptyline, and acridine orange [158]. These compounds possess a tricyclic nucleus and a heterogenic substituent at the central ring. Varga *et al*. [139] refers that their tricyclic nucleus, a quasi-planar structure, and electron donor capacity of the conjugated electron system appears to be critical for the inhibition of QS. Nevertheless, the electronic properties of the substituent in position 9 should also play an important role, justifying the different activities found for the compounds explored.

Table 2. Results of the quorum sensing inhibition assay

Compound	Quorum sensing inhibition (mm)		
	S. marcescens	**wt85**	**EZF+CV026**
Promethazine[a]	18 ± 0.8	40 ± 0.1	41 ± 0.5
MM16	0	0	0
MM17	0	0	48 ± 0.1
MM18	0	0	41 ± 0.8
MM7	0	0	0

[a] promethazine was used as a positive control.

2.3.3. Biofilm formation inhibition

Biofilm formation inhibition was performed with the strains *S. aureus* American Type Culture Collection (ATCC) 25923 and methicillin-resistant *S. aureus* 272123, a strain with strong impact in nosocomial infections [127, 128]. The biofilm inhibition, presented in %, is depicted in **Table 3**. It was observed that compounds **MM17** and **MM18** were effective in inhibiting the formation of biofilm on the methicillin-resistant *S. aureus* (MRSA) strain, showing a reduction of 78 and 79 %, respectively. Compounds **MM7** and **MM16** showed a modest activity of biofilm inhibition in this strain. Regarding *S. aureus* ATCC 25923, none of the tested compounds showed significant activity.

Table 3. Percentage of biofilm inhibition of compounds **MM16-MM18** and **MM7**

Compound	Inhibition of biofilm formation (%)	
	***S. aureus* ATCC 25923**	***S. aureus* MRSA 272123**
Reserpine[a]	22.29 ± 5.10	77.62 ± 1.44
MM16	4.49±0.27	18.16±0.27
MM17	1.91 ± 1.74	78.29 ± 9.27
MM18	0.06 ± 0.99	79.22 ± 1.12
MM7	1.80 ± 2.42	16.07 ± 0.72

a) Reserpine was used as a positive control.

2.3.4. Efflux pump inhibition

Lastly, the compounds were evaluated for their ability to inhibit efflux pumps. The assay was performed on the strain *Salmonella enterica* serovar Typhimurium SL1344, with the *acrA* gene deleted (SE03) and *S. aureus* MRSA 272123, by monitoring the intracellular accumulation of the efflux pump substrate ethidium bromide (EB) through the real-time fluorimetry. Reserpine and carbonyl cyanide 3-chlorophenylhydrazone (CCCP) were used as positive controls. As depicted in **Table 4**, compounds **MM7** and **MM16 – MM18** increase the fluorescence in comparison to the positive control, which can be attributed to the inhibition of the efflux of EB in the tested strains. Nonetheless, for compounds **MM16 – MM18** it is observed a high fluorescence value at *t=0* in relation to the positive control, which indicates a potential intrinsic fluorescence of these compounds (**Figure 28** and **Figure 29**). To clarify this matter, the compounds were tested alone in PBS against a solution of EB

and a solution of EB and the compound together (**Figure 30 – Figure 32**). If the compound presents an irregular fluorescence pattern, or if the fluorescence of the compound with EB is higher than the fluorescence of the compound alone, no conclusions can be drawn, as this is a limitation of the assay. The analysis of the graphs of the variation of fluorescence over the course of the assay showed that compounds **MM16 – MM18** displayed an erratic curve in combination with EB, being their effect considered inconclusive. On the other hand, compound **MM7** showed a regular fluorescence pattern (**Figure 28** and **Figure 29**), confirming that the relative fluorescence index (RFI) result obtained with this compound is related with the inhibition of the efflux pump of the bacterial strains tested, which warranted no further fluorescence studies. This compound showed a 5-fold higher RFI value compared with the respective reference standard on strain SE03. These results are in line with previous studies regarding the inhibition of some efflux pumps by phenothiazines and thioxanthenes[141-144]. Additionally, xanthones and thioxanthones - two classes of tricyclic compounds also structurally related to xanthenes - were recently explored as potential efflux pump inhibitors [140, 159, 160]. Once again, the tricyclic nucleus appears to be an important structural characteristic for the activity as efflux pump inhibitors.

Table 4 Efflux pump inhibition assay for compounds **MM7** and **MM16-18.**

Compound	Relative Fluorescence Index (RFI)	
	***S. aureus* MRSA 272123**	**SE03**
MM16	0.63 ± 0.09	2.75 ± 0.11
MM17	0.33 ± 0.04	2.18 ± 0.04
MM18	0.14 ± 0.10	2.94 ± 0.23
MM7	0.14 ± 0.05	1.66 ± 0.01
Res	0.56 ± 0.04	---
CCCP	---	0.34 ± 0.04

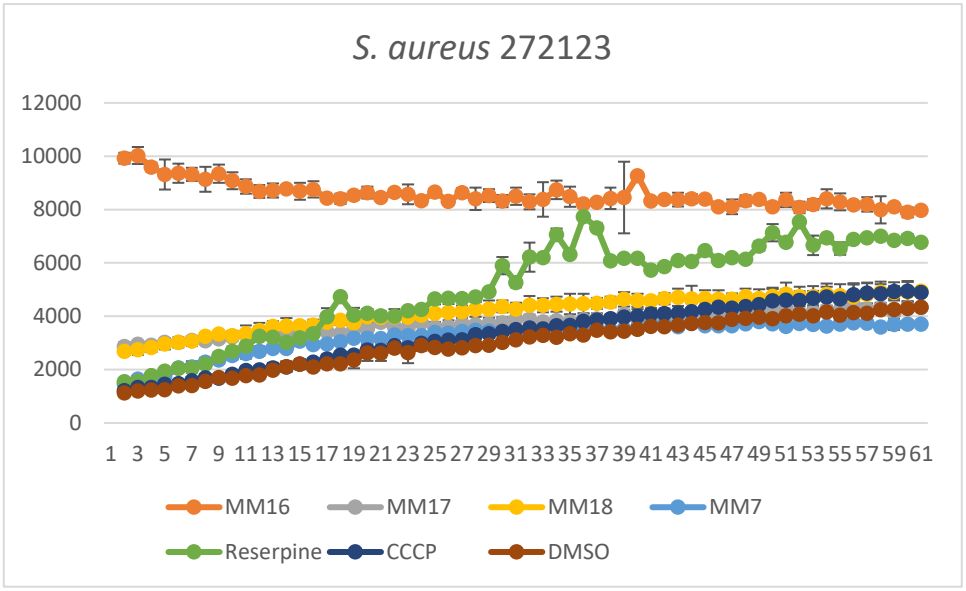

Figure 28. RFI curves of the tested compounds against *S. aureus* 272123.

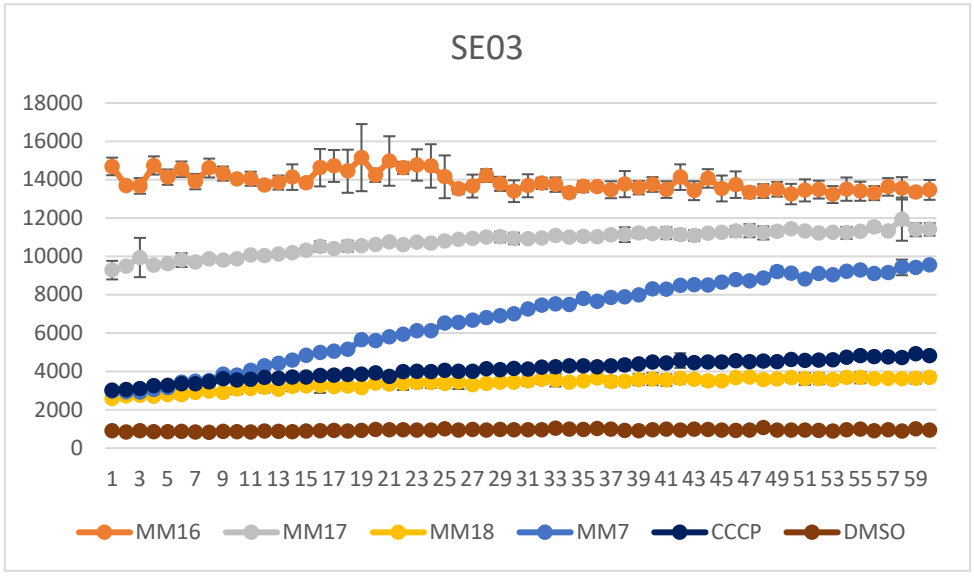

Figure 29. RFI curves of the tested compounds against SE03.

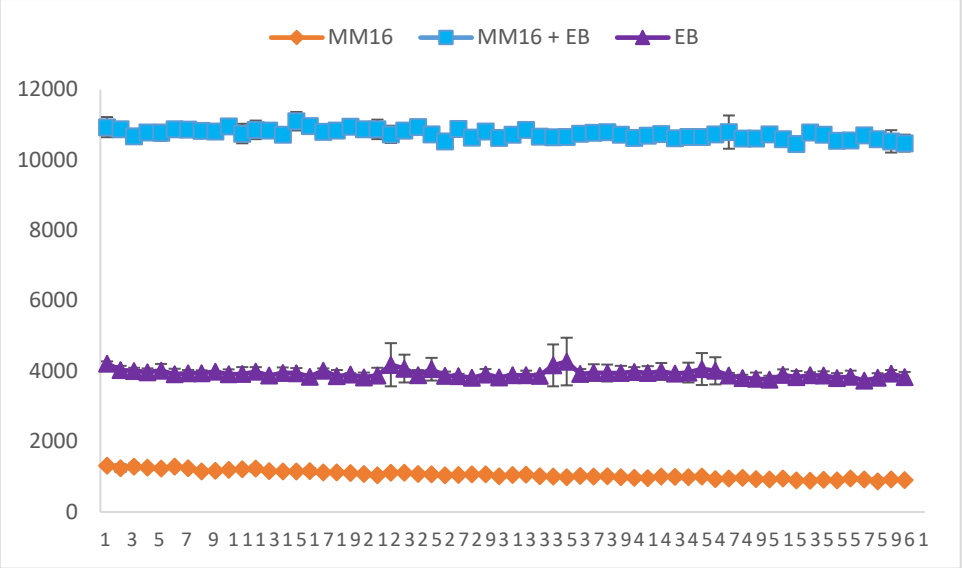

Figure 30. Fluorescence studies of compound **MM16**.

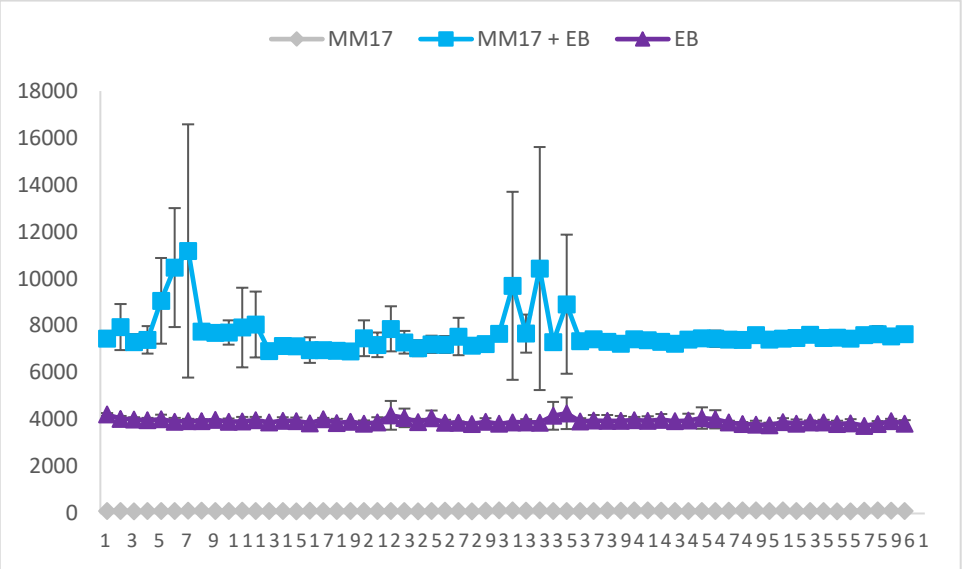

Figure 31. Fluorescence studies of compound **MM17**.

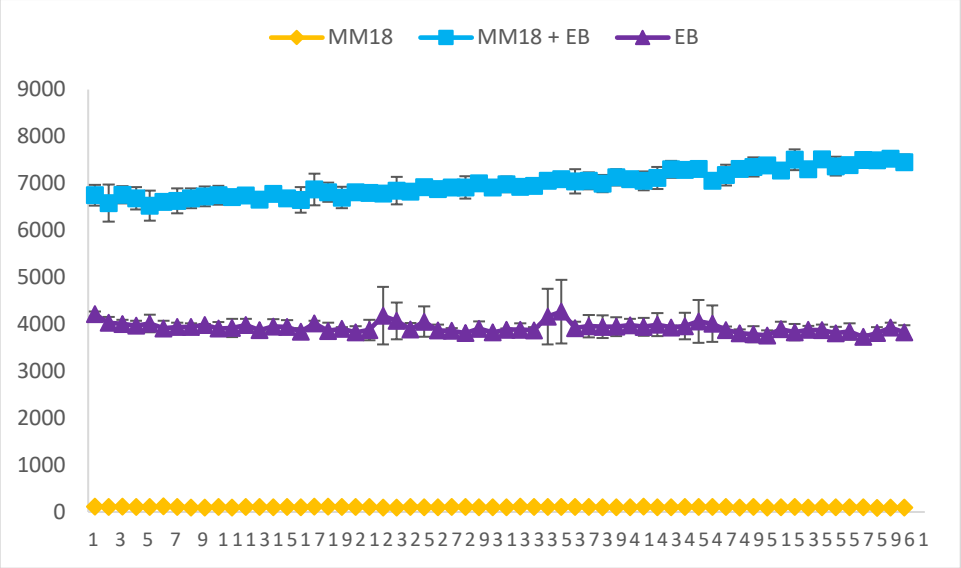

Figure 32. Fluorescence studies of compound **MM18**.

Docking studies were performed for compounds **MM7** and **MM16-18** with the crystal structure of the AcrB (PDB: 4DX5 [161]), and intermolecular interactions were observed between these compounds and the AcrB portion of the AcrAB-TolC efflux system (**Figure 33**). The compounds were predicted to bind in the same sites, with slight variations in the residues they interact with. Compounds **MM16** (**Figure 34**, A and A') and **MM17** (**Figure 34**, B and B') have similar interactions, being able to establish hydrogen interactions between Gln-176, Ser-180, Gln-181, Glu-273, and Asn-274. Compound **MM18** interacts with the residues Ser-48 and Glu-273 (**Figure 34**, C and C'). Interestingly, this compound also interacts with Arg-620 and Tyr-772, present in a different subunit of the efflux pump portion. It is noteworthy that Arg-620 and Gln-176 were previously reported as interaction points with xanthone derivatives in a previous work of our group [159]. Finally, compound **MM7** appears to interact with Leu-177 and Gly-179 (**Figure 34**, D). For compounds **MM16-18**, their capacity to inhibit efflux pumps should be repeated with a different bioassay in which their fluorescent properties have no influence on the results.

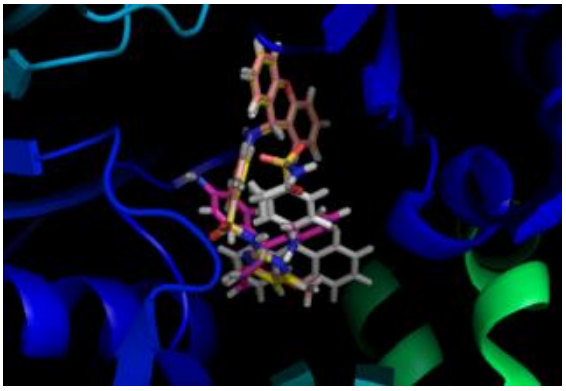

Figure 33. Compounds **MM7** and **MM16-18** in the binding site of the AcrB portion. Crystal structure of the AcrB portion obtained from the Protein Data Bank (PDB: 4DX5 [161])

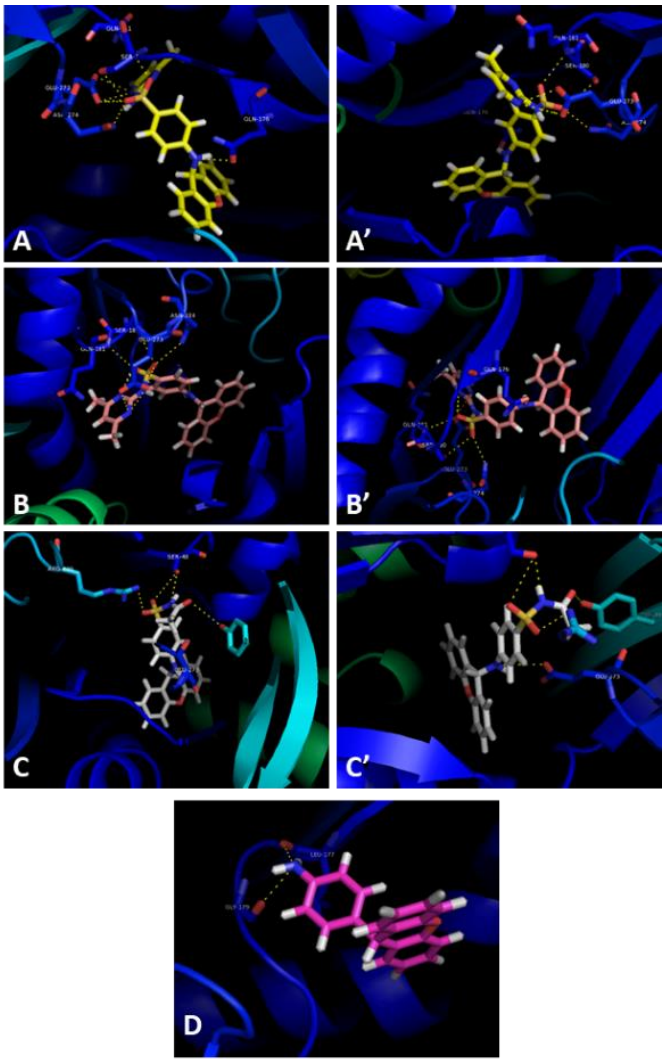

Figure 34. Molecular visualization of compounds **MM16** (A and A'), **MM17** (B and B'), **MM18** (C and C'), and **MM7** (D) A in the AcrB portion of the AcrAB-TolC efflux system. Crystal structure of the AcrB portion obtained from the Protein Data Bank (PDB: 4DX5 [161])

2.4. Conclusion

In summary, four 9-xanthenyl derivatives were synthetized and assessed their antibacterial activity and influence on bacterial mechanisms of resistance, namely, efflux pump inhibition, QS inhibition, and influence on biofilm formation. The compounds herein studied, particularly the xanthene sulfonamide derivatives **MM17** and **MM18**, showed interesting preliminary results regarding their impact on different mechanisms of bacterial resistance. In the future, a comprehensive series of related compounds could be synthesized to allow their assessment against a larger set of bacterial strains and the establishment of a SAR of the 9-xanthenyl derivatives, as well as study their safety, stability, and PK properties. Furthermore, studies on the specific pump being inhibited are warranted, which can be achieved by genetic assays.

2.5. Experimental

2.5.1. Chemical synthesis and characterization

All reagents and solvents were purchased from TCI (Tokyo Chemical Industry Co. Ltd., Chuo-ku, Tokyo, Japan), Acros Organics (Geel, Belgium), Sigma-Aldrich (Sigma-Aldrich Co. Ltd., UK), or Alfa Aesar (Thermo Fisher GmbH, Kandel, Germany) and were used directly without any further purification. All reactions were monitored by TLC, carried out on Merck silica gel 60 (GF254) precoated plates by using appropriate mobile phases. Purification of the synthesized compounds was usually performed by flash column chromatography using Merck silica gel 60 (0.040–0.063 mm). Melting points (mp) were measured by using a Köfler microscope (Wagner and Munz, Munich, Germany) equipped with a Crison TM 65 (Crison Instruments, Barcelona, Spain) and were uncorrected. ^{1}H and ^{13}C NMR spectra were taken in $CDCl_3$ or [D_6]DMSO (Deutero GmbH, Kastellaun, Germany) at rt on Bruker Avance 300 instrument (300.13 or 500.16 MHz for ^{1}H and 75.47 or 125.77 MHz for ^{13}C, Bruker Biosciences Corporation, Billerica, MA, USA) or Bruker AVANCE III (400.14 MHz for ^{1}H and 100.62 MHz for ^{13}C). Chemical shifts are expressed in relative to tetramethylsilane (TMS) as an internal reference.^{13}C-NMR assignments were made by 2D heteronuclear single quantum coherence (HSQC) and heteronuclear multiple bond correlation (HMBC) experiments. For the assignment of each signal to the corresponding proton or carbon, it was considered the automatic numeration provided by MestReNova®, as provided in **Annex I**. High Performance Liquid Chromatography (HPLC) analysis (purity determination by HPLC analysis was performed with a system consisting of Shimadzu LC-

20AD pump, equipped with a Shimadzu DGV-20A5 degasser, a Rheodyne 7725i injector fitted with a 20 µL loop, and a SPD-M20A DAD detector (Kyoto, Japan)). Data acquisition was performed using Shimadzu LCMS Lab Solutions software, version 3.50 SP2. The column used in this study was ACE® - C18 (150 × 4.6 mm I.D., particle size 5 µm) manufactured by Advanced Chromatography Technologies Ltd (Aberdeen, Scotland, UK). The mobile phase composition was water and methanol (85:15 *v/v;* 0.1% acetic acid (AcOH)), all were HPLC grade solvents obtained from Merck Life Science S.L.U. (Darmstadt, Germany). The flow rate was 1.0 mL/min and the ultraviolet (UV) detection wavelength was 254 nm. Analyses were performed at 27 °C in an isocratic mode in a 30 min run. Peak purity index was determined by total peak UV-VIS spectra between 210-800 nm with a step of 4 nm. Compounds **MM16-18** and **MM7** were synthetized as described below, based in methodologies described in previous works [32, 162] .

Synthesis of 4-(9*H*-xanthen-9-yl)aniline (MM7)

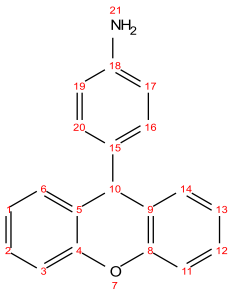

To 0.094 g of xanthydrol (**8**) in 5 mL of glacial acetic acid was added 1 mmol of aniline dissolved in 2 mL of DMF while the mixture was stirred electromagnetically. Stirring was continued at rt and the derivative began to precipitate in minutes. After 3 h, the product was collected through filtration with a vacuum filtration unit possessing a Nylon membrane filter with Ø of 47 mm and pore size of 0.45 µm. After washing with 100 mL of water, the product was dried in a vacuum desiccator over P_2O_5. The crude derivative was dissolved in a minimum volume of THF at rt, and the resulting solution was filtered. Water was then added in small portion until the visualization a sign of cloudiness. Then, the solution was placed in a refrigerator at 8-10 ^oC for slow crystallization. After crystallization was complete, the product was collected by filtration with a nail glass funnel. Compound **5** was obtained as yellowish needles (162.9 mg, 59.1 %)

Compound **MM7**: mp 183 °C (literature [163]: 175-180°C); Purity (HPLC): 99.5%; **^{1}H NMR** (300.13 MHz, DMSO-d_6): δ= 7.19 (ddd, *J* = 8.2, 6.7, 1.9 Hz, 2H, H-2 and H-12), 7.11 (dd, *J* = 8.2, 1.4 Hz, 2H, H-3 and H-11), 7.06 (dd, *J* = 8.2, 1.9 Hz, 2H, H-6 and H-14), 7.01 – 6.93 (m, 4H, H-1, H-13, H-16, H-20), 6.60 (d, *J*= 8.43, 2H, H-17 and H-19), 5.15 (s, 1H, H-10),

3.57 (s,br, 2H, H-21); **^{13}C NMR** (75.47 MHz, DMSO-d_6): δ= 151.2 (C-4 and C-8), 145.1 (C-18), 137.0 (C-15) , 129.8 (C-16 and C-20), 129.5 (C-6 and C-14), 127.8 (C-2 and C-12), 125.1 (C-5 and C-9), 123.3 (C-1 and C-13), 116.5 (C-3 and C-11), 115.5 (C-17 and C-19), 43.6 (C-10) ppm.

Synthesis of 4-((9*H*-xanthen-9-yl)amino)-*N*-(4-methylpyrimidin-2-yl)benzenesulfonamide (MM16)

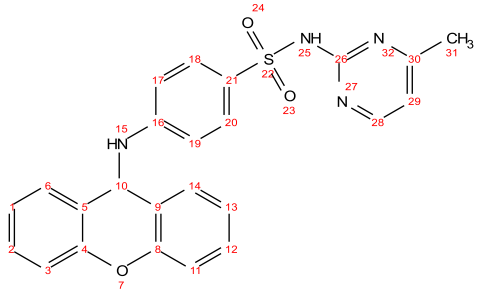

To 0.266g of xanthydrol (**8**) in 5 mL of glacial acetic acid was added 1 mmol of sulfamerazine dissolved in 2 mL of *N*,*N*-dimethylformamide (DMF). Stirring was continued at rt and the derivative began to precipitate in minutes. After 3 h, the product was collected through filtration with a vacuum filtration unit possessing a nylon membrane filter with Ø of 47 mm and pore size of 0.45 µm. After washing with 100 mL of water, the product was dried in a vacuum desiccator over P_2O_5. The crude derivative was dissolved in a minimum volume of tetrahydrofuran (THF) at rt, and the resulting solution was filtered. Water was slowly added until the visualization, was a sign of cloudiness. Then the solution was placed in a refrigerator at 8-10 ºC for crystallization. After crystallization was complete, the product was collected by filtration with a nail glass funnel. Compound **MM16** was obtained as white crystals (298.3 mg, 66.7 %).

Compound **MM16**: mp 207 – 208 °C (literature [32]: 206-207°C); Purity (HPLC): 99.2%; **^{1}H NMR** (300.13 MHz, DMSO-d_6): δ= 11.21 (s, 1H, H-25), 8.32 (d, J = 5.0 Hz, 1H, H-28), 7.68 (d, *J* = 8.6 Hz, 2H, H-18 and H-20), 7.49 (d, *J* = 9.1 Hz, 1H, H-15), 7.43 – 7.27 (m, 4H, H-2, H-6, H-12 and H-14), 7.19 (dd, *J* = 8.2, 1.2 Hz, 2H, H-3 and H-11), 7.09 (td, *J* = 7.3, 1.2 Hz, 2H, H-1 and H-13), 6.84 – 6.90 (m, 3H, H-17, H-19 and H-29), 6.12 (d, *J* = 9.0 Hz, 1H, H-10), 2.30 (s, 3H, H-31) ppm; **^{13}C NMR** (75.47 MHz, DMSO-d_6): δ= 168.1 (C-30), 157.8 (C-26), 156.9 (C-28), 151.3 (C-16), 150.7 (C-4 and C-8), 130.0 (C-18 and C-20), 129.0 (C-2 and C-12), 128.4 (C-6 and C-14), 125.9 (C-21), 123.5 (C-1 and C13), 122.5 (C-5 and C-9), 116.3 (C-3 and C-11), 114.9 (C-29), 110.9 (C-17 and C-19), 46.1 (C-10), 23.4 (C-31) ppm.

Synthesis of 4-((9*H*-xanthen-9-yl)amino)-*N*-(4,6-dimethylpyrimidin-2-yl)benzenesulfonamide (MM17)

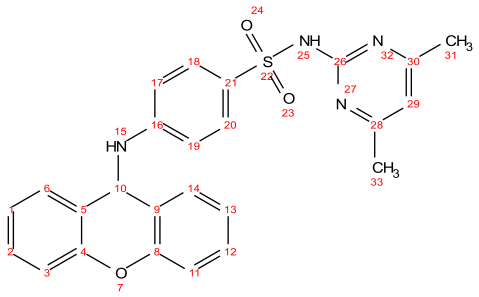

To 0.279g of xanthydrol (**8**) in 5 mL of glacial acetic acid was added 1 mmol of sulfametazine dissolved in 2 mL of DMF. Stirring was continued at rt and the derivative began to precipitate in minutes. After 3 h, the product was collected through filtration with a vacuum filtration unit possessing a Nylon membrane filter with Ø of 47 mm and pore size of 0.45 µm. After washing with 100 mL of water, the product was dried in a vacuum desiccator over P_2O_5. The crude derivative was dissolved in a minimum volume of THF at rt, and the resulting solution was filtered. Water was slowly added until the visualization, was a sign of cloudiness. Then the solution was placed in a refrigerator at 8-10 ºC for crystallization. After crystallization was complete, the product was collected by filtration with a nail glass funnel. Compound **MM17** was obtained as white needles (210.6 mg, 45.8 %).

Compound **MM17**: mp 171 – 173 °C (literature [32]: 174-175°C); Purity (HPLC): 99.9%; **^{1}H NMR** (300.13 MHz, DMSO-d_6): δ= 11.07 (s, 1H, H-25), δ= 7.68 (d, *J* = 8.8 Hz, 2H, H-18 and H-20), 7.46 (d, *J* = 9.1 Hz, 1H, H-15), 7.42 – 7.26 (m, 4H, H-2, H-6, H-12 and H-14), 7.18 (dd, *J* = 8.2, 1.3 Hz, 2H, H-3 and H-11), 7.08 (td, *J* = 7.4, 1.3 Hz, 2H, H-1 and H-13), 6.84 (d, *J* = 8.8 Hz, 2H, H-17 and H-19), 6.76 (s, 1H, H-29), 6.12 (d, *J* = 9.1 Hz, 1H, H-10), 2.24 (s, 6H, H-31 and H-33) ppm; **^{13}C NMR** (75.47 MHz, DMSO-d_6): δ= 167.9 (C-28 and C-30), 157.1 (C-26), 151.6 (C-16), 151.1 (C-4 and C-8), 130.7 (C-18 and C-20), 129.4 (C-2 and C-12), 128.8 (C-6 and C-14), 123.9 (C-1 and C-13), 123.0 (C-5 and C-9), 116.7 (C-3 and C-11), 114.2 (C-29), 111.2(C-17 and C-19), 46.5 (C-10), 23.6 (C-31 and C-33) ppm.

Synthesis of *N*-((4-((9*H*-xanthen-9-yl)amino)phenyl)sulfonyl)acetamide (MM18)

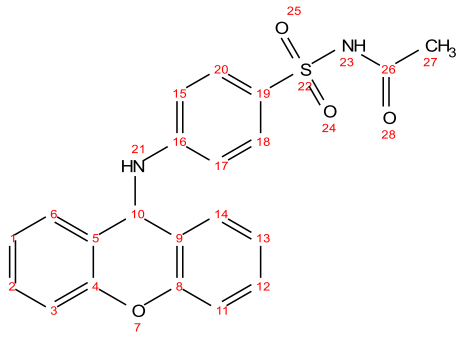

To 0.214 of xanthydrol (**8**) in 5 mL of glacial acetic acid was added 1 mmol of sulfacetamide dissolved in 2 mL of DMF while the mixture was stirred electromagnetically. Stirring was continued at rt and the derivative began to precipitate in minutes. After 3 h, the product was collected through filtration with a vacuum filtration unit possessing a Nylon membrane filter with Ø of 47 mm and pore size of 0.45 µm. After washing with 100 mL of water, the product was dried in a vacuum desiccator over P_2O_5. The crude derivative was dissolved in a minimum volume of THF at rt, and the resulting solution was filtered. Water was then added in a small portions until the visualization, as a sign of cloudiness. Then the solution was placed in a refrigerator at 8-10 ºC for slow crystallization. After crystallization was complete, the product was collected by filtration with a nail glass funnel. Compound **MM18** was obtained as white needles (254.9 mg, 64.7 %).

Compound **MM18**: mp 215 °C (literature [32] 208-208.5°C); Purity (HPLC): 99.9%; **^{1}H NMR** (300.13 MHz, DMSO-d_6): δ= 11.70 (s, 1H, H-25), 7.66 (d, *J* = 9.0 Hz, 1H, H-21), 7.57 (d, *J* = 8.9 Hz, 2H, H-18 and H-20), 7.28 – 7.45 (m, 4H, H2, H-6, H-12 and H-14), 7.20 (dd, *J* = 8.2, 1.2 Hz, 2H, H-3 and H-11), 7.12 (td, *J* = 7.4, 1.3 Hz, 2H, H-1 and H-13), 6.87 (d, *J* = 8.9 Hz, 1H, H-15 and H-17), 6.16 (d, *J* = 9.0 Hz, 1H, H-10), 1.88 (s, 3H, H-27) ppm; **^{13}C NMR** (75.47 MHz, DMSO-d_6): δ= 168.9 (C-26), 152.2 (C-16), 151.1 (C-4 and C-8), 130.2 (C-18 and C-20, 129.5 (C-2 and C-12), 128.8 (C-6 and C-14), 125.1 (C-19), 124.0 (C-1 and C-13), 122.8 (C-5 and C-9), 116.8 (C-3 and C-11), 111.6 (C-15 and C-17), 46.5 (C-10), 23.7 (C-27) ppm.

2.5.2. Biological assays and docking studies

Microorganisms

As Gram-positive strains, *Staphylococcus aureus* ATCC 25923, *Enterococcus faecalis* ATCC 29212, and methicillin and ofloxacin-resistant *Staphylococcus aureus* 272123 clinical

isolate were used. As Gram-negative strains, *Escherichia coli* ATCC 25922, *Pseudomonas aeruginosa* ATCC 27853, the *acrA* gene inactivated mutant *Salmonella enterica* serovar Typhimurium SL1344 (SE03), and clinical isolates of the extended-spectrum β-lactamase producer (ESBL) *E. coli* SA/2 were investigated in this study.

For the QS tests, all bacteria used were Gram-negative. The bacteria used were *Chromobacterium violaceum* wild type 85 (wt85), characterized by the AHL signal molecule-mediated production of the purple violacein pigment, capable of endogenous QS-signal molecule production (*N*-hexanoyl-L-HSL), *C. violaceum* CV026 (CV026), a Tn5 transposase-mutant, AHL-signal molecule indicator strain (produces purple violacein pigment in the presence of AHL), which is incapable of endogenous QS-signal molecule-production, but useful in the detection of external stimuli, *Sphingomonas paucimobilis* Ezf 10-17 (EZF), AHL-producing-strain (used with *C. violaceum* CV026), and *Serratia marcescens* AS-1, characterized by the AHL signal molecule-mediated production of the orange–red pigment prodigiosin (2-methyl-3-pentyl-6-methoxyprodigiosin), capable of endogenous QS-signal molecule production (*N*-hexanoyl-L-HSL), were applied [157].

Docking studies

The crystal structures of the AcrB (PDB: 4DX5) [164], AcrA (PDB: 2F1M) [165], and TolC (PDB: 1EK9) [166] portions of the AcrAB-TolC bacterial efflux system, downloaded from the protein databank (PDB) [167], were used for this study. The structures of the known AcrAB-TolC inhibitors D13-9001, doxorubicin, MBX-3132, minocycline, and phenyl-arginyl-β-naphthylamide, along with the structures of the tested compounds were drawn with ChemDraw (PerkinElmer Informatics, MA, USA) and minimized using ArgusLab. Docking was carried out using AutoDock Vina (Scripps, CA, USA) [168], in the sites described in [169, 170].Since the crystal structure of NorA efflux pump is not available, a homology model was prepared. The model was generated using the Swiss Model server [171] and the sequence was deposited in Uniprot (Q5HHX4) [172], using the EmrD pump from *Escherichia coli* (PDB: 2GFP) as the homolog, as described previously [173]. The top nine poses were collected for each molecule and the lowest docking score value was associated with the most favorable binding conformation. PyMol (Schrödinger, NY, USA) was used for molecular visualization [174].

Antibacterial assay

The antibacterial activity was assessed by determination of the MIC of the compounds using the microdilution method, in a 96-well plate, according to the Clinical and Laboratory

Standard Institute (CLSI) guidelines [175] . The media used was MHB II. The concentrations tested ranged from 64 µg/mL to 4 µg/mL, which were later converted to µM. The MIC was determined by visual inspection. DMSO, in subinhibitory concentrations (1 % *v/v*), was used as a solvent for the compounds.

Inhibition of biofilm formation

Compounds were tested for their ability to inhibit the formation of biofilm. The bacterial strains used were the Gram-positive *S. aureus* ATCC 25923 and *S. aureus* 272123. The detection of biofilm formation was possible with the use of the dye crystal violet (CV; 0.1 % *v/v*). The initial inoculum was incubated in tryptic soy broth (TSB) overnight and then diluted to an OD_{600} of 0.1. Then, the bacterial suspension was added to 96-well microtiter plates and the compounds were added at a concentration of ½ MIC, and for compounds whose MIC is higher than 100 µM, a concentration of 100 µM was used. The final volume in each well was 200 µL. Reserpine was used as the positive control, as it was the same compound used in the efflux pump inhibition assay and it has shown activity in the inhibition of biofilm formation in *S. aureus* strains [176] . The plates were incubated at 30 °C for 48 h, with gentle stirring (100 revolutions per minute (rpm)). After this incubation period, the TSB medium was discarded, and the plates were washed with tap water to remove unattached cells. Afterwards, 200 µL of 0.1 % *v/v* CV solution were added to the wells and incubated for 15 min at rt. Then, the CV solution was removed from the wells, and the plates were washed again with tap water, and 200 µL of 70 % ethanolic solution were added to the wells. The biofilm formation was determined by measuring the OD_{600} using a Multiscan EX ELISA plate reader (Thermo Labsystems, Cheshire, WA, USA). The anti-biofilm effect of the compounds was expressed as the percentage (%) of a decrease in biofilm formation.

Efflux pump inhibition assay

Compounds were evaluated for their ability to inhibit efflux pumps in SE03 and *S. aureus* 272123 strains, through real-time fluorimetry, monitoring the intracellular accumulation of EB, an efflux pump substrate. This was determined by the automated method using a CLARIOstar Plus plate reader (BMG Labtech, Ortenberg, Germany). Reserpine and CCCP were applied at 25 µM as positive controls, and the solvent DMSO was applied at 1 % *v/v*. The bacterial strains were incubated in an appropriate culture media (TSB—*S. aureus* 272123; LB-B—SE03) at 37 °C until they reached an optical density (OD) between 0.4 and 0.6 at λ = 600 nm. The culture was centrifuged at 13,000 × g for 3 min, and the pellet was washed and resuspended with PBS. The suspension was centrifuged again in the same

conditions and resuspended in PBS. The compounds were applied at 50 µM in a solution of a nontoxic concentration of EB (1 µg/ml) in PBS. Then, 50 µL of this solution were transferred into a 96-well black microtiter plate (Greiner Bio-One Hungary Kft, Mosonmagyaróvár, Fertősor, Hungary), and 50 µL of bacterial suspension (OD_{600} 0.4–0.6) were added to each well. The plates were placed into the CLARIOstar plate reader, and the fluorescence was monitored at excitation and emission wavelengths of 530 nm and 600 nm every minute for 1 h on a real-time basis. From the real-time data, the activity of the compounds, namely, the RFI of the last time point (minute 60) of the EB accumulation assay, was calculated according to the following formula:

$$RFI = \frac{RF_{treated} - RF_{untreated}}{RF_{untreated}} \quad (1)$$

where $RF_{treated}$ is the relative fluorescence (RF) at the last time point of EB accumulation curve in the presence of the compound, and $RF_{untreated}$ is the RF at the last time point of the EB accumulation curve of the untreated control, having only the solvent (DMSO) control. The accumulation curves were designed using Microsoft Excel®.

Chapter 3. – Synthesis and biological activity of xanthene-9-carboxylic acid derivatives

Candidate contribution: synthesis and structural characterization of the xanthene-9-carboxylic acid derivatives herein described; discussion of the results obtained in the biological activity assessment.

Introduction adapted from Miguel Maia *et al* *.

* Maia, M. A.; Sousa, E., BACE-1 and γ-Secretase as Therapeutic Targets for Alzheimer's Disease. Pharmaceuticals 2019, 12 (1)

3.1. Introduction

3.1.1. Alzheimer's disease

Alzheimer's disease (AD) is recognized by the World Health Organization (WHO) as a global public health priority [177]. Notwithstanding the advances in the understanding of AD pathogenesis since Alois Alzheimer reported the first case in 1907 [178],there are still a lot of uncertainties regarding the mechanisms involved in disease progression. AD is the most prevalent cause of dementia-acquired progressive cognitive impairment sufficient to impact on activities of daily living, being a major cause of dependence, disability, and mortality. The WHO estimated that in 2010, 35.6 million worldwide were living with dementia. This figure is projected to almost double every 20 years, reaching 65.7 million by 2030 and 115.4 million by 2050 [179]. Europe, with an estimated 10 million cases of dementia in 2010 and acquiring progressively an old population structure, has a projected increase to 14 million cases in 2030 [52].

The main characteristics of Alzheimer's pathology are the presence of amyloid plaques and neurofibrillary tangles (aggregates of hyperphosphorylated tau protein). In addition, neuropil treads, dystrophic neurites, associated astrogliosis, and microglial activation frequently coexist. The downstream consequences of these pathological processes include neurodegeneration with synaptic and neuronal loss leading to macroscopic atrophy [52].

Currently, five drugs are approved for the treatment of AD (tacrine, donepezil, rivastigmine, galantamine and memantine). However, these drugs only relieve symptoms, not being able to impact in the progression of the disease. There is an urgent need for the development of disease modifying therapies or treatments (DMT's) able to prevent, delay, or slow the progression and target the primary pathophysiology mechanisms of AD.

3.1.2. The amyloid hypothesis of AD

The amyloid hypothesis suggests that the accumulation of pathological forms of Aβ, due to an increase of production and/or decreased clearance, is the primary pathological process in AD [179, 180]. The accumulation of Aβ peptides leads to their oligomerization and formation of Aβ plaques. These plaques generate an anti-inflammatory response causing oxidative stress in neurons and disrupting normal kinase and phosphatase activity, resulting in hyperphosphorylation of tau protein and subsequent neurofibrillary tangle formation. This cascade of events leads to abnormal signaling and synaptic impairment, resulting ultimately in neuronal dead and dementia in the AD patient [181].

Aβ is produced by a two-step sequential cleavage of amyloid precursor protein (APP): first BACE1 cleaves APP to generate soluble APPβ (sAPPβ) and a 99 amino acid fragment (C99), which then suffers several cleavage events by γ-secretase to produce peptides of different lengths from 38 to 43 amino acids, being Aβ40 and Aβ42 the main products and both playing a key role in the aggregation of neuritic plaques [182, 183]. Aβ is a normal cellular product that is rapidly cleared, and, at physiological concentrations, it is related with important neuroprotective functions [184, 185]. However, in circumstances of abnormal accumulation, namely overproduction or impaired clearance there is an higher concentration of Aβ, increasing aggregation and toxicity [186].

3.1.3. Amyloid targeting strategies

Following the amyloid hypothesis, where a high brain Aβ level is considered as an important factor in AD pathogenesis, pharmacological intervention to reduce its production or improve the clearance has become a logical approach for AD therapy development.

3.1.3.1. Inhibition of BACE1

BACE1 is a type-1 membrane-anchored aspartyl protease responsible for the first step of the proteolysis of APP, identified in 1999 [187]. BACE1 cleaves APP in the luminal surface of the plasma membrane and releases the soluble ectodomain of APP, leaving C99 (Aβ plus AICD) in the membrane to be subsequently cleaved by GS to generate Aβ peptides of different lengths as described above.

BACE1 protease is characterized by a large catalytic domain which is marked by the centrally located catalytic aspartates Asp32 and Asp228. Free BACE1 features a flap-open conformation that is energetically stable due to the multiple hydrogen bonds in the flap region of the enzyme. When a substrate is bound, BACE-1 assumes a flap-closed or a flap-open conformation, depending on the characteristics of the substrate [181, 188].

Initially, the development of BACE1 inhibitors appeared to be a relatively simple approach. First, the development of successful clinical aspartic proteases inhibitors for other therapeutic areas, namely human immunodeficiency virus (HIV) and hypertension, had established an important knowledge for the development of others aspartic protease inhibitors [189]. Second, the first crystal structure of this secretase, elucidated in 2000, provided powerful information for the structure-based drug design of BACE1 inhibitors [190]. However, progress has been difficulted by combination of properties needed for being efficacious: compounds must fulfill the general rigid prerequisites for a drug aimed for CNS

penetration and, at the same time, be compatible with the large and hydrophobic catalytic pocket of BACE1. Moreover, selectivity toward different aspartyl proteases, namely cathepsin D, BACE2 and renin, have been an additional attrition factor in BACE1 drug discovery.

As described in **Chapter 1 – Introduction**, xanthenes, hydroxyxanthones and azaxanthenes have been explored for the development of potent and selective BACE1 inhibitors. Hence, one of the aims of this thesis was the development of novel xanthene derivatives with improved activity as BACE1 inhibitors and selectivity over other proteases. Considering previous studies on the important moieties for an effective interaction with the catalytic pocket of BACE1 [191], several xanthenes were synthetized, comprising amide and amine groups in position 9, as well as different substituents in the aromatic rings of the xanthene core to improve selectivity. Nonetheless, preliminary results on the activity of the xanthenes synthetized showed no inhibition of BACE1 at a concentration of 10 μM (results not disclosed). In this way and considering previous studies regarding the ability of tricyclic compounds to modulate P-gp activity [192-194], a second approach was followed, assessing the efficacy of the derivatives synthetized in enhancing the elimination of Aβ peptides through P-gp activation, as described below.

3.1.2. P-glycoprotein and amyloid- β export

One important mechanism of Aβ elimination from the brain is via direct transport across the blood-brain barrier (BBB) [195-197]. Several members of the ATP-binding cassette (ABC) transporter superfamily have recently been linked in the development of neurodegenerative disorders, namely AD [198-201], and growing evidence points to a significant role of P-gp, in the export of Aβ.

P-gp utilizes adenosine triphosphate (ATP) to actively export substances across membranes of tissues with excretory or barrier functions. In the brain, P-gp is predominantly expressed on the luminal (blood-facing) surface of the BBB endothelium, where it provides a protective function regulating the passage of a wide variety of endo- and xenobiotic compounds out of the central nervous system [202].

In healthy individuals, Aβ is constitutively produced and cleared from the brain at rates of 7.6% and 8.3%. of total Aβ per hour, respectively [185]. In late-onset Alzheimer's disease (LOAD), this clearance rate is reduced by approximately 30% [202]. Several studies suggest that P-gp is required for the normal clearance of Aβ across the BBB [186, 198, 203-205].

Hence, the use of substances able to modulate P-gp activity can be considered a potential AD therapeutic/ preventive strategy.

Previous studies have shown the ability of tricyclic compounds to modulate P-gp activity [192-194, 206]. Oxygenated xanthones demonstrated their potential for P-gp induction and/ or activation in Caco-2 cells[192] and SW480 cells[193]. A similar effect was observed with thioxanthones and dehydroxylated xanthones derivatives, where Caco-2 cells were protected against paraquat-induced cytotoxicity due to an increase in P-gp expression and/or to P-gp activation [193, 194].

Considering the above-mentioned information, the library of xanthene derivatives planned to include a tricyclic nucleus with aromatics, hydrogen-bound acceptors and donors, important features in the pharmacophore of P-gp activators [192], was assessed on P-gp modulation activity.

3.2. Synthesis of xanthene-9-carboxylic acid derivatives

Xanthene-9-carboxylic acid was used as starting material for the synthesis of different derivatives as depicted in **Scheme 15**, involving four distinctive steps: aromatic halogenation, amide coupling, amide reduction, and Suzuki coupling.

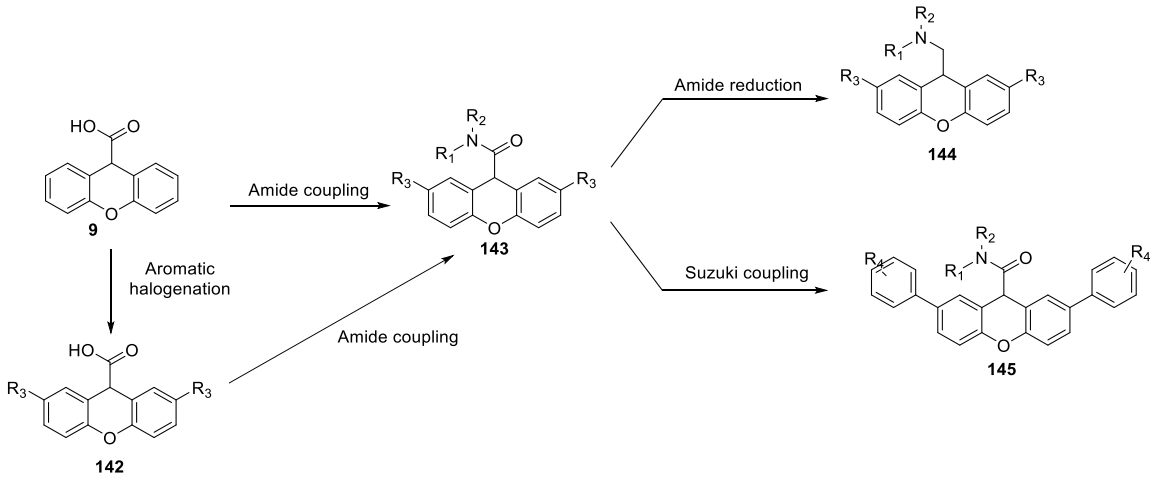

Scheme 15. Synthesis of xanthene-9-carboxylic acid derivatives.

3.2.1. Aromatic halogenation

The aromatic halogenation of xanthene-9-carboxylic acid was performed following a previously reported procedure describing the chlorination of xanthene-9-carboxylic acid with

N-chlorosuccinimide (NCS), under the presence of a catalytic amount of hydrochloric acid and acetic acid as solvent. The same procedure was applied to obtain the dibrominated derivative, using *N*-bromosuccinimide (NBS) instead of NCS (**Scheme 16**) [207]. 2,7-Dichloro-9*H*-xanthene-9-carboxylic acid (**MM52**) and 2,7-dibromo-9*H*-xanthene-9-carboxylic acid (**MM54**) were obtained with a 53% and 56% yield, respectively. For subsequent reactions it was used the dibrominated compound (**MM54**) considering its higher reactivity for Suzuki–Miyaura coupling [208]. An attempt to obtain the monobrominated product was performed, in order to increase molecular diversity and to obtain non-symmetrical compounds. Nonetheless, a mixture of non-brominated, monobrominated and dibrominated product was obtained, and their separation would be very challenging considering their similar polarity, leading to postpone this strategy.

Further details regarding characterization data are provided in section ***3.5****. Experimental*.

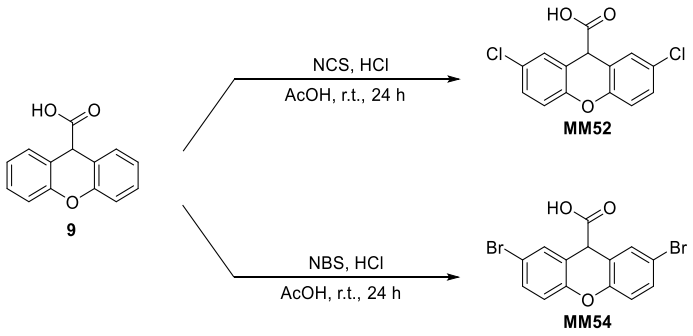

Scheme 16. Aromatic halogenation of xanthene-9-carboxylic acid (**9**).

3.2.2. Amide coupling

The direct union of the carboxylic acid function and the amine does not occur spontaneously at ambient temperature, since the hydroxyl (-OH) group from the carboxylic acid is a bad leaving group. Therefore, it is usually required to first activate the carboxylic acid, by converting the -OH of the acid in a good leaving group. One of the strategies used is the formation of an acyl chloride. The general approach consists in reacting the carboxylic acid with thionyl chloride or oxalyl chloride under reflux to obtain the respective acyl chloride, which react quickly with amines to form amides [209]. However, this strategy comprises some drawbacks, as the rigorous exclusion of water due to their high reactivity and sensitivity to hydrolysis and the need of a large excess of reactant, as well as safety issues [210, 211]. Another commonly strategy is the use of a coupling agent a strategy largely employed in

peptide bond formation. Several suitable reagents have been described for this purpose, with the most popular based on carbodiimide coupling mediated by benzotriazole additives, such as 1-Hydroxybenzotriazole (HOBt) or 1-Hydroxy-7-azabenzotriazole (HOAt). After some concerns raised about the safety of these reagents, particularly their potential explosive nature in large scale, a third generation reagent was developed - (1-cyano-2-ethoxy-2-oxoethylidenaminooxy)-dimethylamino-morpholino-carbenium hexafluorophosphate (COMU, **146**) (**Figure 35**), allowing a similar performance with the previous coupling agents but surpassing safety issues [212, 213]. Based on the above considerations, COMU was chosen as the preferred approach for the synthesis of xanthene carboxamides through the reaction of xanthene-9-carboxylic acid (**9**) and 2,7-dibromo-9*H*-xanthene-9-carboxylic acid (**MM54**) with several aliphatic and aromatic amines.

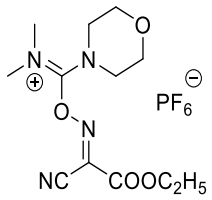

146

Figure 35. (1-Cyano-2-ethoxy-2-oxoethylidenaminooxy)-dimethylamino-morpholino-carbenium hexafluorophosphate (COMU, **146**).

The first series of carboxamides was synthetized in an one-pot reaction in the presence of COMU according to previous described procedures [212]. The general reaction is presented in **Scheme 17** and **Table 5** summarizes the compounds obtained and the corresponding isolated yield. Further details regarding characterization data are provided in section ***3.5****. Experimental*.

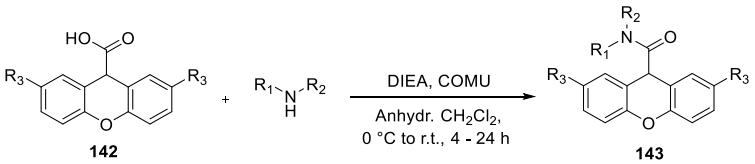

Scheme 17. General reaction for the synthesis of carboxamides using COMU as coupling agent.

Table 5. Carboxamides obtained using COMU as coupling agent and respective isolated yield.

Starting material	Amine	Product	Isolated yield (%)
		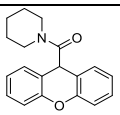 MM30	77
		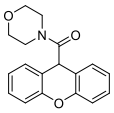 MM32	92
		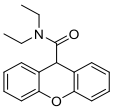 MM36	90
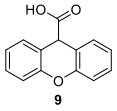 9	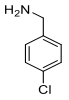	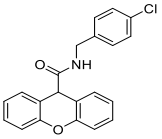 MM48A	52
		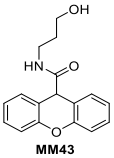 MM43	64
		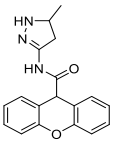 MM42B	24
		 MM42C	20
		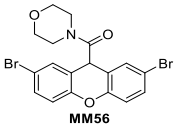 MM56	50
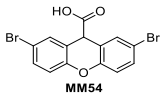 MM54	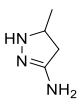	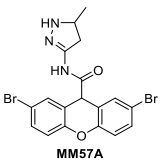 MM57A	24
		 MM57B	29

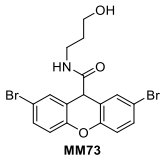

MM73

10

For the structure elucidation of the compounds obtained, ^{1}H and ^{13}C NMR analysis were performed, as well as Heteronuclear Single Quantum Coherence (HSQC) and Heteronuclear Multiple Bond Correlation (HMBC) experiments to assist in the correct attribution of each signal.

The data corresponding to the ^{1}H NMR and ^{13}C NMR of the illustrative example, compound **MM30**, are depicted in Table 6.

Table 6. ^{1}H NMR and ^{13}C NMR data of compound **MM30**.

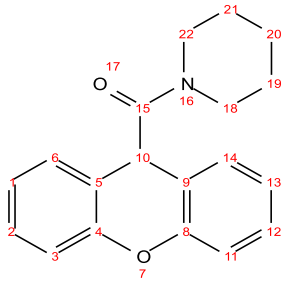

MM30

Protons	**δ_H (multiplicity, integration) ***	**Carbons**	**δC**
H-6 and H-14	7.33 – 7.17 (m, 4H)	C-15	170.2
H-2 and H-12		C-4, C-8	150.1
H-1 and H-13	7.15 – 6.94 (m, 4H)	C-2, C-12	129.0
H-3 and H-11		C-6, C-14	128.2
H-10	5.45 (s, 1H)	C-1, C-13	123.5
H-18	3.56 (t, *J* = 5.0 Hz, 2H)	C-5, C-9	119.2
H-22	3.20 (t, *J* = 5.5 Hz, 2H)	C-3, C-11	117.0
H-19	1.61 – 1.40 (m, 4H)	C-22	47.0
H-21		C-10	45.7
H-20	0.97 (s, 2H)	C-18	44.0
-	-	C-19	25.6
-	-	C-21	25.4
-	-	C-20	24.4

* The values are presented in ppm (δH) relative to $(CH_3)_4Si$ as an internal reference. The coupling constants (*J*) are in Hertz (Hz).
Numbering provided by MestReNova®.

The ^{1}H NMR spectrum of **MM30** showed the presence at highest values of δ_H of two signals, each corresponding to four aromatic protons totalizing eight protons: H-1, H-2, H-3, H-6, H-11, H-12, H-13, and H-14. The aromatic protons most deshielded (at δ_H 7.33 – 7.17 ppm) are protons H-2 and H-12 and protons H-6 and H-14 due to the resonance effect of the aromatic ether, an *ortho*- and *para*- director (**Scheme 18**). The signals corresponding to the remaining aromatic protons, H- 1 and H-13 and H-3 and H-11, are at lower chemical shifts (δ_H 7.15 – 6.94 ppm). The signal with the highest chemical shift corresponding to a non-aromatic proton was attributed to H-10 (δ_H = 5.45 ppm) due to magnetic anisotropy and electron-withdrawing effects of the carbonyl group (C-15). The remain aliphatic signals were attributed to the piperidine protons H-18 – H-22.

Regarding ^{13}C NMR data, the signal with the highest chemical shift value (δ_C = 170.2 ppm) was attributed to C-15, the carbon of the carbonyl group. This high chemical shift value was due to the unprotective effect of the carbonyl group. It was also possible to visualize six signals attributed to the twelve aromatic carbons (δ_C 117.0-150.1 ppm) and six signals corresponding to the six aliphatic carbons: one from the xanthene (C-10) and five from the piperidine group (C-18 – C-22). The ^{13}C NMR assignments of the hydrogenated carbons were determined by HSQC and the quaternary carbons were determined by HMBC experiments.

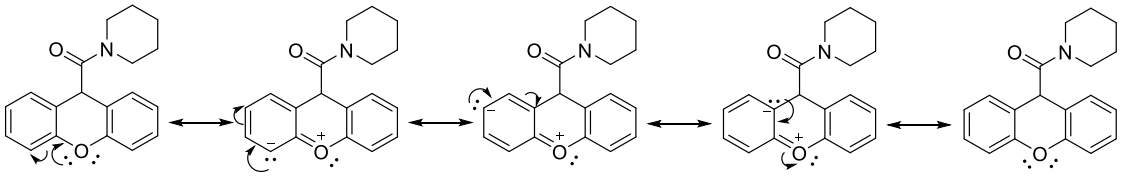

Scheme 18. Resonance effect of the aromatic ether group, an ortho- and para- director.

When diethanolamine and *N*-Boc-1,6-hexanediamine (**Figure 36**) were used as nucleophiles, the amide coupling procedure using COMU as coupling agent provided unsatisfactory results. It was hypothesized that the lower reactivity of these two amines could be associated with some steric hindrance and/ or electron deficiency. Hence, a distinctive protocol was used to provide amide coupling through the synthesis of an acyl fluoride intermediate. Acyl fluorides are attractive derivatives of carboxylic acids that allow straightforward access to a range of high-value products upon subjection to nucleophiles. Acyl fluorides have been shown to have improved stability and reactivity features over the commonly employed acyl chlorides. While the latter are highly reactive and unstable intermediates, the corresponding fluorides are easily isolable, stable to column

chromatography on silica gel, and react less violently. Consequently, acyl fluorides allow for couplings with, for example, more sterically demanding amines or more richly functionalized variants with less byproduct formation compared to acyl chlorides, anhydrides, or activated alternatives [214].

For the coupling procedure through *in situ* formation of acyl fluorides and reaction with amines, it was used a previously described procedure, employing fluoro-*N,N,N′,N′*-bis(tetramethylene)formamidinium hexafluorophosphate (BTFFH, **Figure 36**) as fluorinating agent. *N,N*-Diisopropylethylamine (DIEA) is used as base and anhydrous THF as solvent, and the reaction is performed in a sealed vial, under nitrogen atmosphere and 80 °C, for 4 h [215]. The general reaction is presented in **Scheme 19** and **Table 7** summarizes the compounds obtained and the corresponding isolated yield. Further details regarding characterization data are provided in section ***3.5****. Experimental*.

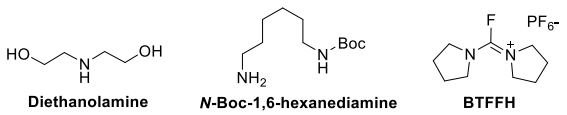

Figure 36. Diethanolamine, N-boc-1,6-hexanediamine and BTFFH.

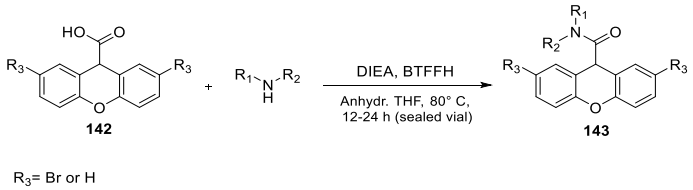

Scheme 19. General reaction for the synthesis of carboxamides through *in situ* formation of acyl fluorides.

Table 7. Carboxamides obtained through *in situ* formation of acyl fluorides.

Starting material	Amine	Product	Isolated yield (%)
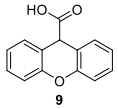 9	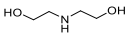	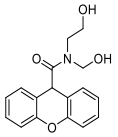 MM59B	94
		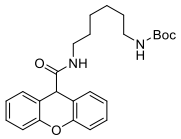 MM61B	98
	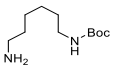	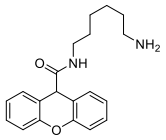 MM63B 1)	88
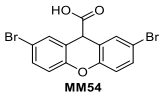 MM54	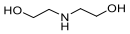	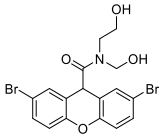 MM74	23

1) Obtained through deprotection of **MM61B**. Details are provided in section ***3.5****. Experimental*

3.2.3. Amide reduction

The reduction of carboxamides to the respective amines was performed using borane-tetrahydrofuran (BH_3.THF) as reducing agent. Comparing with $Li(AlH_4)$, borane is a milder reducing agent and due to its chemoselectivity, it is capable of reducing amides to the correspondent amines with lower probability of reducing other functional groups also present [216, 217]. The general reaction is presented in **Scheme 20**. The amide was dissolved in anhydrous THF and BH_3.THF in excess was added at 0 ºC due to the exothermic character of the reaction. Heat was used as catalyst and the reaction was heated until reflux being stirred under N_2 for 2 h. When all the starting material was consumed, the reaction was cooled to 0 ºC and HCl was added. **Table 8** summarizes the compounds obtained and the corresponding isolated yield. Further details regarding characterization data are provided in section ***3.5****. Experimental*.

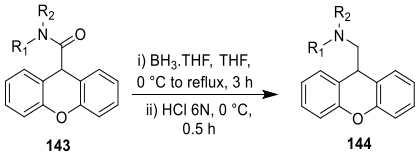

Scheme 20. General reaction for amide reduction using the complex BH_3.THF as reducing agent.

Table 8. Amines obtained through carboxamide reduction.

Amide	Product	Isolated yield (%)
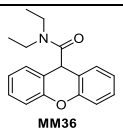 MM36	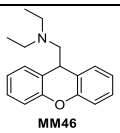 MM46	53
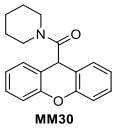 MM30	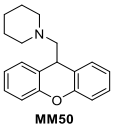 MM50	50

3.2.4. Suzuki-Miyaura coupling

Suzuki-Miyaura coupling (also known as Suzuki coupling) is a metal catalyzed reaction, usually with Pd, between an alkenyl, aryl, or alkynyl organoborane (boronic ester or boronic acid, or in some cases with aryl trifluoroborane) and a triflate or halide, under basic conditions. This reaction allows to create carbon-carbon bonds to obtain conjugated systems of alkenes, styrenes, or biaryl compounds. The catalytic cycle in Suzuki-Miyaura coupling starts with the active catalytic LnPd(0) species, where L represents the ligand stabilising the Pd(0) species. The Pd(0) species can be added directly to the reaction, namey $Pd(PPh_3)_4$, $Pd(dba)_2$ and $Pd(t Bu_3P)_2$. As an alternative to Pd(0) species, Pd(II) species can also be used, which is then reduced *in situ*. Pd(II) species are more stable than the Pd(0) species, nonetheless, typically it is also less reactive as it does require the reduction to generate the active species. Typical examples of Pd(II) species are $Pd(OAc)_2$, $Pd(dppf)Cl_2$ and $PdCl_2(PPh_3)_2$ [208].

Suzuki coupling procedure was applied to compound **MM56** with 2,4-difluorophenylboronic acid. The reaction was performed in THF, with tetrakis(triphenylphosphine)palladium(0) ($Pd(PPh_3)_4$) as catalyst and potassium carbonate as base, at 100 °C for 3 h in a sealed vial. Compound **MM68** was obtained with an isolated yield of 92%. The reaction is depicted in

Scheme 21. Further details regarding characterization data are provided in section ***3.5****. Experimental****.***

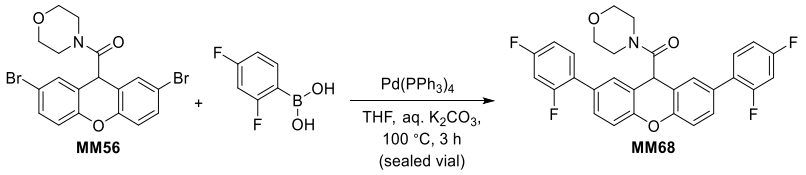

Scheme 21. Synthesis of **MM68** through Suzuki coupling procedure.

3.3 Biological activity results and discussion

3.3.1. Cytotoxicity

Cytotoxicity evaluation of the compounds was studied in RA (retinoic acid) differentiated SH-SY5Y cells to eliminate the compounds with high cytotoxicity and to select the concentration range for further neuroprotection assays. The selected methods of cell viability/cytotoxicity applied were the neutral red uptake assay and MTT (3-(4,5-dimethylthiazol-2-yl)-2,5-diphenyltetrazolium bromide) reduction assay [218, 219].

Neutral red uptake assay

The neutral red uptake assay is one of the most used cytotoxicity tests that allows in vitro quantification of xenobiotic-induced cytotoxicity [220]. It relies on the ability of viable cells to incorporate and bind the supravital dye neutral red. This weak cationic dye penetrates the cell membranes by nonionic passive diffusion and concentrates in the lysosomes, where it binds by electrostatic hydrophobic bonds to anionic and/ or phosphate groups of the lysosomal matrix [218, 221]. The dye is then extracted from the viable cells using an acidified EtOH solution, and the absorbance of the solubilized dye is quantified using a spectrophotometer. As such, cytotoxicity is expressed as a concentration-dependent reduction of the uptake of neutral red after exposure to the xenobiotic under investigation [220].

The uptake of neutral red depends on the capacity of the cells to maintain pH gradients, through the production of ATP. At physiological pH, the dye comprises a net charge close to zero, allowing it to penetrate the membranes of the cell. Then, inside the lysosomes, there is a proton gradient to maintain a pH lower than that of the cytoplasm (**Figure 37**). Consequently, the dye becomes charged and is retained inside the lysosomes. When the

cell dies or the pH gradient is reduced, the dye cannot be retained. Thus, the amount of retained dye is proportional to the number of viable cells [218].

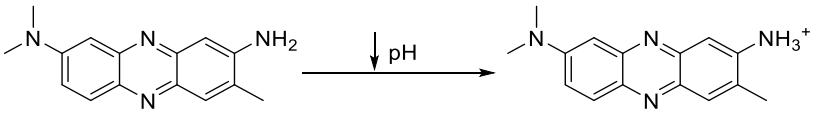

Figure 37. Chemical structures of neutral red outside lysosome, at physiological pH, and positive charged NR inside lysosome, at lower pH than physiological pH.

MTT reduction

The MTT (3-[4,5-dimethylthiazol-2-yl]-2,5 diphenyl tetrazolium bromide) assay allows the measurement of viable cells in high throughput assays (96-well plates), therefore, it is a wide used technique for the determination of cytotoxicity of compounds at different concentrations. The principle of this assay is that for most viable cells mitochondrial activity is constant and thus an increase or decrease in the number of viable cells is linearly associated to mitochondrial activity. The mitochondrial activity of the cells is reflected by the conversion of the tetrazolium salt MTT into formazan crystals, which can be solubilized for homogenous measurement. Therefore, any increase or decrease in the number of viable cells can be detected by measuring the concentration of formazan, reflected in OD using a plate reader at 540 and 720 nm.

Xanthene derivatives **MM7**, **MM29**, **MM30**, **MM32**, **MM36**, **MM42B**, **MM42C**, **MM43**, **MM46**, **MM48A**, **MM50**, **MM52**, **MM54**, **MM56**, **MM57A**, **MM57B**, **MM59B3**, **MM63B**, **MM68**, **MM73** and **MM74** were studied regarding their cytotoxicity at concentrations of 5 µM, 10 µM, 25 µM, and 50 µM with both neutral red uptake assay and MTT reduction assay. **Figure 38** – **Figure 41** resume the results obtained in each assay.

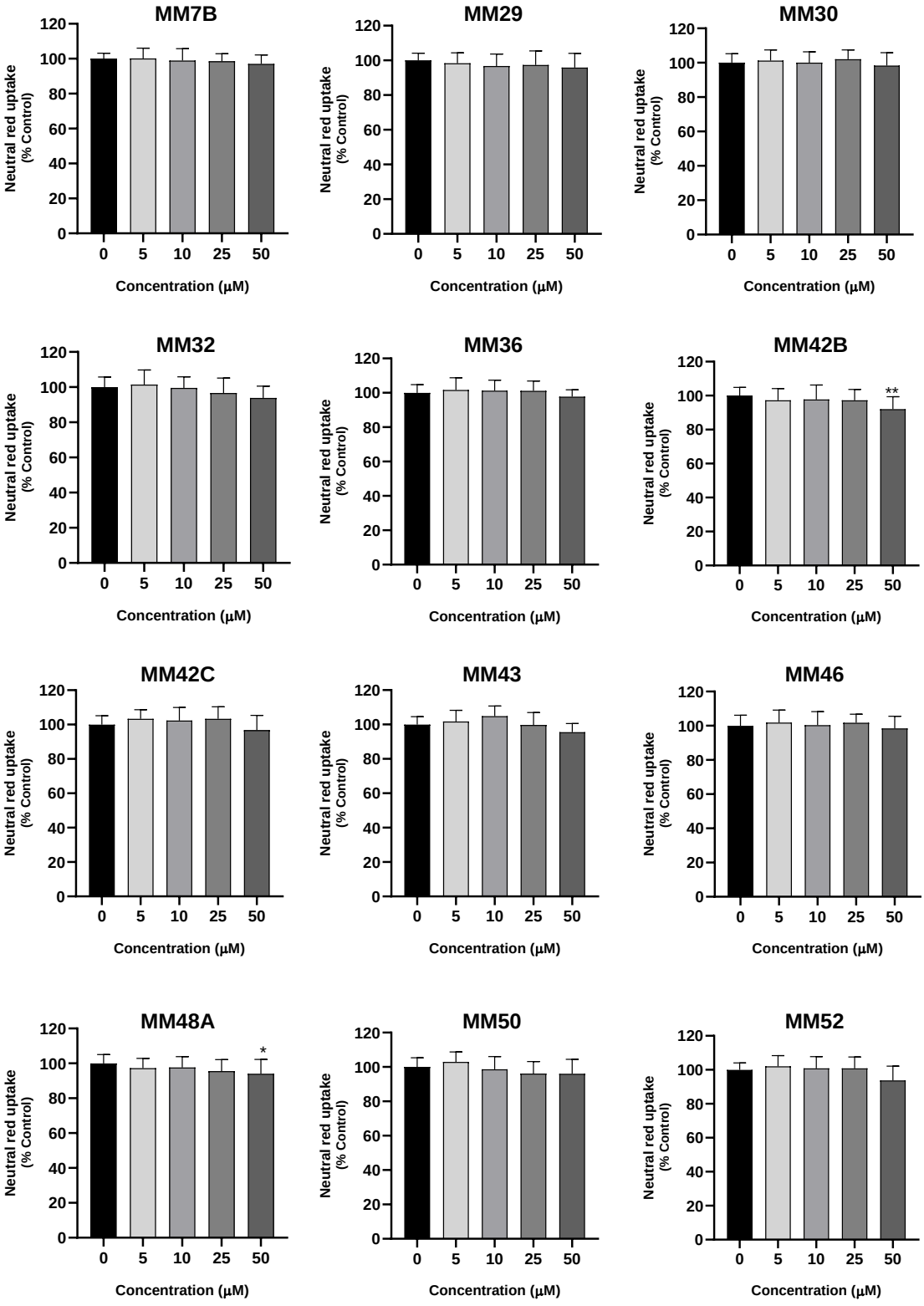

Figure 38. Cytotoxicity evaluation of compounds **MM7**, **MM29**, **MM30**, **MM32**, **MM36**, **MM42B**, **MM42C, MM43**, **MM46**, **MM48A**, **MM50**, **MM52** at concentrations of 5 µM, 10 µM, 25 µM and 50 µM with neutral red uptake assay. Results are expressed as mean + SD from five independent experiences, performed in triplicate. Statistical comparisons were made using One-way ANOVA followed by the Dunnett's multiple comparisons test [*$p < 0.05$; **$p < 0.01$*; versus* control cells (0 µM)]. In all cases, p values < 0.05 were considered significant.

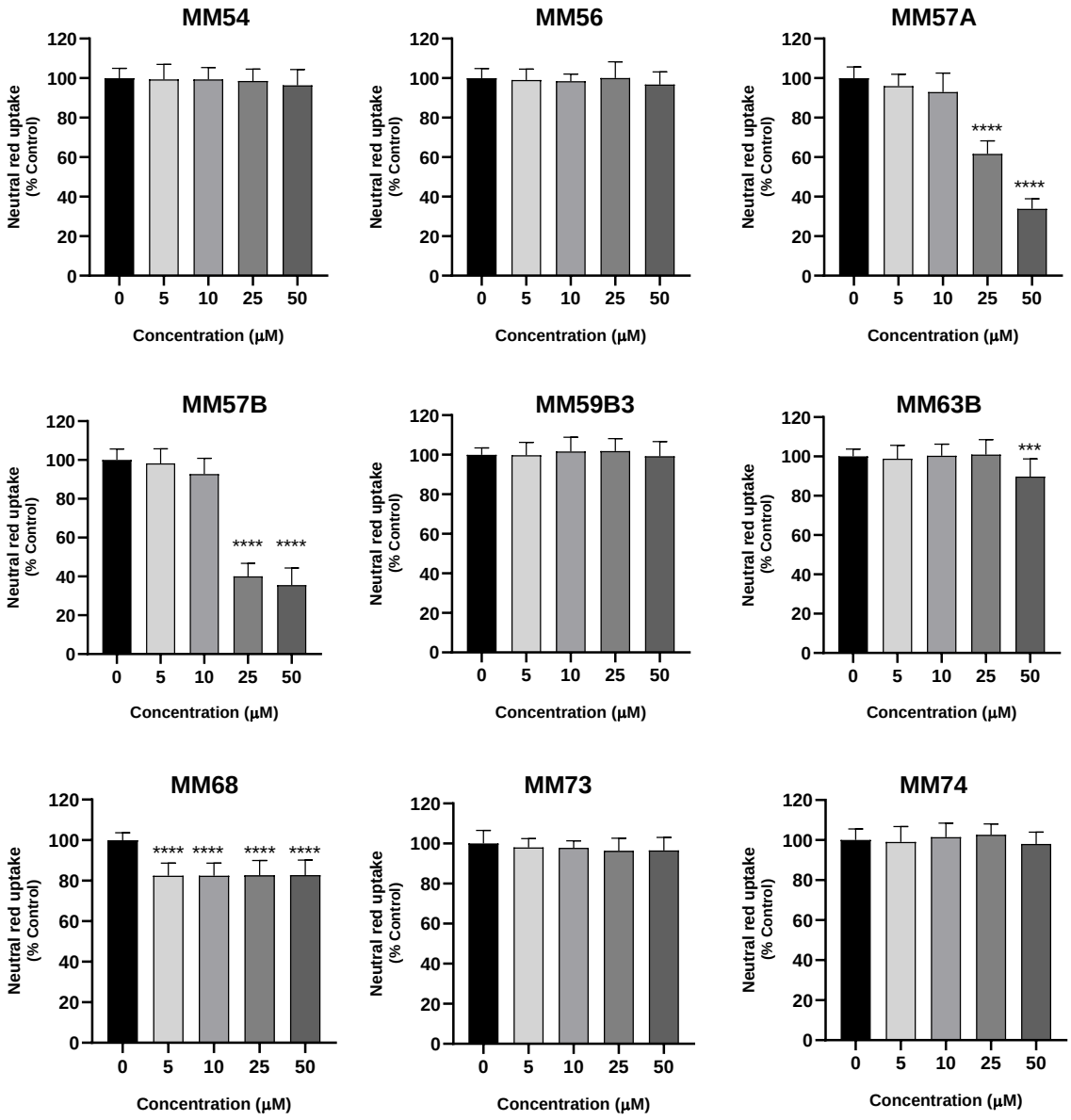

Figure 39. Cytotoxicity evaluation of compounds **MM54**, **MM56**, **MM57A**, **MM57B**, **MM59B3**, **MM63B**, **MM68**, **MM73**, **MM74** at concentrations of 5 µM, 10 µM, 25 µM, and 50 µM with neutral red uptake assay. Results are expressed as mean + SD from five independent experiences, performed in triplicate. Statistical comparisons were made using One-way ANOVA followed by the Dunnett's multiple comparisons test [****p* < 0.001; *****p* < 0.0001 *versus* control cells (0 µM)]. In all cases, *p* values < 0.05 were considered significant.

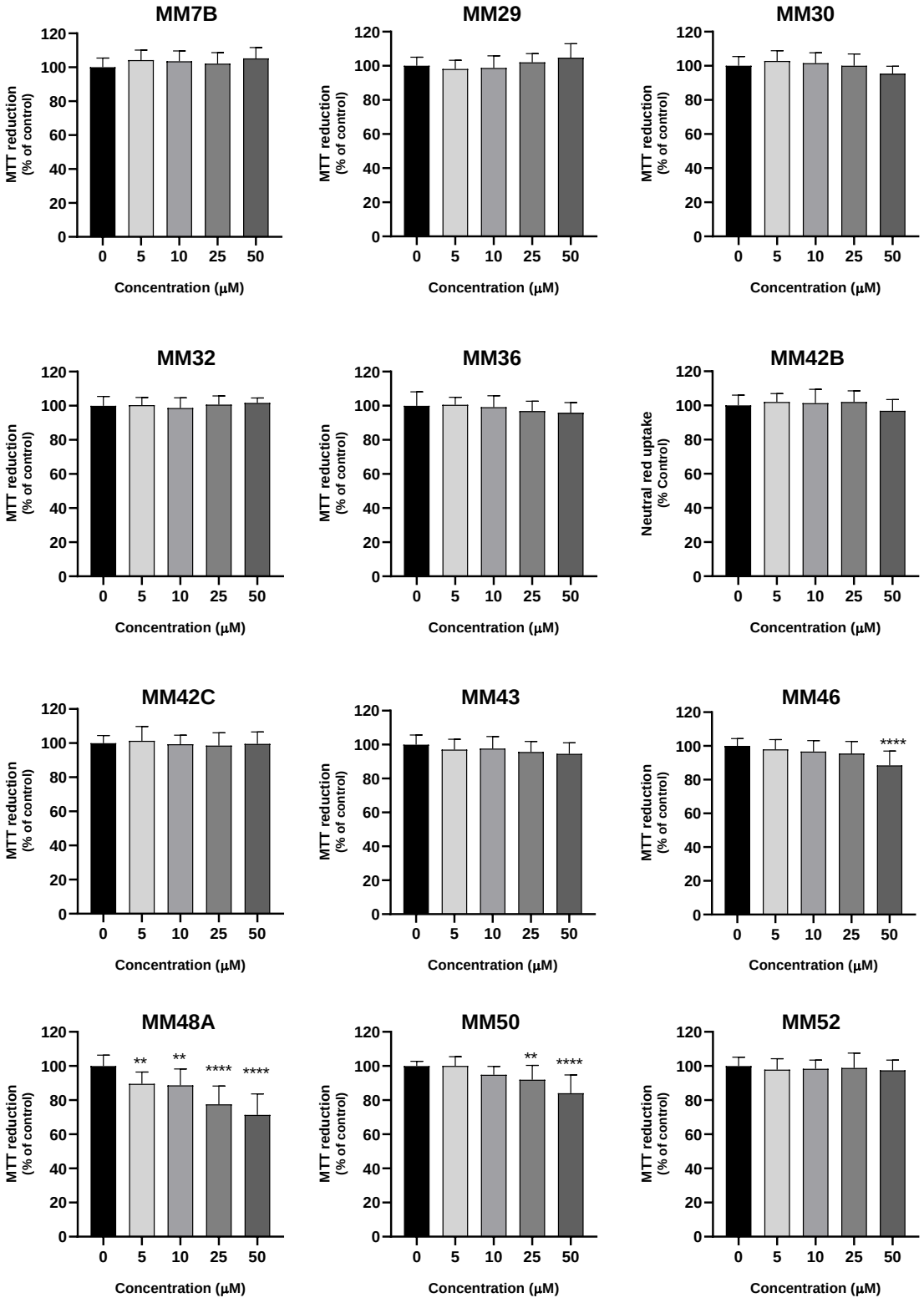

Figure 40. Cytotoxicity evaluation of compounds **MM7**, **MM29**, **MM30**, **MM32**, **MM36**, **MM42B**, **MM43**, **MM46**, **MM48A**, **MM50**, **MM52** at concentrations of 5 µM, 10 µM, 25 µM, and 50 µM with MTT assay. Results are expressed as mean + SD from five independent experiences, performed in triplicate. Statistical comparisons were made using One-way ANOVA followed by the Dunnett's multiple comparisons test [**p < 0.01; ****p < 0.0001 *versus* control cells (0 µM)]. In all cases, p values < 0.05 were considered significant.

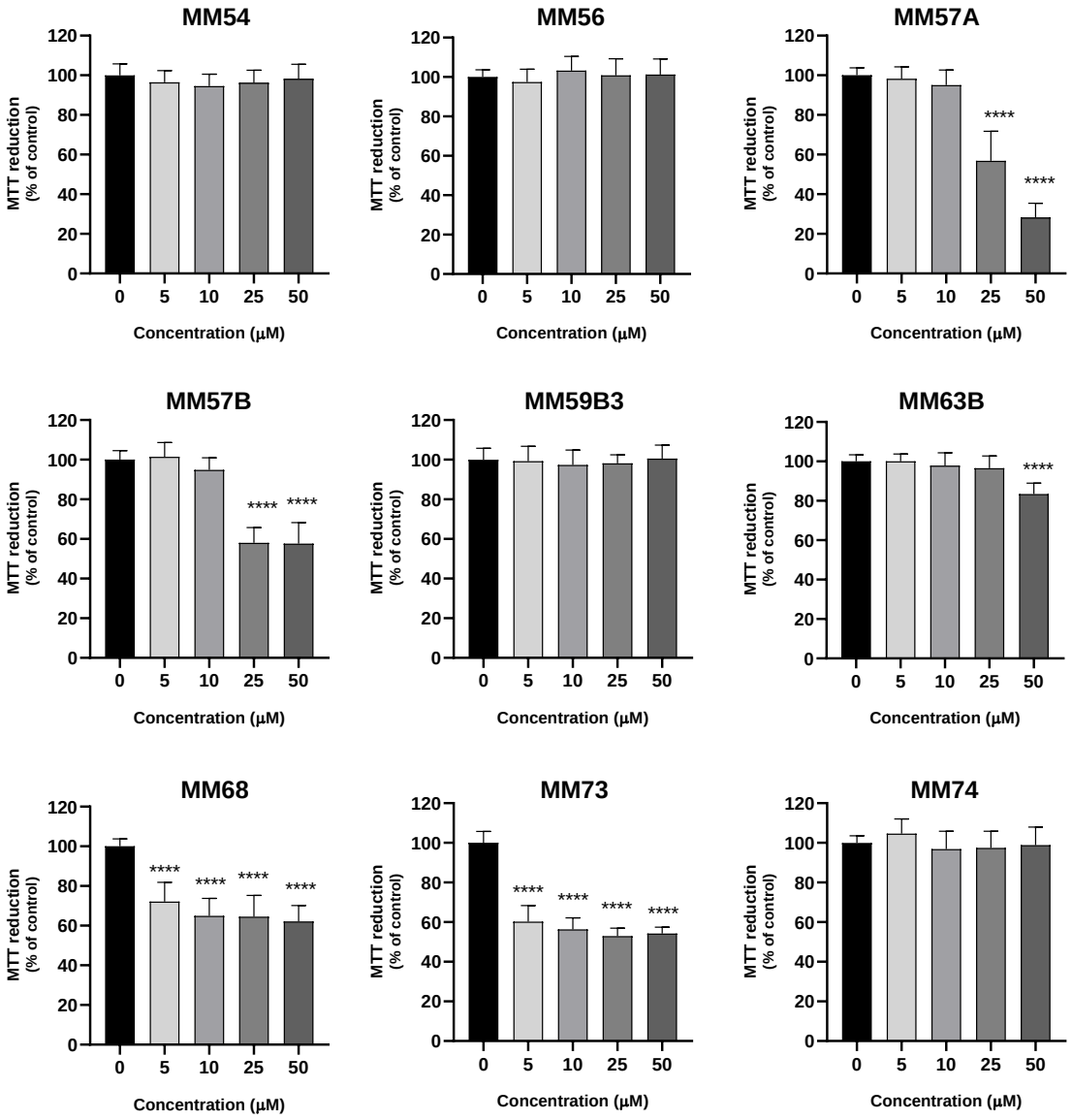

Figure 41. Cytotoxicity evaluation of compounds **MM54**, **MM56**, **MM57A**, **MM57B**, **MM59B3**, **MM63B**, **MM68**, **MM73**, **MM74** at concentrations of 5 μM, 10 μM, 25 μM, and 50 μM with MTT assay. Results are expressed as mean + SD from five independent experiences, performed in triplicate. Statistical comparisons were made using One-way ANOVA followed by the Dunnett's multiple comparisons test [****p < 0.0001 *versus* control cells (0 μM)]. In all cases, p values < 0.05 were considered significant.

In general, xanthene derivatives tested showed to be well tolerated in both the cytotoxicity assays performed in a concentration up to 50 μM. As exceptions, it was observed that compounds **MM42B**, **MM46**, and **MM63B** showed toxicity in the highest concentration tested of 50 μM. Compounds **MM48A**, **MM57A**, and **MM57B** caused a cell viability decline when using a concentration equal or above 25 μM. Lastly, compounds **MM68** and **MM73** showed cytotoxicity at the minimum concentration tested of 5 μM. For this reason, these two compounds did not proceed for further evaluation on neuroprotection studies. It is

observed that the five compounds that showed toxicity at a concentration ≤ 25 μM are halogenated, indicating a potential correlation between the presence of a halogen and their cytotoxicity.

3.3.2. Modulation of P-gp

To evaluate the effect of the tested compounds on P-gp transport activity, rhodamine 123 (RHO 123) (5.0 μM) accumulation, in the presence of the tested compounds (0 – 25 μM) and in the presence or absence of ZOS (5 μM), a specific third generation P-gp inhibitor, was evaluated for 90 min using 10 μM of RA differentiated SH-SY5Y cells [222, 223].

The activation was evaluated by the ratio between the amount of RHO 123 accumulated under inhibition conditions (ZOS, 5μM) and the amount of accumulated RHO 123 in the absence of the P-gp inhibitor [192, 223]

The P-gp activity, expressed as percentage of control cells (0 μM), was calculated through the ratio of fluorescence intensity of RHO 123 accumulation under P-gp inhibition (FI_{IA}) and fluorescence intensity of RHO 123 accumulation under normal condition (FI_{NA}). When P-gp is activated by the tested compound, the amount of RHO 123 being pump out the cells increases, decreasing the fluorescence intensity due to a lower RHO 123 intracellular content. In the presence of a P-gp inhibitor, RHO 123 intracellular content increases leading to a higher fluorescence intensity. Therefore, during the accumulation period of RHO 123, when P-gp is activated, a decrease in fluorescence intensity under normal conditions is detected, lowering RHO 123 accumulation. In contrast, when P-gp activity decreases, the ratio FI_{IA}/ FI_{NA} will be lower, due to a higher FI_{NA}.

Xanthene derivatives **MM7**, **MM29**, **MM30**, **MM32**, **MM36**, **MM42B**, **MM42C**, **MM43**, **MM46**, **MM48A**, **MM50**, **MM52**, **MM54**, **MM56**, **MM57A**, **MM57B**, **MM59B3**, **MM63B** and **MM74** were studied regarding their capacity to modulate P-gp activity. The concentrations tested were 10 μM and 25 μM, excepting for compounds **MM48A**, **MM57A** and **MM57B**, where only the 10μM concentration was tested, once higher concentrations showed cell decline in the cytotoxicity tests. **Figure 42** and **Figure 43** resume the results obtained.

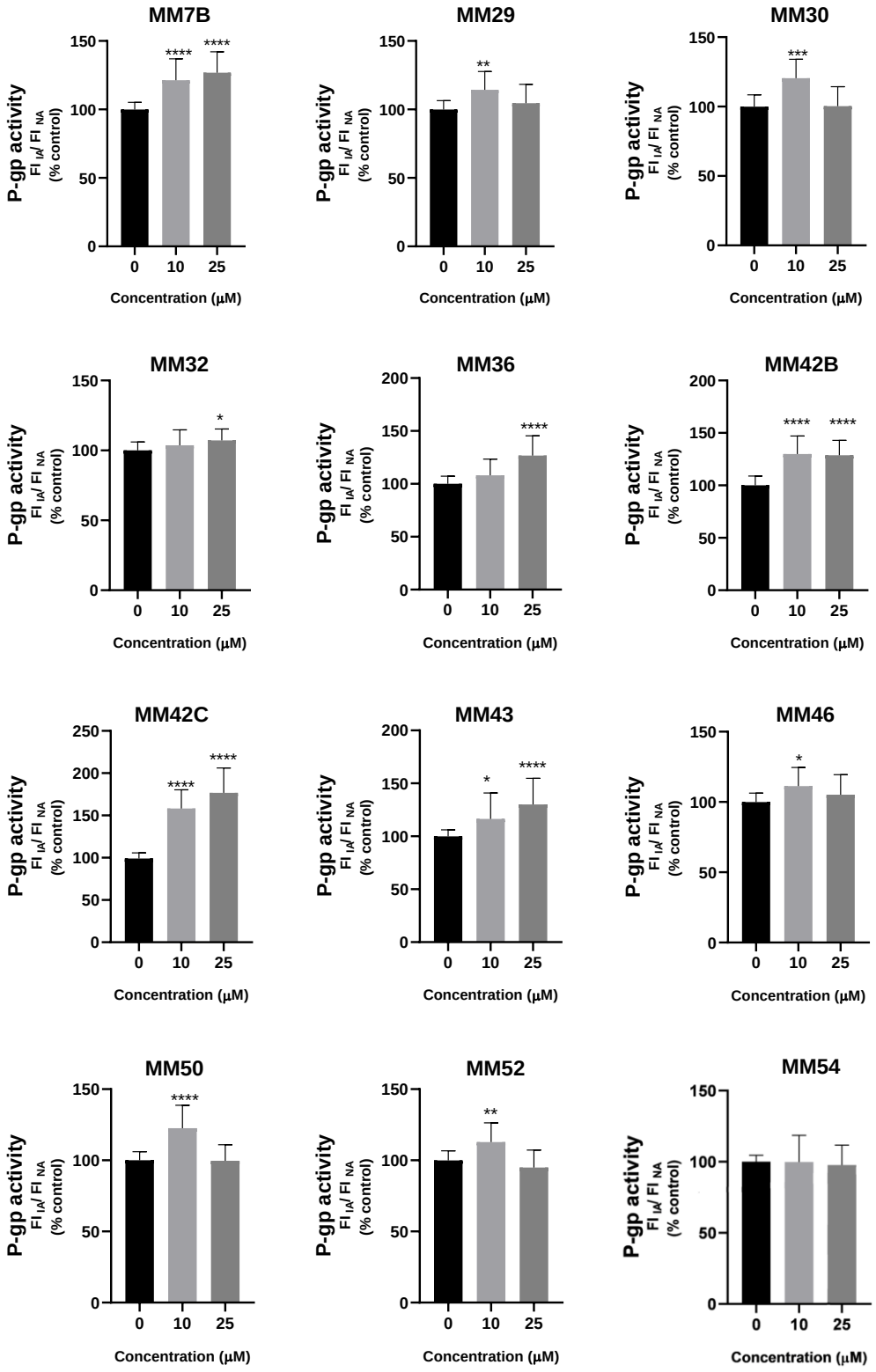

Figure 42. Modulation of P-gp activity by compounds **MM7B**, **MM29**, **MM30**, **MM32**, **MM36**, **MM42B**, **MM42C**, **MM43**, **MM46**, **MM50**, **MM52** and **MM52** at concentrations of 10 μM and 25 μM. Results are expressed as mean + SD from five independent experiences, performed in triplicate. Statistical comparisons were made using One-way ANOVA followed by the Dunnett's multiple comparisons test [*p < 0.05; **p < 0.01; ***p < 0.001; ****p < 0.0001 *versus* control cells (0 μM)]. In all cases, p values < 0.05 were considered significant.

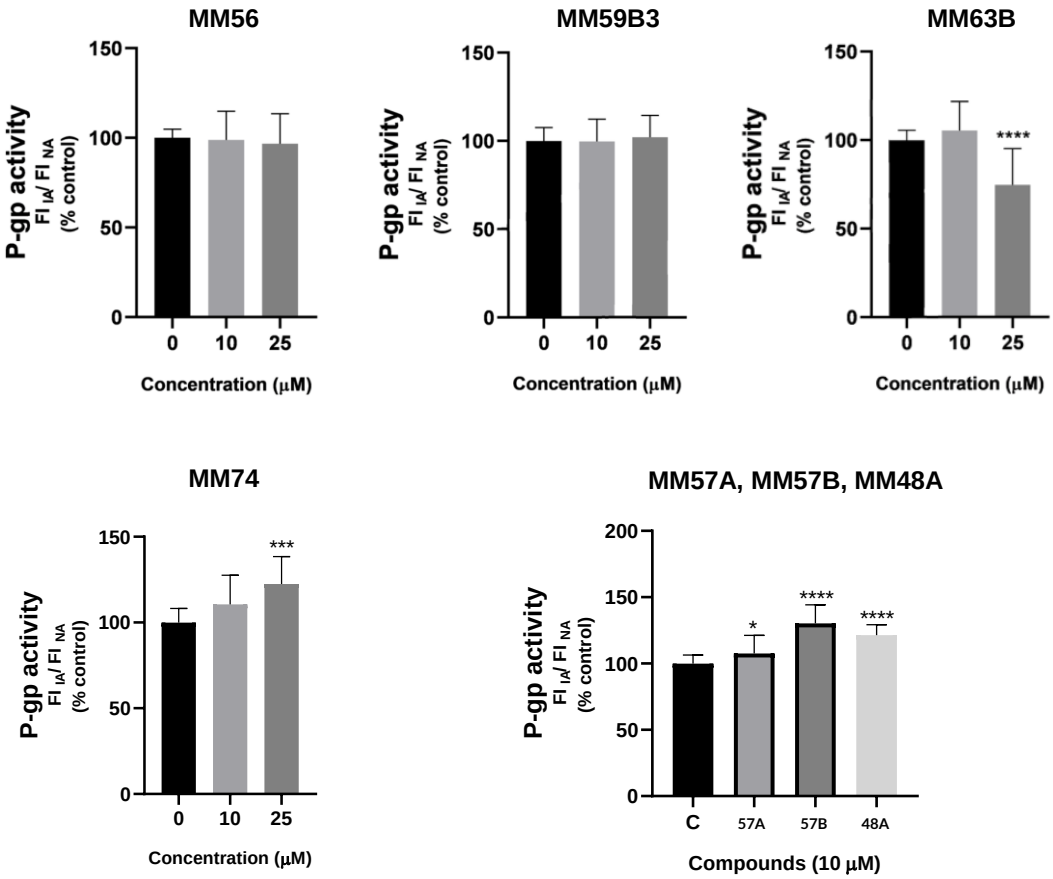

Figure 43. Modulation of P-gp activity by compounds **MM56**, **MM59B3**, **MM63B** and **MM74** at concentrations of 10 μM and 25 μM. For compounds **MM57A**, **MM57B** and **MM48A** only the 10μM concentration was tested. Results are expressed as mean + SD from five independent experiences, performed in triplicate. Statistical comparisons were made using One-way ANOVA followed by the Dunnett's multiple comparisons test [*p < 0.05; ***p < 0.001; ****p < 0.0001 *versus* control cells (0 μM)]. In all cases, p values < 0.05 were considered significant.

Compounds **MM7B**, **MM29**, **MM30**, **MM32**, **MM36**, **MM42B**, **MM42C**, **MM43**, **MM46**, **MM50**, **MM52**, **MM48A**, **MM57A**, **MM57B** and **MM74** showed activation of P-gp activity at least at one of the concentrations tested after 90 min of exposure and when compared to the control cells (0 μM, 100 %). On the other hand, compounds **MM54**, **MM56** and **MM59B3** showed no effect on P-gp activity, and compound **MM63B** showed no activity at a concentration of 10 μM and showed an inhibition activity on P-gp at a concentration of 25 μM.

Compounds **MM7**, **MM36**, **MM42C**, **MM43** and **MM74** showed the most significant and concentration-dependent increase of P-gp activity. These four compounds possess different substituents in position 9: compound **MM7** comprises a free amine, in position *para* to the xanthene moiety, while compound **MM42C**, also possessing a free amine, is an amide comprising a pyrazole ring from one side and the xanthene moiety on the other side. **MM43** is a xanthene carboxamide derived from 3-amino-propanol, while **MM74** is a di-bromo

xanthene carboxamide, derived from diethanolamine with 2,7-dibromo-9*H*-xanthene-9-carboxylic acid. Hence, focus on the most promising compounds for P-gp activation, it was observed that a heterogeneity of functional groups at position 9 of the xanthene moiety were able to activate this transporter. Comparing the results obtained for **MM42C** and **MM57B**, differing only on the absence/ presence, respectively, of the halogen bromo in positions 2,7 of the aromatic rings, it was observed that the halogen is prejudicial for P-gp activation.

The modulation of P-gp activity through the administration of P-gp activators is a therapeutic strategy based on the immediate increase of P-gp activity without interfering with the expression of the efflux pump, allowing a quick and time-limited reduction of the intracellular concentration of potential harmful P-gp substrates [224]. As already mentioned, the impact of tricyclic compounds on P-gp activity have been assessed in different studies [192-194, 206]. In the screening of five thioxanthonic derivatives as possible inducers of P-gp expression and/ or activity [193], a pharmacophore to predict new ligands for P-gp activation was built based on the thioxanthones *in vitro* activity, as well as other molecules previously described as P-gp activators. The best ranked pharmacophore found is composed of three features: one hydrophobic feature, one aromatic ring and one hydrogen bond acceptor group. These three features are observed in all the twenty-two xanthene derivatives tested, which can justify that most of the compounds led to a significant increase in P-gp activity. Hence, the xanthene core proved to be a good scaffold for P-gp activation, namely in the presence of the amide or amine functional groups in position 9.

3.3.3. Neuroprotective effects against iron (III)-induced cytotoxicity

Iron displays several crucial roles in healthy brain functions. Nevertheless, when its homeostasis is disrupted and iron levels are abnormally increased, oxidative stress and cell death can be triggered. Iron may induce oxidative stress due to its central role in reactive oxygen species (ROS) generation, and, consequently, leading to cellular dysfunction or even cellular death [225]. The importance of iron-induced toxicity has been supported by the protective effects demonstrated by iron chelators observed in cell culture models used to study neurodegenerative diseases, such as the SH-SY5Y cell line. Iron has already been implicated in the pathology of several ND, including Parkinson's disease (PD) and Alzheimer´s disease [225-229].

Therefore, considering the prevention of iron-induced cytotoxicity as a potential strategy for neuroprotection, the xanthene derivatives herein described were assessed regarding their ability to protect cells against iron-induced cytotoxicity.

For the experimental studies, iron (III) in the form of the complex ferric nitrilotriacetate (FeNTA) was used, to prevent iron (III) from hydrolysis at physiological pH and allowing its cellular uptake, where it will act as a pro-oxidant through the generation of oxidative stress [230, 231].

Xanthene derivatives **MM7**, **MM29**, **MM30**, **MM32**, **MM36**, **MM42B**, **MM42C**, **MM43**, **MM46**, **MM48A**, **MM50**, **MM52**, **MM54**, **MM56**, **MM57A**, **MM57B**, **MM59B3**, **MM63B**, and **MM74** were studied regarding their activity against FeNTA-induced cytotoxicity at concentrations of 10 µM and 25 µM, except for compounds **MM48A**, **MM57A** and **MM57B**, where only the 10 µM concentration was used. **Figure 44** – **Figure 46** resume the results obtained.

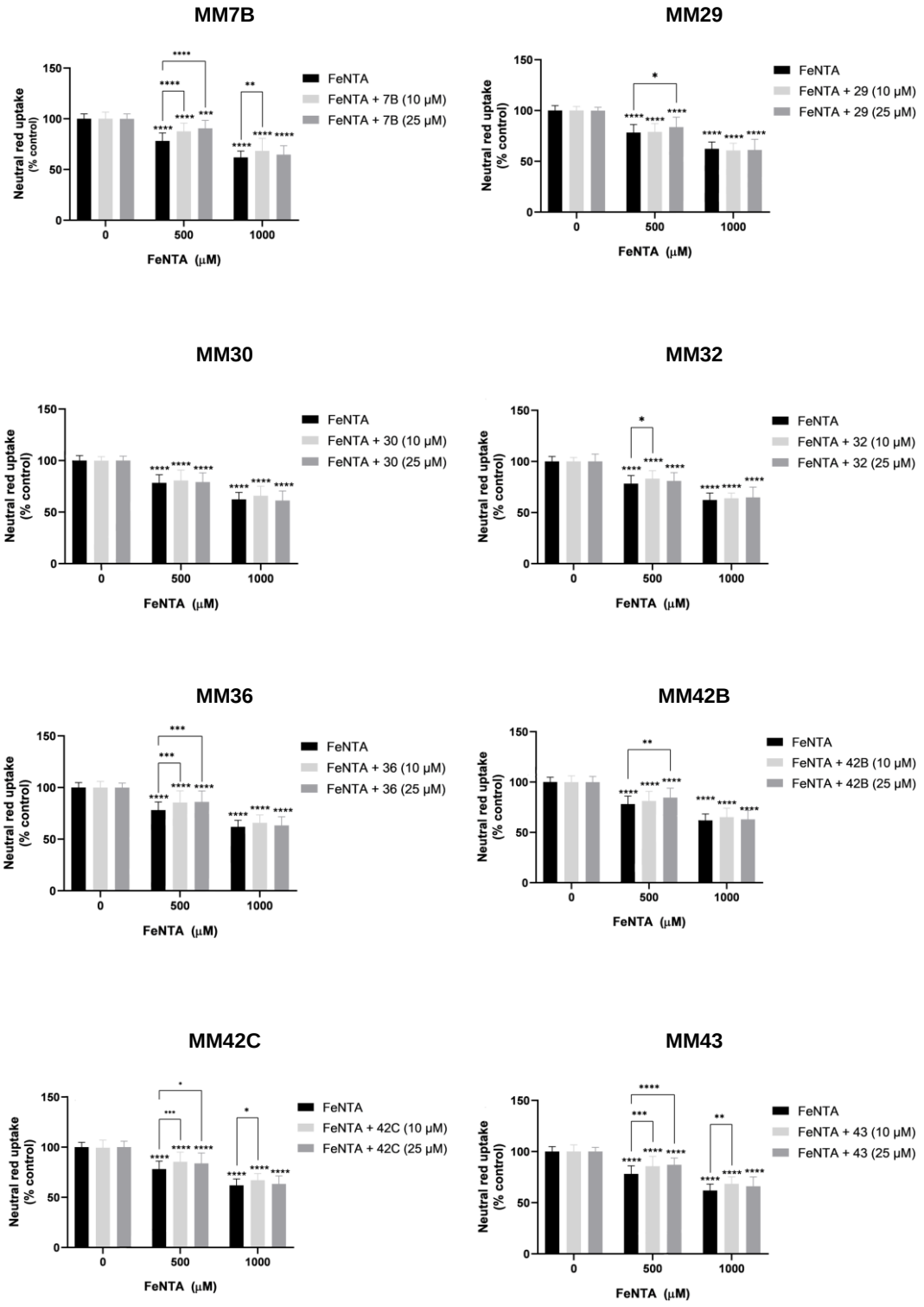

Figure 44. FeNTA (500 and 1000 μM) cytotoxicity towards RA differentiated SH-SY5Y cells, in the presence or absence of the tested compounds **MM7B**, **MM29**, **MM30**, **MM32**, **MM36**, **MM42B**, **MM42C**, **MM43**(10 and 25 μM), evaluated by the neutral red uptake assay, 24 h after exposure. Results are presented as mean + SD from five independent experiments, performed in triplicate. Statistical comparisons were made using Two-way ANOVA, followed by the Tukey's multiple comparisons test (*p < 0.05; **p < 0.01; ***p < 0.001; ****p < 0.0001 *versus* FeNTA alone, at each FeNTA concentration).

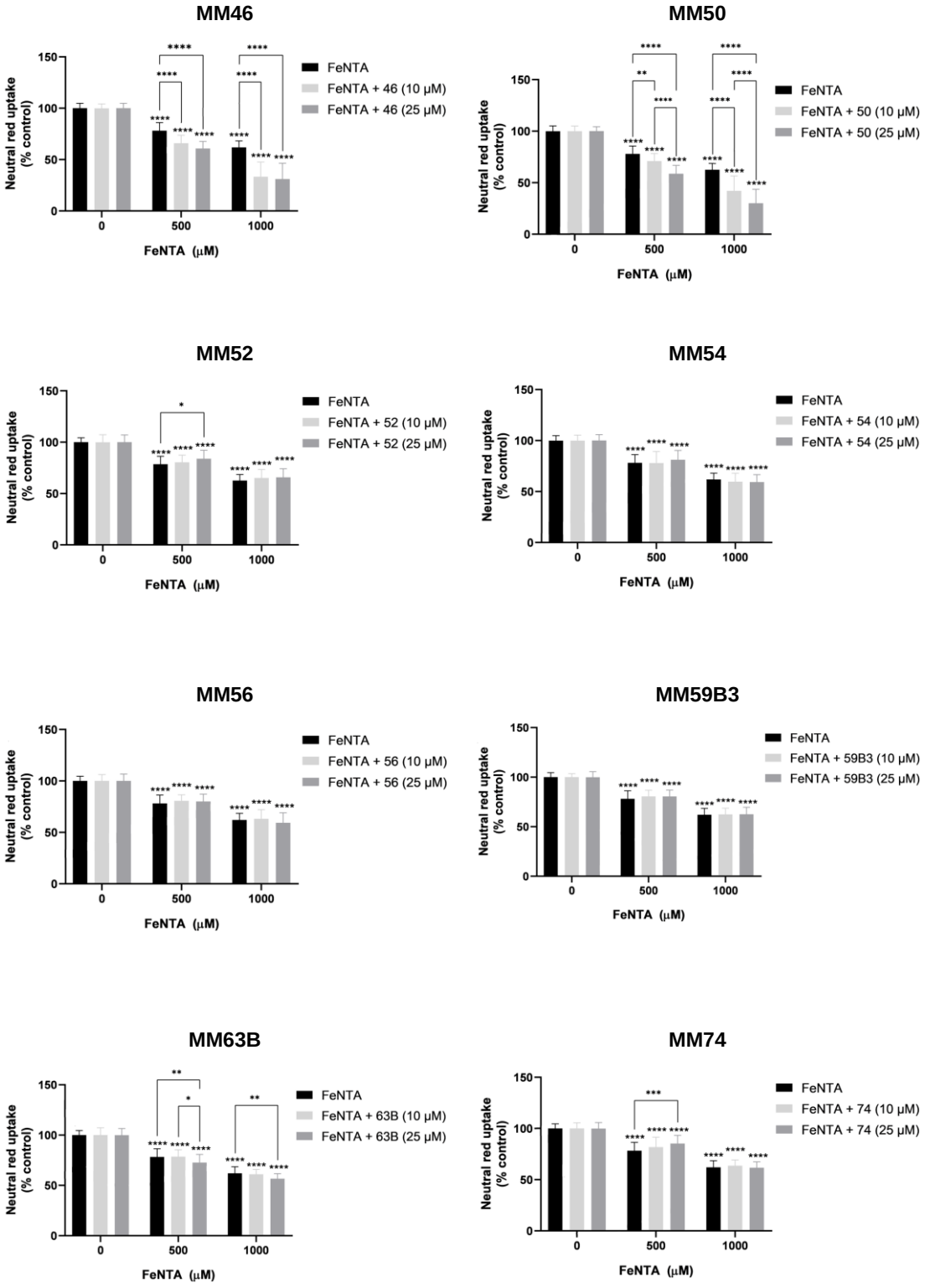

Figure 45. FeNTA (500 and 1000 µM) cytotoxicity towards RA differentiated SH-SY5Y cells, in the presence or absence of the tested compounds **MM46**, **MM50**, **MM52**, **MM54**, **MM56**, **MM59B3**, **MM63B**, **MM74** (10 and 25 µM), evaluated by the neutral red uptake assay, 24 h after exposure. Results are presented as mean + SD from five independent experiments, performed in triplicate. Statistical comparisons were made using Two-way ANOVA, followed by the Tukey's multiple comparisons test (*p < 0.05; **p < 0.01; ***p < 0.001; ****p < 0.0001 *versus* FeNTA alone, at each FeNTA concentration).

MM48A, MM57A, MM57B

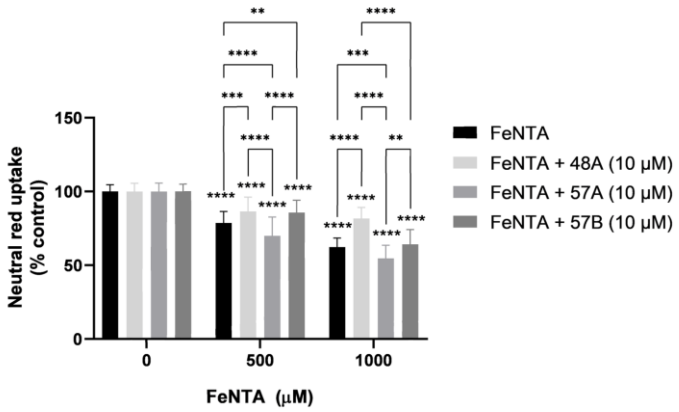

Figure 46. FeNTA (500 and 1000 µM) cytotoxicity towards RA differentiated SH-SY5Y cells, in the presence or absence of the tested compounds **MM48A**, **MM57A** and **MM57B** (10 µM), evaluated by the neutral red uptake assay, 24 h after exposure. Results are presented as mean + SD from five independent experiments, performed in triplicate. Statistical comparisons were made using Two-way ANOVA, followed by the Tukey's multiple comparisons test (**p* < 0.05; ***p* < 0.01; ****p* < 0.001; *****p* < 0.0001 *versus*. FeNTA alone, at each FeNTA concentration).

Compounds **MM7B**, **MM29**, **MM32**, **MM36**, **MM42B**, **MM42C**, **MM43**, **MM48A**, **MM52**, **MM57B** and **MM74** demonstrated potential protection against iron (III)-induced cytotoxicity at least at one of the concentrations tested in the presence of 500µM or 1000 µM of FeNTA.

Compound **MM7B** provided the most interesting results, where the neutral red uptake significantly increased from 78 % (cell viability of FeNTA alone in the concentration of 500 µM) to 88 % and 91 % in the presence of 10 µM and 25 µM of MM7B, respectively. The neuroprotective effect was also observed when used a concentration of FeNTA of 1000 µM.

MM36, **MM42C, MM43** and **MM48A** also showed to provide relevant neuroprotective effect, where it was observed an increase in cell viability in the presence of 10 µM of the compound, comparing with the cell viability of FeNTA alone in the concentration of 500 µM.

On the other hand, compounds **MM46**, **MM50** and **MM57A**, significantly increased FeNTA-induced cytotoxicity. A decreased in cell viability for compound **MM46**, when compared with the obtained results for the neutral red uptake assay of FeNTA alone, was observed at both concentrations of FeNTA used (500 µM and 1000 µM). The cell viability decreased from 78 % (FeNTA alone) to 66 % and 61 % when 10 µM and 25 µM of compound **MM46** were present, respectively, with 500 µM of FeNTA. In the presence of 1000 µM of FeNTA, the cell viability decreased from 62% (FENTA alone) to 33 % and 31 %. Similar results were found for compound **MM50**. Compound **MM57A** led to a more modest decrease, from 78 % (FeNTA alone) to 70 % when 10 µM of compound was present with 500 µM of FeNTA,

and from 62 % (FeNTA alone) to 55 % when 10 μM of compound was present with 1000 μM of FeNTA.

Lastly, compounds **MM30**, **MM54**, **MM56** and **MM59B3** showed no significant effects on the FeNTA-induced cytotoxicity test, at both tested concentrations (10 μM and 25 μM) suggesting that these compounds are absent of neuroprotective properties against iron (III)-induced cytotoxicity, and also do not increase the cytotoxicity associated with FeNTA.

According with the results depicted above, some considerations can be made regarding the SAR of the compounds tested. Comparing the unsatisfactory results obtained with compounds **MM46** and **MM50** – amines obtained through the reduction of amides **MM36** and **MM30**, respectively, the amide group at position 9 of the xanthene seems to be important for the compound's neuroprotection against iron (III)-induced cytotoxicity, and the presence of a tertiary amine leads to obtaining compounds able to increase FeNTA-induced cytotoxicity. Additionally, when comparing the results obtained with the non-brominated compounds **MM32, MM52** and **MM42B** with the corresponding di-brominated derivatives **MM56**, **MM54** and **MM57A**, respectively, the presence of bromine at positions 2,7 of the xanthene moiety seems to have a detrimental effect.
The results obtained regarding the neuroprotective effects of the compounds against iron (III)-induced cytotoxicity can be related with different mechanisms, namely the potential ability of the compounds to chelate iron, decreasing the available concentration of the aggressor agent causing cell damage, or through the elimination of free radicals, being necessary to perform additional studies to understand their mechanism of action. Hence, an assay was performed to evaluate the iron-chelating ability of the compounds that demonstrated potential protection against iron (III)-induced cytotoxicity.

Iron-chelating effects

The interaction of the synthetized compounds with ferric ions was evaluated based on changes in the UV/Vis spectra of the tricyclic derivatives, following the addition of $FeCl_3$ (0 – 1320 μM) (**Figure 47**). The presence of a compound able to chelate Fe(III) is associated with a change of the absorbance spectrum with bathochromic shifts from the original band [232, 233].

Testing the compounds that demonstrated potential protection against iron (III)-induced cytotoxicity – compounds **MM7B**, **MM29**, **MM32**, **MM36**, **MM42B**, **MM42C**, **MM43**, **MM48A**, **MM52**, **MM57B** and **MM74** – it was observed that the sequential additions of $FeCl_3$ solution resulted only in small hyperchromic effects and no bathochromic effects of the absorbance

spectrum from the original band were detected (**Figure 47**). Analysing the chemical structure of the compounds tested, the results obtained are in accordance with the expected, considering that none of the compounds possesses important groups for Fe(III) accommodation, such as catecholate, hydroxamate, or hydroxyacid [234, 235]. Hence, further studies should be performed in order to assess the potential mechanism involved in the protection effect observed with the compounds tested.

MM7B

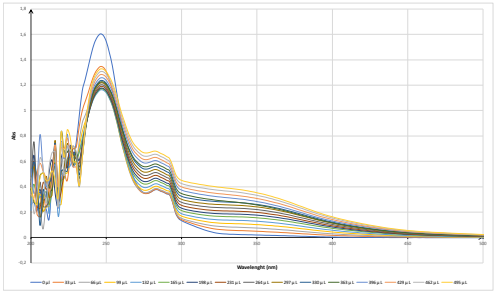

MM29

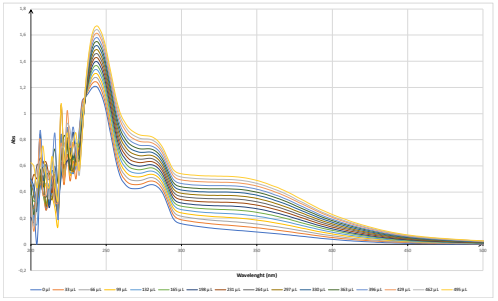

MM32

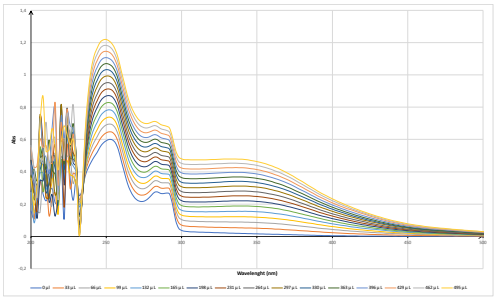

MM36

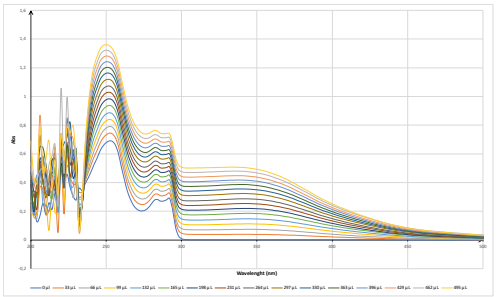

MM42B

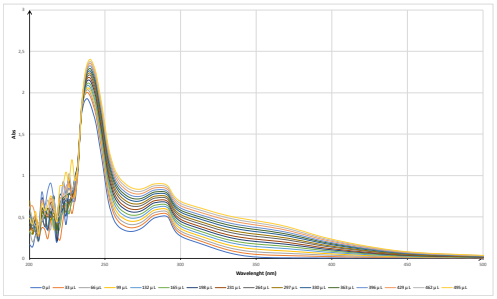

MM42C

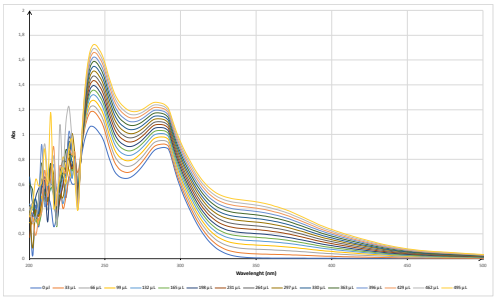

MM43

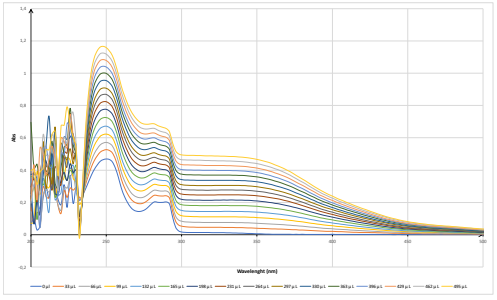

MM48A

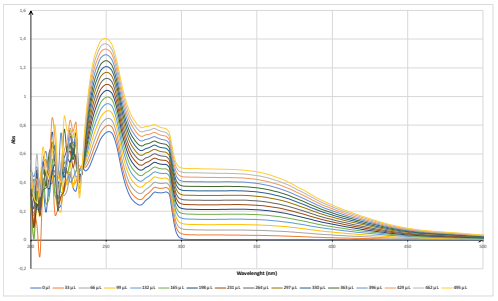

Figure 47. UV/Vis spectra of compounds **MM7B**, **MM29**, **MM32**, **MM36**, **MM42B**, **MM42C**, **MM43**, **MM48A**, **MM52**, **MM57B** and **MM74** in methanolic solution with 1 % of DMSO with sequential additions of $FeCl_3$.

MM52

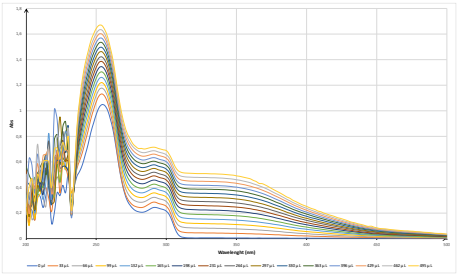

MM57B

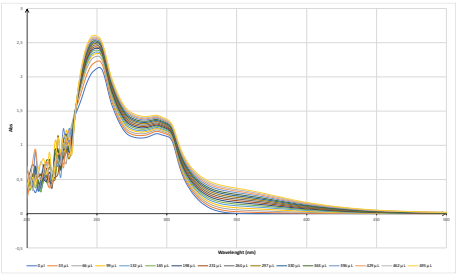

MM74

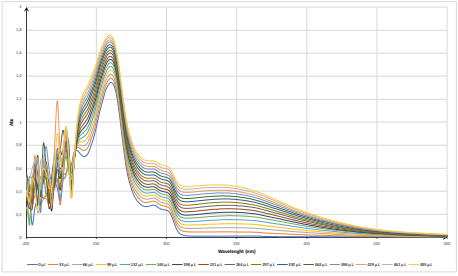

Figure 47. *Cont.*

3.3.4. CNS penetration: *in vitro* parallel artificial membrane permeability assay (PAMPA)-BBB.

One of the main obstacles in the development of drugs aiming for CNS disease is their capacity to penetrate BBB at therapeutic concentrations. The BBB is a very complex interface between blood and the CNS that controls the exchanges between these two compartments [236]. This barrier is composed by endothelial cells with tight junctions that protect the brain from endogenous materials which could damage the brain tissues [237]. Most of the CNS drugs achieve the brain by transcellular passive diffusion, due to the tight junction structure and limited transport pathways. Parallel Artificial Membrane Permeability Assay (PAMPA) is a high throughput technique developed to predict passive permeability through biological membranes. In order to explore the capacity of the preliminary synthetized series of compounds, **MM32, MM42B, MM46, MM48A, MM50, MM57A, MM59B3, MM63B and MM68**, to penetrate into the brain, it was used the PAMPA-BBB method described by Di *et al*. [238], which employed a brain lipid porcine membrane. The *in vitro* permeabilities (*Pe*) of commercial drugs through lipid membrane extract together with compounds **MM32, MM42B, MM46, MM48A, MM50, MM57A, MM59B3, MM63B** and **MM68,** were determined and described in **Table 9**. An assay validation was made comparing the reported permeabilities values of commercial drugs with the experimental

data obtained employing this methodology. A good correlation between experimental-described values was obtained *Pe* (exptl) = 0.9285 (bibl) – 0.942 (R2= 0.9504) (**Figure 48**). From this equation and following the pattern established in the literature for BBB permeation prediction [239] we could classify compounds as CNS + when they present a permeability > 2.77 x 10^{-6} cm/s. **Table 9** resumes the results obtained. It was observed that compounds **MM32, MM42B, MM57A** and **MM63B** are able to cross the BBB by passive permeation (CNS +). Compounds **MM46 and MM59B3** are in the shadow area and could cross or not by passive permeation (CNS+/CNS-) Compounds **MM48A, MM50** and **MM68,** were not soluble in the assay buffer so BBB permeation could not be determined (N.D).

Table 9. Permeability (Pe 10^{-6} cm s^{-1}) in the PAMPA-BBB assay for 10 commercial drugs (used in the experiment validation) and **MM32, MM42B, MM46, MM57A, MM59B3**, and **MM63B** with their predictive penetration in the CNS.[a]

Compound	Bibliography[b]	*Pe* (10^{-6} cm s^{-1})[c]	Prediction
Atenolol	0.8	0.1 ± 0.6	N/A
Caffeine	1.3	0.7 ± 0.8	N/A
Desipramine	12	7.4 ± 2.4	N/A
Enoxacin	0.9	0.3 ± 0.2	N/A
Hydrocortisone	1.9	0.6 ± 0.6	N/A
Ofloxacin	0.8	0.4 ± 0.4	N/A
Piroxicam	2.5	1.0 ± 0.1	N/A
Promazine	8.8	6.8 ± 2.1	N/A
Testosterone	17	17.7 ± 1.3	N/A
Verapamil	16	13.2 ± 1.6	N/A
MM32	N/A	23.3 ± 2.0	CNS +
MM42B	N/A	10.6 ± 1.3	CNS +
MM46	N/A	0.9 ± 0.3	CNS +/ CNS-
MM57A	N/A	7.4 ± 0.5	CNS +
MM59B3	N/A	1.9 ± 0.3	CNS +/ CNS-
MM63B	N/A	4.4 ± 0.8	CNS +

[a] PBS:EtOH (70:30) was used as solvent. [b] Reference Di *et al.* [c] Data are the mean ± SD of 2 independent experiments.

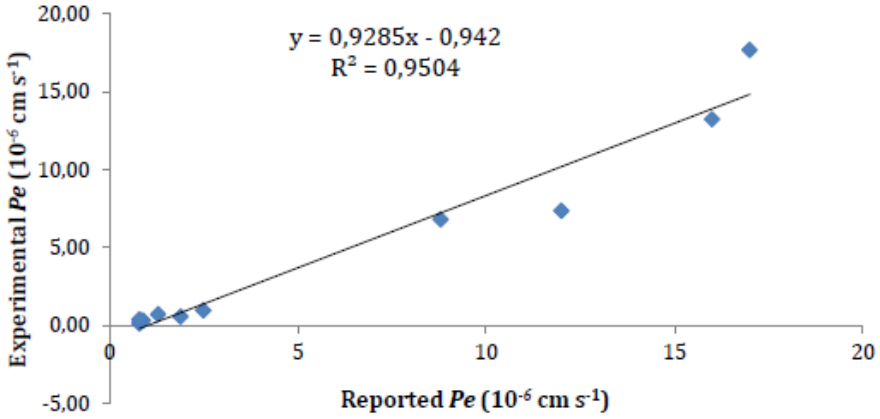

Figure 48. Linear correlation between experimental and reported permeability of commercial drugs using the PAMPA-BBB assay.

For the compounds that showed able to activate P-gp and not evaluated through the PAMPA assay, an *in silico* assessment was performed in order to predict their permeation through the BBB. SwissADME [105], a free available software used to predict physicochemical and pharmacokinetic properties, was used to assess *in silico* BBB permeation and associated parameters of compounds **MM7B**, **MM29**, **MM30, MM36**, **MM42C**, **MM43**, , **MM48A**, **MM50**, **MM52**, **MM54** and **MM57B**. **Table 10** resumes the results obtained.

All the compounds assessed through SwissADME platform showed potential for BBB permeation, according to the yolk of the BOILED-Egg [110]. Additionally, these compounds were assessed considering additional attributes generally considered when designing drugs for CNS, as described by Hassan Pajouhesh and George R. Lenz [240]. Generally, all the compounds comply with the six parameters assessed. MM57B possesses a molecular weight slightly above the reference limit; nonetheless, these specifications should be seen as guidance and evaluated together, and so a singular value out of the reference range should not be seen as limitant.

These results are in line with other tricyclic compounds, including drugs approved for clinical use. One of the first group of antidepressants were the tricyclic antidepressants, which are in use for many years for the treatment of CNS disorders [241, 242]. Xanthene derivatives have also shown to penetrate BBB in *in vitro* and *in vivo* assays and successfully impact different biological pathways of the CNS [12, 54, 243].

Table 10. Prediction of BBB permeation with SwissADME platform [105].

Compound	BBB permeant[a]	Molecular weight (g/mol)	Consensus logP[b]	H-bond donors	H-bond acceptors	Rotatable bonds	TPSA[c] (Å²)
Rules for CNS drugs [240]	**-**	**<450**	**<5**	**<3**	**<7**	**<8**	**<70**
MM7B	yes	273.33	3.86	1	1	1	35
MM29	yes	212.24	2.64	1	2	1	29
MM30	yes	293.36	3.15	0	2	2	30
MM36	yes	281.36	3.5	0	3	3	30
MM42C	yes	305.34	3.18	2	5	1	70
MM43	yes	283.32	2.15	2	3	5	59
MM48A	yes	349.81	3.45	1	2	4	38
MM50	yes	279.38	3.27	0	2	2	12
MM52	yes	295.12	2.47	1	3	1	47
MM54	yes	384.02	2.69	1	3	1	47
MM57B	yes	463.12	3.42	1	3	2	70

[a] Brain permeation. According to the yolk of the BOILED-Egg [110]

[b] Average of five predicted models: XLOGP3 [118], WLOGP [119], MLOGP [120, 121], SILICOS-IT [122]and iLOGP [123]

[c] Topological polar surface area. Calculated from [117]

3.4. Conclusion

In summary, twenty 9-xanthenyl derivatives were synthetized involving four distinctive steps: aromatic halogenation, amide coupling, amide reduction, and Suzuki coupling. In generally, the synthesis strategies employed showed to be suitable for the obtention of the compounds required. For the amide coupling reaction, COMU proved to be an adequate coupling agent for the generally of the amines used. Nonetheless, when diethanolamine and *N*-Boc-1,6-hexanediamine were used as nucleophiles, COMU provided unsatisfactory results; for these two amines, the amide coupling *via in situ* formation of acyl fluoride showed to be adequate.

The compounds obtained were assessed regarding their cytotoxicity, BBB penetration, P- gp activation and protection against iron-induced toxicity. In generally, the xanthene derivatives tested showed to be well tolerated in both the cytotoxicity assays performed in a concentration up to 50 µM. Regarding their ability on P-gp activation, a highlight is made for compounds **MM7**, **MM36**, **MM42C**, **MM43 and MM74**, which showed the most significant and concentration-dependent increase of P-gp activity. These five compounds also showed to provide protection against iron-induced cytotoxicity. Additionally, *in silico* predictions showed their potential to penetrate the BBB and reach CNS, which is a crucial factor to allow for their biological activity. Nonetheless, *in vitro* studies are warranted to confirm their BBB penetration. Further studies on the most potent compound (**MM42C**), comprising different functionalization of the xanthene tricyclic and different length of the chain connecting with the 1*H*-pyrazol-3-amine ring will allow to explore derivatives and structure-P-gp activation activity relationship.

3.5. Experimental

3.5.1. Chemical synthesis and characterization

General information

All reagents and solvents were purchased from TCI (Tokyo Chemical Industry Co. Ltd., Chuo-ku, Tokyo, Japan), Acros Organics (Geel, Belgium), Sigma-Aldrich (Sigma-Aldrich Co. Ltd., UK), or Alfa Aesar (Thermo Fisher GmbH, Kandel, Germany) and were used directly without any further purification. All reactions were monitored by TLC, carried out on Merck silica gel 60 (GF254) precoated plates using with appropriate mobile phases. Purification of the synthesized compounds was usually performed by flash column chromatography using Merck silica gel 60 (0.040–0.063

mm). Melting points (mp) were measured by using a Köfler microscope (Wagner and Munz, Munich, Germany) equipped with a Crison TM 65 (Crison Instruments, Barcelona, Spain) and were uncorrected. ^{1}H and ^{13}C NMR spectra were taken in $CDCl_3$, [D_6]DMSO, methanol-d_4, acetone-d_6 or tetrahydrofuran-d_8 (Deutero GmbH, Kastellaun, Germany) at rt on Bruker Avance 300 instrument (300.13 or 500.16 MHz for ^{1}H and 75.47 or 125.77 MHz for ^{13}C, Bruker Biosciences Corporation, Billerica, MA, USA) or Bruker AVANCE III (400.14 MHz for ^{1}H and 100.62 MHz for ^{13}C). Chemical shifts are expressed in relative to tetramethylsilane (TMS) as an internal reference.^{13}C NMR assignments were made by 2D HSQC and HMBC experiments. For the assignment of each signal to the corresponding proton or carbon, it was considered the automatic numeration provided by MestReNova®, as provided in **Annex I**. HPLC Analysis (Purity determinations by HPLC analysis were performed with a system consisted of Shimadzu LC-20AD pump, equipped with a Shimadzu DGV-20A5 degasser, a Rheodyne 7725i injector fitted with a 20 µL loop, and a SPD-M20A DAD detector (Kyoto, Japan). Data acquisition was performed using Shimadzu LCMS Lab Solutions software, version 3.50 SP2. The column used in this study was ACE - C18 (150 × 4.6 mm I.D., particle size 5 µm) manufactured by Advanced Chromatography Technologies Ltd (Aberdeen, Scotland, UK). The mobile phase composition was water and methanol (85:15 *v/v*; 0.1 % AcOH), all were HPLC grade solvents obtained from Merck Life Science S.L.U. (Darmstadt, Germany). The flow rate was 1.0 mL/min and the UV detection wavelength was 254 nm. Analyses were performed at 27 °C in an isocratic mode in a 30 min run. Peak purity index was determined by total peak UV-Vis spectra between 210-800 nm with a step of 4 nm. High-resolution mass spectrometry (HRMS) was performed on an LTQ OrbitrapTM XL hybrid mass spectrometer (Thermo Fischer Scientific, Bremen, Germany) controlled by LTQ Tune Plus 2.5.5 and Xcalibur 2.1.0. at CEMUP— University of Porto, Portugal or in a electrospray ionization (ESI) mode in Centro de Apoio Cientifico e Tecnolóxico á Investigación (CACTI, University of Vigo, Pontevedra, Spain) and on a Q Exactive Focus Hybrid Quadrupole Orbitrap Mass Spectrometer (Thermo Fisher Scientific), controlled by Q Exactive Focus (Exactive Series) 2.9 and Thermo Scientific Xcalibur 4.1.31.9 software.

3.5.1.2. Synthesis, purification, and structural characterization

Synthesis of piperidin-1-yl(9*H*-xanthen-9-yl)methanone (MM30)

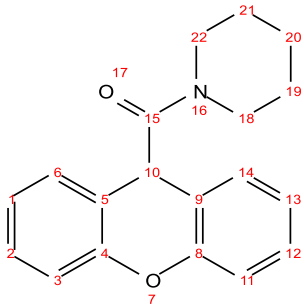

To a 25 mL round-bottom flask containing 5 mL of anhydrous CH_2Cl_2 and a magnetic stirrer bar, xanthene-9-carboxylic (**9**, 0.226 g, 1.0 mmol) was added. While stirring, DIEA (0.35 mL, 2 mmol) and piperidine (0.12 mL, 1.2 mmol) were added and the reaction was cooled to 0°C with an ice bath. After 10 min, COMU (0.642 g, 1.5 mmol) was added, and the reaction was warmed up slowly to rt and left overnight. The mixture was then diluted with CH_2Cl_2 (40 mL) and washed with 1 N HCl (2 × 10 mL), 1 N $NaHCO_3$ (2 × 10mL) and brine (1 × 10 mL). The organic phase was then dried with Na_2SO_{4N}, filtered and the solvent evaporated. The crude product was purified by silica gel flash chromatography (ethyl acetate (EtOAc)/hexane 20:80). Compound **MM30** was obtained as an off-white solid (227.3 mg, 77 %).

Compound MM30: off-white solid (227.3 mg, 77 %); mp: 156 °C ; ^{1}H NMR (300 MHz, $CDCl_3$) δ 7.33 – 7.17 (m, 4H, H-2, H-6, H-12, H-14), 7.15 – 6.94 (m, 4H, H-1, H-3, H-11, H-13), 5.45 (s, 1H, H-10), 3.56 (t, *J* = 5.4 Hz, 2H, H-18), 3.20 (t, *J* = 5.4 Hz, 2H, H-22), 1.61 – 1.40 (m, 4H, H-19, H-21), 0.97 (s, 2H, H-20); ^{13}C NMR (75 MHz, $CDCl_3$) δ 170.2 (C-15), 150.1 (C-4, C-8), 129.0 (C-2, C-12), 128.2 (C-6, C-14), 123.5 (C-1, C-13), 119.2 (C-5, C-9), 117.0 (C-3, C-11), 47.0 (C-22), 45.7 (C-10), 44.0 (C-18), 25.6 (C-19), 25.4 (C-21), 24.4 (C-20). HRMS (ESI): m/z calculated for $C_{19}H_{19}NO_2$ [M+H]: 294.14886; found: 294.14877.

Synthesis of morpholino(9*H*-xanthen-9-yl)methanone (MM32)

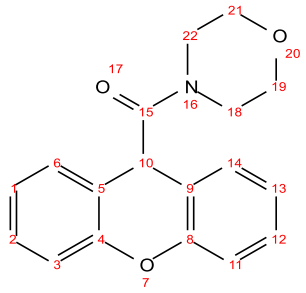

To a 25 mL round-bottom flask containing 5 mL of anhydrous CH_2Cl_2 and a magnetic stirrer bar, xanthene-9-carboxylic (**9**, 0.226 g, 1.0 mmol) was added. While stirring, DIEA (0.35 mL, 2 mmol) and morpholine (0.11 mL, 1.2 mmol) were added and the reaction was cooled to 0°C with an ice bath. After 10 min COMU (0.642 g, 1.5 mmol) was added, and the reaction was warmed up slowly to rt and left overnight. The mixture was then diluted with CH_2Cl_2 (40 mL) and washed with 1 N HCl (2 × 10 mL), 1 N $NaHCO_3$ (2 × 10mL) and brine (1 × 10 mL). The organic phase was then dried with Na_2SO_4, filtered and the solvent evaporated. The crude product was purified by silica gel flash chromatography (EtOAc/hexane 30:70). Compound **MM32** was obtained as an off-white solid (275.2 mg, 92 %).

Compound MM32: off-white solid (275.2 mg, 92 %); mp: 160-161 °C, literature: 159-161 °C [244]; ^{1}H NMR (300 MHz, $CDCl_3$) δ 7.32 – 7.20 (m, 4H, H-2, H-6, H-12, H-14)), 7.13 – 7.02 (m, 4H, H-1, H-3, H-11, H-13), 5.45 (s, 1H, H-10), 3.61 (s, 4H, H-19, H-21), 3.16 (d, *J* = 27.1 Hz, 4H, H-18, H-22); ^{13}C NMR (75 MHz, $CDCl_3$) δ 170.3 (C-15), 149.8 (C-4, C-8), 129.2 (C-2, C-12), 128.0 (C-6, C-14), 123.6 (C-1, C-13), 118.5 (C-5, C-9), 117.1 (C-3, C-11), 66.7 (C-21), 65.9 (C-19), 46.3 (C-18), 45.6 (C-10), 43.0 (C-22).; HRMS (ESI): m/z calculated for $C_{18}H_{17}NO_3$ [M+H]: 296.12812; found: 296.12804.

Synthesis of *N,N*-diethyl-9*H*-xanthene-9-carboxamide (MM36)

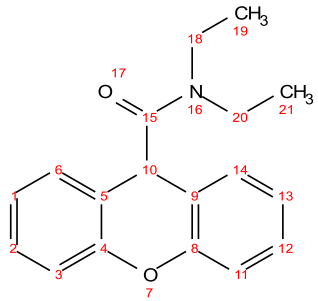

To a 25 mL round-bottom flask containing 5 mL of anhydrous CH_2Cl_2 and a magnetic stirrer bar, xanthene-9-carboxylic (**9**, 0.226 g, 1.0 mmol) was added. While stirring, DIEA (0.35 mL, 2 mmol) and diethylamine (0.12 mL, 1.2 mmol) were added and the reaction was cooled to 0°C with an ice bath. After 10 min COMU (0.642 g, 1.5 mmol) was added, and the reaction was warmed up slowly to rt and left overnight. The mixture was then diluted with CH_2Cl_2 (40 mL) and washed with 1 N HCl (2 × 10 mL), 1 N $NaHCO_3$ (2 × 10mL) and brine (1 × 10 mL). The organic phase was then dried with Na_2SO_4, filtered and the solvent evaporated. The crude product was purified by silica gel flash chromatography (EtOAc/hexane 20:80). Compound **MM36** was obtained as an off-white solid (254.3 mg, 90 %).

Compound MM36: off-white solid (254.3 mg, 90 %); mp: 104 - 105 °C ; ^{1}H NMR (300 MHz, $CDCl_3$) δ 7.30 – 7.19 (m, 4H, H-2, H-6, H12, H-14), 7.13 – 6.99 (m, 4H, H-1, H-3, H-11, H-13), 5.41 (s, 1H, H-10), 3.35 (q, *J* = 7.1 Hz, 2H, H-18), 3.20 (q, *J* = 7.1 Hz, 2H, H-20), 1.10 (t, *J* = 7.1 Hz, 3H, H-19), 0.68 (t, *J* = 7.1 Hz, 3H, H-21); ^{13}C NMR (75 MHz, $CDCl_3$) δ 171.3 (C-15), 150.3 (C-4, C-8), 129.0 (C-2, C-12), 128.2 (C-6, C-14), 123.5 (C-1, C-13), 119.3 (C-5, C-9), 117.1 (C-3, C-11), 45.3 (C-10), 42.0 (C-20), 40.7 (C-18), 13.2 (C-21), 12.6 (C-19).; HRMS (ESI): m/z calculated for $C_{18}H_{19}NO_2$ [M+H]: 282.14886; found: 282.14885.

Synthesis of *N*-(5-methyl-1*H*-pyrazol-3-yl)-9*H*-xanthene-9-carboxamide (MM42B)

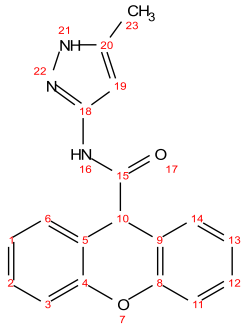

To a 25 mL round-bottom flask containing 5 mL of anhydrous CH_2Cl_2 and a magnetic stirrer bar, xanthene-9-carboxylic (**9**, 0.226 g, 1.0 mmol) was added. While stirring, DIEA (0.35 mL, 2 mmol) and 3-amino-5 metil-1H-pirazole (0.117g, 1.2 mmol) were added and the reaction was cooled to 0°C with an ice bath. After 10 min COMU (0.642 g, 1.5 mmol) was added, and the reaction was warmed up slowly to rt and left overnight. The mixture was then diluted with CH_2Cl_2 (40 mL) and washed with 1 N HCl (2 × 10 mL), 1 N $NaHCO_3$ (2 × 10mL) and brine (1 × 10 mL). The organic phase was then dried with Na_2SO_4, filtered and the solvent evaporated. The crude product was purified by silica gel flash chromatography (EtOAc/hexane 20:80). Compound **MM42B** was obtained as an off-white solid (65.7 mg, 24 %).

Compound MM42B: off-white solid (65.7 mg, 24 %); mp: 143 – 144 °C ; ^{1}H NMR (300 MHz, $CDCl_3$) δ 7.41 (dd, *J* = 7.9, 1.7 Hz, 2H, H-6, H-14), 7.32 – 7.25 (m, 2H, H-2, H-12), 7.18 (dd, *J* = 8.2, 1.4 Hz, 2H, H-3, H-11), 7.04 (td, *J* = 7.9, 1.4 Hz, 3H, H-1, H-13), 6.56 (s, 1H, H-10), 5.27 (s, 1H, H-19), 2.27 (s, 3H, H-23); ^{13}C NMR (75 MHz, $CDCl_3$) δ 174.3 (C-15), 154.5 (C-20), 152.3 (C-4, C-8), 151.5 (C-18), 129.3 (C-6, C-14), 129.1 (C-2, C-12), 123.5 (C-1, C-13), 119.5 (C-5, C-9), 117.2 (C-3, C-11), 90.2 (C-19), 43.1(C-10), 14.6 (C-23); HRMS (ESI): m/z calculated for $C_{18}H_{15}N_3O_2$ [M+H]: 306.12370; found: 306.12395.

Synthesis of (3-amino-5-methyl-1*H*-pyrazol-1-yl)(9*H*-xanthen-9-yl)methanone (MM42C)

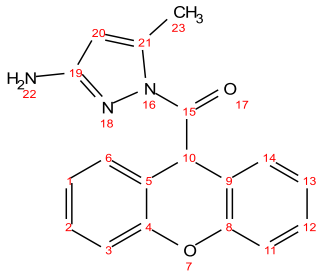

To a 25 mL round-bottom flask containing 5 mL of anhydrous CH_2Cl_2 and a magnetic stirrer bar, xanthene-9-carboxylic (**9**, 0.226 g, 1.0 mmol) was added. While stirring, DIEA (0.35 mL, 2 mmol) and 3-amino-5 metil-1*H*-pirazole (0.117g, 1.2 mmol) were added and the reaction was cooled to 0°C with an ice bath. After 10 min COMU (0.642 g, 1.5 mmol) was added, and the reaction was warmed up slowly to rt and left overnight. The mixture was then diluted with CH_2Cl_2 (40 mL) and washed with 1 N HCl (2 × 10 mL), 1 N $NaHCO_3$ (2 × 10mL) and brine (1 × 10 mL). The organic phase was then dried with Na_2SO_4, filtered and the solvent evaporated. The crude product was purified by silica gel flash chromatography (EtOAc/hexane 40:60). Compound **MM42C** was obtained as an off-white solid (55.7 mg, 20 %).

Compound MM42C: off-white solid (55.7 mg, 20 %); mp: 147 – 148 °C ; ^{1}H NMR (300 MHz, $CDCl_3$) δ 7.38 (dd, *J* = 7.6, 1.6 Hz, 2H, H-6, H-14), 7.28 – 7.24 (m, 2H, H-2, H-12), 7.17 (dd, *J* = 8.1, 1.4 Hz, 2H, H-3, H-11), 7.03 (td, *J* = 7.6, 1.5 Hz, 2H, H-1, H-13), 6.51 (s, 1H, H-10), 5.72 (s, 1H, H-20), 2.40 (s, 3H, H-23); ^{13}C NMR (75 MHz, $CDCl_3$) δ 171.7 (C-15), 156.0 (C-19), 152.3 (C-4, C-8), 146.6 (C-21), 129.1(C-6, C-14), 129.0 (C-2, C-12), 123.4 (C-1, C-13), 119.9 (C-5, C-9), 117.2 (C-3, C-11), 103.0 (C-20), 43.0 (C-10), 15.0 (C-23).; HRMS (ESI): m/z calculated for $C_{18}H_{15}N_3O_2$ [M+H]: 306.12370; found: 306.12363.

Synthesis of *N*-(3-hydroxypropyl)-9*H*-xanthene-9-carboxamide (MM43)

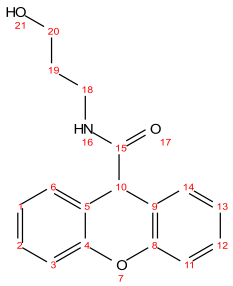

To a 25 mL round-bottom flask containing 5 mL of anhydrous CH_2Cl_2 and a magnetic stirrer bar, xanthene-9-carboxylic (**9**, 0.226 g, 1.0 mmol) was added. While stirring, DIEA (0.35 mL, 2 mmol) and 3-amino-1-propanol (0.901g, 1.2 mmol) were added and the reaction was cooled to 0°C with an ice bath. After 10 min COMU (0.642 g, 1.5 mmol) was added, and the reaction was warmed up slowly to rt and left overnight. The mixture was then diluted with CH_2Cl_2 (40 mL) and washed with 1 N HCl (2 × 10 mL), 1 N $NaHCO_3$ (2 × 10mL) and brine (1 × 10 mL). The organic phase was then dried with Na_2SO_4, filtered and the solvent evaporated. The crude product was purified by silica gel flash chromatography (EtOAc/hexane 80:20). Compound **MM43** was obtained as an off-white solid (181.0 mg, 64 %).

Compound MM43: off-white solid (181.0 mg, 64 %); mp: 220 – 221 °C ; ^{1}H NMR (300 MHz, DMSO-d_6) δ 8.40 (t, *J* = 5.6 Hz, 1H, H-16), 7.36 – 7.02 (m, 8H, H-1, H-2, H-3, H-6, H-11, H-12, H-13, H-14), 4.90 (s, 1H, H-10), 4.44 (t, *J* = 5.2 Hz, 1H, H-21), 3.41 (d, *J* = 6.5 Hz, 2H, H-20), 3.09 (q, *J* = 6.5 Hz, 2H, H-18), 1.55 (p, *J* = 6.5 Hz, 2H, H-19); ^{13}C NMR (75 MHz, DMSO-d_6) δ 171.3 (C-15), 151.0 (C-4, C-8), 128.6 (C-2, C-12), 128.5 (C-6, C-14), 123.3 (C-1, C-13), 120.3 (C-5, C-9), 116.4 (C-3, C-11), 58.3 (C-20), 45.0 (C-10), 36.0 (C-18), 32.3 (C-19); HRMS (ESI): m/z calculated for $C_{17}H_{17}NO_3$ [M+H]: 284.12812; found: 284.12812.

Synthesis of *N*-((9*H*-xanthen-9-yl)methyl)-*N*-ethylethanamine (MM46)

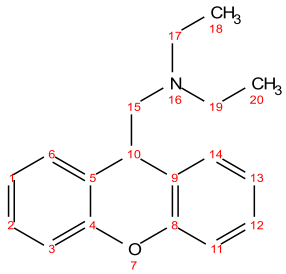

N,N-Diethyl-9*H*-xanthene-9-carboxamide (**36**, 0.422g 1.5 mmol) was added to a 25 mL round-bottom flask containing 5 mL of anhydrous THF and a magnetic stirrer bar, under an ice bath and nitrogen atmosphere. After 15 min, a solution of borane-tetrahydrofuran complex BH_3.THF 1.0 M (7.5 mL, 7.5 mmol) was slowly added, and the reaction was placed at reflux for 2 h. The reaction was cooled to rt and 5 mL of HCl 6N was slowly added to the reaction. The acid was neutralized with Na_2CO_3 and the product extracted with 40 mL of CH_2Cl_2, and then washed with 1 N HCl (2 × 10 mL), 1 N $NaHCO_3$ (2 × 10 mL) and brine (1 × 10 mL). The organic phase was then dried with Na_2SO_4, filtered and the solvent evaporated. The crude product was purified by silica gel flash chromatography (CH_2Cl_2/hexane 30:70). Compound **MM46** was obtained as an off-white solid (213.0 mg, 53 %).

Compound MM46: off-white solid (213.0 mg, 53 %); mp: 89 – 90 °C ; ^{1}H NMR (300 MHz, $CDCl_3$) δ 7.52 (dt, *J* = 7.5, 1.4 Hz, 2H, H-6, H-14), 7.27 – 7.23 (m, 2H, H-2, H-12), 7.19 – 7.09 (m, 4H, H-1, H-3, H-11, H-13), 5.00 (t, *J* = 6.2 Hz, 1H, H-10), 2.82 – 2.66 (m, 6H, H-15, H-17, H-19), 0.92 (td, *J* = 7.3, 1.1 Hz, 6H, H-18, H-20); ^{13}C NMR (75 MHz, $CDCl_3$) δ 154.0 (C-4, C-8), 129.2 (C-6, C-14), 128.2 (C-2, C-12), 126.4 (C-5, C-9), 124.0 (C-3, C-11), 117.0 (C-1, C-13, 64.8 (C-15), 53.7 (C-17, C-19), 37.1 (C-10), 8.3 (C-18, C-20); HRMS (ESI): m/z calculated for $C_{18}H_{21}NO$ [M+H]: 268.1696; found: 268.1699.

Synthesis of *N*-(4-chlorobenzyl)-9*H*-xanthene-9-carboxamide (MM48A)

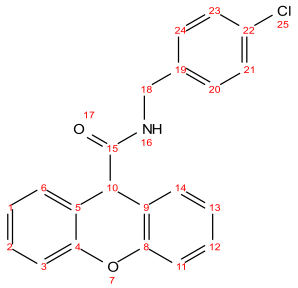

To a 25 mL round-bottom flask containing 5 mL of anhydrous CH_2Cl_2 and a magnetic stirrer bar, xanthene-9-carboxylic (**9**, 0.226 g, 1.0 mmol) was added. While stirring, DIEA (0.35 mL, 2 mmol) and 4-chlorobenzylamine (0.169g, 1.2 mmol) were added and the reaction was cooled to 0°C with an ice ba th. After 10 min COMU (0.642 g, 1.5 mmol) was added, and the reaction was warmed up slowly to rt and left overnight. The mixture was then diluted with CH_2Cl_2 (40 mL) and washed with 1 N HCl (2 × 10 mL), 1 N $NaHCO_3$ (2 × 10mL) and brine (1 × 10 mL). The organic phase was then dried with Na_2SO_4, filtered and the solvent evaporated. The crude was dissolved in a minimum volume of EtOAc atrt, and the resulting solution was filtered. Hexane was slowly added until the visualization a sign of cloudiness. Then the solution was placed in a refrigerator at 8-10 ºC for crystallization. After crystallization, the product was collected by filtration with a nail glass funnel. Compound **MM48A** was obtained as white needles (181.7 mg, 52 %).

Compound MM48A: white needles (181.7 mg, 52 %); mp: 197 °C ; ^{1}H NMR (300 MHz, $CDCl_3$) δ 7.47 – 7.28 (m, 4H, H-6, H-14,H-2, H-12), 7.22 – 7.08 (m, 6H, H-1, H-3, H-11, H-13, H-21, H-23), 6.94 – 6.85 (m, 2H, H-20, H-24), 5.62 (t, *J* = 6.1 Hz, 1H, H-16), 4.96 (s, 1H, H-10), 4.27 (d, *J* = 6.1 Hz, 2H, H-18); ^{13}C NMR (75 MHz, $CDCl_3$) δ 172.1 (C-15), 151.1 (C-4, C-8), 136.6 (C-19), 133.2 (C-22), 129.6 (C-6, C-14), 129.5 (C-2, C-12), 128.8 (C-21, C-23), 128.4 (C-20, C-24), 124.0 (C-1, C-13), 119.0 (C-5, C-9), 117.2 (C-3, C-11), 47.1 (C-10), 42.9 (C-18); HRMS (ESI): m/z calculated for $C_{21}H_{16}ClNO_2$ [M+H]: 350.09423; found: 350.09497.

Synthesis of 1-((9*H*-xanthen-9-yl)methyl)piperidine (MM50)

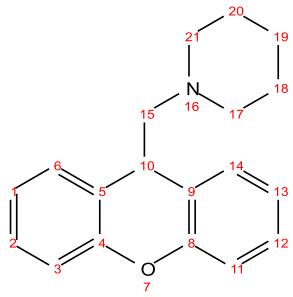

Piperidin-1-yl(9*H*-xanthen-9-yl)methanone (**MM30**, 0.279 g 1.0 mmol) was added to a 25 mL round-bottom flask containing 5 mL of anhydrous THF and a magnetic stirrer bar, under an ice bath and nitrogen atmosphere. After 15 min, a solution of borane-tetrahydrofuran complex BH_3.THF 1.0 M (7.8 mL, 7 mmol) was slowly added, and the reaction was placed at reflux for 2 h. The reaction was cooled to rt and 5 mL of HCl 6N was slowly added to the reaction. The acid was neutralized with Na_2CO_3 and the product extracted with 40 mL of CH_2Cl_2, and then washed with 1 N HCl (2 × 10 mL), 1 N $NaHCO_3$ (2 × 10mL) and brine (1 × 10 mL). The organic phase was then dried with Na_2SO_4, filtered and the solvent evaporated. The crude product was purified by silica gel flash chromatography (CH_2Cl_2/hexane 30:70). Compound **MM50** was obtained as an off-white solid (133.5.0 mg, 50 %).

Compound MM50: off-white solid (133.5.0 mg, 50 %); mp: 139 – 140 °C ; ^{1}H NMR (300 MHz, $CDCl_3$) δ 7.55 (dd, *J* = 7.5, 1.6 Hz, 2H, H-6, H-14), 7.25 (td, *J* = 7.4, 1.8 Hz, 2H, C-2, C-12), 7.20 – 7.07 (m, 4H, H-1, H-3, H-11, H-13), 5.13 (t, *J* = 6.1 Hz, 1H, H-10), 2.96 – 2.64 (m, 6H, H-15, H-17, H-21), 1.57 – 1.30 (m, 6H, H-18, H-19, H-20); ^{13}C NMR (75 MHz, $CDCl_3$) δ 154.0 (C-4, C-8), 129.3 (C-6, C-14), 128.2 (C-2, C-12), 126.6 (C-5, C-9), 123.9 (C-1, C-13), 117.0 (C-3, C-11), 66.0 (C-15), 59.9 (C-17, C-21), 37.0 (C-10), 22.5 (C-19), 20.1 (C-18,C-20). HRMS (ESI): m/z calculated for $C_{19}H_{21}NO$ [M+H]: 280.16959; found: 280.16956.

Synthesis of 2,7-dichloro-9*H*-xanthene-9-carboxylic acid (MM52)

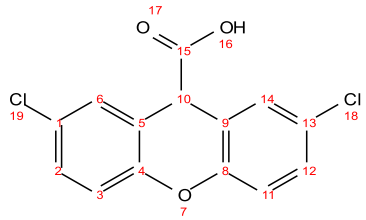

To a suspension of 0.226 g (1 mmol) of xanthene-9-carboxylic (**9**) and 0.334 g (2.5 mmol) of *N*-chlorosuccinimide (NCS) in 2 mL of acetic acid was added 0.05 mL of conc. HCl. The mixture was stirred at rt for 12 h and quenched by the addition of 10 mL of purified water. The precipitated solid was removed by filtration, rinsed with water, and dried in a desiccator. The crude was then dissolved in a minimum volume of EtOAc at rt, and the resulting solution was filtered. Hexane was slowly added until the visualization a sign of cloudiness. Then the solution was placed in a refrigerator at 8-10 ºC for crystallization. After crystallization, the product was collected by filtration with a nail glass funnel. Compound **MM52** was obtained as white needles (22.6 mg, 8 %).

Compound MM52: white needles (22.6 mg, 8 %); mp: found 275 – 277 °C, literature: 273-275 °C [207]; ^{1}H NMR (300 MHz, DMSO-d_6) δ 7.46 (d, J = 2.6 Hz, 2H, H-6, H-14), 7.39 (dd, J = 8.7, 2.6 Hz, 2H, H-2, H-12), 7.21 (d, J = 8.7 Hz, 2H, H-3, H-11), 5.09 (s, 1H, H-10); ^{13}C NMR (75 MHz, DMSO-d_6) δ 171.9 (C-15), 149.6 (C-4, C-8), 129.2 (C-6, C-14), 129.0 (C-2, C-12), 127.2 (C-1, C-13), 121.0 (C-5, C-9), 118.3 (C-3, C-11), 44.0 (C-10).

Synthesis of 2,7-dibromo-9*H*-xanthene-9-carboxylic (MM54)

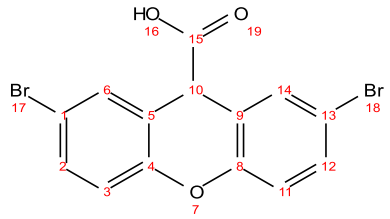

To a suspension of 2.262 g (10 mmol) of xanthene-9-carboxylic (**9**) and 4.550 g (25 mmol) of *N*-bromosuccinimide (NBS) in 20 mL of acetic acid was added 0.5 mL of

conc. HCl. The mixture was stirred at rt for 12 h and quenched by the addition of 100 mL of purified water. The precipitated solid was removed by filtration, rinsed with water, and dried in a desiccator. The crude product was purified by silica gel flash chromatography (EtOAc/hexane/ formic acid 30:70:0.1). Compound **MM54** was obtained as an off-white solid (2151.8 mg, 56 %).

Compound MM54: off-white solid (2151.8 mg, 56 %); mp: 250 °C; ^{1}H NMR (300 MHz, DMSO-d_6) δ 7.58 (d, *J* = 2.4 Hz, 2H, H-6, H-14), 7.51 (dd, *J* = 8.6, 2.5 Hz, 2H, H-2, H-12), 7.15 (d, *J* = 8.6 Hz, 2H, H-3, H-11)), 5.10 (s, 1H, H-10); ^{13}C NMR (75 MHz, DMSO-d_6) δ 171.9 C-15), 150.0 (C-4, C-8), 132.1 (C-2, C-12), 131.9 (C-6, C-14), 121.5 (C-5, C-9), 118.8 (C-3, C-11), 115.0 (C-1, C-13), 43.8 (C-10).

Synthesis of (2,7-dibromo-9*H*-xanthen-9-yl)(morpholino)methanone (MM56)

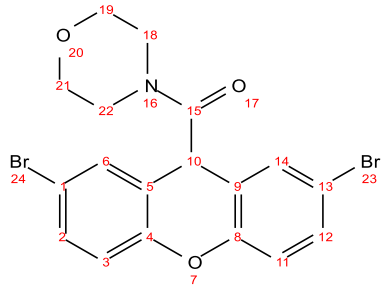

0.384 g (1.0 mmol) of 2,7-dibromo-9*H*-xanthene-9-carboxylic (**MM54**) was added to a 25 mL round-bottom flask containing 5 mL of anhydrous CH_2Cl_2 and a magnetic stirrer bar. While stirring, DIEA (0.35 mL, 2 mmol) and morpholine (1.2 mmol) were added and the reaction was cooled to 0°C with an ice bath. After 10 min COMU (0.642 g, 1.5 mmol) was added, and the reaction was warmed up slowly to rt and left overnight. The mixture was then diluted with CH_2Cl_2 (40 mL) and washed with 1 N HCl (2 × 10 mL), 1 N $NaHCO_3$ (2 × 10mL) and brine (1 × 10 mL). The organic phase was then dried with Na_2SO_4, filtered and the solvent evaporated. The crude product was purified by silica gel flash chromatography (EtOAc/hexane 20:80). Compound **MM56** was obtained as a yellowish solid (224.9 mg, 50 %).

Compound MM56: yellowish solid (224.9 mg, 50 %); mp: 171 – 172 °C ; ^{1}H NMR (300 MHz, $CDCl_3$) δ 7.38 (dd, *J* = 8.7, 2.4 Hz, 2H, H-2, H-12), 7.33 (d, *J* = 2.3 Hz, 2H, H-6, H-14), 6.98 (d, *J* = 8.7 Hz, 2H, H-3, H-11), 5.35 (s, 1H, H-10), 3.65 (s, 4H,H-19, H-21), 3.33 (s, 4H, H-18, H-22); ^{13}C NMR (75 MHz, $CDCl_3$) δ 169.4 (C-15), 149.2 (C-

4, C-8), 132.5 (C-2, C-12), 130.6 (C-6, C-14), 120.4 (C-5, C-9), 119.1 (C-3, C-11), 116.2 (C-1, C-13), 44.2 (C-10).; HRMS (ESI): m/z calculated for $C_{18}H_{15}Br_2NO_3$ [M+H]: 451.94914; found: 451.94928.

Synthesis of 2,7-dibromo-N-(5-methyl-1H-pyrazol-3-yl)-9*H*-xanthene-9-carboxamide (MM57A)

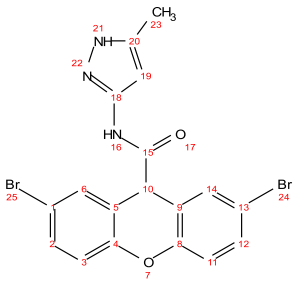

0.384 g (1.0 mmol) of 2,7-dibromo-9*H*-xanthene-9-carboxylic (**MM54**) was added to a 25 mL round-bottom flask containing 5 mL of anhydrous CH_2Cl_2 and a magnetic stirrer bar. While stirring, DIEA (0.35 mL, 2 mmol) and 3-amino-5-metil-1*H*-pirazole (0.117 g, 1.2 mmol) were added and the reaction was cooled to 0°C with an ice bath. After 10 min COMU (0.642 g, 1.5 mmol) was added, and the reaction was warmed up slowly to rt and left overnight. The mixture was then diluted with CH_2Cl_2 (40 mL) and washed with 1 N HCl (2 × 10 mL), 1 N $NaHCO_3$ (2 × 10mL) and brine (1 × 10 mL). The organic phase was then dried with Na_2SO_4, filtered and the solvent evaporated. The crude product was purified by silica gel flash chromatography (EtOAc/hexane 15:85). Compound **MM57A** was obtained as an off-white solid (111.2 mg, 24 %).

Compound MM57A: off-white solid (111.2 mg, 24 %); mp: 163 °C ; ^{1}H NMR (300 MHz, $CDCl_3$) δ 7.54 (d, J = 2.3 Hz, 2H, H-6, H-14), 7.39 (dd, *J* = 8.8, 2.3 Hz, 2H, H-2, H-12), 7.05 (d, *J* = 8.8 Hz, 2H, H-3, H-11), 6.49 (s, 1H, H-10), 5.39 (s,br, 1H, H-16), 5.31 (s, 1H, H-19), 2.27 (s, 3H, H-23); ^{13}C NMR (75 MHz, $CDCl_3$) δ 173.0 (C-15), 155.1 (C-4, C-8), 151.4 (C-18), 151.1 (C-4, C-8), 132.3 (C-2, C-12), 131.9 (C-6, C-14), 120.9 (C-5, C-9), 119.0 (C-3, C-11), 115.9 (C-1, C-13, 90.6 (C-19), 42.7 (C-10), 14.5 (C-23).; HRMS (ESI): m/z calculated for $C_{18}H_{13}Br_2N_3O_2$ [M+H]: 461.94473; found: 461.94568.

Synthesis of (3-amino-5-methyl-1H-pyrazol-1-yl)(2,7-dibromo-9*H*-xanthen-9-yl)methanone (MM57B)

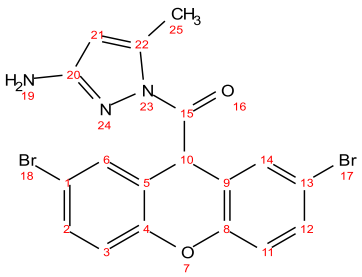

0.384 g (1.0 mmol) of 2,7-dibromo-9*H*-xanthene-9-carboxylic (**MM54**) was added to a 25 mL round-bottom flask containing 5 mL of anhydrous CH_2Cl_2 and a magnetic stirrer bar. While stirring, DIEA (0.35 mL, 2 mmol) and 3-amino-5-metil-1*H*-pirazole (0.117 g, 1.2 mmol) were added and the reaction was cooled to 0°C with an ice bath. After 10 min COMU (0.642 g, 1.5 mmol) was added, and the reaction was warmed up slowly to rt and left overnight. The mixture was then diluted with CH_2Cl_2 (40 mL) and washed with 1 N HCl (2 × 10 mL), 1 N $NaHCO_3$ (2 × 10mL) and brine (1 × 10 mL). The organic phase was then dried with Na_2SO_4, filtered and the solvent evaporated. The crude product was purified by silica gel flash chromatography (EtOAc/hexane 15:85). Compound **MM57B** was obtained as an off-white solid (133.6 mg, 29 %).

Compound MM57B: off-white solid (133.6 mg, 29 %); mp: 157 – 158 °C ; ^{1}H NMR (300 MHz, $CDCl_3$) δ 7.50 (d, *J* = 2.4 Hz, 2H, H-6, H-14), 7.37 (dd, *J* = 8.7, 2.4 Hz, 2H, H-2, H-12), 7.04 (d, *J* = 8.7 Hz, 2H, H-3, H-11), 6.43 (s, 1H, H-10), 5.76 (s, 1H, H-21), 4.05 (br,s, 2H, H-19), 2.42 (s, 3H, H-25); ^{13}C NMR (75 MHz, $CDCl_3$) δ 170.3 (C-15), 156.2 (C-20), 151.0 (C-4, C-8), 146.5 (C-22), 132.0 (C-2, C-12), 131.6 (C-6, C-14), 121.3 (C-5, C-9), 118.8 (C-3, C-11), 115.7 (C-1, C-13), 103.5 (C-21), 42.5 (C-10), 14.8 (C-25); HRMS (ESI): m/z calculated for $C_{18}H_{13}Br_2N_3O_2$ [M+H]: 461.94473; found: 461.94491.

Synthesis of *N,N*-bis(2-hydroxyethyl)-9*H*-xanthene-9-carboxamide (MM59B3)

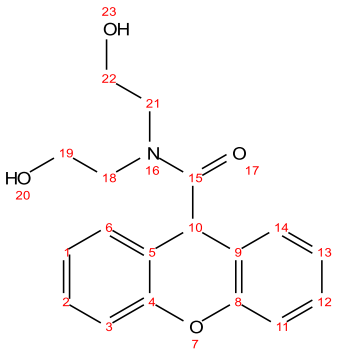

0.294 g (1.3 mmol) of xanthene-9-carboxylic and 0.474 g (1.5 mmol) of BTFFH was added to a 5 mL vial containing 3 mL of anhydrous THF and a magnetic stirrer bar. While stirring under nitrogen atmosphere, DIEA (0.78 mL, 4.5 mmol) was added and the reaction stand stirring. After 30 min, diethanolamine (0.10 mL, 1 mmol) was added, the vial sealed, and the reaction was warmed up to 80ºC and left for 4 h (CAUTION: Heating THF at 80ºC causes overpressure in the vial). The mixture was then diluted with EtOAc (40 mL) and washed with water (2 × 10 mL) and brine (1 × 10 mL). The organic phase was then dried with Na_2SO_4, filtered and the solvent evaporated. The crude product was purified by silica gel flash chromatography (100 % EtOAc). Compound **MM59B3** was obtained as a yellowish oil (294.7 mg, 94 %).

Compound MM59B3: yellowish oil (294.7 mg, 94 %); ^{1}H NMR (300 MHz, DMSO-d_6) δ 7.34 – 7.21 (m, 4H, H-2, H-6, H-12, H-149), 7.16 – 7.01 (m, 4H, H-1, H-3, H-12, H-13), 5.68 (s, 1H, H-10), 5.05 (t, *J* = 5.3 Hz, 1H, H-20), 4.70 (t, *J*= 5.0 Hz, 1H, H-23), 3.89 (t, *J* = 5.3 Hz, 2H, H-18), 3.68 (q, *J* = 5.3 Hz, 2H, H-19), 3.50 – 3.37 (m, 4H, H-21, H-22); ^{13}C NMR (75 MHz, DMSO-d_6) δ 172.4 (C-15), 150.9 (C-4, C-8), 128.4 (C-6, C-14), 128.3 (C-2, C-12), 123.2 (C-1, C-13), 121.0 (C-5, C-9), 116.3 (C-3, C-11), 59.3 (C-19), 58.6 (C-21), 51.3 (C-18), 48.5 (C-22), 39.2 (C-10).; HRMS (ESI): m/z calculated for $C_{18}H_{19}Br_2NO_4$ [M+H]: 314.13869; found: 314.13919.

Synthesis of *tert*-butyl (6-(9*H*-xanthene-9-carboxamido)hexyl)carbamate (MM61B)

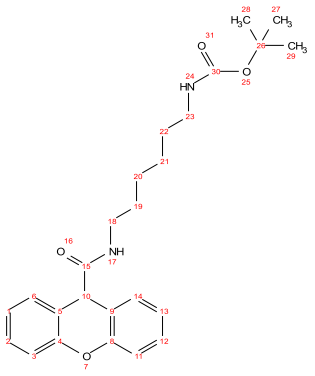

0.294 g (1.3 mmol) of xanthene-9-carboxylic and 0.474 g (1.5 mmol) of BTFFH was added to a 5 mL vial containing 3 mL of anhydrous THF and a magnetic stirrer bar. While stirring under nitrogen atmosphere, DIEA (0.78 mL, 4.5 mmol) was added, and the reaction stand stirring. After 30 min, *N*-boc-1,6-hexanediamine (0.02 mL, 1 mmol) was added, the vial sealed, and the reaction was warmed up to 80ºC and left for 4 h (CAUTION: Heating THF at 80ºC causes overpressure in the vial). The mixture was then diluted with EtOAc (40 mL) and washed with water (2 × 10 mL) and brine (1 × 10 mL). The organic phase was then dried with Na_2SO_4, filtered and the solvent evaporated. The crude product was purified by silica gel flash chromatography (EtOAc/hexane 60:40). Compound **MM61B** was obtained as a white solid (415.3 mg, 98 %).

Compound MM61B: yellowish oil (294.7 mg, 94 %); ^{1}H NMR (300 MHz, DMSO-d_6) δ 8.38 (t, *J* = 5.6 Hz, 1H, H-17), 7.34 – 7.23 (m, 4H, H-2, H-6, H-12, H-14), 7.16 – 7.03 (m, 4H, H-1, H-3, H-11, H-13), 6.77 (t, *J* = 5.8 Hz, 1H, H-24), 4.89 (s, 1H, H-10), 3.02 (q, *J* = 6.5 Hz, 2H, H-18), 2.87 (q, *J* = 6.6 Hz, 2H, H-23), 1.37 (s, 13H, H-19, H-22, H-29, H-30, H-31), 1.22 (q, *J* = 3.7 Hz, 4H, H-20, H-21); ^{13}C NMR (75 MHz, DMSO-d_6) δ 171.6 (C-15), 156.0 (C-25), 151.3 (C-4, C-8), 129.0 (C-6, C-14), 128.9 (C-2, C-12), 123.7 (C-1, C-13), 120.8 (C-5, C-9), 116.8 (C-3, C-11), 77.8 (C-28), 45.5 (C-10), 29.9 (C-22), 29.4 (C-19), 28.7 (C-29, C-30, C-31), 26.4 (C-20, C-21).

Synthesis of *N*-(6-aminohexyl)-9*H*-xanthene-9-carboxamide (MM63B)

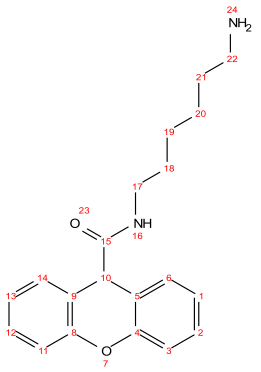

To a solution of *tert*-butyl (6-(9*H*-xanthene-9-carboxamido)hexyl)carbamate (**MM61B**, 0.042 g, 0.1 mmol) in CH_2Cl_2 at 0 ºC was added trifluoroacetic acid (TFA) (0.02 mL, 0.3 mmol). The ice bath was removed and the reaction mixture was stirred at rt for 3 h. The solvents were removed in vacuo and the residue was diluted with CH_2Cl_2. The mixture was then diluted with $CHCl_3$ (20 mL) and neutralized with NaOH 15%, washed with water (2 × 10 mL and brine (1 × 10 mL). The organic phase was then dried with Na_2SO_4, filtered and the solvent evaporated. The solvent was removed in vacuo to provide the product. Compound **MM63B** was obtained as an off-white solid (34.6 mg, 88 %).

Compound MM63B: off-white solid (34.6 mg, 88 %); mp: 142 – 143 °C; ^{1}H NMR (300 MHz, Methanol-d_4) δ 7.34 – 7.22 (m, 4H, H-2, H-6, H-12, H-14), 7.15 – 7.03 (m, 4H, H-1, H-3, H-11, H-13), 4.88 (s, 1H, H-10), 3.16 (t, *J* = 6.9 Hz, 2H, H-17), δ = 2.59 (t, J = 7.1 Hz, 2H, H-22), 1.55 – 1.38 (m, 4H, H-18, H-21)), 1.33 – 1.24 (m, 4H, H-19, H-20).; ^{13}C NMR (75 MHz, Methanol-d_4) δ 175.0 (C-15), 152.8 (C-4, C-8), 130.0 (C-6, C-14), 129.6 (C-2, C-12), 124.4 (C-3, C-11), 120.9 (C-5, C-9), 117.9 (C-1, C-13), 42.2 (C22) 40.4 (C-17), 33.2 (C-21), 30.3 (C-18), 27.6 (C-20), 27.5 (C-19); HRMS (ESI): m/z calculated for $C_{20}H_{24}N_2O_2$ [M+H]: 325.19105; found: 325.19126.

Synthesis of (2,7-bis(2,4-difluorophenyl)-9*H*-xanthen-9-yl)(morpholino)methanone (MM68)

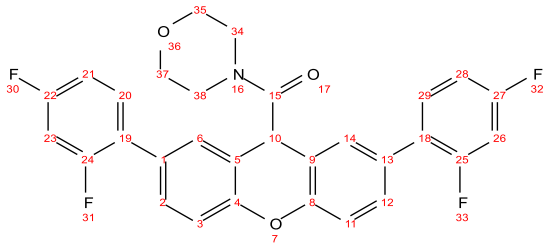

0.136 g (0.3 mmol) of (2,7-dibromo-9*H*-xanthen-9-yl)(morpholino)methanone **(MM56)**, 0189g (1.2 mmol) of 2,4-difluorophenylboronic acid, 0.069g (0.06 mmol) of tetrakis(triphenylphosphine)palladium(0) and 3 mmol of potassium carbonate (2.5 mL of a 2M aq. solution) were added to a 10 mL vial containing 3 mL of sonicated THF and a magnetic stirrer bar. The vial was sealed under nitrogen and placed in a 100 °C oil bath and stirred for 3 h. The mixture was then diluted with CH_2Cl_2 (40 mL) and washed with 1 N HCl (2 × 10 mL), 1 N $NaHCO_3$ (2 × 10mL) and brine (1 × 10 mL). The organic phase was then dried with Na_2SO_4, filtered and the solvent evaporated. The crude product was purified by silica gel flash chromatography (EtOAc/hexane 20:80). Compound **MM68** was obtained as a yellowish solid (143.9 mg, 92 %).

Compound MM68: yellowish solid (143.9 mg, 92 %).; mp: 187 – 188 °C ; ^{1}H NMR (300 MHz, DMSO-d_6) δ 7.59 (td, J = 9.0, 6.6 Hz, 2H, H-6, H-14), 7.48 (dt, *J* = 8.4, 1.9 Hz, 2H, H-2, H-12), 7.43 – 7.35 (m, 4H, H-23, H-26), 7.29 (d, *J* = 8.4 Hz, 2H, H-3, H-11), 7.21 (tdd, *J* = 8.5, 2.6, 1.0 Hz, 2H, H-21, H-28), 5.78 (s, 1H, H-10), 4.02 (s, 2H, H-38), 3.66 (s, 2H, H-37), 3.53 (s, 2H, H-35), 3.43 (s, 2H, H-34); ^{13}C NMR (75 MHz, DMSO-d_6) δ 170.2 (C-15), 160.7 (C22, C-27), 157.5 (C-24, C-25), 150.9 (C-4, C-8), 131.8 (C-1, C-13), 129.4 (C-20, C-29), 129.2 (C-2, C-12), 128.7 (C-6, C-14), 123.9 (C-18, C-19), 120.9 (C-5, C-9), 116.9 (C-3, C-11), 112.3 and 112.1 (C-21, C-28), 105.0, 104.6 and 104. 3 (C-23, C-26), 66.2 (C-35, C-37), 46.4 (C-34), 42.6 (C-38).; HRMS (ESI): m/z calculated for $C_{30}H_{21}F_4NO_3$ [M+H]: 520.15303; found: 520.15287.

Synthesis of 2,7-dibromo-*N*-(3-hydroxypropyl)-9*H*-xanthene-9-carboxamide (MM73)

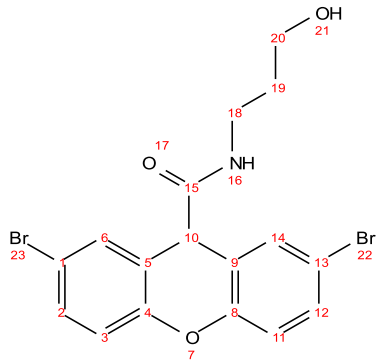

0.384 g (1.0 mmol) of 2,7-dibromo-9*H*-xanthene-9-carboxylic (**MM54**) was added to a 25 mL round-bottom flask containing 5 mL of anhydrous CH_2Cl_2 and a magnetic stirrer bar. While stirring, DIEA (0.35 mL, 2 mmol) and 3-amino-1-propanol (0.09 mL, 1.2 mmol) were added and the reaction was cooled to 0°C with an ice bath. After 10 min COMU (0.642 g, 1.5 mmol) was added, and the reaction was warmed up slowly to rt and left overnight. The crude product was directly purified by silica gel flash chromatography (EtOAc/CH_2Cl_2 10:90). Compound **MM73** was obtained as an off-white solid (43.4.0 mg, 10 %).

Compound MM73: off-white solid (43.4.0 mg, 10 %).; mp: 274 °C ; ^{1}H NMR (300 MHz, DMSO-d_6) δ 8.41 (t, *J* = 5.6 Hz, 1H, H-16), 7.53 – 7.45 (m, 4H, H-2, H-6, H-12, H-14), 7.13 (d, *J* = 8.6 Hz, 2H, H-13, H-11), 4.91 (s, 1H, H-10), 4.46 (t, *J* = 5.1 Hz, 1H, H-21), 3.41 (s, 2H, under H_2O signal, H-20), 3.11 (td, *J* = 6.8, 5.6 Hz, 2H, H-18), 1.56 (p, *J* = 6.8 Hz, 2H, H-19); ^{13}C NMR (75 MHz, DMSO-d_6) δ 170.7 (C-15), 150.4 (C-4, C-8), 132.0 (C-6, C-14), 131.4 (C-2, C-12), 122.8 (C-5, C-9), 119.2 (C-3, C-11), 115.3 (C-1, C-13), 58.6 (C-20), 45.0 (C-10), 36.6 (C-18), 32.6 (C-19); HRMS (ESI): m/z calculated for $C_{17}H_{15}Br_2NO_3$ [M+H]: 439.94915; found: 439.94924.

Synthesis of 2,7-dibromo-*N*,*N*-bis(2-hydroxyethyl)-9*H*-xanthene-9-carboxamide (MM74)

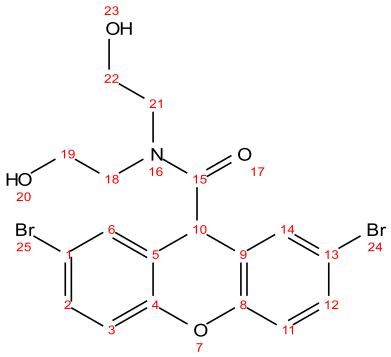

0.250g (0.65 mmol) of 2,7-dibromo-9*H*-xanthene-9-carboxylic (**MM54**) and 0.237 g (0.75 mmol) of BTFFH were added to a 5 mL vial containing 3 mL of anhydrous THF and a magnetic stirrer bar. While stirring under nitrogen atmosphere, DIEA (0.39 mL, 2.25 mmol) was added and the reaction stand stirring. After 30 min, diethanolamine (0.05 mL, 0.5 mmol) was added, the vial sealed, and the reaction was warmed up to 80 ºC and left for 4 h (CAUTION: Heating THF at 80 ºC causes overpressure in the vial). The mixture was directly purified by silica gel flash chromatography (EtOAc/hexane 70:30). Compound **MM74** was obtained as a yellowish oil (54.3 mg, 23 %).

Compound MM74: yellowish oil (54.3 mg, 23 %); ^{1}H NMR (300 MHz, Acetone-d_6) δ 7.63 (dd, *J* = 2.4, 0.8 Hz, 2H, H-6, H14), 7.45 (dd, *J* = 8.7, 2.4 Hz, 2H, H-2, H-12)), 7.09 (d, *J* = 8.7 Hz, 2H, H-3, H-11), 5.84 (s, 1H, H-10), 4.10 (t, *J* = 5.0 Hz, 2H, H-18), 3.96 – 3.87 (m, 2H, H-19), 3.66 (t, *J* = 5.4 Hz, 2H, H-22), 3.56 (t, *J* = 5.4 Hz, 2H, H-21); ^{13}C NMR (75 MHz, Acetone-d_6) δ 172.3 (C-15), 150.7 (C-4, C-8), 131.3 (C-2, C-12), 131.0 (C-6, C-14), 123.3 (C-5, C-9), 118.5 (C-3, C-11), 114.9 (C-1, C-13), 59.9 (C-22), 58.7 (C-19), 51.9 (C-18), 49.1 (C-21), 39.6 (C-10). HRMS (ESI): m/z calculated for $C_{18}H_{17}Br_2NO_4$ [M+H]: 469.95579; found: 469.93700.

3.5.2. Biological assays

3.5.2.1. Cytotoxicity, modulation of P-gp and FeNTA

General information

SH-SY5Y neuroblastoma cell line (American Type Culture Collection, ATCC, Manassas, Virginia); Dulbecco modified eagle medium, DMEM (Gibco, Lenexa, KS); Heat-inactivated

fetal bovine serum FBS (PAN-Biotech, Germany); penicillin-streptomycin [10,000 U/mL penicillin, 10 mg/mL streptomycin] (PAN-Biotech, Germany); Non-essential amino acids (100x) without (w/o): L-Glutamine (PAN-Biotech, Germany); trypsin-Ethylenediaminetetraacetic acid (EDTA) (0.25 %), phenol red (Gibco, Lenexa, KS); retinoic Acid (RA) (Sigma-Aldrich, Germany); DMSO (Merck KGaA, Germany); Hank's balanced salt solution, HBSS, w/o: Ca^{2+} and Mg^{2+}, w/o: phenol red, w: 0.35 g/L $NaHCO_3$ (PAN-Biotech, Germany); zosuquidar (ZOS) hydrochloride (Sigma-Aldrich, Germany); rhodamine 123 (Sigma-Aldrich, Germany); HBSS, w: Ca^{2+} and Mg^{2+}, w/o: phenol red, w/o: $NaHCO_3$ (PAN-Biotech, Germany); triton X-100 (Sigma-Aldrich, Germany); $FeCl_3$ (Sigma-Aldrich, Germany); nitrilotriacetic acid (Sigma-Aldrich, Germany); *tert*-butyl hydroperoxide (Sigma-Aldrich, Germany); phenazine methosulfate (Sigma-Aldrich, Germany); dichloro-dihydrofluorescein diacetate (Abcam, UK); erastin (Merck KGaA, Germany); okadaic acid, phosphatases 1 (PP1) and phosphatase-2A (PP2A) inhibitor (ab120375) (Abcam, UK); beta-amyloid (25-35) (GenScript, UK); acetylcholinesterase Assay Kit (ab138871) (Abcam, UK); microplate reader (Reader Synergy HT, BioTek, Vermont, US); t-25 cm^2 flasks; 96-well plates; 24-well plates.

SH-SY5Y culture and differentiation

SH-SY5Y cells were culture to confluence in 25-cm^2 flasks containing DMEM culture medium supplemented with 10% FBS, 1% penicillin–streptomycin and 1% non-essential amino acids in a humid atmosphere of 5% CO_2 at 37º C. At day -1, cells were seeding at density of 25,000 cells/cm^2, in 96- or 24-well plates, according to the type of assay performed, and the differentiation (day 0) was performed resorting to treatment with retinoic acid at a final concentration of 10 µM in DMEM culture medium supplemented with 3% FBS, 1% penicillin–streptomycin and 1% non-essential amino acids. At day 7 of the differentiation treatment, the cells were used in the experiments.

Compounds preparation

The compounds tested were previously weighed and dissolved in DMSO at 50 mM stock solution.

Cytotoxicity evaluation

Experimental design

The effect of each compound at concentrations of 5, 10, 25, and 50 µM on cell viability was tested to determine the optimal concentration range for the next studies. From the stock solution, the different concentrations were prepared in medium and the differentiated SH-SY5Y cells (day 7), previously seeding in 96-well plates, were exposed and then incubated for a period of 24 h at 37ºC. Cells were divided into groups, in triplicate, treated with: (i)

differentiation medium only (control) and (ii) differentiation medium containing the increasing concentrations to be tested for each compound. Cell viability was measured using MTT reduction and Neutral Red uptake assays.

MTT reduction assay

Cell viability was measured using MTT assay**,** 24 h following experimental treatment. A solution of MTT at a final concentration of 0.5 mg/mL was prepared in medium (from 5 mg/mL stock solution) and 150 µL was added to each well, after aspiration of the culture medium from the exposure. The plate was incubated for an additional 1 h at 37ºC. After removal MTT medium, 150 µL of DMSO was added to each well and the OD was measured at 550 nm using a microplate reader. The absorbance of the control group was considered as 100 % of the cell viability.

Neutral red uptake assay

In addition, the complementary neutral red uptake assay was used to confirm the results. A solution of neutral red at a final concentration of 50 µg/mL was prepared in medium (from 3,300 µg/mL stock solution) and 150 µL was added to each well, after aspiration of the culture medium from the exposure. The plate was incubated for an additional 1 h at 37 ºC. After removal neutral red medium, 150 µL of neutral red desorption solution (1% glacial acetic acid solution, 50% EtOH, 49% distilled water) was added to each well and the OD was measured at 540/590 nm using a microplate reader. The absorbance of the control group was considered as 100% of the cell viability.

Modulation of P-gp activity

Reagent preparation

ZOS was prepared according to the manufacturer's instructions at 5 mM stock solution. From the stock solution, a final concentration solution per well of 5 µM ZOS in HBSS (w: Ca^{2+} and Mg^{2+}) was prepared for the assay. Rhodamine 123 was prepared as well according to the manufacturer's instructions at 20 mM stock solution. Then, from the stock solution, a final concentration solution per well of 10 µM Rhodamine 123 in HBSS (w: Ca^{2+} and Mg^{2+}) was prepared. As a lysis solution, triton X-100 1% was prepared in in HBSS (w: Ca^{2+} and Mg^{2+}).

Experimental design

The effect of each compound at concentrations of 10 and 25 μM on P-gp activity was tested to classify the compounds into activators or inhibitors of their activity. From the stock solution, the different concentrations to be tested of the compounds per well were prepared in HBSS (w: Ca^{2+} and Mg^{2+}) and the differentiated SH-SY5Y cells (day 7), previously seeding in 24-well plates, were exposed by being divided into groups, in triplicate, treated with: (i) 400 μL of HBSS (w: Ca^{2+} and Mg^{2+}) (control in the absence of the P-gp inhibitor); (ii) 200 μL of HBSS (w: Ca^{2+} and Mg^{2+}) and 200 μL of HBSS (w: Ca^{2+} and Mg^{2+}) containing the concentrations to be tested for each compound; (iii) 200 μL of HBSS (w: Ca^{2+} and Mg^{2+}) and 200 μL of HBSS (w: Ca^{2+} and Mg^{2+}) containing ZOS (control under inhibition conditions) and (iv) 200 μL of HBSS (w: Ca^{2+} and Mg^{2+}) containing ZOS and 200 μL of HBSS (w: Ca^{2+} and Mg^{2+}) containing the concentrations to be tested for each compound.

Upon removal of the differentiation medium, the cells were exposed to the previously described conditions and incubated for 30 min at 37ºC. Subsequently, 50 μL of HBSS (w: Ca^{2+} and Mg^{2+}) containing rhodamine 123 was added to all wells with the plate being incubated for an additional 90 min at 37 ºC. Consequently, after aspiration of the exposure conditions, the cells were carefully washed twice with HBSS (w: Ca^{2+} and Mg^{2+}) and finally 400 μL of triton X-100 were added to each well. The plate was protected from the light by covering it with aluminum foil and left at rt for 30 min with subsequent fluorescence intensity reading at an excitation wavelength of 485 and emission wavelength of 528 nm.

Iron (III)-induced cytotoxicity (FeNTA)

Reagent preparation

NTA stock solution was prepared at a concentration of 250 mM, pH 7,4. Afterwards, $FeCl_3$ stock solution at a concentration of 100 mM was prepared in NTA and left to stabilize for at least 15 minutes protected from light. From the FeNTA complex stock solution, a 50 mM concentration solution was prepared in medium from which the concentrations to be tested in the assay were prepared.

Experimental design

The effects of FeNTA complex at 100, 250, 500, 750, 1000 and 1500 μM at 24 hours were previously evaluated in SH-SY5Y-differentiated cells. The optimal concentration of 500 and 1000 μM per well were selected based on the significant decrease in cell viability assessed by the Neutral Red uptake assay.

The effect of the compounds and deferiprone at concentrations of 10 and 25 μM was evaluated on attenuation of iron (III)-induced cytotoxicity. From the stock solution, the

different concentrations of the compounds to be tested per well were prepared in medium and the differentiated SH-SY5Y cells (day 7), previously seeding in 96-well plates, were exposed by being divided into groups, in triplicate, treated with: (i) 200 µL of differentiation medium (control); (ii) 100 µL of differentiation medium and 100 µL of each FeNTA concentration to be tested; (iii) 100 µL of differentiation medium and 100 µL of each compound concentration to be tested (control of every compound) and (iv) 100 µL of each compound concentration and 100 µL of each FeNTA concentration to be tested.

Upon removal of the differentiation medium, the cells were pretreated with the different compounds for 30 minutes at 37ºC prior to addition of 500 and 1000 µM FeNTA in the corresponding wells. Then, the cells were incubated for 24 hours, after which cell viability was measured by the Neutral Red uptake assay.

Iron (III)-chelating effects

The UV/Vis spectra were obtained in a methanolic solution with 1% DMSO at room temperature using a path length of 1 cm on a HITACHI UH5300 spectrophotometer from 200 nm to 600 nm using the software HITACHI. The iron chelating effects were evaluated according with a published protocol [245]. Briefly, an intermediate solution of the compounds in a concentration of 1.0×10^{-3} M was prepared in DMSO, which was used to prepare the final solution in methanol in the following concentration 1.0×10^{-4} M. An intermediate solution of $FeCl_3$, prepared in deionized water in the concentration of 0.1 M, was used to prepare the final solution also in deionized water in the concentration of 1.0×10^{-3} M. Fifteen additions of 33 µL of the iron (III) solution were added to 2 mL of the compounds under study.

3.5.2.2. CNS penetration: in vitro parallel artificial membrane permeability assay (PAMPA)- BBB.

Prediction of the brain penetration was evaluated using a parallel artificial membrane permeability assay (PAMPA) [238]. Caffeine, enoxacine, hydrocortisone, desipramine, ofloxacine, piroxicam, testosterone, promazine, verapamile, atenolol, phosphate buffer saline solution at pH 7.4 (PBS), EtOH and dodecane were purchased from Sigma, Acros organics, Merck, Aldrich and Fluka. The porcine polar brain lipid (PBL) (catalog no. 141101) was from Avanti Polar Lipids. The donor plate was a 96-well filtrate plate (Multiscreen® IP Sterile Plate PDVF membrane, pore size is 0.45 µM, catalog no. MAIPS4510) and the acceptor plate was an indented 96-well plate

(Multiscreen®, catalog no. MAMCS9610) both from Millipore. Filter PDVF membrane units (diameter 30 mm, pore size 0.45 µm) from Symta were used to filtered the samples. A 96-well plate UV reader (Thermoscientific, Multiskan spectrum) was used for the UV measurements. Quality control compounds (3-5 mg of caffeine, enoxacine, hydrocortisone, desipramine, ofloxacine, piroxicam, testosterone, 12 mg of promazine, and 25 mg of verapamile and atenolol] were dissolved in EtOH (1,000 µL). 100 Microlitres of this compound stock solution was taken and 1,400 µL of EtOH and 3,500 µL of PBS pH=7.4 buffer were added to reach 30% of EtOH concentration in the experiment. These solutions were filtered. The acceptor 96-well microplate was filled with 180 µL of PBS/EtOH (70/30). The donor 96-well plate was coated with 4 µL of porcine brain lipid in dodecane (20 mg/mL) and after 5 min, 180 µL of each compound solution was added. 1-2 mg of every compound to be determined their ability to pass the brain barrier were dissolved in 1,500 µL of EtOH and 3,500 µL of PBS pH=7.4 buffer, filtered and then added to the donor 96-well plate. Then the donor plate was carefully put on the acceptor plate to form a “sandwich”, which was left undisturbed for 2h and 30 min at 25 °C. During this time the compounds diffused from the donor plate through the brain lipid membrane into the acceptor plate. After incubation, the donor plate was removed. UV plate reader determined the concentration of the compounds under assessment and the quality control compounds in the acceptor and the donor wells. Every sample was analyzed at three to five wavelengths, in 3 wells and in two independent runs. Results are given as the mean [standard deviation (SD)] and the average of the two runs is reported. Ten quality control compounds (previously mentioned) of known BBB permeability were included in each experiment to validate the analysis set.

Chapter 4 - Synthesis and biological activity of benzhydryl derivatives

4.1. Introduction

4.1.1. *Trypanosoma brucei* and Human African Trypanosomiasis

Trypanosoma brucei is the causal agent of Human African Trypanosomiasis (HAT), a vector-borne neglected disease transmitted by insects of Glossina genus, the tsetse fly [246, 247]. Also known as sleeping sickness, the disease is found in sub-Saharan Africa, where the World Health Organization have been made efforts to eradicate the disease. Although a significant reduction of infections have been accomplished (from about 25,000 cases in 1995 to about 1,000 cases in 2019) [248] HAT continues to be a life-threatening disease, mostly for poor rural populations. The therapeutic arsenal to treat HAT is scarce, mainly based on a few old drugs, and present some safety concerns and limited efficacy [246, 247]. Hence, the development of a safe and efficacious drugs for the treatment of HAT would represent a beneficial impact for populations suffering with this disease.

The urea and carbamate functionalities have been proved to represent important functionalities in the development of antiparasitic agents [249-252]. For instance, Suramin (**146**, **Figure 49**), a urea derivative, is used as an effective therapy during the early stage of sleeping sickness caused by *Trypanosoma brucei* [250, 251]. Compound **148,** an urea analogue of the hit compound 2-(2-benzamido)ethyl-4-phenylthiazole (**147**), showed an IC_{50} (*T.brucei*) of 9 nM with a SI > 18,000) (**Figure 50**) [252]. Mebendazole (**149**, **Figure 51**) a benzimidazole carbamate compound currently used in as a preventive chemotherapy agent for soil-transmitted helminthiasis [253], has been proposed as an agent for other parasitic infections, namely for trypanosomes [254, 255].

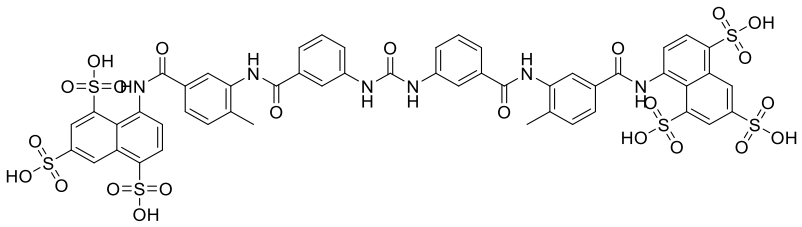

Figure 49. Suramin (**146**).

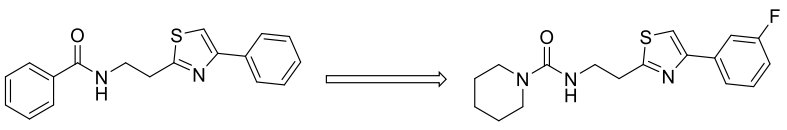

147

IC_{50} (*T.brucei*) = 632 nM

148

IC_{50} (*T.brucei*) = 9 nM

Figure 50. Compound **147** and compound **148**.

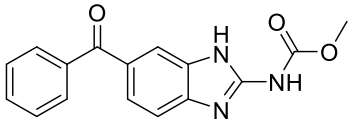

Figure 51. Mebendazole (**149**).

Considering the above-mentioned information, novel urea and carbamates derivatives were synthesized and their activity against *T.brucei* were assessed. Diphenylacetic acid (**150**) was chosen as starting material, considering its structural similarity with the xanthene moiety, though representing a more flexible structure and allowing to increase molecular diversity on the library developed. Additionally, the benzhydryl moiety has been extensively used in medicinal chemistry programs and proved to be able to provide several bioactive compounds [256-260].

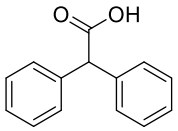

150

Figure 52. Diphenylacetic acid (**150**).

4.2. Synthesis of diphenylacetic acid derivatives

Diphenylacetic acid (**150**, **Figure 52**) was used as starting material for the synthesis of urea and carbamate derivatives through continuous flow synthesis, applying the DPPA-mediated Curtius rearrangement procedure (**Scheme 22**).

Continuous flow procedures have become a widely used technique in organic and medicinal chemistry, allowing the application of old and novel chemistry in a safer, reproducible, and scalable fashion [261]. Moreover, this technique allows the application of in-line extraction and purification procedures, improving automation on synthesis with several gains in a laboratory of organic chemistry. Additionally, moving from batch to continuous chemical processing is now an important goal for the pharmaceutical, specialty chemical, and flavor and fragrance industries [262]. In this work, following previous reports on the application of continuous flow Curtius rearrangement and its significance in modern drug discovery [263, 264], new benzhydryl carbamate and urea derivatives were synthetized through a continuous DPPA-mediated Curtius rearrangement procedure.

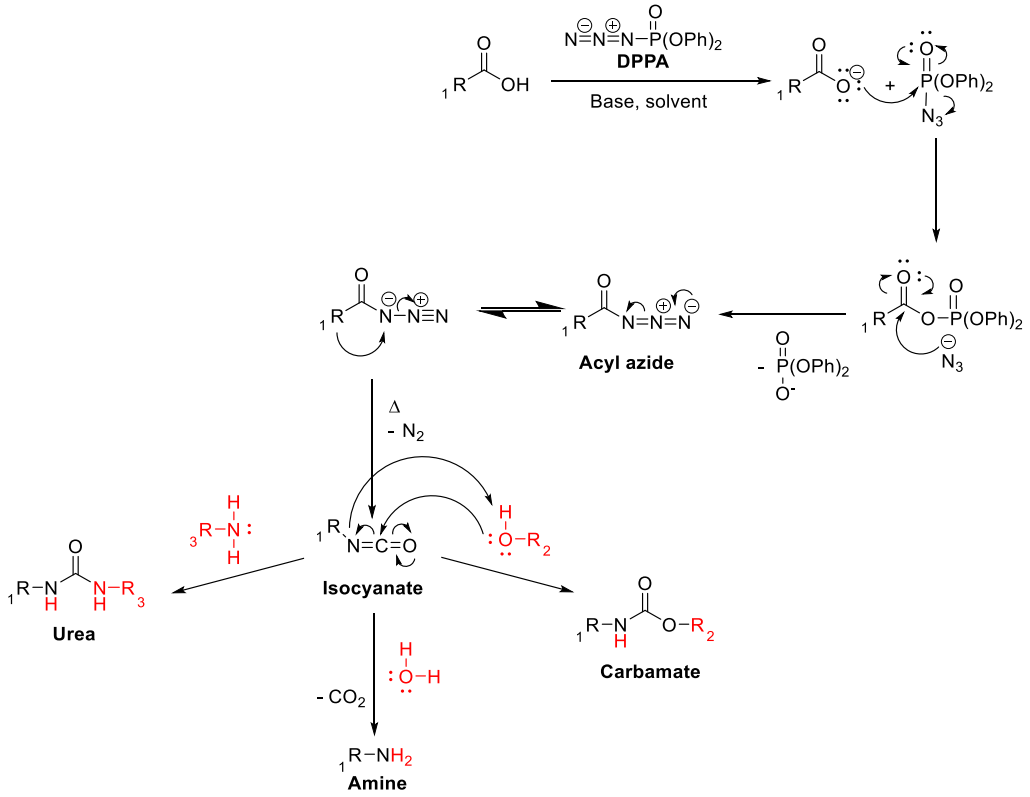

Scheme 22. DPPA-mediated Curtius rearrangement mechanism [265, 266].

4.2.1. Synthesis of benzhydryl carbamates

Six benzhydryl carbamates were synthetized according to **Scheme 23**. In a general procedure, a mixture of triethylamine (2 equiv.), the appropriate alcohol (3 equiv.), diphenylacetic acid (1 equiv.) and diphenylphosphoryl azide (DPPA) (1 mmol) were homogenized in 4 mL of toluene with stirring for 15 min. The obtained mixture flowed directly into a continuous flow chemistry (CFC) reactor (10 mL volume). A total flow rate of 0.25 mL/min, equating to a reactor residence time of 40 min at a temperature of 105 °C, was used to ensure complete conversion. The resulting flow stream was then collected to a round bottom flask and the solvent evaporated. Silica gel flash chromatography allowed to obtain the pure carbamate with an isolated yield of 59 – 80%. **Table 11** summarizes the compounds obtained and the corresponding isolated yield. Further details regarding characterization data are provided in section *4.6. Experimental data*.

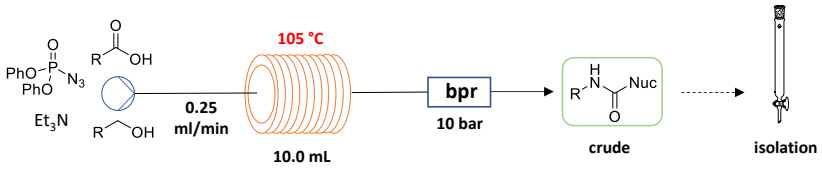

Scheme 23. Synthesis of benzhydryl carbamates through a continuous DPPA-mediated Curtius rearrangement procedure.

Table 11. Benzhydryl carbamates obtained through a continuous DPPA-mediated Curtius rearrangement procedure.

Starting material	Alcohol	Product	Isolated yield (%)
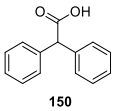 150	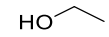	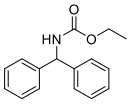 MM81	50
	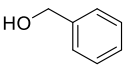	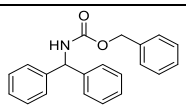 MM85	59
	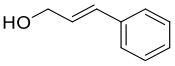	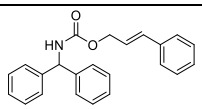 MM88	54
		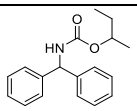 MM90	66
	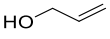	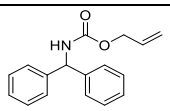 MM91	84
	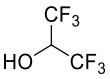	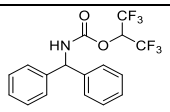 MM92	80

4.2.2. Synthesis of benzhydryl ureas

Employing amines as nucleophile, six benzhydryl ureas were synthetized according to **Scheme 24**. Distinctively from the previous scheme for the synthesis of carbamates, in this time the nucleophile (amine) is not present in the solution flowed through the flow reactor. This modification in the procedure was needed due to the reactivity of amines with the intermediate acyl azide, leading to the formation of amides (**Scheme 25**) [267]. Hence, for the synthesis of ureas, the flow procedure was used to form the isocyanate intermediate. The resulting flow stream was then collected to a round bottom flask containing the amine,

allowing the formation of the urea derivative at rt. Silica gel flash chromatography allowed to obtain the pure ureas with an isolated yield of 35 – 93%. **Table 12** summarizes the compounds obtained and the corresponding isolated yield. Further details regarding characterization data are provided in section ***4.6****. Experimental data*.

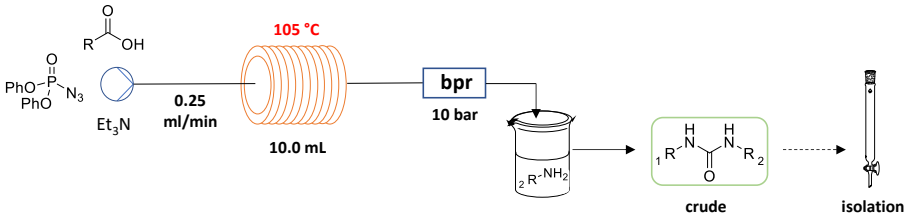

Scheme 24. Synthesis of benzhydryl carbamates through a continuous DPPA-mediated Curtius rearrangement procedure.

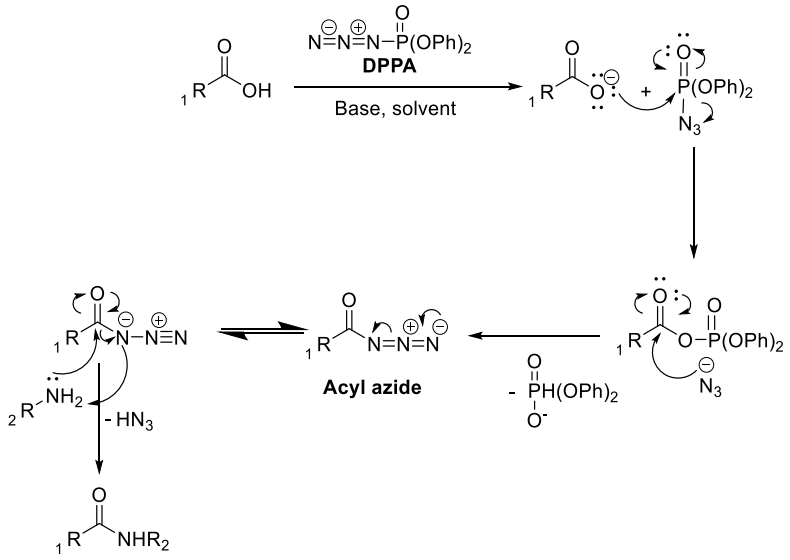

Scheme 25. DPPA-mediated amide bond formation.

Table 12. Benzhydryl ureas obtained through a continuous DPPA-mediated Curtius rearrangement procedure.

Starting material	Amine	Product	Isolated yield (%)
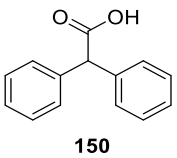 **150**	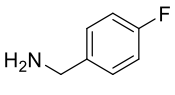	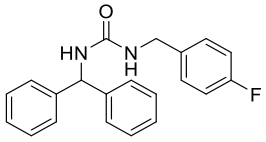 **MM94**	93
		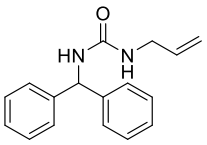 **MM95**	73
	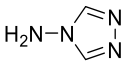	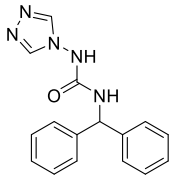 **MM96**	83
	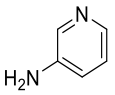	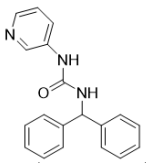 **MM97**	84
	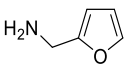	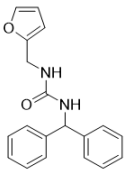 **MM98**	82
	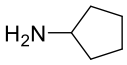	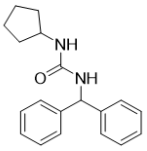 **MM99**	35

4.3. Flow *versus* batch assessment

In order to assess the impact on the reaction's yield of the procedure used - continuous flow or batch procedure - a comparative study was performed, assessing the yield obtained for each of the twelve derivatives obtained. **Table 13** and **Table 14** depict the yield obtained in the synthesis of the benzhydryl carbamates through flow and batch procedure. For the synthesis of the benzhydryl carbamates, the quantity of unreacted starting material (SM) (diphenyl acetic acid) present in the crude product was also quantified.

Table 13. Yield obtained in the synthesis of the benzhydryl carbamates through flow and batch procedures and unreacted SM.

	Yield (%)		Unreacted SM (%)	
Entry	**Flow[a]**	**Batch[a,b]**	**Flow[a]**	**Batch[a,b]**
MM81	50	60	13	7
MM85	60	91	8	1
MM88	45	93	9	2
MM90	24	42	5	n.d.
MM91	57	78	5	n.d.
MM92	39	79	41	2

[a] Yield calculated from crude NMR using an internal standard
[b] i) toluene, DPPA, TEA, rt, 0.5 h; ii) 110 °C, 0.5 h; iii) alcohol, 110 °C, 2.0 h.
n.d.: not detected

Table 14. Yield obtained in the synthesis of the benzhydryl ureas through flow and batch procedures.

	Yield (%)	
Entry	**Flow[a]**	**Batch[a,b]**
MM94	89	97
MM95	71	96
MM96	51	98
MM97	82	85
MM98	78	96
MM99	67	74

[a] Yield calculated from crude NMR using an internal standard
[b] i) toluene, DPPA, TEA, rt, 0.5 h; ii) 110 °C, 0.5 h; iii) amine, 110 °C, 2.0 h.
n.d.: not detected

Unexpectedly, it was observed that the flow procedure led to a lower yield comparing with the batch procedure, for all the carbamate and urea derivatives synthetized. As previously mentioned, the application of continuous flow techniques provides several advantages regarding safety, reproducibility, and scalability comparing with the traditional batch procedure. An improved reaction yield is also expected, considering the precise control over the reaction conditions, namely temperature and stoichiometry. Nonetheless, in this procedure such improved yield was not observed. In an attempt to understand the reasons

for the results obtained, three possible causes were hypothesized as potential responsible for the lowest performance of the flow technique:

i) Unreacted SM: the first step of the Curtius rearrangement reaction is the formation of the acyl azide, reacting the carboxylic acid group with DPPA. This step was performed stirring at room temperature for 15 min at the flow procedure and for 30 min at the batch procedure, and such difference in the reaction time may have led to higher levels of unreacted starting material in the flow procedure. However, as depicted in **Table 13**, with exception of **MM92,** a lower percentage of unreacted diphenyl acetic acid is observed (bellow 13%), which suggests that this should not be the single reason for the unsatisfactory yields obtained in the flow procedure.

ii) Incomplete conversion acyl azide -> isocyanate: the formation of the isocyanate intermediate is a crucial step for the subsequent reaction with a nucleophile. An incomplete conversion may also have impacted the yield obtained in flow, namely due to insufficient temperature. Beyond the 5 ºC difference used in flow *versus* the batch procedure, considering that this conversion is exothermic, the temperature in the batch procedure may be higher than 105°C, favoring the conversion of the acyl azide in isocyanate and, consequently, the reaction yield.

iii) Dimer formation (traces of water): as depicted in **Scheme 22**, the presence of water in the reaction medium/system would lead to the formation of an amine; thus, the amine will act as a nucleophile and react with another isocyanate intermediate, forming a dimer connected by a urea group. The formation of this by-product may be reduced in the batch procedure, once this is an open system, allowing the water molecules to escape under temperature conditions above its boiling point.

Further studies would allow to assess the impact of 1) residence time; 2) temperature; 3) anhydrous conditions in the continuous flow Curtius rearrangement procedure, in order to achieve an improved process for the synthesis of carbamate and urea derivatives. Additionally, the integration of an automated flash chromatography system with the flow reactor would provide the continuous synthesis and isolation of the desire products, enhancing automation and scalability.

4.4. Biological activity results and discussion

4.4.1. Activity against *Trypanosoma brucei*

The twelve compounds obtained - six carbamate and six urea derivatives - were assessed regarding their potential to inhibit the growth of *T.brucei*. Additionally, and following previous disclosures of xanthene derivatives with antitrypanosoma activity [86, 247], twenty-one xanthene derivatives (described in **Chapter 3**) were also evaluated.

A stock solution of 10 mg/mL was prepared in DMSO, and the compounds were kept at -20 °C until the assay was performed. Then, a first assay was performed for a preliminary minimum inhibitory concentration (MIC) determination, using concentrations ranging from 100 – 0.01 µg/mL (10-fold dilutions). Compounds were considered effective and advanced to the IC_{50} determination if MIC < 1 µg/mL. The dye used was Alamar blue, and the fluorescence was measured in a BMG FLUOstar Omega (excitation: 544 nm, emission: 595 nm). The results obtained in the first assay are depicted in **Table 15** and **Table 16** for xanthene derivatives and diphenylacetic acid derivatives, respectively.

Table 15. Preliminary MIC determination for *T. brucei* of xanthene derivatives.

Compound	MIC (µg/mL	MIC (µM)
MM7B	10	36.6
MM29	100	471.1
MM30	100	340.9
MM32	100	338.6
MM36	10	35.5
MM42B	10	32.8
MM42C	100	327.5
MM43	100	352.9
MM46	10	37.4
MM48A	100	285.9
MM50	10	35.8
MM52	100	338.8
MM54	100	260.4
MM56B	10	22.1
MM57A	100	215.9
MM57B	100	215.9
MM59B3	100	319.1
MM63B	1	3.1
MM68	10	19.2
MM73	100	226.7
MM74	100	212.3

Table 16. Preliminary MIC determination for *T. brucei* of diphenyl acetic acid derivatives.

Compound	MIC (µg/mL)	MIC (µM)
MM81	100	391.7
MM85	10	31.5
MM88	10	29.1
MM90	10	35.3
MM91	10	37.4
MM92	10	26.5
MM94	10	29.9
MM95	100	375.5
MM96	100	340.9
MM97	10	33.0
MM98	10	32.6
MM99	1	3.4

The urea derivative **MM99,** comprising a urea moiety with a terminal cyclopentane ring, showed the best result in the *in vitro* assay performed, with a MIC = 3.4 µM. This compound has a 8-fold improved activity comparing with the second most active compound – **MM92** – which contains a carbamate moiety with a 1,1,1,3,3,3-hexafluoro-2-methylpropane terminal. **MM99** is the only derivative comprising a terminal cycloalkane ring. Other compounds comprising different terminal cycloalkane ring, with carbamate or urea moieties, should be obtained in further studies in order to confirm if this moiety provides improved activity for *T. brucei*.

Regarding the xanthene derivatives, **MM63B** showed to be the post potent derivative in this series, with a MIC = 3.1 µM. These results are in line with prior studies, reporting interesting activities of xanthenes comprising a carboxamide moiety with a long alkyl chain with a terminal nitrogen [85, 86]. The next two most active compounds are **MM68** and **MM56**, xanthene carboxamides comprising a morpholine moiety in the central position of the xanthene and substituted in positions 2,7 of the xanthene aromatic rings with bromo and 2,4-difluorophenyl, respectively. Together with the results from compound **MM32** (xanthene scaffold unsubstituted), it indicates that the inclusion of bromine in these positions of the tricyclic moiety improves activity. Considering the results of **MM68**, the presence of a bulky group also appears to be benefic (**Figure 53**).

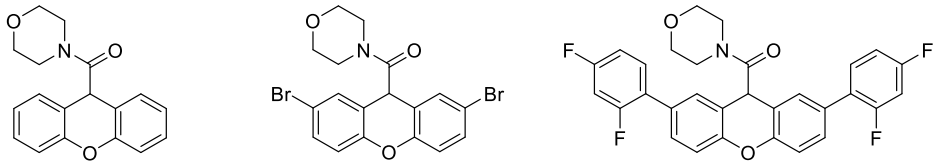

MM32 MIC= 338.6 (µM)

MM56 MIC= 22.1 (µM)

MM68 MIC= 19.2 (µM)

Figure 53. Comparison of the MIC of compounds **MM32**, **MM56** and **MM68**.

Xanthene derivative **MM63B** and diphenyl acetic acid derivative **MM99** were investigated in an additional assay, for the determination of IC_{50} values against *T. brucei*, using concentrations ranging from 3.2 – 0.05 µg/mL (2-fold dilutions). The dye used was Alamar blue, and the fluorescence was measured in a BMG FLUOstar Omega (excitation: 544 nm, emission: 595 nm). The results are depicted in **Table 17**.

Table 17. Determination of IC_{50} for for *T. brucei*.

Compound	IC_{50} (µg/mL)	IC_{50} (µM)
MM63B	2.346 ± 0.467	7.2
MM99	0.318 ± 0.097	1.1

Compounds **MM63B** and **MM99** showed interesting values of IC_{50}, of 7.2 µM and 1.1 µM, respectively, against *T. brucei.* Hence, in other to assess the safety of these compounds, their cytotoxicity was evaluated and the selectivity index (SI) calculated. IC_{50} in HeLa cells was determined, using concentrations ranging from 100 – 1.5 µg/mL (2-fold dilutions). The dye used was Alamar blue, and the fluorescence was measured in a BMG FLUOstar Omega (excitation: 544 nm, emission: 595 nm). Selectivity index was calculated through the ratio IC_{50} (HeLa cells) / IC_{50} (*T. brucei)*. **Table 18** and **Table 19** depict the results obtained.

Table 18. MIC determination for HeLa cells.

Compound	MIC (µg/mL)	MIC (µM)
MM63B	100	308.2
MM99	100	339.7

Table 19. Determination of IC_{50} for HeLa cells and selectivity index.

Compound	IC_{50} (µg/mL)	IC_{50} (µM)	Selectivity index
MM63B	3.38	6.508	0.9
MM99	57.64	>100	181.4

Compound **MM63** showed an IC_{50} of 3.38 µg/mL for HeLa cells. Considering the results obtained for *T. brucei*, it results to an undesired selectivity index below 1, showing that compound **MM63** does not represent a suitable compound for further studies once it possesses cytotoxic issues. On the other side, compound **MM99** showed an IC_{50} of 57.64 µg/mL for HeLa cells, representing a selectivity index for *T. brucei* of 181.4. These results shows that compound **MM99** has an adequate selectivity for *T. brucei* parasite comparing with HeLa cells, indicating a potential suitability for administration without causing cytotoxicity issues. Hence, compound **MM99** was chosen for an *in vivo* assay, to study the tolerability in a BALB/c mice, at doses as high as 150 mg/kg, according to the scheme in **Table 20**.

Table 20. Application scheme of compound **MM99** in BALB/c mice for tolerability study.

Time point (h)	Dose applied (mg/kg)	Cumulative dose
0	20	20
2	30	50
4	50	100
6	50	150

Compound **MM99** showed to be well tolerated at the cumulative dose of 150 mg/kg. Hence, considering the preliminary results regarding cytotoxicity and efficacy obtained, compound **MM99** will be further study in a *in vivo* model to assess its *in vivo* efficacy. These results will allow to confirm the results obtained *in vitro* and support the further development of the compound, namely move on to a hit-to-lead optimization process, to improve their pharmacodynamic and pharmacokinetic properties. Additionally, studies regarding the molecular target should be performed, namely, assessing the impact of the compounds on trypanothione reductase, a vulnerable target for drugs that disrupt the natural redox defense systems of the parasite [268].

4.5. Conclusion

In summary, six carbamate and six urea derivatives comprising a benzhydryl moiety were obtained, through a straightforward process employing continuous flow synthesis and DPPA-mediated Curtius rearrangement. The compounds herein obtained, as well as twenty-one xanthene derivatives described in the previous chapter were assessed regarding their ability to inhibit T. brucei growth. The urea derivative **MM99** showed the most promising result in the *in vitro* assay performed, with an IC_{50} = 1.1 µM and a selectivity index of 181.4. Additionally, this compound showed to be well tolerated in an *in vivo* assay, at the cumulative dose of 150 mg/kg. Further modifications on the urea **MM99**, namely adding substituents to the cyclopentane ring and/or on the aromatic rings, would provide additional information on the structure activity of this class of compounds.

4.6. Experimental data

4.6.1. Chemical synthesis and characterization

4.6.1.1. General information

All reagents and solvents were purchased from TCI (Tokyo Chemical Industry Co. Ltd., Chuo-ku, Tokyo, Japan), Acros Organics (Geel, Belgium), Sigma-Aldrich (Sigma-Aldrich Co. Ltd., UK), or Alfa Aesar (Thermo Fisher GmbH, Kandel, Germany) and were used directly without any further purification. All reactions were monitored by Thin-layer chromatography (TLC), carried out on Merck silica gel 60 (GF254) precoated plates by using appropriate mobile phases. Purification of the synthesized compounds was usually performed by flash column chromatography using Merck silica gel 60 (0.040–0.063 mm). Melting points (mp) were measured by using a Köfler microscope (Wagner and Munz, Munich, Germany) equipped with a Crison TM 65 (Crison Instruments, Barcelona, Spain) and were uncorrected. ^{1}H and ^{13}C NMR spectra were taken in $CDCl_3$ or $[D_6]$DMSO (Deutero GmbH, Kastellaun, Germany) at rt on 400 MHz instrument. ^{13}C-NMR spectra were recorded on the same instruments (100 MHz). Chemical shifts are expressed in relative to tetramethylsilane (TMS) as an internal reference.^{13}C-NMR assignments were made by 2D HSQC and HMBC experiments. For the assignment of each signal to the corresponding proton or carbon, it was considered the automatic numeration provided by MestReNova®, as provided in **Annex 1**. Continuous flow experiments were performed on a *Vapourtec easy-Scholar E-Series flow reactor* system, comprising a 10 mL volume reactor.

4.6.1.2. Synthesis, purification and structural characterization

Synthesis of ethyl benzhydrylcarbamate (MM81)

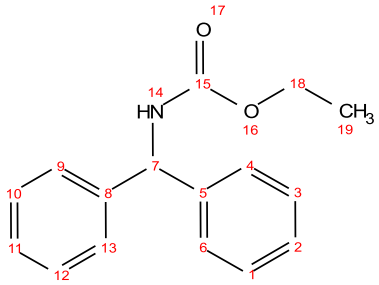

A mixture of triethylamine (0.14 mL, 1 mmol), absolute EtOH (0.09 mL, 1.5 mmol), diphenylacetic acid (**161**) (0.106 g, 0.5 mmol) and DPPA (0.138g, 0.5 mmol) were homogenized in 4 mL of toluene with stirring for 15 min. The obtained mixture flowed directly into a CFC reactor (10 mL volume). A total flow rate of 0.25 mL/min, equating to a reactor residence time of 40 min at a temperature of 105 °C, was used to ensure complete conversion. The resulting flow stream was then collected to a round bottom flask and the solvent evaporated. The crude product was purified by silica gel flash chromatography (EtOAc/hexane 10:90). Compound **MM81** was obtained as a beige powder (63.9 mg, 50 %).

Compound MM81: white powder (63.9 mg, 50 %); mp: 127 – 128 °C; ^{1}H NMR (400 MHz, $CDCl_3$) δ 7.38 – 7.20 (m, 10H, H-1 – H-4, H-6, H-9 – H13), 5.96 (s, 1H, H-7), 5.28 (s, 1H, H-14), 4.13 (q, *J* = 7.1 Hz, 2H, H-18), 1.30 – 1.18 (m, 3H, H-19); ^{13}C NMR (101 MHz, $CDCl_3$) δ 156.0 (C-15), 142.0 (C-5, C-8), 128.8 (C-1, C-3, C-10, C-12), 127.6 (C-2, C-11), 127.4 (C-4, C-6, C-9, C-13), 61.3 (C-18), 58.9 (C-7), 14.7 (C-19). ; HRMS (ESI): m/z calculated for $C_{16}H_{17}NO_2$ [M+Na^+]: 278.11515; found: 278.11800.

Synthesis of benzyl benzhydrylcarbamate (MM85)

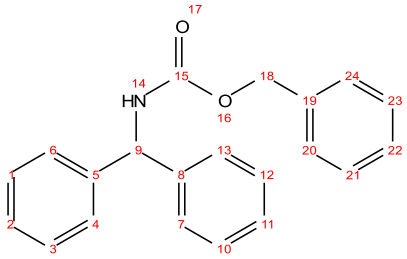

A mixture of triethylamine (0.14 mL, 1 mmol), benzyl alcohol (0.21 mL, 1.5 mmol), diphenylacetic acid (**161**) (0.106 g, 0.5 mmol) and DPPA (0.138g, 0.5 mmol) were homogenized in 4 mL of toluene with stirring for 15 min. The obtained mixture flowed directly into a CFC reactor (10 mL volume). A total flow rate of 0.25 mL/min, equating to a reactor residence time of 40 min at a temperature of 105 °C, was used to ensure complete conversion. The resulting flow stream was then collected to a round bottom flask and the solvent evaporated. The crude product was purified by silica gel flash chromatography (EtOAc/hexane 10:90). Compound **MM85** was obtained as a white powder (93.0 mg, 59 %).

Compound MM85: white powder (93.0 mg, 59 %); mp: 99 – 100 °C; ^{1}H NMR (400 MHz, $CDCl_3$) δ 7.39 – 7.21 (m, 15H, (H-1 – H-4, H-6, H-7, H-10 – H-13, H-20 – H-24), 5.99 (d, *J* = 8.1 Hz, 1H, H-9), 5.40 (s, 1H, H-14), 5.12 (s, 2H, H-18); ^{13}C NMR (101 MHz, $CDCl_3$) δ 155.6 (C-15), 141.6 (C-5, C-8), 136.3 (C-19), 128.8 (C-21, C-23), 128.7 (C-1, C-3,C-10, C-12, 128.5 (C-20, C-24), 127.8 (C-22) , 127.5 (C-2, C-11), 127.2 (C-4, C-6, C-9, C-13), 67.0 (C-18), 58.8 (C-9); HRMS (ESI): m/z calculated for $C_{21}H_{19}NO_2$ [M+Na^+]: 340.13080; found: 340.13448.

Synthesis of cinnamyl benzhydrylcarbamate (MM88)

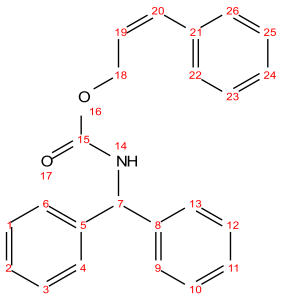

A mixture of triethylamine (0.14 mL, 1 mmol), *trans*-cinnamyl alcohol (0.205 g,1.5 mmol), diphenylacetic acid (**161**) (0.106 g, 0.5 mmol) and DPPA (0.138g, 0.5 mmol) were homogenized in 4 mL of toluene with stirring for 15 min. The obtained mixture flowed directly into a CFC reactor (10 mL volume). A total flow rate of 0.25 mL/min, equating to a reactor residence time of 40 min at a temperature of 105 °C, was used to ensure complete conversion. The resulting flow stream was then collected to a round bottom flask and the solvent evaporated. The crude product was purified by silica gel flash chromatography (EtOAc/hexane 10:90). Compound **MM88** was obtained as a white powder (54.0 mg, 31 %).

Compound MM88: white powder (54.0 mg, 31 %); mp: 119 – 120 °C ; ^{1}H NMR (400 MHz, $CDCl_3$) δ 7.44 – 7.19 (m, 15H, H-1 – H-4, H-6, H-9 – H-13, H-22 – H-26), 6.64 (d, *J* = 15.8 Hz, 1H, H-20), 6.29 (d, *J* = 15.8 Hz, 1H, H-19), 6.00 (d, *J* = 8.1 Hz, 1H, H-7), 5.39 (s, 1H, H-14), 4.75 (dd, *J* = 6.3, 1.4 Hz, 2H, H-18); ^{13}C NMR (101 MHz, $CDCl_3$) δ 155.5 (C-15), 141.7 (C-5, C-8), 136.3 (C-21), 133.8 (C-20), 128.7 (C-1, C-3, C-10, C-12), 128.6 (C-23, C-25), 128.0 (C-24), 127.5 (C-2, C-11), 127.3 (C-4, C-6, C-9, C-13, 126.6 (C-22, C-26), 123.7 (C-19), 65.7 (C-18), 58.9 (C-7); HRMS (ESI): m/z calculated for $C_{23}H_{21}NO_2$ [M+ Na^+]: 366.14645; found: 366.15081.

Synthesis of *sec*-butyl benzhydrylcarbamate (MM90)

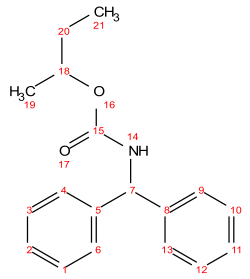

A mixture of triethylamine (0.28 mL, 1 mmol), 2-butanol (0.28 mL, 3 mmol), diphenylacetic acid (**161**) (0.212 g, 1 mmol) and DPPA (0.275 g, 1 mmol) were homogenized in 4 mL of toluene with stirring for 15 min. The obtained mixture flowed directly into a CFC reactor (10 mL volume). A total flow rate of 0.25 mL/min, equating to a reactor residence time of 40 min at a temperature of 105 °C, was used to ensure complete conversion. The resulting flow stream was then collected to a round bottom flask and the solvent evaporated. The crude product was purified by silica gel flash chromatography (EtOAc/hexane 10:90). Compound **MM90** was obtained as a white powder (193.7 mg, 66 %).

Compound MM90: white powder (193.7 mg, 66 %); mp: 70 – 71 °C ; ^{1}H NMR (400 MHz, $CDCl_3$) δ 7.37 – 7.19 (m, 10H, H-1 – H-4, H-6, H-9 – H-13), 5.96 (s, 1H, H-7), 5.25 (s, br, 1H, H-14), 4.76 (h, *J* = 6.3 Hz, 1H, H-18), 1.51 (s, 2H, H-20), 1.20 (s, 3H, H-19), 0.89 (s, 3H, H-21); ^{13}C NMR (101 MHz, $CDCl_3$) δ 155.7 (C-15), 141.9 (C-5, C-8), 128.6 (C-1, C-3, C-10, C-12), 127.4 (C-2, C-11), 127.2 (C-4, C-6, C-9, C-13), 58.8 (C-7), 29.0 (C-20), 19.7 (C-19), 9.6 (C-21) ; HRMS (ESI): m/z calculated for $C_{18}H_{21}NO_2$ [M+ Na^+]: 306.14645; found: 306.14974.

Synthesis of allyl benzhydrylcarbamate (MM91)

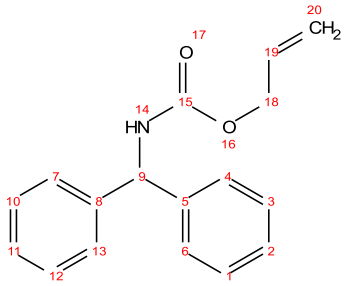

A mixture of triethylamine (0.28 mL, 2 mmol), allyl alcohol (0.20 mL, 3 mmol), diphenylacetic acid (**161**) (0.212 g, 1 mmol) and DPPA (0.275 g, 1 mmol) was homogenized in 4 mL of toluene with stirring for 15 min. The obtained mixture flowed directly into a CFC reactor (10 mL volume). A total flow rate of 0.25 mL/min, equating to a reactor residence time of 40 min at a temperature of 105 C, was used to ensure complete conversion. The resulting flow stream was then collected to a round bottom flask and the solvent evaporated. The crude product was purified by silica gel flash chromatography (EtOAc/hexane 10:90). Compound **MM91** was obtained as a white powder (224.3 mg, 84 %).

Compound MM91: white powder (224.3 mg, 84 %); mp: 72 °C ; ^{1}H NMR (400 MHz, $CDCl_3$) δ 7.38 – 7.22 (m, 10H, H4 – H-6, H-7 – H13), 5.98 (d, *J* = 9.5 Hz, 1H, H-9), 5.91 (s, 1H, H-19), 5.45 – 5.24 (m, 2H, H-20), 5.21 (d, *J* = 9.5 Hz, 1H, H-14), 4.59 (dt, *J* = 5.6, 1.4 Hz, 2H, H-18); ^{13}C NMR (101 MHz, $CDCl_3$) δ 155.4 (C-15), 141.7 (C-5, C-8), 132.7 (C-19), 128.7 (C-1, C-3, C-10, C-12), 127.5 (C-2, C-12), 127.2 (C-4, C-6, C-7, C-13), 117.9 (C-20), 65.8 (C-18), 58.8 (C-9) ; HRMS (ESI): m/z calculated for $C_{17}H_{17}NO_2$ [M+ Na^+]: 290.11515; found: 290.11789.

Synthesis of 1,1,1,3,3,3-hexafluoropropan-2-yl benzhydrylcarbamate (MM92)

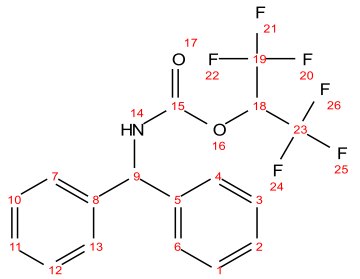

A mixture of triethylamine (0.28 mL, 2 mmol), 1,1,1,3,3,3-hexafluoro-2-propanol (0.32 mL, 3 mmol), diphenylacetic acid (**161**) (0.212 g, 1 mmol) and DPPA (0.275 g, 1 mmol) were homogenized in 4 mL of toluene with stirring for 15 min. The obtained mixture flowed directly into a CFC reactor (10 mL volume). A total flow rate of 0.25 mL/min, equating to a reactor residence time of 40 min at a temperature of 105 °C, was used to ensure complete conversion. The resulting flow stream was then collected to a round bottom flask and the solvent evaporated. The crude product was purified by silica gel flash chromatography (EtOAc/hexane 5:95). Compound **MM92** was obtained as a white powder (321.8 mg, 80 %).

Compound MM92: white powder (321.8 mg, 80 %); mp: 108 – 109 °C; ^{1}H NMR (400 MHz, $CDCl_3$) δ 7.39 – 7.21 (m, 10H, H-4 – H-6, H-7 – H13), 5.98 (d, *J* = 7.8 Hz, 1H, H-9), 5.76 – 5.62 (m, 2H, H-14, H-18).; ^{13}C NMR (101 MHz, $CDCl_3$) δ 151.7 (C-15), 140.2 (C-5, C-8), 128.9 (C-1, C-3, C-10, C-12), 128.0 (C-2, C-11), 127.1 (C-4, C-6, C-7, C-13), 122.0 and 119.1 (C-19, C-13), 68.1, 67.8 and 67.4 (C-18), 59.6 (C-9) ; HRMS (ESI): m/z calculated for $C_{17}H_{13}F_6NO_2$ [M+ Na^+]: 400.07427; found: 400.07979.

Synthesis of 1-benzhydryl-3-(4-fluorobenzyl)urea (MM94)

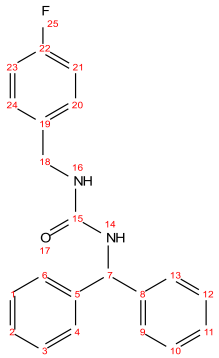

A mixture of triethylamine (0.28 mL, 2 mmol), diphenylacetic acid (**161**) (0.212 g, 1 mmol) and DPPA (0.275 g, 1 mmol) were homogenized in 4 mL of toluene with stirring for 15 min. The obtained mixture flowed directly into a CFC reactor (10 mL volume). A total flow rate of 0.25 mL/min, equating to a reactor residence time of 40 min at a temperature of 105 °C, was used to ensure complete conversion. The resulting flow stream was then collected to a round bottom flask containing 4-fluorobenzylamine (0.34 mL, 3 mmol) solubilized in 2 mL of toluene. After stirring for 15 min at rt the solvent was evaporated. The crude product was purified by silica gel flash chromatography (EtOAc/hexane 30:70). Compound **MM94** was obtained as yellowish powder (313.4 mg, 93 %).

Compound MM94: white powder (313.4 mg, 93 %); mp: 138 – 140 °C; ^{1}H NMR (400 MHz, DMSO-d_6) δ 7.34 – 7.17 (m, 12H, H-1 – H-4, H-6, H9 – H-13, H-20, H-24), 7.13 – 7.06 (m, 2H, H-21, H-23), 6.99 (d, J = 8.6 Hz, 1H, H-14), 6.38 (t, J = 6.1 Hz, 1H, H-16), 5.90 (d, J = 8.6 Hz, 1H, H-7), 4.19 (d, J = 6.1 Hz, 2H, H-18); ^{13}C NMR (101 MHz, DMSO-d_6) δ 162.7 and 160.3 (C-22), 157.7 (C-15), 144.1 (C-5, C-8), 137.4 (C-19), 129.4 and 129.3 (C-20, C-24), 128.8 (C-1, C-3, C-10, C-12), 127.4 (C-2, C-11), 127.2 (C-4, C-6, C-9, C-13), 115.5 and 115.3 (C-21, C-23), 57.4 (C-7) , 42.6 (C-18).

Synthesis of 1-benzhydryl-3-(4-fluorobenzyl)urea (MM95)

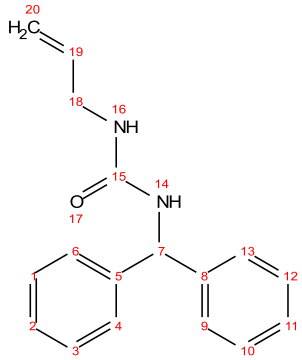

A mixture of triethylamine (0.28 mL, 2 mmol), diphenylacetic acid (**161**) (0.212 g, 1 mmol) and DPPA (0.275 g, 1 mmol) were homogenized in 4 mL of toluene with stirring for 15 min. The obtained mixture flowed directly into a CFC reactor (10 mL volume). A total flow rate of 0.25 mL/min, equating to a reactor residence time of 40 min at a temperature of 105 °C, was used to ensure complete conversion. The resulting flow stream was then collected to a round bottom flask containing allylamine (0.23 mL, 3 mmol) solubilized in 2 mL of toluene. After stirring for 15 min at rt the solvent was evaporated. The crude product was purified by silica gel flash chromatography (EtOAc/hexane 30:70). Compound **MM95** was obtained as a white powder (195.6 mg, 73 %).

Compound MM95: white powder (195.6 mg, 73 %); mp: 132 °C; ^{1}H NMR (400 MHz, $CDCl_3$) δ 7.34 – 7.18 (m, 10H, H-1 – H-4, H-6, H-9 – H-13), 5.92 (d, *J* = 7.1 Hz, 1H, H-7), 5.76 (ddt, *J* = 17.2, 10.5, 5.7 Hz, 1H, H-19), 5.35 (d, *J* = 7.1 Hz, 1H, H-14), 5.11 – 4.98 (m, 2H, H-20), 4.75 (t, *J* = 5.7 Hz, 1H, H-16), 3.71 (tt, *J* = 5.7, 1.8 Hz, 2H, H-18); ^{13}C NMR (101 MHz, $CDCl_3$) δ 157.4 (C-15), 142.2 (C-5, C-8), 135.2 (C-19), 128.6 (C-1, C-3, C-10, C-12), 127.4 (C-2, C-11) 127.3 (C-4, C-6, C-9, C-13), 115.5 (C-20), 58.5 (C-7), 42.9 (C-18). ; HRMS (ESI): m/z calculated for $C_{17}H_{18}N_2O$ [M+ Na^+]: 289.13113; found: 289.13429.

Synthesis of 1-benzhydryl-3-(4*H*-1,2,4-triazol-4-yl)urea (MM96)

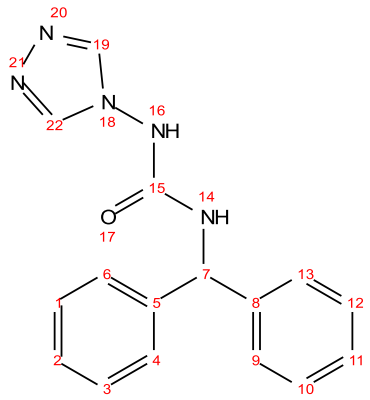

A mixture of triethylamine (0.28 mL, 2 mmol), diphenylacetic acid (**161**) (0.212 g, 1 mmol) and DPPA (0.275 g, 1 mmol) was homogenized in 4 mL of toluene with stirring for 15 min. The obtained mixture flowed directly into a CFC reactor (10 mL volume). A total flow rate of 0.25 mL/min, equating to a reactor residence time of 40 min at a temperature of 105 °C, was used to ensure complete conversion. The resulting flow stream was then collected to a round bottom flask containing 4-amino-4*H*-1,2,4-triazole (0.255 g, 3 mmol) solubilized in 2 mL of toluene. After stirring for 15 min at rt the solvent was evaporated. The crude product was purified by silica gel flash chromatography (MeOH/EtOAc 10:90). Compound **MM96** was obtained as a white powder (244.1 mg, 83 %).

Compound MM96: white powder (244.1 mg, 83 %); mp: 230 °C; ^{1}H NMR (400 MHz, DMSO-d_6) δ 9.49 (s, 1H, H-16), 8.57 (s, 2H, H-19, H-22), 8.16 (d, *J* = 8.6 Hz, 1H, H-14), 7.37 – 7.19 (m, 10H, H-4 – H-6, H-9 – H-13), 5.97 (d, *J* = 8.6 Hz, 1H, H-7); ^{13}C NMR (101 MHz, DMSO-d_6) δ 156.0 (C-15), 145.1 (C-19, C-22), 143.0 (C-5, C-8), 128.9 (C-1, C-3, C-10, C-12), 127.6 (C-4, C-6, C-9, C-13), 127.5 (C-2, C-11), 57.6 (C-7).

Synthesis of 1-benzhydryl-3-(pyridin-3-yl)urea (MM97)

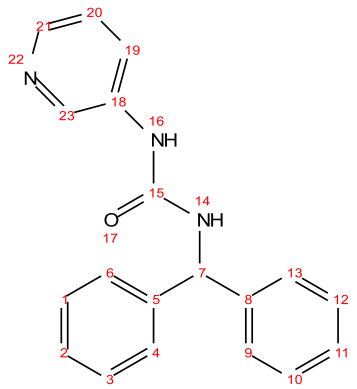

A mixture of triethylamine (0.28 mL, 2 mmol), diphenylacetic acid (**161**) (0.212 g, 1 mmol) and DPPA (0.275 g, 1 mmol) was homogenized in 4 mL of toluene with stirring for 15 min. The obtained mixture flowed directly into a CFC reactor (10 mL volume). A total flow rate of 0.25 mL/min, equating to a reactor residence time of 40 min at a temperature of 105 °C, was used to ensure complete conversion. The resulting flow stream was then collected to a round bottom flask containing 3-aminopyridine (0.285 g, 3 mmol) solubilized in 2 mL of toluene. After stirring for 15 min at rt the solvent was evaporated. The crude product was purified by silica gel flash chromatography (EtOAc/hexane 80:20). Compound **MM97** was obtained as a white powder (258.3 mg, 84 %).

Compound MM97: white powder (258.3 mg, 84 %); mp: 173 – 174 °C; ^{1}H NMR (400 MHz, DMSO-d_6) δ 8.62 (s, 1H, H-16), 8.50 (d, J = 2.7 Hz, 1H, H-23)), 8.10 (dd, J = 4.6, 1.5 Hz, 1H, H-21), 7.86 (ddd, J = 8.3, 2.6, 1.5 Hz, 1H, H-19), 7.38 – 7.19 (m, 12H, H-1 – H-4, H-6, H-9 – H-14, H-20), 5.96 (d, J = 8.0 Hz, 1H, H-7); ^{13}C NMR (101 MHz, DMSO-d_6) δ 154.7 (C-15), 143.4 (C-5, C-8), 142.8 (C-21), 139.9 (C-23), 137.3 (C-18), 129.0 (C-1, C-3, C-10, C-12), 127.5 (C-2, C-11), 127.4 (C-4, C-6, C-9, C-13), 124.8 (C-19), 124.0 (C-20), 57.4 (C-7); HRMS (ESI): m/z calculated for $C_{19}H_{17}N_3O$ [M+ Na^+]: 304.14444; found: 304.14764.

Synthesis of 1-benzhydryl-3-(furan-2-ylmethyl)urea (MM98)

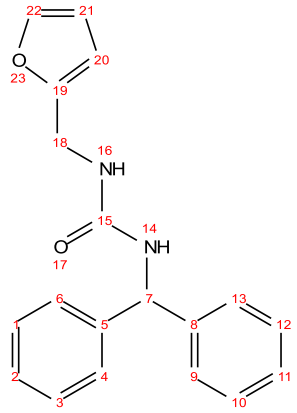

A mixture of triethylamine (0.28 mL, 2 mmol), diphenylacetic acid (**161**) (0.212 g, 1 mmol) and DPPA (0.275 g, 1 mmol) was homogenized in 4 mL of toluene with stirring for 15 min. The obtained mixture flowed directly into a CFC reactor (10 mL volume). A total flow rate of 0.25 mL/min, equating to a reactor residence time of 40 min at a temperature of 105 °C, was used to ensure complete conversion. The resulting flow stream was then collected to a round bottom flask containing furfurylamine (0.26 mL, 3 mmol) solubilized in 2 mL of toluene. After stirring for 15 min at rt the solvent was evaporated. The crude product was purified by silica gel flash chromatography (EtOAc/hexane 20:80). Compound **MM98** was obtained as a white powder (254.0 mg, 82 %).

Compound MM98: white powder (254.0 mg, 82 %); mp: 131 – 132 °C; ^{1}H NMR (400 MHz, DMSO-d_6) δ 7.53 (dd, J = 1.9, 0.9 Hz, 1H, H-22), 7.34 – 7.16 (m, 10H, H-1 – H-4, H-6, H-9 – H-13), 6.94 (d, J = 8.5 Hz, 1H, H-14), 6.35 (dd, J = 3.2, 1.9 Hz, 1H, H-21), 6.27 (t, J = 5.8 Hz, 1H, H-16), 6.16 (dq, J = 3.2, 0.9 Hz, 1H, H-20), 5.89 (d, J = 8.5 Hz, 1H, H-7), 4.19 (dd, J = 5.8, 0.9 Hz, 2H, H-18); ^{13}C NMR (101 MHz, DMSO-d_6) δ 157.3 (C-15), 153.9 (C-19), 144.0 (C-5, C-8), 142.4 (C-22), 128.8 (C-1, C-3, C-10, C-12), 127.3 (C-4, C-6, C-9, C-13), 127.2 (C-2, C-11), 110.8 (C-21), 106.7 (C-20), 57.3 (C-7), 36.8 (C-18). ; HRMS (ESI): m/z calculated for $C_{19}H_{18}N_2O_2$ [M+ H^+]: 307.14410; found: 307.14727.

Synthesis of 1-benzhydryl-3-cyclopentylurea (MM99)

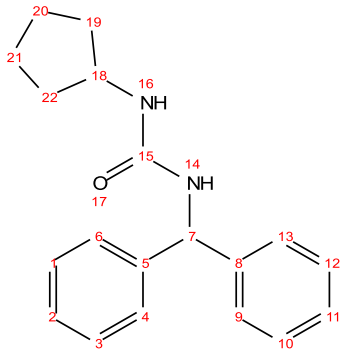

A mixture of triethylamine (0.28 mL, 2 mmol), diphenylacetic acid (**161**) (0.212 g, 1 mmol) and DPPA (0.275 g, 1 mmol) was homogenized in 4 mL of toluene with stirring for 15 min. The obtained mixture flowed directly into a CFC reactor (10 mL volume). A total flow rate of 0.25 mL/min, equating to a reactor residence time of 40 min at a temperature of 105 °C, was used to ensure complete conversion. The resulting flow stream was then collected to a round bottom flask containing cyclopentylamine (0.30 mL, 3 mmol) solubilized in 2 mL of toluene. After stirring for 15 min at rt the solvent was evaporated. The crude product was purified by silica gel flash chromatography (EtOAc/hexane 30:70). Compound **MM99** was obtained as a white powder (137.0 mg, 35 %).

Compound MM99: white powder (137.0 mg, 35 %); mp: 163 °C; ^{1}H NMR (400 MHz, DMSO-d_6) δ 7.38 – 7.13 (m, 10H, H-1 – H-4, H-6, H-9 – H-13), 6.65 (d, J = 8.5 Hz, 1H, H-14), 5.91 – 5.81 (m, 2H, H-7, H-16), 3.86 – 3.79 (m, 1H, H-18), 2.00 – 1.72 (m, 2H, H-20, H-21), 1.76 – 1.55 (m, 2H, H-19, H-22), 1.59 – 1.40 (m, 2H, H-20, H-21), 1.32 – 1.19 (m, 2HH-19, H-22); ^{13}C NMR (101 MHz, DMSO-d_6) δ 157.3 (C-15), 144.3 (C-5, C-8), 128.8 (C-1, C-3, C-10, C-12), 127.3 (C-4, C-6, C-9, C-13), 127.1 (C-2, C-11), 57.2 (C-7), 51.4 (C-18), 33.5 (C-19, C-22), 23.6 (C-20, C-21). ; HRMS (ESI): m/z calculated for $C_{19}H_{22}N_2O$ [M+ H^+]: 295.18049; found: 295.18396.

4.6.2. Biological assays

4.6.2.1. Activity against *Trypanosoma brucei*

T. brucei culturing and evaluation of trypanocidal activity

Bloodstream form T. brucei (strain 221) were cultured at 37 ºC in modified HMI9 medium supplemented with 5% fetal calf serum. Trypanocidal activity was assessed by growing parasites in the presence of various concentrations of the novel compounds and determining the levels which inhibited growth by 50% (IC_{50}). *T. brucei* in the logarithmic phase of growth were diluted back to 2.5×10^4/mL and aliquoted into 96-well plates. The compounds were then added at a range of concentrations and the plates incubated at 37 °C. Each drug concentration was tested in triplicate. Resazurin was added after 48 h and the plates incubated for a further 16 h and the plates then read in BMG FLUOstar Omega plate reader. Results were analysed using GraphPad Prism.

Chapter 5 – General conclusions

Xanthenes represents an important scaffold in Medicinal Chemistry and their synthesis and biological activity are being extensive explored. A comprehensive review of the synthesis strategies of xanthene derivatives and their biological activities was included in Chapter I. Concerning synthesis, one strategy commonly used is the one-step conjugation of simple building blocks, namely phenols, aldehydes, and benzynes intermediates, allowing to obtain the respective derivatives in good yields. However, these methodologies have a limited versatility, and few derivatives are obtained from each technique, being from a Medicinal Chemistry perspective an important limitation. Further modification and functionalization of aromatic rings are also widely explored and described by several authors. Through standard and simple procedures, the carbonyl in position 9 is easily converted into different function groups, namely alkyl, alcohol, or carboxylic acid, which can be subsequent transformed in different derivatives.

Concerning the biological applications, the xanthene nucleus showed to be versatile and suitable towards obtaining compounds for different biological targets. As expected, the substitution pattern of the xanthene core will define the capability to interact with specific targets and lead to the respective pharmacological response. Additionally, another essential aspect to be considered is the drug-likeness of the compounds developed, which should present appropriate ADMET properties to allow its progression from pre-clinical assessment to clinical evaluation.
In this thesis, 36 small molecules, with a xanthene or a benzhydryl moiety, were synthesized and fully characterized, and studied regarding their biological activity: antibacterial, antiparasitic and neuroprotection.

In Chapter 2, starting with xanthydrol, four compounds were obtained from the conjugation of xanthydrol with sulfonamides and aniline and were fully characterized. Compounds were obtained through crystallization without need of chromatographic column purification.

In Chapter 3, xanthene-9-carboxylic acid was used as starting material for the synthesis of a series of 20 compounds, involving four distinctive steps: aromatic halogenation, amide coupling, amide reduction, and Suzuki coupling. The diversity of synthetic techniques employed allowed the obtention of derivatives with distinct polar and electronic properties, comprising the presence of different functional groups on position 9 of the xanthene moiety, namely amides and amines, as well as modification of the aromatic rings through halogenation and Suzuki coupling.

Lastly, in Chapter 4, diphenylacetic acid was used as scaffold for the synthesis of ureas and carbamates through continuous flow synthesis, applying the DPPA-mediated Curtius

rearrangement procedure. Twelve compounds were obtained (six ureas and six carbamates) through a simple procedure, with isolated yields ranging from 35 – 93 %.

Xanthene sulfonamides **MM16-18** and compound **MM7** were assessed concerning their antibacterial activity and influence on bacterial mechanisms of resistance, namely, efflux pump inhibition, QS inhibition, and influence on biofilm formation. Particularly, the xanthene sulfonamide derivatives **MM17** and **MM18** showed interesting preliminary results regarding their impact on different mechanisms of bacterial resistance. In the future, a comprehensive series of related compounds must be synthesized to allow their assessment against a larger set of bacterial strains and the establishment of a structure-activity relationship of the 9-xanthenyl derivatives, as well as study their safety, stability, and PK properties. Furthermore, studies on the specific pump being inhibited are warranted, which can be achieved by genetic assays.

From the series of xanthene derivatives and their impact on P-gp modulation, a highlight is made for compounds **MM7**, **MM36**, **MM42C**, **MM43**, **MM74**, which showed the most significant and concentration-dependent increase of P-gp activity demonstrating the ability to increase the RHO 123 efflux and, consequently, leading to the reduction of its intracellular accumulation. These five compounds also showed to provide protection against iron-induced cytotoxicity, another potential strategy for neuroprotection. In particular, compound **MM42C** showed an increase in P-gp activity in 58% and 76% in the concentration of 10 μM and 25 μM, respectively. Further studies comprising the synthesis of derivatives of **MM42C**, comprising different functionalization of the xanthene tricyclic and different length of the chain connecting with the 1*H*-pyrazol-3-amine ring will allow to explore derivatives with improved P-gp activation activity.
Of utmost importance, the xanthene derivatives that showed to be P-gp activators, also show to be able to penetrate BBB to reach CNS, through in vitro or *in silico* studies. The compounds showed to comply with the principal attributes generally considered when designing drugs for CNS, namely logP, TPSA and molecular weight. A future interesting approach would be to assess the capacity of P-gp activation by the benzhydryl carbamates and urea derivatives obtained, considering the structural similarities of this series of compounds comparing with the xanthene derivatives, though comprising a different hydrophobic scaffold.

P-gp activation is a potential strategy against the abnormal accumulation of Aβ, which is considered one of the main pathological processes involved in neuronal damage and the development of Alzheimer's disease. This strategy would allow to prevent Aβ-associated toxicity without interfering with BACE1 activity, once questions have been raised regarding

the suitability of BACE1 as a drug target for AD [269] . Nonetheless, the clinical application of P- gp activation can lead to repercussions on the pharmacokinetic of other pharmacological agents, once P-gp promotes the efflux of several clinical drugs, reducing their bioavailability and promoting their elimination [224]. Alzheimer's disease has a higher prevalence in the elderly, a segment of population generally polymedicated, where drug interactions represent an important concern. Hence, P-gp activation on such population as a therapeutic strategy against Alzheimer's disease should be carefully assessed in a case-by case scenario, under risk–benefit ratio assessment. On the other hand, Alzheimer's disease is considered a multifactorial disease, where several and independent pathological pathways are involved. Several hypotheses have arisen in an attempt to identify the principal pathological factors in AD: (i) amyloid cascade hypothesis; (ii) tau hypothesis; (iii) metal ion hypothesis; (iv) oxidative stress hypothesis; (v) cholinergic hypothesis [52, 270]. Hence, a relevant strategy to fight AD would be the development of a multitarget-direct ligand (MTDL), capable of acting in more than one pathological mechanism and consequently effectively slow or stop the neuronal damage and the progression of the disease.

Lastly, xanthene-9-carboxylic acid and diphenylacetic acid derivatives were assessed regarding their ability to inhibit *T. brucei* growth. The urea derivative **MM99** showed the most promising result in the *in vitro* assay performed, with an IC_{50} = 1.1 µM and a selectivity index of 181.4y. Further modifications on the urea **MM99**, namely adding substituents to the cyclopentane ring and/or on the aromatic rings, would provide additional information on the structure activity of this class of compounds.

Overall, the main achievements of this thesis were:

- A comprehensive review of the strategies of synthesis of xanthenes and their biological application was performed, and hopefully will provide guidance to medicinal chemists, highlighting the best techniques to value this important scaffold and make significant advances in obtaining novel xanthenes that may become useful pharmacological tools;
- Thirty-six compounds were synthetized, starting with a xanthene or diphenyl moiety, 24 of which were synthetized from the first time;
- four compounds were found to be active against different mechanisms of bacterial resistance: efflux pump inhibition, QS inhibition, and influence on biofilm formation.
- fourteen compounds were found to be P-gp activators, where the most potent compound was **MM42C** providing an increase in Pg-p activity of 58% and 76% in the concentration of 10 µM and 25 µM, respectively. All the 14 compounds showed

to be permeant to BBB, 6 in an *in vitro* assay and the remain compounds in a *in silico* prediction.

- eleven compounds showed to provide protection against iron-induced cytotoxicity, another potential strategy for neuroprotection, and a dual effect, P-activation and iron-induced cytotoxicity protection was found for the most promising hits, **MM7**, **MM36**, **MM42C**, **MM43** and **MM74**.
- two compounds were found to inhibit *T. brucei* growth with an $IC_{50} \leq 7.2$ μM, where the most potent compound was a benzhydryl urea derivative, **MM99**, with an $IC_{50} =$ 1.1 μM and a SI =181.4. This compound also showed to be tolerated at the cumulative dose of 150 mg/kg in an *in vivo* study.

Further investigations concerning the most promising compounds, synthetizing analogues and providing a structure activity relationship, are needed. Additionally, a scale-up process should be developed, providing enough material for further studies, namely safety, stability, and PK studies. Considering the low solubility of some of the compounds obtained due to the tricyclic nucleus, a solid-state study can be performed to find a (potential) suitable polymorph combining enhance dissolution with adequate stability. Converting a crystalline state to an amorphous state is also a potential alternative; nonetheless, the development of a formulation is often necessary to assure the stability of the amorphous form.

The work presented in this thesis is a significant step in the discovery of suitable synthetic routs to easily obtain novel benzhydryl and xanthenes with biological activity, hopefully leading to a compound with clinical relevance.

Chapter 6 – References

References

1. Cao, J. Q.; Yao, Y.; Chen, H.; Qiao, L.; Zhou, Y. Z.; Pei, Y. H., A New xanthene from Blumea riparia. *Chinese Chemical Letters* **2007,** *18* (3), 303-305.
2. Bai, M.; Zheng, C.-J.; Nong, X.-H.; Zhou, X.-M.; Luo, Y.-P.; Chen, G.-Y., Four New Insecticidal Xanthene Derivatives from the Mangrove-Derived Fungus Penicillium sp. JY246. *Marine Drugs* **2019,** *17* (12), 649.
3. Richardson, S. N.; Nsiama, T. K.; Walker, A. K.; McMullin, D. R.; Miller, J. D., Antimicrobial dihydrobenzofurans and xanthenes from a foliar endophyte of Pinus strobus. *Phytochemistry (Elsevier)* **2015,** *117*, 436-443.
4. Bongard, R. D.; Lepley, M.; Gastonguay, A.; Syrlybaeva, R. R.; Talipov, M. R.; Jones Lipinski, R. A.; Leigh, N. R.; Brahmbhatt, J.; Kutty, R.; Rathore, R.; Ramchandran, R.; Sem, D. S., Discovery and characterization of halogenated xanthene inhibitors of DUSP5 as potential photodynamic therapeutics. *Journal of Photochemistry and Photobiology A: Chemistry* **2019,** *375*, 114-131.
5. FDA, Food and drug administration compliance program guidance manual. Chapter 09 – Food and color additives. Retrieved 11 May 2020, from https://www.fda.gov/media/71661/download. **2019**.
6. Khairy, Y.; Mohammed, M. I.; Elsaeedy, H. I.; Yahia, I. S., Synthesis, optical limiting and properties of Rhodamine B-doped PMMA polymeric films/glass substrate: New trends in polymeric composites. *Optik* **2020,** *212*, 164687.
7. Lee, D.; Swamy, K. M. K.; Hong, J.; Lee, S.; Yoon, J., A rhodamine-based fluorescent probe for the detection of lysosomal pH changes in living cells. *Sensors and Actuators B: Chemical* **2018,** *266*, 416-421.
8. Sen, R. N.; Sarkar, N. N., The condensation of primary alcohols with resorcinol and other hydroxy aromatic compounds. *Journal of the American Chemical Society* **1925,** *47*, 1079-1091.
9. Casiraghi, G.; Casnati, G.; Catellani, M.; Corina, M., A Convenient One-Step Synthesis of Xanthene Derivatives. *Synthesis* **1974,** *1974* (08), 564-564.
10. Böβ, E.; Hillringhaus, T.; Nitsch, J.; Klussmann, M., Lewis acid-catalysed one pot synthesis of substituted xanthenes. *Organic & Biomolecular Chemistry* **2011,** *9* (6), 1744.
11. Sousa, S. C. A.; Fernandes, T. A.; Fernandes, A. C., Highly Efficient Deoxygenation of Aryl Ketones to Arylalkanes Catalyzed by Dioxidomolybdenum Complexes. *European Journal of Organic Chemistry* **2016,** *2016* (18), 3109-3112.
12. Vieira, E.; Huwyler, J.; Jolidon, S.; Knoflach, F.; Mutel, V.; Wichmann, J., Fluorinated 9H-xanthene-9-carboxylic acid oxazol-2-yl-amides as potent, orally available mGlu1 receptor enhancers. *Bioorganic & Medicinal Chemistry Letters* **2009,** *19* (6), 1666-1669.
13. Knight, D. W.; Little, P. B., The first efficient method for the intramolecular trapping of benzynes by phenols: a new approach to xanthenes. *Journal of the Chemical Society, Perkin Transactions 1* **2001,** (15), 1771-1777.
14. A. Birkett, M.; W. Knight, D.; G. Giles, R.; B. Mitchell, M., Directed deprotonation of 7-methyl-1-aminobenzotriazole: an approach to ortho-substituted benzyne precursors. *Journal of the Chemical Society, Perkin Transactions 1* **1998,** (15), 2301-2306.
15. Knight, D. W.; Little, P. B., 1-Aminobenzotriazole functionalisation using directed metallation: new routes to chromanes and chromenes using intramolecular benzyne trapping by alcohols. *Journal of the Chemical Society, Perkin Transactions 1* **2000,** (15), 2343-2355.
16. Zhang, B.; Xiang, S.-K.; Zhang, L. H.; Cui, Y.; Jiao, N., Organocatalytic Asymmetric Intermolecular Dehydrogenative α-Alkylation of Aldehydes Using Molecular Oxygen as Oxidant. *Organic Letters* **2011,** *13* (19), 5212-5215.
17. Lin, M.-Y.; Xu, K.; Jiang, Y.-Y.; Liu, Y.-G.; Sun, B.-G.; Zeng, C.-C., Intermolecular Electrochemical C(sp 3)-H/N-H Cross-coupling of Xanthenes with N -alkoxyamides: Radical

Pathway Mediated by Ferrocene as a Redox Catalyst. *Advanced Synthesis & Catalysis* **2018,** *360* (8), 1665-1672.
18. Yang, Y.-Z.; Song, R.-J.; Li, J.-H., Intermolecular Anodic Oxidative Cross-Dehydrogenative C(sp3)–N Bond-Coupling Reactions of Xanthenes with Azoles. *Organic Letters* **2019,** *21* (9), 3228-3231.
19. Shao, X.; Tian, L.; Wang, Y., C-N Coupling of Azoles or Imides with Carbocations Generated by Electrochemical Oxidation. *European Journal of Organic Chemistry* **2019,** *2019* (25), 4089-4094.
20. Brandhofer, T.; Özdemir, A.; Gini, A.; Mancheño, O. G., Double Cu-Catalyzed Direct Csp3 −H Azidation/CuAAC Reaction: A Direct Approach towards Demanding Triazole Conjugates. *Chemistry - A European Journal* **2019,** *25* (16), 4077-4086.
21. Sarma, D.; Majumdar, B.; Sarma, T. K., Visible-light induced enhancement in the multi-catalytic activity of sulfated carbon dots for aerobic carbon-carbon bond formation. *Green Chemistry* **2019,** *21* (24), 6717-6726.
22. Kuo, C.-W.; Fang, J.-M., Synthesis of xanthenes, indanes, and tetrahydronaphthalenes via intramolecular phenyl-carbonyl coupling reactions. *Synthetic Communications* **2001,** *31* (6), 877-892.
23. Okuma, K.; Nojima, A.; Matsunaga, N.; Shioji, K., Reaction of Benzyne with Salicylaldehydes: General Synthesis of Xanthenes, Xanthones, and Xanthols. *Organic Letters* **2009,** *11* (1), 169-171.
24. Kentaro, O.; Akiko, N.; Yuki, N.; Nahoko, M.; Noriyoshi, N.; Kosei, S., Reaction of Benzyne with Formamides and Acetylimidazole. *Bulletin of the Chemical Society of Japan* **2011,** *84* (3), 328-332.
25. Bristol, J. A.; Gold, E. H.; Lovey, R. G.; Long, J. F., Gastric antisecretory agents. 1. Antisecretory and antiulcer activity of 5H-[1]benzopyrano[2,3-b]pyridin-5-ylureas and 5H-[1]benzothiopyrano[2,3-b]pyridin-5-ylureas. *Journal of Medicinal Chemistry* **1981,** *24* (8), 927-932.
26. Carmen De La Fuente, M.; Domínguez, D., Synthesis of chromeno[4,3,2-cd]isoindolin-2-ones and chromeno[4,3,2-de]isoquinolin-3-ones. Electrophilic versus anionic cyclization of carbamates. *Tetrahedron* **2004,** *60* (44), 10019-10028.
27. Clark, S.; Francis, P. S.; Conlan, X. A.; Barnett, N. W., Determination of urea using high-performance liquid chromatography with fluorescence detection after automated derivatisation with xanthydrol. *Journal of Chromatography A* **2007,** *1161* (1), 207-213.
28. Hirota, K.; Kawase, M.; Ohmori, S.; Kishie, T., High-performance liquid chromatographic method for the determination of plasma allantoin. *Journal of Chromatography B: Biomedical Sciences and Applications* **1983,** *277*, 165-172.
29. Herbert, P.; Santos, L.; Bastos, M.; Barros, P.; Alves, A., New HPLC Method to Determine Ethyl Carbamate in Alcoholic Beverages Using Fluorescence Detection. *Journal of Food Science* **2002,** *67* (5), 1616-1620.
30. Zhang, J.; Liu, G.; Zhang, Y.; Gao, Q.; Wang, D.; Liu, H., Simultaneous Determination of Ethyl Carbamate and Urea in Alcoholic Beverages by High-Performance Liquid Chromatography Coupled with Fluorescence Detection. *Journal of Agricultural and Food Chemistry* **2014,** *62* (13), 2797-2802.
31. BOWDEN, R. S. T., The Estimation of Blood Urea by the Xanthydrol Reaction. *Journal of Small Animal Practice* **1962,** *3* (4), 217-218.
32. Moskalyk, R. E.; Chatten, L. G., Alkylation by secondary alcohols. I. The reaction of xanthydrol with some N1-monosubstituted sulfanilamides and related compounds. *Canadian Journal of Chemistry* **1967,** *45* (13), 1411-1424.
33. Gorokhov, V. Y.; Makhova, T. V., Synthesis and Antibactericidal Activities of Amines and Imines Containing (Aza, Thio)Xanthene Rings. *Pharmaceutical Chemistry Journal* **2016,** *50* (8), 530-533.

34. Wang, S.-Y.; Ji, S.-J., Novel Reaction of Indoles and Pyrrole with Pyrillium Catalyzed by Ceric Ammonium Nitrate (CAN). *Synlett* **2007,** *2007* (14), 2222-2226.
35. Eshghi, H.; Bakavoli, M.; Abedini-Torghabeh, J.; Rahimizadeh, M., Efficient synthesis of novel 9H-xanthen-9-yl derivatives of bidentate heterocyclic nucleophiles by Fe(HSO4)3 as a catalyst. *Chinese Chemical Letters* **2012,** *23* (10), 1153-1156.
36. Liu, L.-Y.; Wang, B.; Yang, H.-M.; Chang, W.-X.; Li, J., The direct substitutions of 9H-xanthen-9-ol with indoles in a room temperature ionic liquid medium BmimBF4. *Tetrahedron Letters* **2011,** *52* (43), 5636-5639.
37. Xiao, J., Merging Organocatalysis with Transition Metal Catalysis: Highly Stereoselective α-Alkylation of Aldehydes. *Organic Letters* **2012,** *14* (7), 1716-1719.
38. Vázquez, R.; de la Fuente, M. C.; Castedo, L.; Domínguez, D., A Short Synthesis of (±)-Clavizepine. *Synlett* **1994,** *1994* (06), 433-434.
39. Batzly, R.; Lorz, E. Process for the manufacture of xanthene carboxylic acid derivatives, US2956063A. US2956063A, 1960.
40. Coburn, C., A. ; Rosenblum, S., B. ; Kozlowski, J., A. ; Soll, R.; Wu, H.; Hu, B.; Zhong, B.; Wang, D.; Shen, C.; Sun, F. Tetracyclic xanthene derivatives and methods of use thereof for treatment of viral diseases. WO2012122716, 2012.
41. Vieira, E.; Huwyler, J.; Jolidon, S.; Knoflach, F.; Mutel, V.; Wichmann, J., 9H-Xanthene-9-carboxylic acid [1,2,4]oxadiazol-3-yl- and (2H-tetrazol-5-yl)-amides as potent, orally available mGlu1 receptor enhancers. *Bioorganic & Medicinal Chemistry Letters* **2005,** *15* (20), 4628-4631.
42. Wu, C.-P.; Van Schalkwyk, D. A.; Taylor, D.; Smith, P. J.; Chibale, K., Reversal of chloroquine resistance in Plasmodium falciparum by 9H-xanthene derivatives. *International Journal of Antimicrobial Agents* **2005,** *26* (2), 170-175.
43. KISS, Z. Drug combinations to treat drug resistant tumors. WO2008105872A1, 2008.
44. Pestel, S.; Reichl, R.; Meissner, H.; Pohl, G.; Pieper, M. P.; Germeyer, S.; Speck, G.; Morschhaeuser, G. Xanthene-carboxylic acid esters of tropenol and scopine as m3 antagonists, method for producing the same and use thereof as medicaments, CA2471578A1. CA2471578A1, 2002.
45. Xu, X.; Xu, X.; Li, H.; Xie, X.; Li, Y., Iron-Catalyzed, Microwave-Promoted, One-Pot Synthesis of 9-Substituted Xanthenes by a Cascade Benzylation−Cyclization Process. *Organic Letters* **2010,** *12* (1), 100-103.
46. Huang, X.; Zhang, T., Cascade Nucleophilic Addition−Cyclic Michael Addition of Arynes and Phenols/Anilines Bearing Ortho α,β-Unsaturated Groups: Facile Synthesis of 9-Functionalized Xanthenes/Acridines. *The Journal of Organic Chemistry* **2010,** *75* (2), 506-509.
47. Giri, R.; Goodell, J. R.; Xing, C.; Benoit, A.; Kaur, H.; Hiasa, H.; Ferguson, D. M., Synthesis and cancer cell cytotoxicity of substituted xanthenes. *Bioorganic & Medicinal Chemistry* **2010,** *18* (4), 1456-1463.
48. Huang, H.; La, D. S.; Cheng, A. C.; Whittington, D. A.; Patel, V. F.; Chen, K.; Dineen, T. A.; Epstein, O.; Graceffa, R.; Hickman, D.; Kiang, Y. H.; Louie, S.; Luo, Y.; Wahl, R. C.; Wen, P. H.; Wood, S.; Fremeau, R. T., Structure- and Property-Based Design of Aminooxazoline Xanthenes as Selective, Orally Efficacious, and CNS Penetrable BACE Inhibitors for the Treatment of Alzheimer's Disease. *Journal of Medicinal Chemistry* **2012,** *55* (21), 9156-9169.
49. Nowick, J. S.; Ballester, P.; Ebmeyer, F.; Rebek, J., Convergent functional groups.9. Complexation in new molecular clefts. *Journal of the American Chemical Society* **1990,** *112* (24), 8902-8906.
50. Catanzaro, E.; Seghetti, F.; Calcabrini, C.; Rampa, A.; Gobbi, S.; Sestili, P.; Turrini, E.; Maffei, F.; Hrelia, P.; Bisi, A.; Belluti, F.; Fimognari, C., Identification of a new tamoxifen-xanthene hybrid as pro-apoptotic anticancer agent. *Bioorganic Chemistry* **2019,** *86*, 538-549.
51. Nowick, J. S.; Ballester, P.; Ebmeyer, F.; Rebek, J., Convergent functional groups. 9. Complexation in new molecular clefts. *Journal of the American Chemical Society* **1990,** *112* (24), 8902-8906.

52. Maia, M. A.; Sousa, E., BACE-1 and γ-Secretase as Therapeutic Targets for Alzheimer's Disease. *Pharmaceuticals* **2019,** *12* (1), 41.
53. Erkkinen, M. G.; Kim, M.-O.; Geschwind, M. D., Clinical Neurology and Epidemiology of the Major Neurodegenerative Diseases. *Cold Spring Harbor Perspectives in Biology* **2018**.
54. Epstein, O.; Bryan, M. C.; Cheng, A. C.; Derakhchan, K.; Dineen, T. A.; Hickman, D.; Hua, Z.; Human, J. B.; Kreiman, C.; Marx, I. E.; Weiss, M. M.; Wahl, R. C.; Wen, P. H.; Whittington, D. A.; Wood, S.; Zheng, X. M.; Fremeau, R. T.; White, R. D.; Patel, V. F., Lead Optimization and Modulation of hERG Activity in a Series of Aminooxazoline Xanthene β-Site Amyloid Precursor Protein Cleaving Enzyme (BACE1) Inhibitors. *Journal of Medicinal Chemistry* **2014,** *57* (23), 9796-9810.
55. Finlayson, K.; Witchel, H. J.; McCulloch, J.; Sharkey, J., Acquired QT interval prolongation and HERG: implications for drug discovery and development. *European Journal of Pharmacology* **2004,** *500* (1), 129-142.
56. Hitchcock, S. A., Structural Modifications that Alter the P-Glycoprotein Efflux Properties of Compounds. *Journal of Medicinal Chemistry* **2012,** *55* (11), 4877-4895.
57. Cheng, Y.; Brown, J.; Judd, T. C.; Lopez, P.; Qian, W.; Powers, T. S.; Chen, J. J.; Bartberger, M. D.; Chen, K.; Dunn, R. T.; Epstein, O.; Fremeau, R. T.; Harried, S.; Hickman, D.; Hitchcock, S. A.; Luo, Y.; Minatti, A. E.; Patel, V. F.; Vargas, H. M.; Wahl, R. C.; Weiss, M. M.; Wen, P. H.; White, R. D.; Whittington, D. A.; Zheng, X. M.; Wood, S., An Orally Available BACE1 Inhibitor That Affords Robust CNS Aβ Reduction without Cardiovascular Liabilities. *ACS Medicinal Chemistry Letters* **2015,** *6* (2), 210-215.
58. Chen, J. J.; Liu, Q.; Yuan, C.; Gore, V.; Lopez, P.; Ma, V.; Amegadzie, A.; Qian, W.; Judd, T. C.; Minatti, A. E.; Brown, J.; Cheng, Y.; Xue, M.; Zhong, W.; Dineen, T. A.; Epstein, O.; Human, J.; Kreiman, C.; Marx, I.; Weiss, M. M.; Hitchcock, S. A.; Powers, T. S.; Chen, K.; Wen, P. H.; Whittington, D. A.; Cheng, A. C.; Bartberger, M. D.; Hickman, D.; Werner, J. A.; Vargas, H. M.; Everds, N. E.; Vonderfecht, S. L.; Dunn, R. T., II; Wood, S.; Fremeau, R. T., Jr.; White, R. D.; Patel, V. F., Development of 2-aminooxazoline 3-azaxanthenes as orally efficacious β-secretase inhibitors for the potential treatment of Alzheimer's disease. *Bioorganic & Medicinal Chemistry Letters* **2015,** *25* (4), 767-774.
59. May, P. C.; Dean, R. A.; Lowe, S. L.; Martenyi, F.; Sheehan, S. M.; Boggs, L. N.; Monk, S. A.; Mathes, B. M.; Mergott, D. J.; Watson, B. M.; Stout, S. L.; Timm, D. E.; Smith LaBell, E.; Gonzales, C. R.; Nakano, M.; Jhee, S. S.; Yen, M.; Ereshefsky, L.; Lindstrom, T. D.; Calligaro, D. O.; Cocke, P. J.; Greg Hall, D.; Friedrich, S.; Citron, M.; Audia, J. E., Robust Central Reduction of Amyloid-β in Humans with an Orally Available, Non-Peptidic β-Secretase Inhibitor. *The Journal of Neuroscience* **2011,** *31* (46), 16507-16516.
60. Fielden, M. R.; Werner, J.; Jamison, J. A.; Coppi, A.; Hickman, D.; Dunn, R. T.; Trueblood, E.; Zhou, L.; Afshari, C. A.; Lightfoot-Dunn, R., Retinal Toxicity Induced by a Novel β-secretase Inhibitor in the Sprague-Dawley Rat. *Toxicologic Pathology* **2015,** *43* (4), 581-592.
61. Im, E.; Kazlauskas, A., The role of cathepsins in ocular physiology and pathology. *Experimental Eye Research* **2007,** *84* (3), 383-388.
62. Low, J. D.; Bartberger, M. D.; Chen, K.; Cheng, Y.; Fielden, M. R.; Gore, V.; Hickman, D.; Liu, Q.; Allen Sickmier, E.; Vargas, H. M.; Werner, J.; White, R. D.; Whittington, D. A.; Wood, S.; Minatti, A. E., Development of 2-aminooxazoline 3-azaxanthene β-amyloid cleaving enzyme (BACE) inhibitors with improved selectivity against Cathepsin D. *MedChemComm* **2017,** *8* (6), 1196-1206.
63. Hicken, E. J.; Hunt, K. W.; Rodriguez, M. E.; Tang, T. P.; Siu, M. Compounds for treating neurodegenerative diseases. WO2013148851A1, 2013, 2013.
64. Reprinted (adapted) with permission from Y. Cheng, J. B., T.C. Judd, P. Lopez, W. Qian, T.S. Powers, J.J. Chen, M.D. Bartberger, K. Chen, R.T. Dunn, O. Epstein, R.T. Fremeau, S. Harried, D. Hickman, S.A. Hitchcock, Y. Luo, A.E. Minatti, V.F. Patel, H.M. Vargas, R.C. Wahl, M.M. Weiss, P.H. Wen, R.D. White, D.A. Whittington, X.M. Zheng, S. Wood, An Orally Available BACE1 Inhibitor That

Affords Robust CNS Aβ Reduction without Cardiovascular Liabilities, ACS Medicinal Chemistry Letters, 6 (2015) 210-215, doi:10.1021/ml500458t. Copyright 2015 American Chemical Society.
65. Adapted from J.D. Low, M. D. B., K. Chen, Y. Cheng, M.R. Fielden, V. Gore, D. Hickman, Q. Liu, E. Allen Sickmier, H.M. Vargas, J. Werner, R.D. White, D.A. Whittington, S. Wood, A.E. Minatti, Development of 2-aminooxazoline 3-azaxanthene β-amyloid cleaving enzyme (BACE) inhibitors with improved selectivity against Cathepsin D, MedChemComm, 8 (2017) 1196-1206, doi:10.1039/C7MD00106A, with permission from The Royal Society of Chemistry.
66. Wichmann, J.; Bleicher, K.; Vieira, E.; Woltering, T.; Knoflach, F.; Mutel, V., Alkyl diphenylacetyl, 9H-xanthene- and 9H-thioxanthene-carbonyl carbamates as positive allosteric modulators of mGlu1 receptors. *Il Farmaco* **2002,** *57* (12), 989-992.
67. Song, Y.; Yang, Y.; Wu, L.; Dong, N.; Gao, S.; Ji, H.; Du, X.; Liu, B.; Chen, G., Synthesis and cytotoxicity of N-substituted dibenzo[a,j]xanthene-3,11-dicarboxamide derivatives. *Molecules* **2017,** *22* (4), 517/1-517/12.
68. Di Micco, S.; Mazue, F.; Daquino, C.; Spatafora, C.; Delmas, D.; Latruffe, N.; Tringali, C.; Riccio, R.; Bifulco, G., Structural basis for the potential antitumour activity of DNA-interacting benzo[kl]xanthene lignans. *Organic & Biomolecular Chemistry* **2011,** *9* (3), 701-710.
69. Cytotoxicity, Cell Cycle Arrest, Antioxidant Activity and Interaction of Dibenzoxanthenes Derivatives with DNA. *DNA and Cell Biology* **2012,** *31* (9), 1468-1474.
70. Jia, Z.; Yang, H.-H.; Liu, Y.-J.; Wang, X.-Z., Novel ethanocycloheptono [3,4,5-kl]benzo[a]xanthene induces apoptosis in BEL-7402 cells. *Molecular and Cellular Biochemistry* **2018,** *445* (1-2), 145-156.
71. Thompson, J. F.; Agarwala, S. S.; Smithers, B. M.; Ross, M. I.; Scoggins, C. R.; Coventry, B. J.; Neuhaus, S. J.; Minor, D. R.; Singer, J. M.; Wachter, E. A., Phase 2 Study of Intralesional PV-10 in Refractory Metastatic Melanoma. *Annals of Surgical Oncology* **2015,** *22* (7), 2135-2142.
72. Singer, J.; Wachter, E. A.; Swift, L.; Zhang, C.; Trippett, T.; Narendran, A. In Vitro and Xenograft Anti-Tumor Activity of a Halogenated-Xanthene Against Refractory Pediatric Solid Tumors. US20190350893, 2019.
73. clinicaltrials.gov. Retrieved 04 november 2020, from https://www.clinicaltrials.gov/.
74. Recruiting and Active, Not Recruiting clinical trials with PV-10 registered on clinicaltrials.gov." Retrieved 04 november 2020, from https://www.clinicaltrials.gov/ct2/results?term=pv-10&Search=Apply&recrs=a&recrs=d&age_v=&gndr=&type=&rslt=.
75. Yunnikova, L. P.; Voronina, É. V., Synthesis of xanthene and thioxanthene derivatives and study of their antimicrobial activity. *Pharmaceutical Chemistry Journal* **1996,** *30* (11), 695-696.
76. Yunnikova, L. P.; Gorokhov, V. Y.; Makhova, T. V.; Aleksandrova, G. A., Synthesis and antimicrobial activity of amines with azaxanthene fragments. *Pharmaceutical Chemistry Journal* **2013,** *47* (3), 139-141.
77. Amininasab, S. M.; Esmaili, S.; Taghavi, M.; Shami, Z., Fabrication and characterization of novel high-performance fluorinated polyimides with xanthene pendent architecture: Study of thermal, photophysical, antibacterial and heavy metal ion adsorption behavior. *Journal of Fluorine Chemistry* **2016,** *192*, 48-57.
78. Amininasab, S. M.; Esmaili, S.; Taghavi, M.; Shami, Z., Synthesis and characterization of new fluorinated photoactive polyamides based on xanthene pendant: Evaluation of antibacterial and heavy metal ions removal behavior. *International Journal of Polymer Analysis and Characterization* **2016,** *21* (8), 686-696.
79. Amininasab, S. M.; Esmaili, S.; Shami, Z., High-performance polyimides based on pyridine and xanthene pendant groups; synthesis, characterization, photoactivity, thermal, antibacterial, and Cr(VI) ion adsorption properties. *High Performance Polymers* **2019,** *32* (4), 371-382.
80. Amininasab, S. M.; Esmaili, S.; Shami, Z., Synthesis of polyamides contains pyridine and xanthene pendant group: study of optical, thermal, antibacterial activity and hexavalent chromium ion adsorption. *Journal of Macromolecular Science, Part A* **2020,** *57* (1), 35-45.

81. Carr, A. A.; Grunwell, J. F.; Sill, A. D.; Meyer, D. R.; Sweet, F. W.; Scheve, B. J.; Grisar, J. M.; Fleming, R. W.; Mayer, G. D., Bis-basic-substituted polycyclic aromatic compounds. A new class of antiviral agents. 7. Bisalkamine esters of 9-oxoxanthene-2,7-dicarboxylic acid, 3,6-bis-basic ethers of xanthen-9-one, and 2,7-bis(aminoacyl)xanthen-9-ones-xanthenes, and -thioxanthenes. *Journal of Medicinal Chemistry* **1976,** *19* (9), 1142-8.
82. Reddi Mohan Naidu, K.; Satheesh Krishna, B.; Anil Kumar, M.; Arulselvan, P.; Ibrahim Khalivulla, S.; Lasekan, O., Design, Synthesis and Antiviral Potential of 14-Aryl/Heteroaryl-14H-dibenzo[a,j]xanthenes Using an Efficient Polymer-Supported Catalyst. *Molecules* **2012,** *17* (6), 7543-7555.
83. Lenard, J.; Vanderoef, R., Photoinactivation of influenza virus fusion and infectivity by Rose Bengal. *Photochemistry and Photobiology* **1993,** *58* (4), 527-531.
84. Lenard, J.; Rabson, A.; Vanderoef, R., Photodynamic inactivation of infectivity of human immunodeficiency virus and other enveloped viruses using hypericin and rose bengal: inhibition of fusion and syncytia formation. *Proceedings of the National Academy of Sciences* **1993,** *90* (1), 158-162.
85. Chibale, K.; Visser, M.; Yardley, V.; Croft, S. L.; Fairlamb, A. H., Synthesis and evaluation of 9,9-dimethylxanthene tricyclics against trypanothione reductase, Trypanosoma brucei, Trypanosoma cruzi and Leishmania donovani. *Bioorganic & Medicinal Chemistry Letters* **2000,** *10* (11), 1147-1150.
86. Chibale, K.; Visser, M.; van Schalkwyk, D.; Smith, P. J.; Saravanamuthu, A.; Fairlamb, A. H., Exploring the potential of xanthene derivatives as trypanothione reductase inhibitors and chloroquine potentiating agents. *Tetrahedron* **2003,** *59* (13), 2289-2296.
87. Jarrahpour, A.; Ebrahimi, E.; De Clercq, E.; Sinou, V.; Latour, C.; Djouhri Bouktab, L.; Brunel, J. M., Synthesis of mono-, bis-spiro- and dispiro-β-lactams and evaluation of their antimalarial activities. *Tetrahedron* **2011,** *67* (45), 8699-8704.
88. Becker, K.; Tilley, L.; Vennerstrom, J. L.; Roberts, D.; Rogerson, S.; Ginsburg, H., Oxidative stress in malaria parasite-infected erythrocytes: host-parasite interactions. *Int J Parasitol* **2004,** *34* (2), 163-189.
89. Cui, L.; Miao, J.; Cui, L., Cytotoxic Effect of Curcumin on Malaria Parasite Plasmodium falciparum: Inhibition of Histone Acetylation and Generation of Reactive Oxygen Species. *Antimicrobial Agents and Chemotherapy* **2007,** *51* (2), 488.
90. Savvides, S. N.; Karplus, P. A., Kinetics and crystallographic analysis of human glutathione reductase in complex with a xanthene inhibitor. *J Biol Chem* **1996,** *271* (14), 8101-8107.
91. Banerjee, A. G.; Kothapalli, L. P.; Sharma, P. A.; Thomas, A. B.; Nanda, R. K.; Shrivastava, S. K.; Khatanglekar, V. V., A facile microwave assisted one pot synthesis of novel xanthene derivatives as potential anti-inflammatory and analgesic agents. *Arabian Journal of Chemistry* **2016,** *9* (Suppl._1), S480-S489.
92. Hafez, H. N.; Hegab, M. I.; Ahmed-Farag, I. S.; El-Gazzar, A. B. A., A facile regioselective synthesis of novel spiro-thioxanthene and spiro-xanthene-9',2-[1,3,4]thiadiazole derivatives as potential analgesic and anti-inflammatory agents. *Bioorganic & Medicinal Chemistry Letters* **2008,** *18* (16), 4538-4543.
93. Jiang, B.-C.; Liu, T.; Gao, Y.-J., Chemokines in chronic pain: cellular and molecular mechanisms and therapeutic potential. *Pharmacology & Therapeutics* **2020,** *212*, 107581.
94. Naya, A.; Sagara, Y.; Ohwaki, K.; Saeki, T.; Ichikawa, D.; Iwasawa, Y.; Noguchi, K.; Ohtake, N., Design, Synthesis, and Discovery of a Novel CCR1 Antagonist. *Journal of Medicinal Chemistry* **2001,** *44* (9), 1429-1435.
95. Kwon, Y.; Song, P.; Yoon, J. H.; Ghim, J.; Kim, D.; Kang, B.; Lee, T. G.; Kim, J.-A.; Choi, J.-K.; Youn, I. K.; Lee, H.-K.; Ryu, S. H., Xanthene Derivatives Increase Glucose Utilization through Activation of LKB1-Dependent AMP-Activated Protein Kinase. *PLOS ONE* **2014,** *9* (9), e108771.

96. Coughlan K; Valentine R; Ruderman N; A., S., AMPK activation: a therapeutic target for type 2 diabetes? . *Diabetes, Metabolic Syndrome and Obesity: Targets and Therapy* **2014,** *7*, 241-253.
97. Patarakijavanich, P.; Vilasinee, H. S.; Kongkiatpaiboon, S.; Chewchinda, S., A review of the antidiabetic potential of Mangifera indica leaf extract. *Songklanakarin J. Sci. Technol.* **2019,** *41* (4), 942-950.
98. Nishiyama, T.; Ishida, T.; Miyazaki, S.; Tsuji, R.; Yamada, F., 9H-xanthene-2,7-diols as antioxidant for autoxidation of tetralin. *Bulletin of the Chemical Society of Japan* **1993,** *66* (8), 2430-1.
99. Yamamura, T.; Arashima, M.; Nakatani, K.; Ishida, T.; Yamada, F.; Nishiyama, T., 9H-Xanthene-2,7-diols as antioxidants for autoxidation of linoleic acid. *Journal of the American Oil Chemists' Society* **1995,** *72* (4), 497-500.
100. Yamamura, T.; Ishida, T.; Tatara, H.; Nishiyama, T., Chain-breaking fused heterocyclic antioxidants: antioxidant activities of 9H-xanthene-2,7-diols and α-tocopherol upon liposomal membranes. *Journal of the American Oil Chemists' Society* **1997,** *74* (6), 739-744.
101. Nishiyama, T.; Sakita, K.; Fuchigami, T.; Fukui, T., Antioxidant activities of fused heterocyclic compounds, xanthene-2,7-diols with BHT or catechol skeleton. *Polymer Degradation and Stability* **1998,** *62* (3), 529-534.
102. Kancheva, V. D.; Saso, L.; Angelova, S. E.; Foti, M. C.; Slavova-Kasakova, A.; Daquino, C.; Enchev, V.; Firuzi, O.; Nechev, J., Antiradical and antioxidant activities of new bio-antioxidants. *Biochimie* **2012,** *94* (2), 403-415.
103. Ilangovan, A.; Anandhan, K.; Prasad, K. M.; Vijayakumar, P.; Renganathan, R.; Ananth, D. A.; Sivasudha, T., Synthesis, DNA-binding study, and antioxidant activity of 14-aryl-14H-dibenzo[a,j]xanthene derivatives. *Medicinal Chemistry Research* **2015,** *24* (1), 344-355.
104. Kaiser, C.; Pavloff, A. M.; Garvey, E.; Fowler, P. J.; Tedeschi, D. H.; Zirkle, C. L.; Nodiff, E. A.; Saggiomo, A. J., Analogs of phenothiazines. 4. Effect of structure upon neuropharmacological activity of some chlorpromazine analogs of the diphenylmethane type. *Journal of Medicinal Chemistry* **1972,** *15* (6), 665-73.
105. Daina, A.; Michielin, O.; Zoete, V., SwissADME: a free web tool to evaluate pharmacokinetics, drug-likeness and medicinal chemistry friendliness of small molecules. *Scientific Reports* **2017,** *7* (1), 42717.
106. Guengerich, F. P., CYTOCHROME P-450 3A4: Regulation and Role in Drug Metabolism. *Annual Review of Pharmacology and Toxicology* **1999,** *39* (1), 1-17.
107. Furumiya, K.; Mizutani, T., Inhibition of Human CYP3A4, UGT1A6, and P-glycoprotein with Halogenated Xanthene Food Dyes and Prevention by Superoxide Dismutase. *Journal of Toxicology and Environmental Health, Part A* **2008,** *71* (19), 1307-1313.
108. Mizutani, T., Toxicity of Xanthene Food Dyes by Inhibition of Human Drug-Metabolizing Enzymes in a Noncompetitive Manner. *Journal of Environmental and Public Health* **2009,** *2009*, 953952.
109. Delaney, J. S., ESOL: Estimating Aqueous Solubility Directly from Molecular Structure. *Journal of Chemical Information and Computer Sciences* **2004,** *44* (3), 1000-1005.
110. Daina, A.; Zoete, V., A BOILED-Egg To Predict Gastrointestinal Absorption and Brain Penetration of Small Molecules. *ChemMedChem* **2016,** *11* (11), 1117-21.
111. Cortes, C.; Vapnik, V., Support-vector networks. *Machine Learning* **1995,** *20* (3), 273-297.
112. Lipinski, C. A.; Lombardo, F.; Dominy, B. W.; Feeney, P. J., Experimental and computational approaches to estimate solubility and permeability in drug discovery and development settings. *Adv Drug Deliv Rev* **2001,** *46* (1-3), 3-26.
113. Martin, Y. C., A bioavailability score. *Journal of Medicinal Chemistry* **2005,** *48* (9), 3164-70.
114. Baell, J. B.; Holloway, G. A., New substructure filters for removal of pan assay interference compounds (PAINS) from screening libraries and for their exclusion in bioassays. *Journal of Medicinal Chemistry* **2010,** *53* (7), 2719-40.

115. Teague, S. J.; Davis, A. M.; Leeson, P. D.; Oprea, T., The Design of Leadlike Combinatorial Libraries. *Angew Chem Int Ed Engl* **1999,** *38* (24), 3743-3748.
116. O'Boyle, N. M.; Banck, M.; James, C. A.; Morley, C.; Vandermeersch, T.; Hutchison, G. R., Open Babel: An open chemical toolbox. *Journal of Cheminformatics* **2011,** *3* (1), 33.
117. Ertl, P.; Rohde, B.; Selzer, P., Fast calculation of molecular polar surface area as a sum of fragment-based contributions and its application to the prediction of drug transport properties. *Journal of Medicinal Chemistry* **2000,** *43* (20), 3714-7.
118. Cheng, T.; Zhao, Y.; Li, X.; Lin, F.; Xu, Y.; Zhang, X.; Li, Y.; Wang, R.; Lai, L., Computation of octanol-water partition coefficients by guiding an additive model with knowledge. *Journal of Chemical Information and Modeling* **2007,** *47* (6), 2140-8.
119. Wildman, S. A.; Crippen, G. M., Prediction of Physicochemical Parameters by Atomic Contributions. *Journal of Chemical Information and Computer Sciences* **1999,** *39* (5), 868-873.
120. Moriguchi, I.; Hirono, S.; Qian, L.; Nakagome, I.; Matsushita, Y., Simple Method of Calculating Octanol/Water Partition Coefficient. *Chemical & Pharmaceutical Bulletin* **1992,** *40* (1), 127-130.
121. Moriguchi, I.; Hirono, S.; Nakagome, I.; Hirano, H., Comparison of Reliability of log P Values for Drugs Calculated by Several Methods. *Chemical & Pharmaceutical Bulletin* **1994,** *42* (4), 976-978.
122. *SILICOS-IT. Retrieved 05 november 2020, from http://silicos-it.be.s3-website-eu-west-1.amazonaws.com/software/filter-it/1.0.2/filter-it.html*.
123. Daina, A.; Michielin, O.; Zoete, V., iLOGP: a simple, robust, and efficient description of n-octanol/water partition coefficient for drug design using the GB/SA approach. *Journal of Chemical Information and Modeling* **2014,** *54* (12), 3284-301.
124. O'Neill, J. Antimicrobial resistance : tackling a crisis for the health and wealth of nations / the Review on Antimicrobial Resistance chaired by Jim O'Neill. https://wellcomecollection.org/works/rdpck35v (accessed 12.04.2021).
125. Kong, Q.; Yang, Y., Recent advances in antibacterial agents. *Bioorganic & Medicinal Chemistry Letters* **2021,** *35*, 127799.
126. Talebi Bezmin Abadi, A.; Rizvanov, A. A.; Haertlé, T.; Blatt, N. L., World Health Organization Report: Current Crisis of Antibiotic Resistance. *BioNanoScience* **2019,** *9* (4), 778-788.
127. Del Pozo, J. L., Biofilm-related disease. *Expert Review of Anti-infective Therapy* **2018,** *16* (1), 51-65.
128. Malhas, A. M.; Lawton, R.; Reidy, M.; Nathwani, D.; Clift, B. A., Causative organisms in revision total hip & knee arthroplasty for infection: Increasing multi-antibiotic resistance in coagulase-negative Staphylococcus and the implications for antibiotic prophylaxis. *The Surgeon* **2015,** *13* (5), 250-255.
129. Rutherford, S. T.; Bassler, B. L., Bacterial Quorum Sensing: Its Role in Virulence and Possibilities for Its Control. *Cold Spring Harbor Perspectives in Medicine* **2012,** *2* (11).
130. Rasmussen, T. B.; Givskov, M., Quorum-sensing inhibitors as anti-pathogenic drugs. *International Journal of Medical Microbiology* **2006,** *296* (2), 149-161.
131. Fuqua, C.; Greenberg, E. P., Listening in on bacteria: acyl-homoserine lactone signalling. *Nature Reviews Molecular Cell Biology* **2002,** *3* (9), 685-695.
132. Du, D.; Wang-Kan, X.; Neuberger, A.; van Veen, H. W.; Pos, K. M.; Piddock, L. J. V.; Luisi, B. F., Multidrug efflux pumps: structure, function and regulation. *Nature Reviews Microbiology* **2018,** *16* (9), 523-539.
133. Alav, I.; Sutton, J. M.; Rahman, K. M., Role of bacterial efflux pumps in biofilm formation. *Journal of Antimicrobial Chemotherapy* **2018,** *73* (8), 2003-2020.
134. Maia, M.; Resende, D. I. S. P.; Durães, F.; Pinto, M. M. M.; Sousa, E., Xanthenes in Medicinal Chemistry – Synthetic strategies and biological activities. *European Journal of Medicinal Chemistry* **2021,** *210*, 113085.

135. Barmak, A.; Niknam, K.; Mohebbi, G.; Pournabi, H., Antibacterial studies of hydroxyspiro[indoline-3,9-xanthene]trione against spiro[indoline3,9-xanthene]trione and their use as acetyl and butyrylcholinesterase inhibitors. *Microbial Pathogenesis* **2019,** *130*, 95-99.
136. Patil, V. S.; Padalkar, V. S.; Phatangare, K. R.; Umape, P. G.; Borase, B. N.; Sekar, N., Synthesis, Characterization, and Antibacterial Activity of Novel (1H-Benzo[d]imidazole-2-yl)-6-(diethylamino)-3H-one-xanthene, Phenoxazine, and Oxazine. *Journal of Heterocyclic Chemistry* **2015,** *52* (1), 124-129.
137. Kaya, M.; Demir, E.; Bekci, H., Synthesis, characterization and antimicrobial activity of novel xanthene sulfonamide and carboxamide derivatives. *Journal of Enzyme Inhibition and Medicinal Chemistry* **2013,** *28* (5), 885-893.
138. Khaki, D.; Amininasab, S. M.; Namazi, H., Novel poly(imide-ether)s based on xanthene and a corresponding composite reinforced with a GO grafted hyperbranched polymer: fabrication, characterization, and thermal, photophysical, antibacterial and chromium adsorption properties. *New Journal of Chemistry* **2020,** *44* (40), 17346-17359.
139. Gabor Varga, Z.; Agnes Szabo, M.; Schelz, Z.; Szegedi, E.; Amaral, L.; Molnar, J., Quorum Sensing Inhibition by Phenothiazines and Related Compounds. *Letters in Drug Design & Discovery* **2011,** *8* (2), 133-137.
140. Durães, F.; Palmeira, A.; Cruz, B.; Freitas-Silva, J.; Szemerédi, N.; Gales, L.; da Costa, P. M.; Remião, F.; Silva, R.; Pinto, M.; Spengler, G.; Sousa, E., Antimicrobial Activity of a Library of Thioxanthones and Their Potential as Efflux Pump Inhibitors. *Pharmaceuticals* **2021,** *14* (6), 572.
141. Kristiansen, M. M.; Leandro, C.; Ordway, D.; Martins, M.; Viveiros, M.; Pacheco, T.; Kristiansen, J. E.; Amaral, L., Phenothiazines alter resistance of methicillin-resistant strains of Staphylococcus aureus (MRSA) to oxacillin in vitro. *International Journal of Antimicrobial Agents* **2003,** *22* (3), 250-253.
142. Kristiansen, M. M.; Leandro, C.; Ordway, D.; Martins, M.; Viveiros, M.; Pacheco, T.; Molnar, J.; Kristiansen, J. E.; Amaral, L., Thioridazine reduces resistance of methicillin-resistant staphylococcus aureus by inhibiting a reserpine-sensitive efflux pump. *In Vivo* **2006,** *20* (3), 361.
143. Amaral, L.; Martins, A.; Spengler, G.; Molnar, J., Efflux pumps of Gram-negative bacteria: what they do, how they do it, with what and how to deal with them. *Frontiers in Pharmacology* **2014,** *4* (168).
144. Kaatz, G. W.; Moudgal, V. V.; Seo, S. M.; Kristiansen, J. E., Phenothiazines and thioxanthenes inhibit multidrug efflux pump activity in Staphylococcus aureus. *Antimicrob Agents Chemother* **2003,** *47* (2), 719-726.
145. Campbell, K. L., Sulphonamides: updates on use in veterinary medicine. *Veterinary Dermatology* **1999,** *10* (3), 205-215.
146. Wainwright, M.; Kristiansen, J. E., On the 75th anniversary of Prontosil. *Dyes and Pigments* **2011,** *88* (3), 231-234.
147. al-Rashida, M.; Hussain, S.; Hamayoun, M.; Altaf, A.; Iqbal, J., Sulfa Drugs as Inhibitors of Carbonic Anhydrase: New Targets for the Old Drugs. *BioMed Research International* **2014,** *2014*, 162928.
148. Loubatières-Mariani, M.-M., La découverte des sulfamides hypoglycémiants. *J. Soc. Biol.* **2007,** *201* (2), 121-125.
149. Siddiqui, N.; Pandeya, S. N.; Khan, S. A.; Stables, J.; Rana, A.; Alam, M.; Arshad, M. F.; Bhat, M. A., Synthesis and anticonvulsant activity of sulfonamide derivatives-hydrophobic domain. *Bioorganic & Medicinal Chemistry Letters* **2007,** *17* (1), 255-259.
150. Okolotowicz, K. J.; Dwyer, M.; Ryan, D.; Cheng, J.; Cashman, E. A.; Moore, S.; Mercola, M.; Cashman, J. R., Novel tertiary sulfonamides as potent anti-cancer agents. *Bioorganic & Medicinal Chemistry* **2018,** *26* (15), 4441-4451.
151. Andrea, S.; Takashi, O.; Antonio, M.; Claudiu, T. S., Anticancer and Antiviral Sulfonamides. *Current Medicinal Chemistry* **2003,** *10* (11), 925-953.

152. Phillips, R. F.; Frank, V. S., XANTHYDROL AS A REAGENT FOR THE IDENTIFICATION OF SULFONAMIDES. *The Journal of Organic Chemistry* **1944,** *09* (1), 9-12.
153. Westcott, W. L. Reactions of xanthydrol with the amino acids and cytochrome C. University of Utah, 1953.
154. Tacic, A.; Nikolic, V.; Nikolic, L.; Savic, I., Antimicrobial sulfonamide drugs. *Advanced technologies* **2017,** *6* (1), 58-71.
155. Connor, E. E., Sulfonamide antibiotics. *Primary Care Update for OB/GYNS* **1998,** *5* (1), 32-35.
156. Seydel, J. K., Sulfonamides, Structure-Activity Relationship, and Mode of Action: Structural Problems of the Antibacterial Action of 4-Aminobenzoic Acid (PABA) Antagonists. *Journal of Pharmaceutical Sciences* **1968,** *57* (9), 1455-1478.
157. Gajdács, M.; Spengler, G., Standard operating procedure (SOP) for disk diffusion-based quorum sensing inhibition assays. *Acta Pharmaceutica Hungarica* **2020,** *89* (4), 117-125.
158. Gajdács, M.; Spengler, G., The Role of Drug Repurposing in the Development of Novel Antimicrobial Drugs: Non-Antibiotic Pharmacological Agents as Quorum Sensing-Inhibitors. *Antibiotics* **2019,** *8* (4), 270.
159. Durães, F.; Resende, D. I. S. P.; Palmeira, A.; Szemerédi, N.; Pinto, M. M. M.; Spengler, G.; Sousa, E., Xanthones Active against Multidrug Resistance and Virulence Mechanisms of Bacteria. *Antibiotics* **2021,** *10* (5), 600.
160. Durães, F.; Cravo, S.; Freitas-Silva, J.; Szemerédi, N.; Martins-da-Costa, P.; Pinto, E.; Tiritan, M. E.; Spengler, G.; Fernandes, C.; Sousa, E.; Pinto, M., Enantioselectivity of Chiral Derivatives of Xanthones in Virulence Effects of Resistant Bacteria. *Pharmaceuticals* **2021,** *14* (11).
161. Eicher, T., Cha, H., Seeger, M.A., Brandstaetter, L., El-Delik, J., Bohnert, J.A., Kern, W.V., Verrey, F., Gruetter, M.G., Diederichs, K., Pos, K.M. 4DX5. https://www.rcsb.org/structure/4DX5 (accessed 14.04.2021).
162. Zhu, Z.; Espenson, J. H., Organic Reactions Catalyzed by Methylrhenium Trioxide: Dehydration, Amination, and Disproportionation of Alcohols. *The Journal of Organic Chemistry* **1996,** *61* (1), 324-328.
163. Shen, G.; Zhao, L.; Wang, Y.; Xia, W.; Yang, M.; Zhang, T., Palladium–copper catalyzed C(sp3)–C(sp2) bond C–H activation cross-coupling reaction: selective arylation to synthesize 9-aryl-9H-xanthene and 9,9-diaryl-xanthene derivatives. *RSC Advances* **2016,** *6* (88), 84748-84751.
164. Eicher, T.; Cha, H.-j.; Seeger, M. A.; Brandstätter, L.; El-Delik, J.; Bohnert, J. A.; Kern, W. V.; Verrey, F.; Grütter, M. G.; Diederichs, K.; Pos, K. M., Transport of drugs by the multidrug transporter AcrB involves an access and a deep binding pocket that are separated by a switch-loop. *Proceedings of the National Academy of Sciences* **2012,** *109* (15), 5687.
165. Mikolosko, J.; Bobyk, K.; Zgurskaya, H. I.; Ghosh, P., Conformational Flexibility in the Multidrug Efflux System Protein AcrA. *Structure* **2006,** *14* (3), 577-587.
166. Koronakis, V.; Sharff, A.; Koronakis, E.; Luisi, B.; Hughes, C., Crystal structure of the bacterial membrane protein TolC central to multidrug efflux and protein export. *Nature* **2000,** *405* (6789), 914-919.
167. Sussman, J. L.; Lin, D.; Jiang, J.; Manning, N. O.; Prilusky, J.; Ritter, O.; Abola, E. E., Protein Data Bank (PDB): database of three-dimensional structural information of biological macromolecules. *Acta Crystallogr D Biol Crystallogr* **1998,** *54* (Pt 6 Pt 1), 1078-84.
168. Trott, O.; Olson, A. J., AutoDock Vina: improving the speed and accuracy of docking with a new scoring function, efficient optimization, and multithreading. *J Comput Chem* **2010,** *31* (2), 455-461.
169. Shi, X.; Chen, M.; Yu, Z.; Bell, J. M.; Wang, H.; Forrester, I.; Villarreal, H.; Jakana, J.; Du, D.; Luisi, B. F.; Ludtke, S. J.; Wang, Z., In situ structure and assembly of the multidrug efflux pump AcrAB-TolC. *Nature Communications* **2019,** *10* (1), 2635.
170. Aron, Z.; Opperman, T. J., The hydrophobic trap—the Achilles heel of RND efflux pumps. *Research in Microbiology* **2018,** *169* (7), 393-400.

171. Waterhouse, A.; Bertoni, M.; Bienert, S.; Studer, G.; Tauriello, G.; Gumienny, R.; Heer, F. T.; de Beer, T. A P.; Rempfer, C.; Bordoli, L.; Lepore, R.; Schwede, T., SWISS-MODEL: homology modelling of protein structures and complexes. *Nucleic Acids Research* **2018,** *46* (W1), W296-W303.
172. The UniProt Consortium, UniProt: the universal protein knowledgebase. *Nucleic Acids Research* **2016,** *45* (D1), D158-D169.
173. Zárate, S. G.; Morales, P.; Świderek, K.; Bolanos-Garcia, V. M.; Bastida, A., A Molecular Modeling Approach to Identify Novel Inhibitors of the Major Facilitator Superfamily of Efflux Pump Transporters. *Antibiotics (Basel)* **2019,** *8* (1).
174. Seeliger, D.; de Groot, B. L., Ligand docking and binding site analysis with PyMOL and Autodock/Vina. *J Comput Aided Mol Des* **2010,** *24* (5), 417-22.
175. CLSI, *Methods for Dilution Antimicrobial Susceptibility Tests for Bacteria that Grow Aerobically*. 11th ed.; Clinical and Laboratory Standards Institute Wayne, PA, USA: 2008.
176. Parai, D.; Banerjee, M.; Dey, P.; Mukherjee, S. K., Reserpine attenuates biofilm formation and virulence of Staphylococcus aureus. *Microbial Pathogenesis* **2020,** *138*, 103790.
177. Duthey B. Background Paper 6.11 Alzheimer Disease and other Dementias, Update on 2004. World Health Organization, 2013.
178. Stelzmann, R. A.; Norman Schnitzlein, H.; Reed Murtagh, F., An english translation of alzheimer's 1907 paper, "über eine eigenartige erkankung der hirnrinde". *Clinical Anatomy* **1995,** *8* (6), 429-431.
179. Lane, C. A.; Hardy, J.; Schott, J. M., Alzheimer's disease. *European Journal of Neurology* **2018,** *25* (1), 59-70.
180. Suzuki, K.; Iwata, A.; Iwatsubo, T., The past, present, and future of disease-modifying therapies for Alzheimer's disease. *Proceedings of the Japan Academy, Series B* **2017,** *93* (10), 757-771.
181. Ghosh, A. K.; Cárdenas, E. L.; Osswald, H. L., The Design, Development, and Evaluation of BACE1 Inhibitors for the Treatment of Alzheimer's Disease. In *Alzheimer's Disease II*, Wolfe, M. S., Ed. Springer International Publishing: Cham, 2017; pp 27-85.
182. Suzuki, K.; Iwata, A.; Iwatsubo, T., The past, present, and future of disease-modifying therapies for Alzheimer's disease. *Proc Jpn Acad Ser B Phys Biol Sci* **2017,** *93* (10), 757-771.
183. Bursavich, M. G.; Harrison, B. A.; Blain, J. F., Gamma Secretase Modulators: New Alzheimer's Drugs on the Horizon? *J Med Chem* **2016,** *59* (16), 7389-409.
184. Brothers, H. M.; Gosztyla, M. L.; Robinson, S. R., The Physiological Roles of Amyloid-β Peptide Hint at New Ways to Treat Alzheimer's Disease. *Frontiers in Aging Neuroscience* **2018,** *10*.
185. Bateman, R. J.; Munsell, L. Y.; Morris, J. C.; Swarm, R.; Yarasheski, K. E.; Holtzman, D. M., Human amyloid-β synthesis and clearance rates as measured in cerebrospinal fluid in vivo. *Nature Medicine* **2006,** *12* (7), 856-861.
186. Vogelgesang, S.; Cascorbi, I.; Schroeder, E.; Pahnke, J.; Kroemer, H. K.; Siegmund, W.; Kunert-Keil, C.; Walker, L. C.; Warzok, R. W., Deposition of Alzheimer's β-amyloid is inversely correlated with P-glycoprotein expression in the brains of elderly non-demented humans. *Pharmacogenetics and Genomics* **2002,** *12* (7).
187. Vassar, R.; Bennett, B. D.; Babu-Khan, S.; Kahn, S.; Mendiaz, E. A.; Denis, P.; Teplow, D. B.; Ross, S.; Amarante, P.; Loeloff, R.; Luo, Y.; Fisher, S.; Fuller, J.; Edenson, S.; Lile, J.; Jarosinski, M. A.; Biere, A. L.; Curran, E.; Burgess, T.; Louis, J. C.; Collins, F.; Treanor, J.; Rogers, G.; Citron, M., Beta-secretase cleavage of Alzheimer's amyloid precursor protein by the transmembrane aspartic protease BACE. *Science* **1999,** *286* (5440), 735-41.
188. Cole, D. C.; Manas, E. S.; Stock, J. R.; Condon, J. S.; Jennings, L. D.; Aulabaugh, A.; Chopra, R.; Cowling, R.; Ellingboe, J. W.; Fan, K. Y.; Harrison, B. L.; Hu, Y.; Jacobsen, S.; Jin, G.; Lin, L.; Lovering, F. E.; Malamas, M. S.; Stahl, M. L.; Strand, J.; Sukhdeo, M. N.; Svenson, K.; Turner, M. J.; Wagner, E.; Wu, J.; Zhou, P.; Bard, J., Acylguanidines as Small-Molecule β-Secretase Inhibitors. *Journal of Medicinal Chemistry* **2006,** *49* (21), 6158-6161.

189. Hamada, Y.; Kiso, Y., New directions for protease inhibitors directed drug discovery. *Biopolymers* **2016,** *106* (4), 563-79.
190. Hong, L.; Koelsch, G.; Lin, X.; Wu, S.; Terzyan, S.; Ghosh, A. K.; Zhang, X. C.; Tang, J., Structure of the protease domain of memapsin 2 (beta-secretase) complexed with inhibitor. *Science* **2000,** *290* (5489), 150-3.
191. Maia, M. A.; Sousa, E., BACE-1 and γ-Secretase as Therapeutic Targets for Alzheimer's Disease. *Pharmaceuticals* **2019,** *12* (1).
192. Martins, E.; Silva, V.; Lemos, A.; Palmeira, A.; Puthongking, P.; Sousa, E.; Rocha-Pereira, C.; Ghanem, C. I.; Carmo, H.; Remião, F.; Silva, R., Newly Synthesized Oxygenated Xanthones as Potential P-Glycoprotein Activators: In Vitro, Ex Vivo, and In Silico Studies. *Molecules* **2019,** *24* (4).
193. Silva, R.; Palmeira, A.; Carmo, H.; Barbosa, D. J.; Gameiro, M.; Gomes, A.; Paiva, A. M.; Sousa, E.; Pinto, M.; Bastos Mde, L.; Remião, F., P-glycoprotein induction in Caco-2 cells by newly synthetized thioxanthones prevents paraquat cytotoxicity. *Arch Toxicol* **2015,** *89* (10), 1783-800.
194. Silva, R.; Sousa, E.; Carmo, H.; Palmeira, A.; Barbosa, D. J.; Gameiro, M.; Pinto, M.; de Lourdes Bastos, M.; Remião, F., Induction and activation of P-glycoprotein by dihydroxylated xanthones protect against the cytotoxicity of the P-glycoprotein substrate paraquat. *Archives of Toxicology* **2014,** *88* (4), 937-951.
195. Shibata, M.; Yamada, S.; Kumar, S. R.; Calero, M.; Bading, J.; Frangione, B.; Holtzman, D. M.; Miller, C. A.; Strickland, D. K.; Ghiso, J.; Zlokovic, B. V., Clearance of Alzheimer's amyloid-β1-40 peptide from brain by LDL receptor–related protein-1 at the blood-brain barrier. *The Journal of Clinical Investigation* **2000,** *106* (12), 1489-1499.
196. Roberts, K. F.; Elbert, D. L.; Kasten, T. P.; Patterson, B. W.; Sigurdson, W. C.; Connors, R. E.; Ovod, V.; Munsell, L. Y.; Mawuenyega, K. G.; Miller-Thomas, M. M.; Moran, C. J.; Cross III, D. T.; Derdeyn, C. P.; Bateman, R. J., Amyloid-β efflux from the central nervous system into the plasma. *Annals of Neurology* **2014,** *76* (6), 837-844.
197. Deane, R.; Bell, D. R.; Sagare, A.; Zlokovic, V. B., Clearance of Amyloid-β Peptide Across the Blood-Brain Barrier: Implication for Therapies in Alzheimers Disease. *CNS & Neurological Disorders - Drug Targets* **2009,** *8* (1), 16-30.
198. Lam, F. C.; Liu, R.; Lu, P.; Shapiro, A. B.; Renoir, J.-M.; Sharom, Frances J.; Reiner, P. B., β-Amyloid efflux mediated by p-glycoprotein. *Journal of Neurochemistry* **2001,** *76* (4), 1121-1128.
199. Pahnke, J.; Langer, O.; Krohn, M., Alzheimer's and ABC transporters — new opportunities for diagnostics and treatment. *Neurobiology of Disease* **2014,** *72*, 54-60.
200. Wolf, A.; Bauer, B.; Hartz, A., ABC Transporters and the Alzheimer's Disease Enigma. *Frontiers in Psychiatry* **2012,** *3*.
201. Abuznait, A. H.; Kaddoumi, A., Role of ABC Transporters in the Pathogenesis of Alzheimer's Disease. *ACS Chemical Neuroscience* **2012,** *3* (11), 820-831.
202. Chai, A. B.; Leung, G. K. F.; Callaghan, R.; Gelissen, I. C., P-glycoprotein: a role in the export of amyloid-β in Alzheimer's disease? *The FEBS Journal* **2020,** *287* (4), 612-625.
203. Dahlgren, K. N.; Manelli, A. M.; Stine, W. B., Jr.; Baker, L. K.; Krafft, G. A.; LaDu, M. J., Oligomeric and Fibrillar Species of Amyloid-β Peptides Differentially Affect Neuronal Viability *. *Journal of Biological Chemistry* **2002,** *277* (35), 32046-32053.
204. Bartels, A. L.; Kortekaas, R.; Bart, J.; Willemsen, A. T. M.; de Klerk, O. L.; de Vries, J. J.; van Oostrom, J. C. H.; Leenders, K. L., Blood–brain barrier P-glycoprotein function decreases in specific brain regions with aging: A possible role in progressive neurodegeneration. *Neurobiology of Aging* **2009,** *30* (11), 1818-1824.
205. Gil-Martins, E.; Barbosa, D. J.; Silva, V.; Remião, F.; Silva, R., Dysfunction of ABC transporters at the blood-brain barrier: Role in neurological disorders. *Pharmacology & Therapeutics* **2020,** *213*, 107554.
206. Silva, V.; Gil-Martins, E.; Rocha-Pereira, C.; Lemos, A.; Palmeira, A.; Puthongking, P.; Sousa, E.; de Lourdes Bastos, M.; Remião, F.; Silva, R., Oxygenated xanthones as P-glycoprotein

modulators at the intestinal barrier: in vitro and docking studies. *Medicinal Chemistry Research* **2020,** *29* (6), 1041-1057.
207. Research Corporation Technologies, Inc., Amino acid protecting groups, 1991. WO9108190A1.
208. Blakemore, D., Chapter 1 Suzuki–Miyaura Coupling. In *Synthetic Methods in Drug Discovery: Volume 1*, The Royal Society of Chemistry: 2016; Vol. 1, pp 1-69.
209. Leggio, A.; Belsito, E. L.; De Luca, G.; Di Gioia, M. L.; Leotta, V.; Romio, E.; Siciliano, C.; Liguori, A., One-pot synthesis of amides from carboxylic acids activated using thionyl chloride. *RSC Advances* **2016,** *6* (41), 34468-34475.
210. Valeur, E.; Bradley, M., Amide bond formation: beyond the myth of coupling reagents. *Chemical Society Reviews* **2009,** *38* (2), 606-631.
211. Montalbetti, C. A. G. N.; Falque, V. M., Amide bond formation and peptide coupling. *Tetrahedron* **2005,** *61*, 10827-10852.
212. El-Faham, A.; Albericio, F., COMU: A third generation of uronium-type coupling reagents. *Journal of Peptide Science* **2010,** *16* (1), 6-9.
213. El-Faham, A.; Funosas, R. S.; Prohens, R.; Albericio, F., COMU: A Safer and More Effective Replacement for Benzotriazole-Based Uronium Coupling Reagents. *Chemistry – A European Journal* **2009,** *15* (37), 9404-9416.
214. Scattolin, T.; Deckers, K.; Schoenebeck, F., Direct Synthesis of Acyl Fluorides from Carboxylic Acids with the Bench-Stable Solid Reagent (Me4N)SCF3. *Organic Letters* **2017,** *19* (21), 5740-5743.
215. Due-Hansen, M. E.; Pandey, S. K.; Christiansen, E.; Andersen, R.; Hansen, S. V. F.; Ulven, T., A protocol for amide bond formation with electron deficient amines and sterically hindered substrates. *Organic & Biomolecular Chemistry* **2016,** *14* (2), 430-433.
216. Bailey, C. L.; Joh, A. Y.; Hurley, Z. Q.; Anderson, C. L.; Singaram, B., Controlled Reduction of Tertiary Amides to the Corresponding Alcohols, Aldehydes, or Amines Using Dialkylboranes and Aminoborohydride Reagents. *The Journal of Organic Chemistry* **2016,** *81* (9), 3619-3628.
217. *Clayden, J.; Greeves, N.; Warren, S., Organic Chemistry. OUP Oxford: 2012*.
218. Repetto, G.; del Peso, A.; Zurita, J. L., Neutral red uptake assay for the estimation of cell viability/cytotoxicity. *Nature Protocols* **2008,** *3* (7), 1125-1131.
219. Jaszczyszyn, A.; Gąsiorowski, K., Limitations of the MTT Assay in Cell Viability Testing. *Advances in Clinical and Experimental Medicine* **2008,** *17*, 525-529.
220. Ates, G.; Vanhaecke, T.; Rogiers, V.; Rodrigues, R. M., Assaying Cellular Viability Using the Neutral Red Uptake Assay. In *Cell Viability Assays: Methods and Protocols*, Gilbert, D. F.; Friedrich, O., Eds. Springer New York: New York, NY, 2017; pp 19-26.
221. Nemes, Z.; Dietz, R.; Lüth, J. B.; Gomba, S.; Hackenthal, E.; Gross, F., The pharmacological relevance of vital staining with neutral red. *Experientia* **1979,** *35* (11), 1475-1476.
222. Martins, E.; Silva, V.; Lemos, A.; Palmeira, A.; Puthongking, P.; Sousa, E.; Rocha-Pereira, C.; Ghanem, C. I.; Carmo, H.; Remião, F.; Silva, R., Newly Synthesized Oxygenated Xanthones as Potential P-Glycoprotein Activators: In Vitro, Ex Vivo, and In Silico Studies. *Molecules* **2019,** *24* (4), 707.
223. Chai, A. B.; Hartz, A. M. S.; Gao, X.; Yang, A.; Callaghan, R.; Gelissen, I. C., New Evidence for P-gp-Mediated Export of Amyloid-β Peptides in Molecular, Blood-Brain Barrier and Neuronal Models. *International Journal of Molecular Sciences* **2021,** *22* (1), 246.
224. Silva, R.; Vilas-Boas, V.; Carmo, H.; Dinis-Oliveira, R. J.; Carvalho, F.; de Lourdes Bastos, M.; Remião, F., Modulation of P-glycoprotein efflux pump: induction and activation as a therapeutic strategy. *Pharmacology & Therapeutics* **2015,** *149*, 1-123.
225. Whitnall, M.; Richardson, D. R., Iron: A New Target for Pharmacological Intervention in Neurodegenerative Diseases. *Seminars in Pediatric Neurology* **2006,** *13* (3), 186-197.
226. Barreiro, S.; Silva, B.; Long, S.; Pinto, M.; Remião, F.; Sousa, E.; Silva, R., Fiscalin Derivatives as Potential Neuroprotective Agents. *Pharmaceutics* **2022,** *14* (7).

227. Eid, R.; Arab, N. T. T.; Greenwood, M. T., Iron mediated toxicity and programmed cell death: A review and a re-examination of existing paradigms. *Biochimica et Biophysica Acta (BBA) - Molecular Cell Research* **2017,** *1864* (2), 399-430.
228. Salvador, G. A.; Uranga, R. M.; Giusto, N. M., Iron and mechanisms of neurotoxicity. *Int J Alzheimers Dis* **2010,** *2011*, 720658.
229. Cheignon, C.; Tomas, M.; Bonnefont-Rousselot, D.; Faller, P.; Hureau, C.; Collin, F., Oxidative stress and the amyloid beta peptide in Alzheimer's disease. *Redox Biology* **2018,** *14*, 450-464.
230. Eid, R.; Arab, N. T.; Greenwood, M. T., Iron mediated toxicity and programmed cell death: A review and a re-examination of existing paradigms. *Biochim Biophys Acta Mol Cell Res* **2017,** *1864* (2), 399-430.
231. Jiang, D.; Li, X.; Williams, R.; Patel, S.; Men, L.; Wang, Y.; Zhou, F., Ternary complexes of iron, amyloid-beta, and nitrilotriacetic acid: binding affinities, redox properties, and relevance to iron-induced oxidative stress in Alzheimer's disease. *Biochemistry* **2009,** *48* (33), 7939-47.
232. Cidade, H.; Rocha, V.; Palmeira, A.; Marques, C.; Tiritan, M. E.; Ferreira, H.; Lobo, J. S.; Almeida, I. F.; Sousa, M. E.; Pinto, M., In silico and in vitro antioxidant and cytotoxicity evaluation of oxygenated xanthone derivatives. *Arabian Journal of Chemistry* **2020,** *13* (1), 17-26.
233. Resende, D.; Almeida, M. C.; Maciel, B.; Carmo, H.; Sousa Lobo, J.; Dal Pozzo, C.; Cravo, S. M.; Rosa, G. P.; Kane-Pagès, A.; do Carmo Barreto, M.; Almeida, I. F.; de Sousa, M. E.; Pinto, M. M. M., Efficacy, Stability, and Safety Evaluation of New Polyphenolic Xanthones Towards Identification of Bioactive Compounds to Fight Skin Photoaging. *Molecules* **2020,** *25* (12).
234. d'Hardemare Adu, M.; Torelli, S.; Serratrice, G.; Pierre, J. L., Design of iron chelators: syntheses and iron (III) complexing abilities of tripodal tris-bidentate ligands. *Biometals* **2006,** *19* (4), 349-66.
235. Liu, Z. D.; Hider, R. C., Design of iron chelators with therapeutic application. *Coordination Chemistry Reviews* **2002,** *232* (1), 151-171.
236. Cardoso, F. L.; Brites, D.; Brito, M. A., Looking at the blood–brain barrier: Molecular anatomy and possible investigation approaches. *Brain Research Reviews* **2010,** *64* (2), 328-363.
237. Van Asperen, J.; Mayer, U.; Van Tellingen, O.; Beijnen, J. H., The Functional Role of P-Glycoprotein in the Blood–Brain Barrier. *Journal of Pharmaceutical Sciences* **1997,** *86* (8), 881-884.
238. Di, L.; Kerns, E. H.; Fan, K.; McConnell, O. J.; Carter, G. T., High throughput artificial membrane permeability assay for blood–brain barrier. *European Journal of Medicinal Chemistry* **2003,** *38* (3), 223-232.
239. Crivori, P.; Cruciani, G.; Carrupt, P.-A.; Testa, B., Predicting Blood−Brain Barrier Permeation from Three-Dimensional Molecular Structure. *Journal of Medicinal Chemistry* **2000,** *43* (11), 2204-2216.
240. Pajouhesh, H.; Lenz, G. R., Medicinal chemical properties of successful central nervous system drugs. *NeuroRx* **2005,** *2* (4), 541-53.
241. Fedi, V.; Guidi, A.; Altamura, M., Tricyclic structures in medicinal chemistry: an overview of their recent uses in non-CNS pathologies. *Mini Rev Med Chem* **2008,** *8* (14), 1464-84.
242. Samanidou, V. F.; Nika, M. K.; Papadoyannis, I. N., Chapter 11 - HPLC and its Essential Role in the Analysis of Tricyclic Antidepressants in Biological Samples. In *Recent Advances in Medicinal Chemistry*, Atta ur, R.; Choudhary, M. I.; Perry, G., Eds. Elsevier: 2014; pp 332-380.
243. Vieira, E.; Huwyler, J.; Jolidon, S.; Knoflach, F.; Mutel, V.; Wichmann, J., 9H-Xanthene-9-carboxylic acid [1,2,4]oxadiazol-3-yl- and (2H-tetrazol-5-yl)-amides as potent, orally available mGlu1 receptor enhancers. *Bioorg Med Chem Lett* **2005,** *15* (20), 4628-31.
244. Xie, Q.; Zhu, Z.; Li, L.; Ni, C.; Hu, J., A General Protocol for C−H Difluoromethylation of Carbon Acids with TMSCF2Br. *Angewandte Chemie International Edition* **2019,** *58* (19), 6405-6410.
245. Moradkhani, S.; Ayatollahi, A. M.; Ghanadian, M.; Moin, M. R.; Razavizadeh, M.; Shahlaei, M., Phytochemical Analysis and Metal-chelation Activity of Achillea tenuifolia Lam. *Iran J Pharm Res* **2012,** *11* (1), 177-83.

246. Ferrigno, F.; Biancofiore, I.; Malancona, S.; Ponzi, S.; Paonessa, G.; Graziani, R.; Bresciani, A.; Gennari, N.; Di Marco, A.; Kaiser, M.; Summa, V.; Harper, S.; Ontoria, J. M., Discovery of 2-(1H-imidazo-2-yl)piperazines as a new class of potent and non-cytotoxic inhibitors of Trypanosoma brucei growth in vitro. *Bioorganic & Medicinal Chemistry Letters* **2018,** *28* (23), 3689-3692.
247. Olmo, E. d.; Diaz-González, R.; Escarcena, R.; Carvalho, L.; Bustos, L. A.; Navarro, M.; Feliciano, A. S., Diamine and aminoalcohol derivatives active against Trypanosoma brucei. *Bioorganic & Medicinal Chemistry Letters* **2012,** *22* (1), 440-443.
248. Organization, W.-W. H. Human African trypanosomiasis (sleeping sickness). https://www.who.int/health-topics/human-african-trypanosomiasis#tab=tab_1 (accessed 23/08/2022).
249. Li, K.; Grooms, G. M.; Khan, S. M.; Hernandez, A. G.; Witola, W. H.; Stec, J., Novel acyl carbamates and acyl / diacyl ureas show in vitro efficacy against Toxoplasma gondii and Cryptosporidium parvum. *International Journal for Parasitology: Drugs and Drug Resistance* **2020,** *14*, 80-90.
250. Ghosh, A. K.; Brindisi, M., Urea Derivatives in Modern Drug Discovery and Medicinal Chemistry. *Journal of Medicinal Chemistry* **2020,** *63* (6), 2751-2788.
251. Wiedemar, N.; Hauser, D. A.; Mäser, P., 100 Years of Suramin. *Antimicrob Agents Chemother* **2020,** *64* (3).
252. Patrick, D. A.; Wenzler, T.; Yang, S.; Weiser, P. T.; Wang, M. Z.; Brun, R.; Tidwell, R. R., Synthesis of novel amide and urea derivatives of thiazol-2-ethylamines and their activity against Trypanosoma brucei rhodesiense. *Bioorganic & Medicinal Chemistry* **2016,** *24* (11), 2451-2465.
253. Mrus, J.; Baeten, B.; Engelen, M.; Silber, S. A., Efficacy of single-dose 500 mg mebendazole in soil-transmitted helminth infections: a review. *Journal of Helminthology* **2018,** *92* (3), 269-278.
254. Ochola, D. O. K.; Prichard, R. K.; Lubega, G. W., CLASSICAL LIGANDS BIND TUBULIN OF TRYPANOSOMES AND INHIBIT THEIR GROWTH IN VITRO. *Journal of Parasitology* **2002,** *88* (3), 600-604, 5.
255. Cañete, R.; Escobedo, A. A.; Almirall, P.; González, M. E.; Brito, K.; Cimerman, S., Mebendazole in parasitic infections other than those caused by soil-transmitted helminths. *Trans R Soc Trop Med Hyg* **2009,** *103* (5), 437-42.
256. Roy, D.; Panda, G., Benzhydryl Amines: Synthesis and Their Biological Perspective. *ACS Omega* **2020,** *5* (1), 19-30.
257. Desmarchelier, A.; Ortiz, P.; Harutyunyan, S. R., Tertiary α-diarylmethylamines derived from diarylketimines and organomagnesium reagents. *Chemical Communications* **2015,** *51* (4), 703-706.
258. Onur, S.; Köse, M.; Koçer, F.; Tümer, F., Synthesis, characterization and antibacterial effect of diarylmethylamine-based imines. *Journal of Molecular Structure* **2020,** *1214*, 128150.
259. Jolidon, S.; Alberati, D.; Dowle, A.; Fischer, H.; Hainzl, D.; Narquizian, R.; Norcross, R.; Pinard, E., Design, synthesis and structure-activity relationship of simple bis-amides as potent inhibitors of GlyT1. *Bioorg Med Chem Lett* **2008,** *18* (20), 5533-6.
260. Naito, R.; Takeuchi, M.; Morihira, K.; Hayakawa, M.; Ikeda, K.; Shibanuma, T.; Isomura, Y., Selective muscarinic antagonists. I. Synthesis and antimuscarinic properties of 4-piperidyl benzhydrylcarbamate derivatives. *Chem Pharm Bull (Tokyo)* **1998,** *46* (8), 1274-85.
261. Bonner, A.; Loftus, A.; Padgham, A. C.; Baumann, M., Forgotten and forbidden chemical reactions revitalised through continuous flow technology. *Organic & Biomolecular Chemistry* **2021,** *19* (36), 7737-7753.
262. Baumann, M.; Moody, T. S.; Smyth, M.; Wharry, S., A Perspective on Continuous Flow Chemistry in the Pharmaceutical Industry. *Organic Process Research & Development* **2020,** *24* (10), 1802-1813.

263. Baumann, M.; Baxendale, I. R.; Ley, S. V.; Nikbin, N.; Smith, C. D.; Tierney, J. P., A modular flow reactor for performing Curtius rearrangements as a continuous flow process. *Organic & Biomolecular Chemistry* **2008,** *6* (9), 1577-1586.
264. Baumann, M.; Leslie, A.; Moody, T. S.; Smyth, M.; Wharry, S., Tandem Continuous Flow Curtius Rearrangement and Subsequent Enzyme-Mediated Impurity Tagging. *Organic Process Research & Development* **2021,** *25* (3), 452-456.
265. Ghosh, A. K.; Brindisi, M.; Sarkar, A., The Curtius Rearrangement: Applications in Modern Drug Discovery and Medicinal Chemistry. *ChemMedChem* **2018,** *13* (22), 2351-2373.
266. Ghosh, A. K.; Sarkar, A.; Brindisi, M., The Curtius rearrangement: mechanistic insight and recent applications in natural product syntheses. *Organic & Biomolecular Chemistry* **2018,** *16* (12), 2006-2027.
267. Joullie, M. M.; Lassen, K. M., Evolution of amide bond formation. *ARKIVOC* **2010,** *2010* (8), 189-250.
268. Battista, T.; Colotti, G.; Ilari, A.; Fiorillo, A., Targeting Trypanothione Reductase, a Key Enzyme in the Redox Trypanosomatid Metabolism, to Develop New Drugs against Leishmaniasis and Trypanosomiases. *Molecules* **2020,** *25* (8), 1924.
269. McDade, E.; Voytyuk, I.; Aisen, P.; Bateman, R. J.; Carrillo, M. C.; De Strooper, B.; Haass, C.; Reiman, E. M.; Sperling, R.; Tariot, P. N.; Yan, R.; Masters, C. L.; Vassar, R.; Lichtenthaler, S. F., The case for low-level BACE1 inhibition for the prevention of Alzheimer disease. *Nature Reviews Neurology* **2021,** *17* (11), 703-714.
270. Savelieff, M. G.; Nam, G.; Kang, J.; Lee, H. J.; Lee, M.; Lim, M. H., Development of Multifunctional Molecules as Potential Therapeutic Candidates for Alzheimer's Disease, Parkinson's Disease, and Amyotrophic Lateral Sclerosis in the Last Decade. *Chemical Reviews* **2019,** *119* (2), 1221-1322.

Annex I - HPLC and NMR spectra and electrospray ESI data

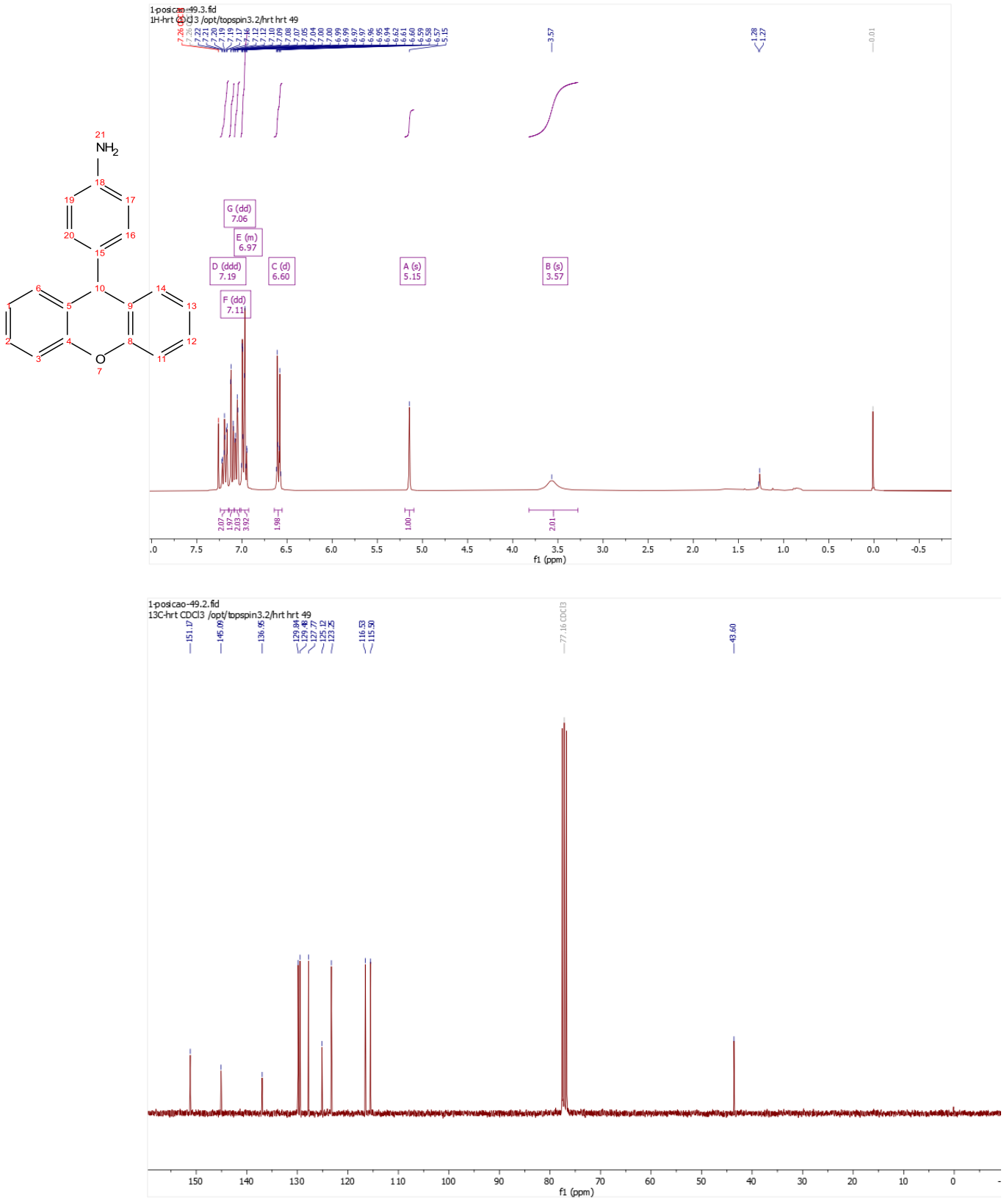

Figure 54. ^{1}H and ^{13}C NMR of compound **MM7**.

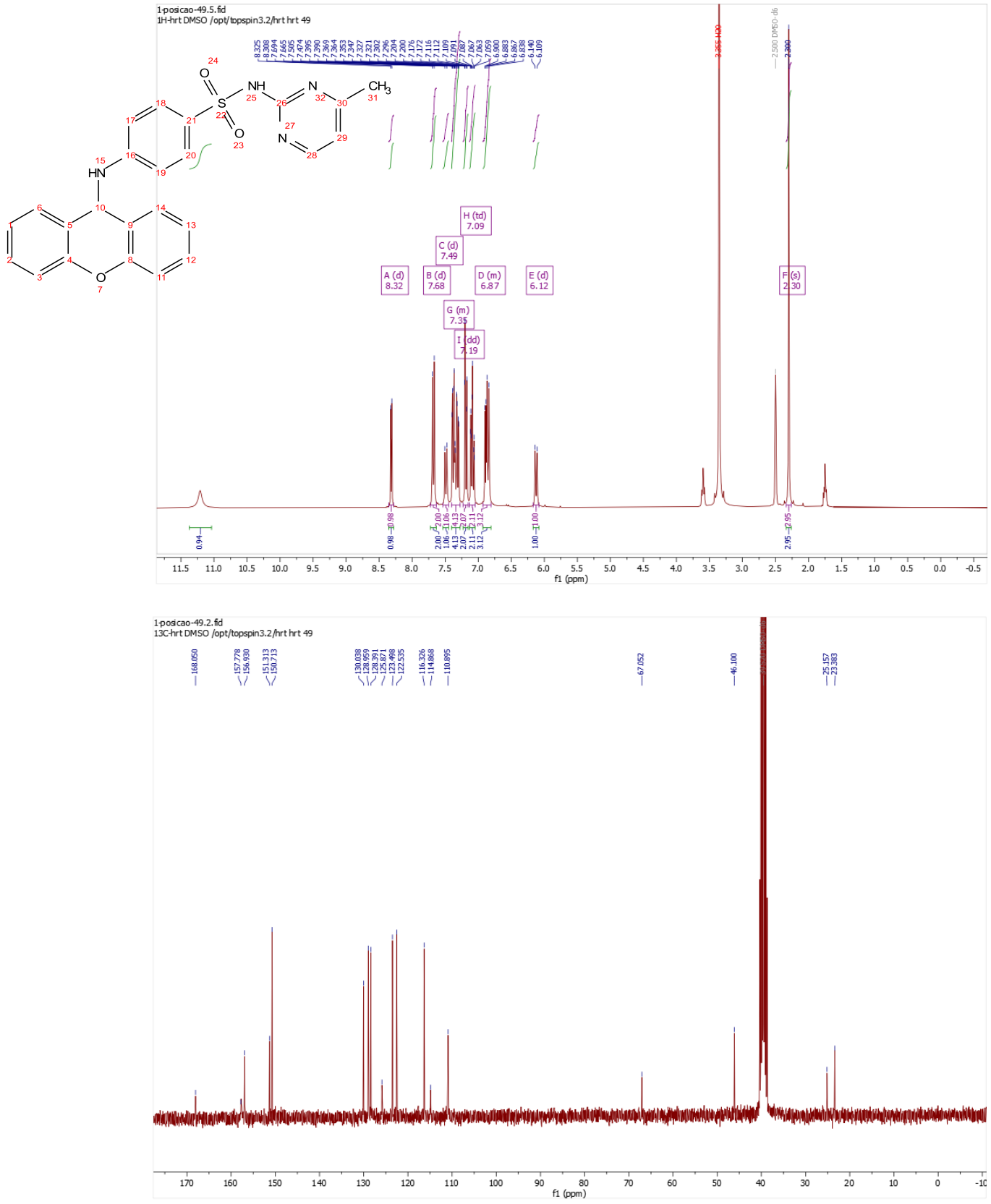

Figure 55. ^{1}H NMR (top, 300.13 MHz, DMSO-d_6) and ^{13}C NMR (bottom, 75.48 MHz, DMSO-d_6) for compound **MM16**.

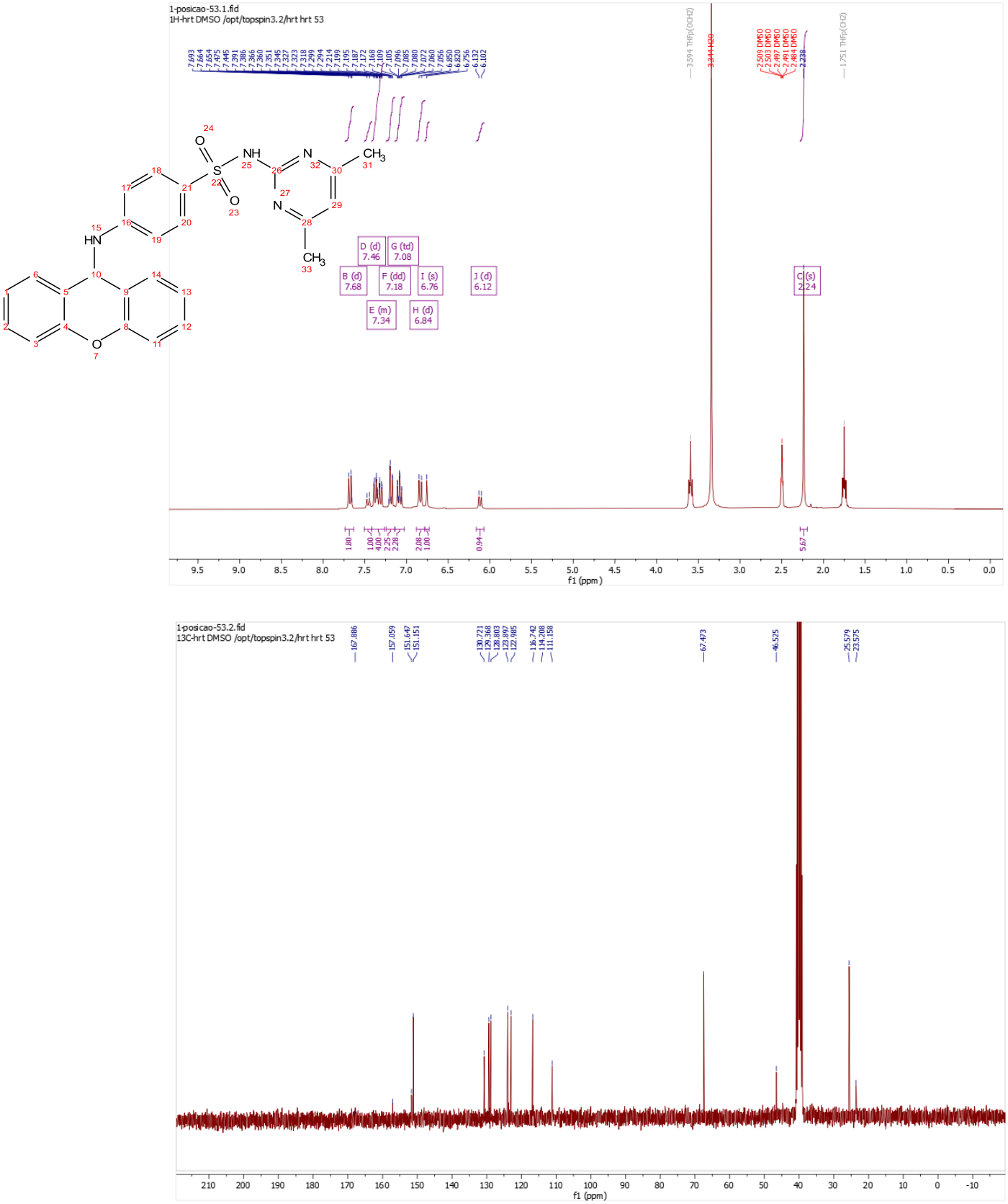

Figure 56. ^{1}H and ^{13}C NMR of compound **MM17**.

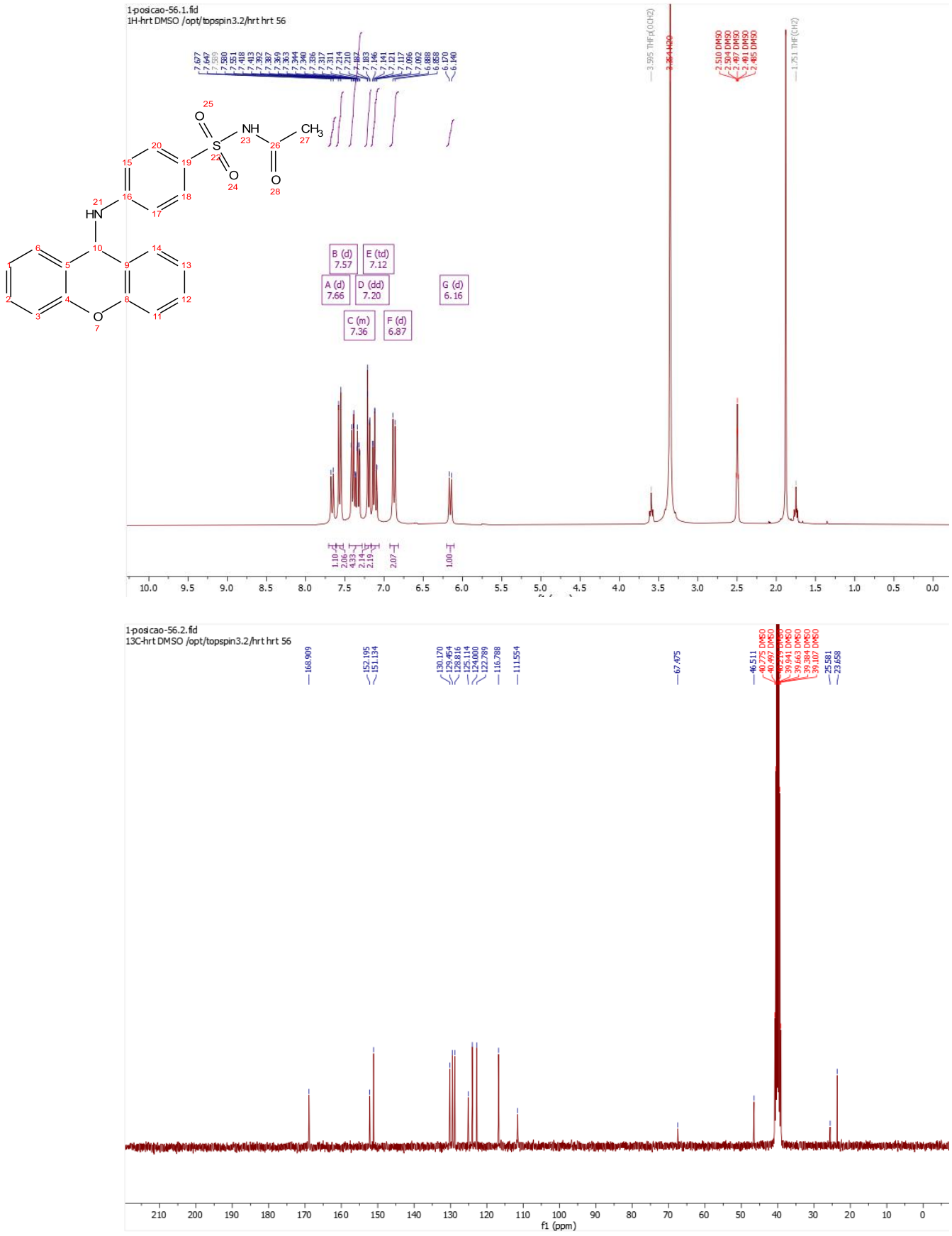

Figure 57. ^{1}H and ^{13}C NMR of compound **MM18**.

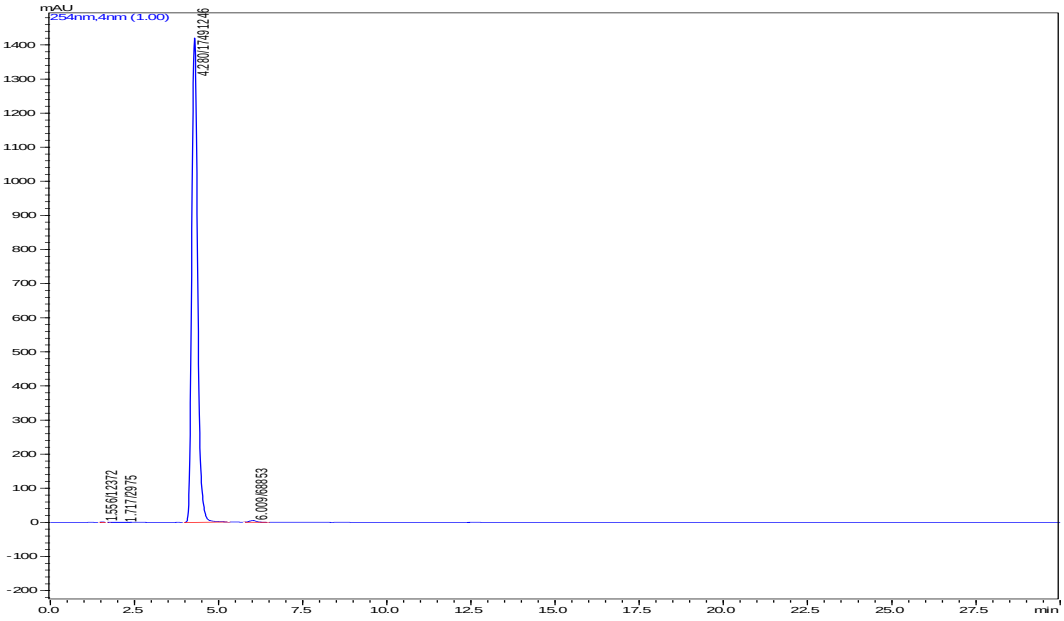

Figure 58. Chromatogram (HPLC) of compound **MM7**. Purity (% a/a): 99.5%.

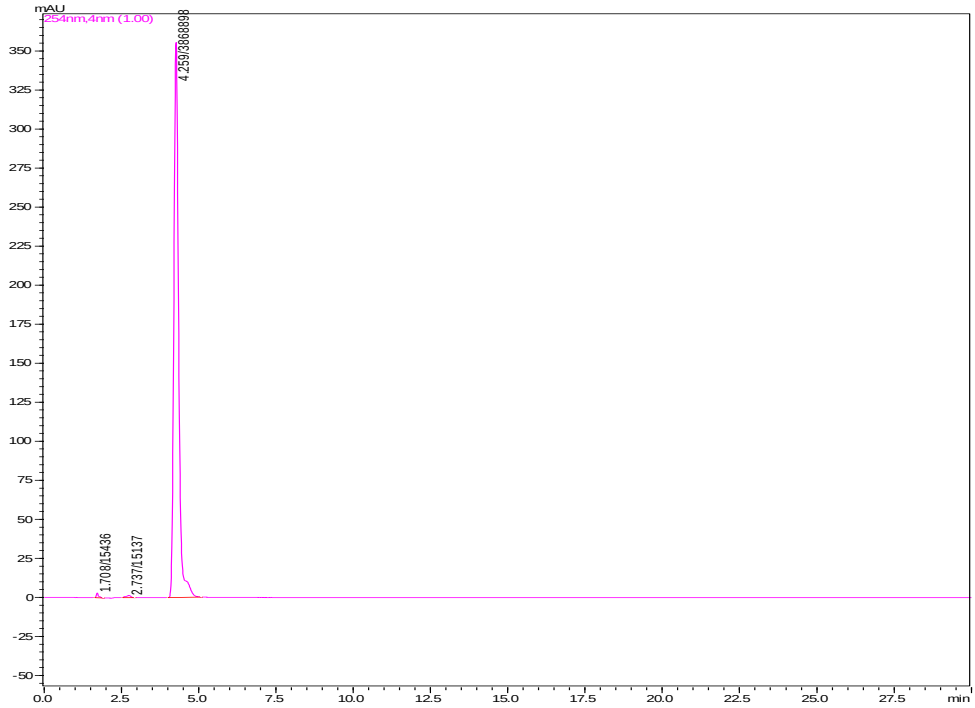

Figure 59. Chromatogram (HPLC) of compound **MM16**. Purity (% a/a): 99.2%.

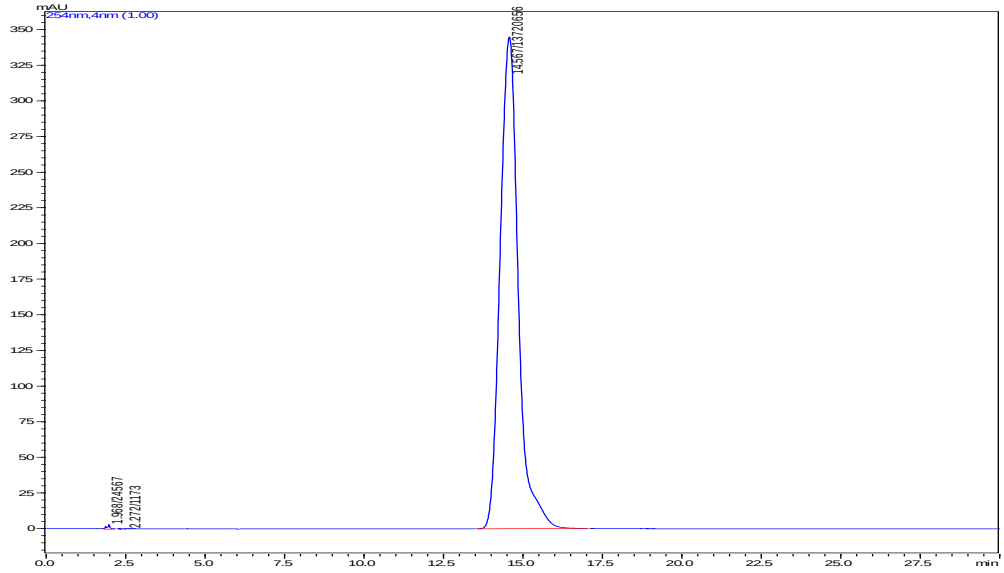

Figure 60. Chromatogram (HPLC) of compound **MM17**. Purity (% a/a): 99.9%.

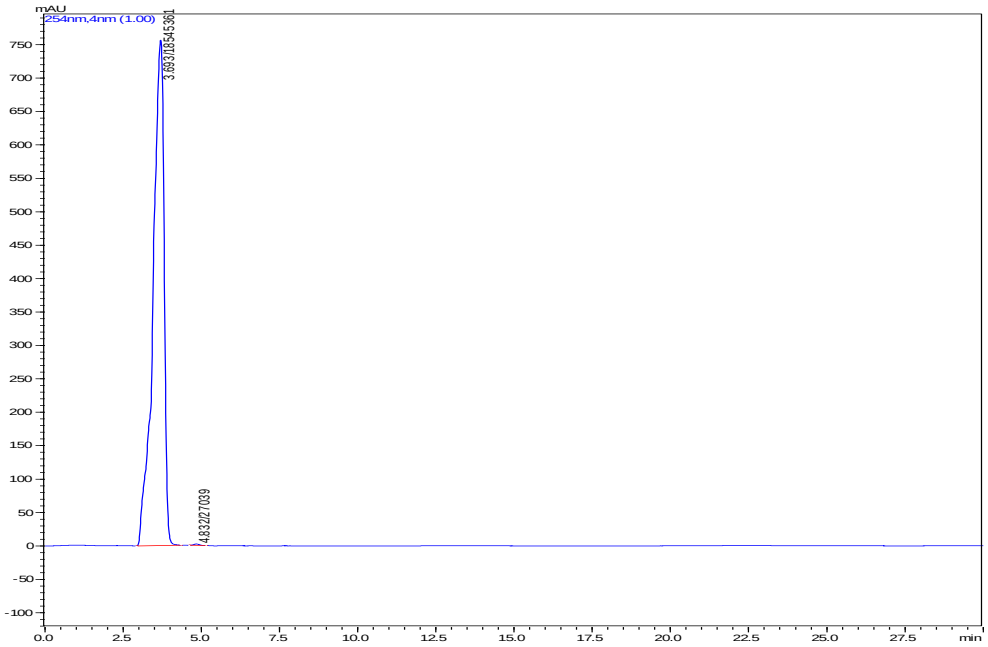

Figure 61. Chromatogram (HPLC) of compound **MM18**. Purity (% a/a): 99.9%.

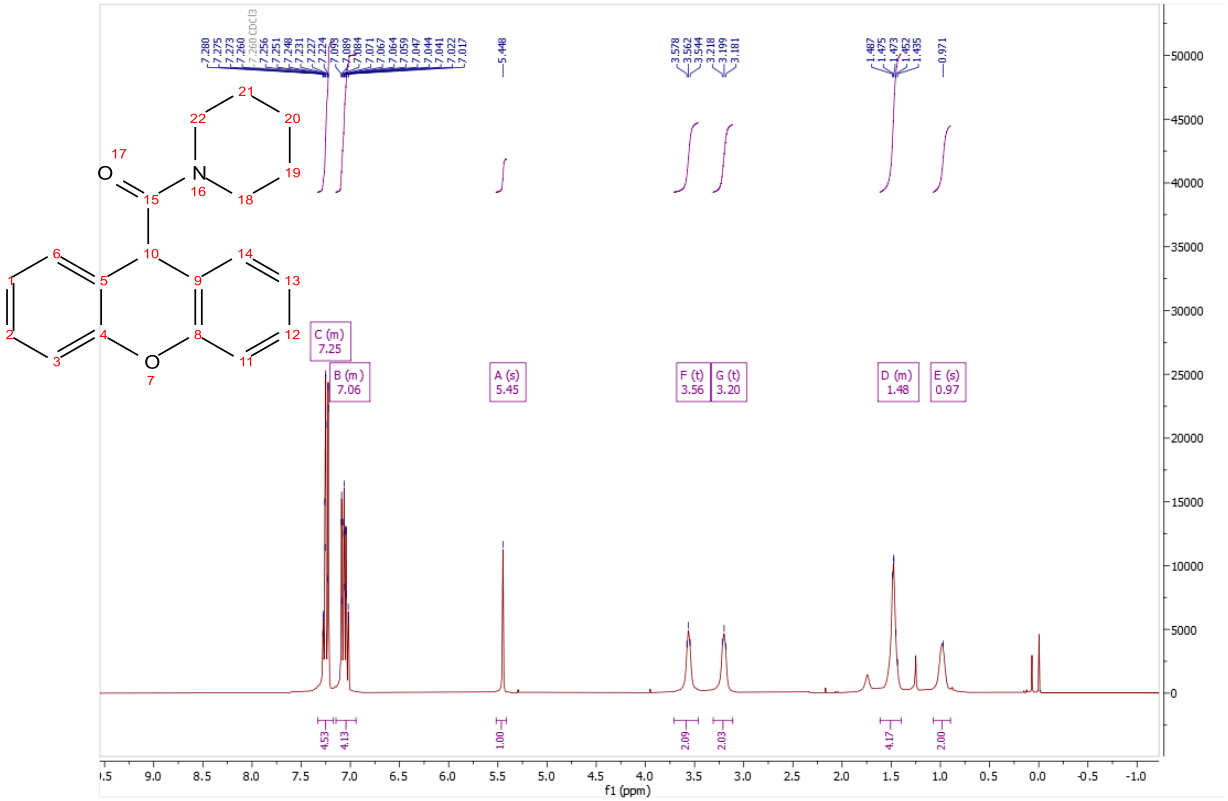

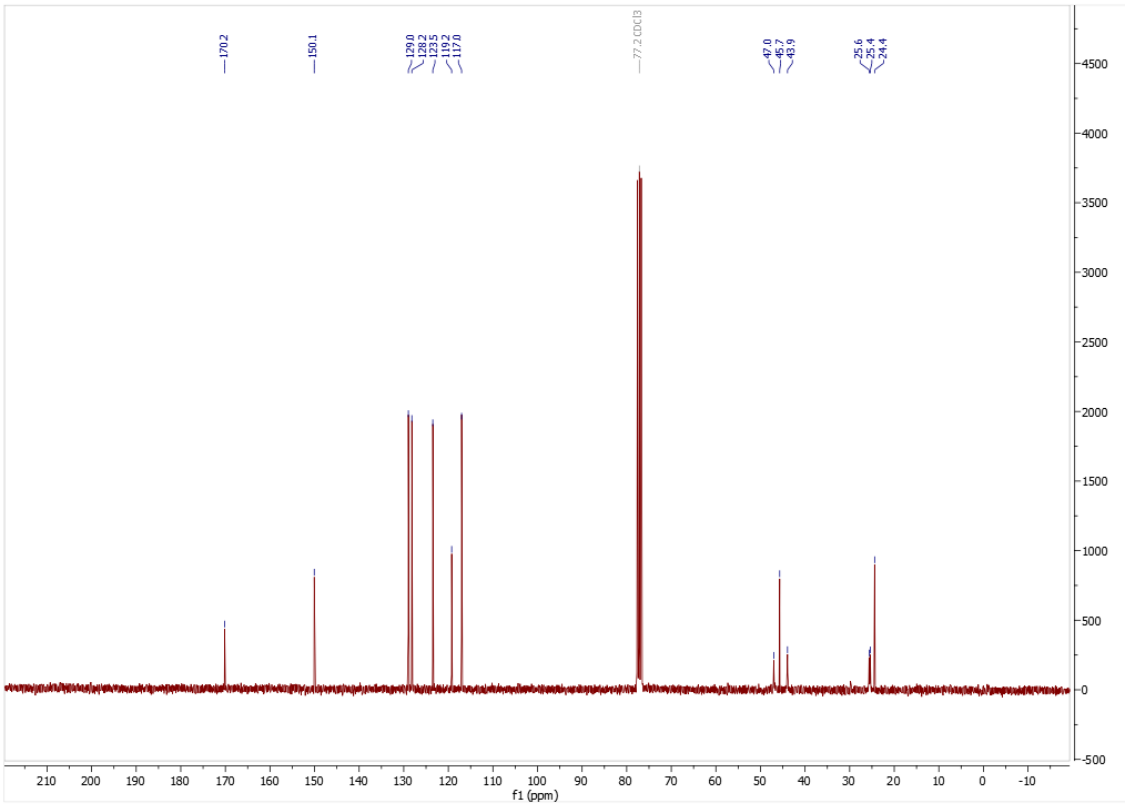

Figure 62. ^{1}H NMR (top, 300.13 MHz, $CDCl_3$) and ^{13}C NMR (bottom, 75.48 MHz, $CDCl_3$) for compound **MM30**.

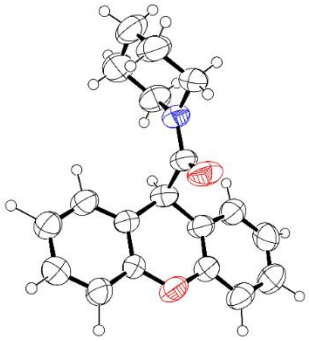

Figure 63. ORTEP view of the crystal structure of compound **MM30**.

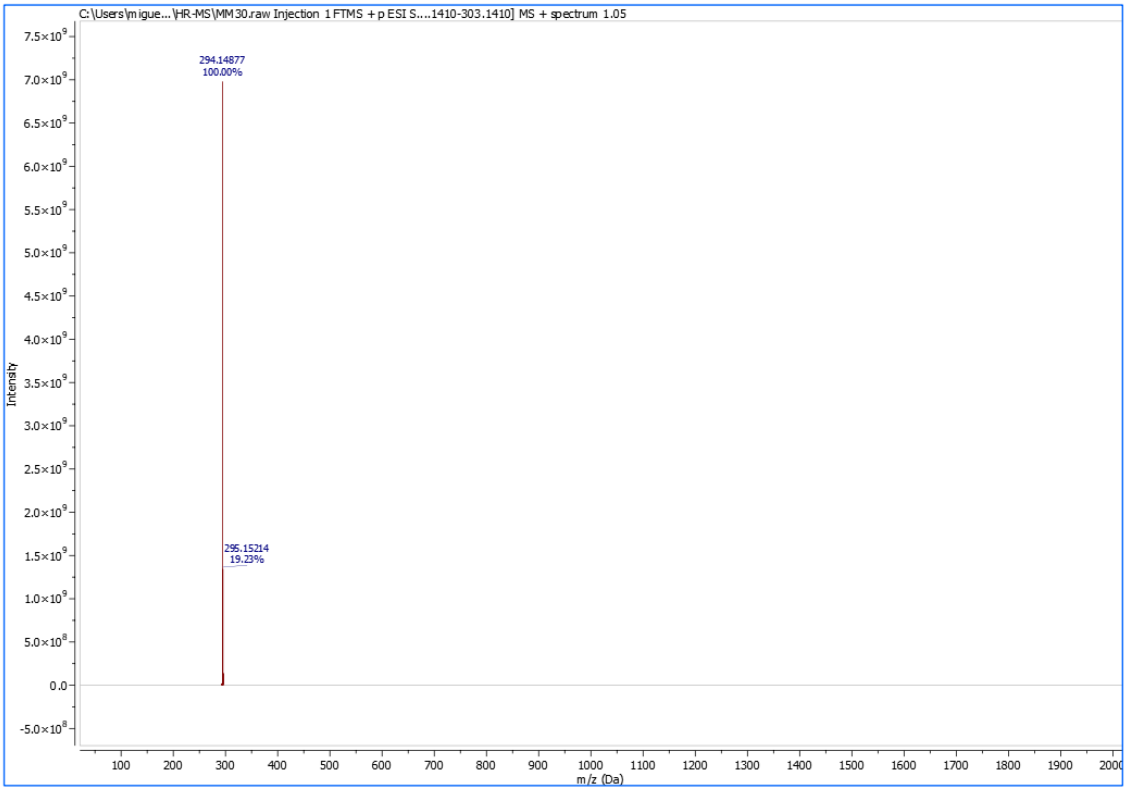

Meas. m/z	Formula	Adduct	Predicted m/z	Error [ppm]
294.1488	$C_{19}H_{19}NO_2$	H^+	294.1489	-0.300

Figure 64. Electrospray ESI data for compound **MM30**.

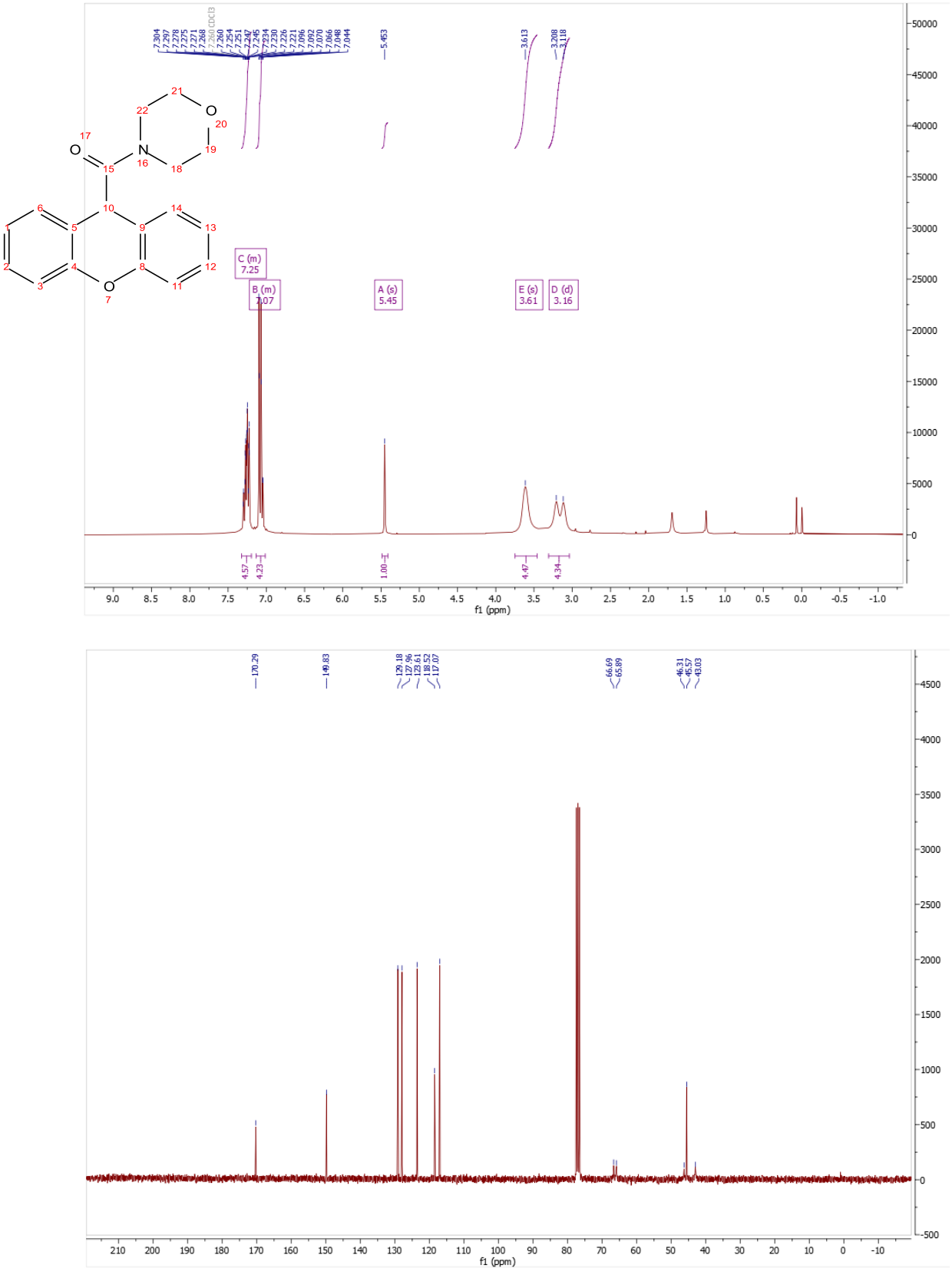

Figure 65. ^{1}H NMR (top, 300.13 MHz, $CDCl_3$) and ^{13}C NMR (bottom, 75.48 MHz, $CDCl_3$) for compound **MM32**.

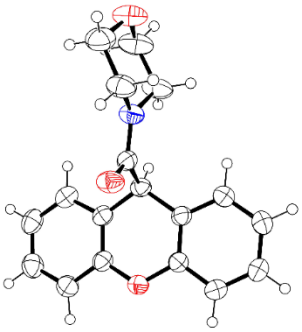

Figure 66. ORTEP view of the crystal structure of compound **MM32**.

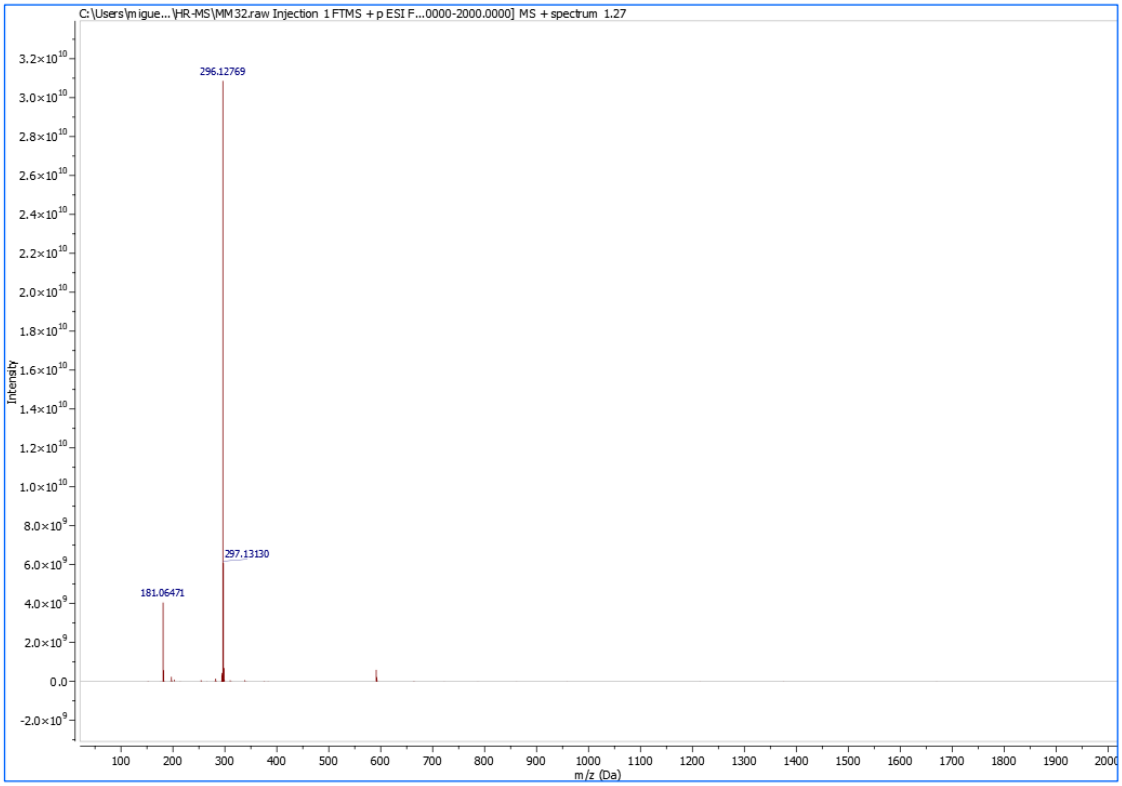

Meas. m/z	Formula	Adduct	Predicted m/z	Error [ppm]
296.1281	$C_{18}H_{17}N0_3$	H^+	296.1277	-1.452

Figure 67. Electrospray ESI data for compound **MM32**.

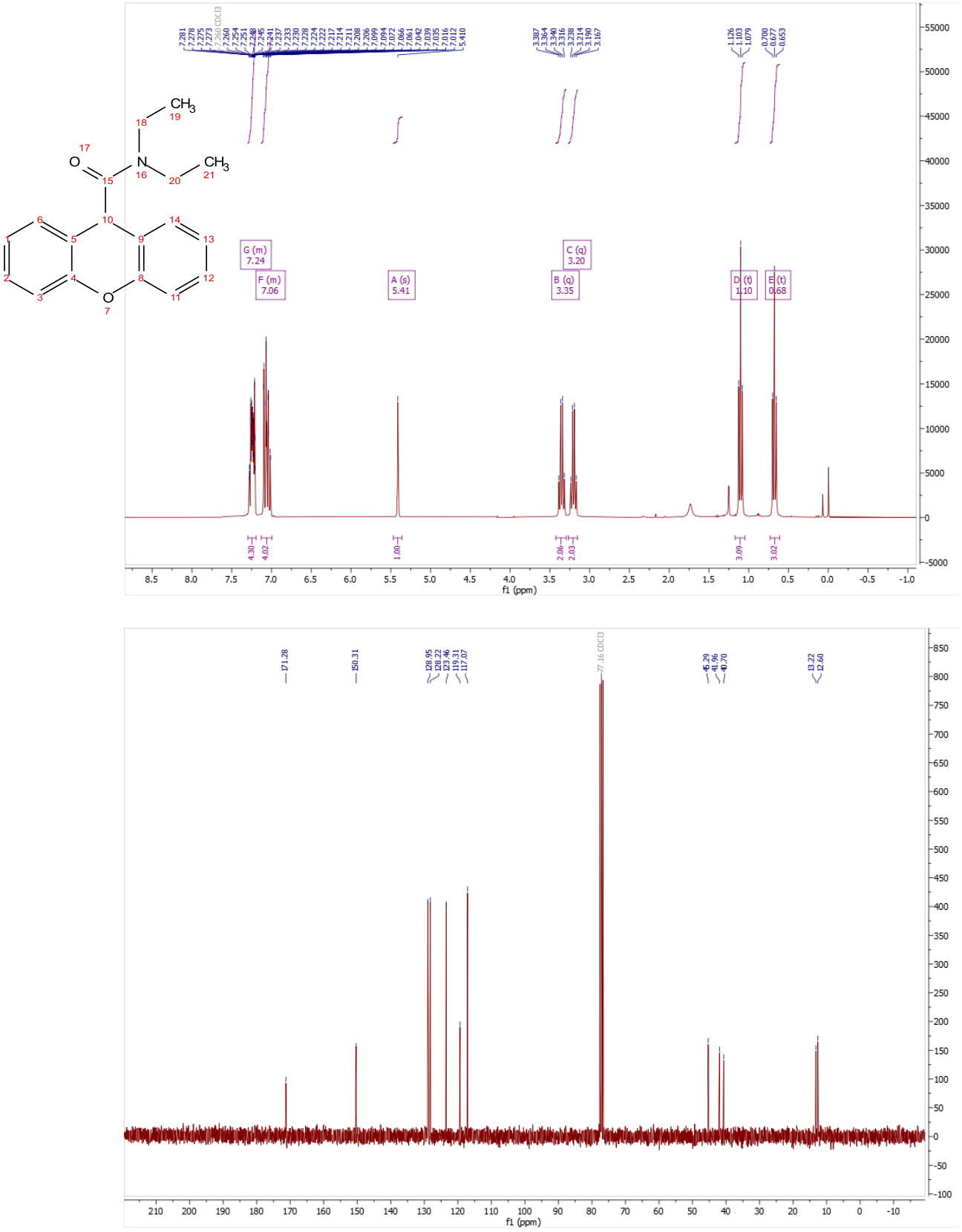

Figure 68. ^{1}H NMR (top, 300.13 MHz, $CDCl_3$) and ^{13}C NMR (bottom, 75.48 MHz, $CDCl_3$) for compound **MM36**.

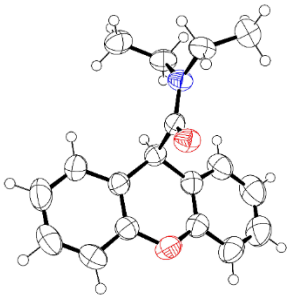

Figure 69. ORTEP view of the crystal structure of compound **MM36**.

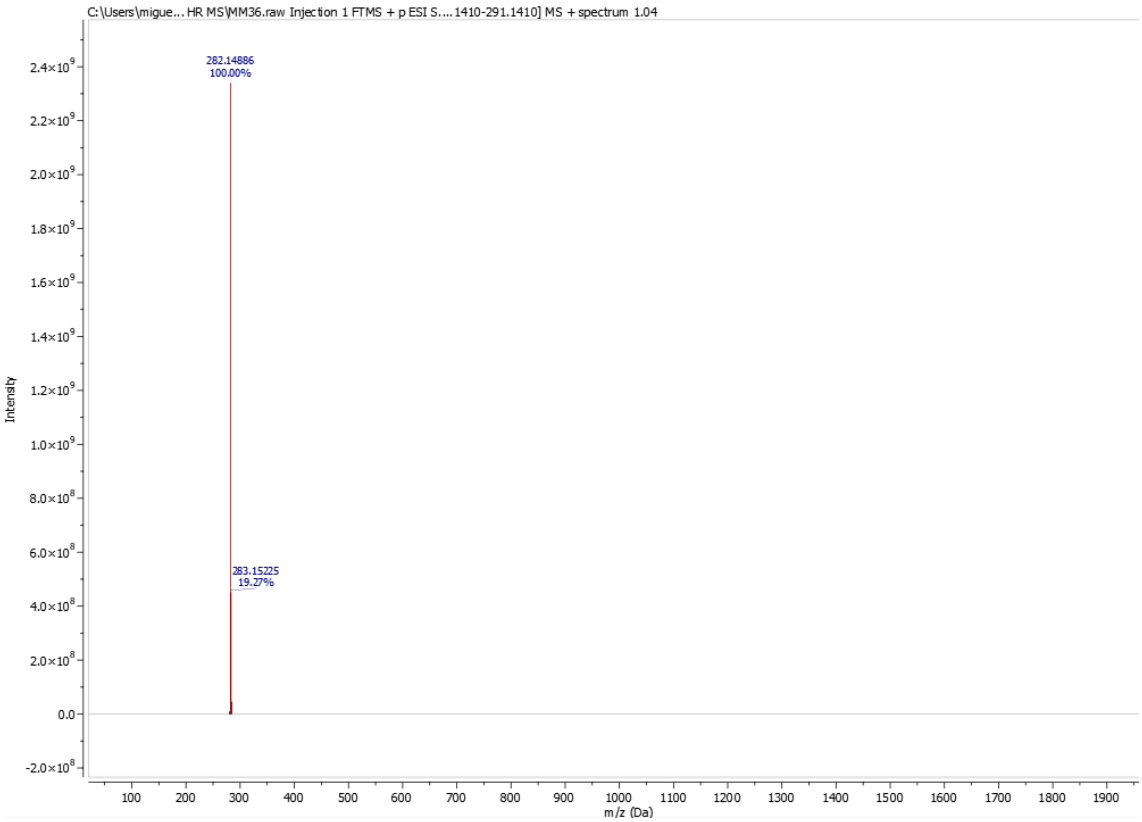

Meas. m/z	Formula	Adduct	Predicted m/z	Error [ppm]
282.1489	$C_{18}H_{19}N0_2$	H^+	282.1489	0.024

Figure 70. Electrospray ESI data for compound **MM36**.

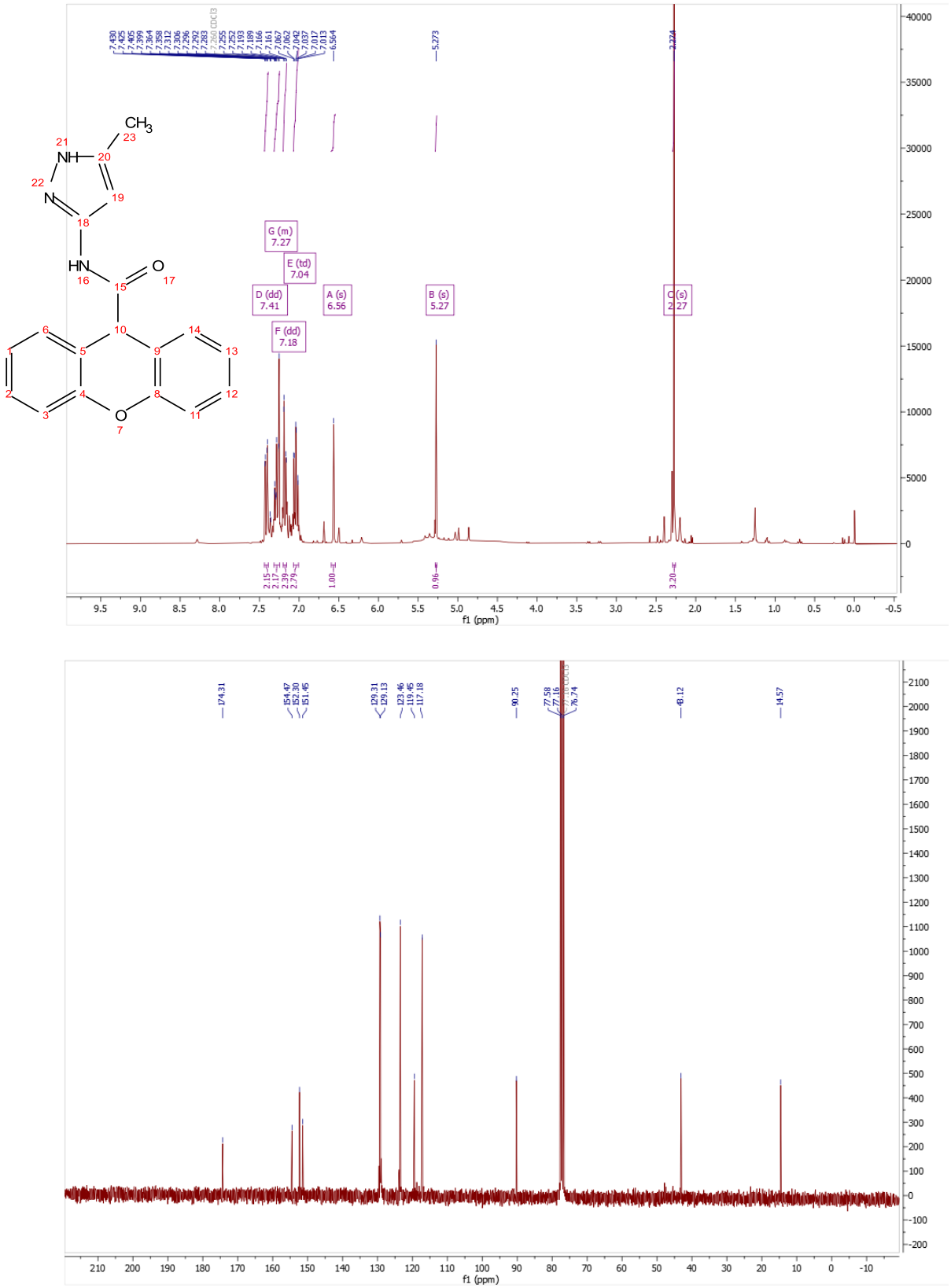

Figure 71. ^{1}H NMR (top, 300.13 MHz, $CDCl_3$) and ^{13}C NMR (bottom, 75.48 MHz, $CDCl_3$) for compound **MM42B**.

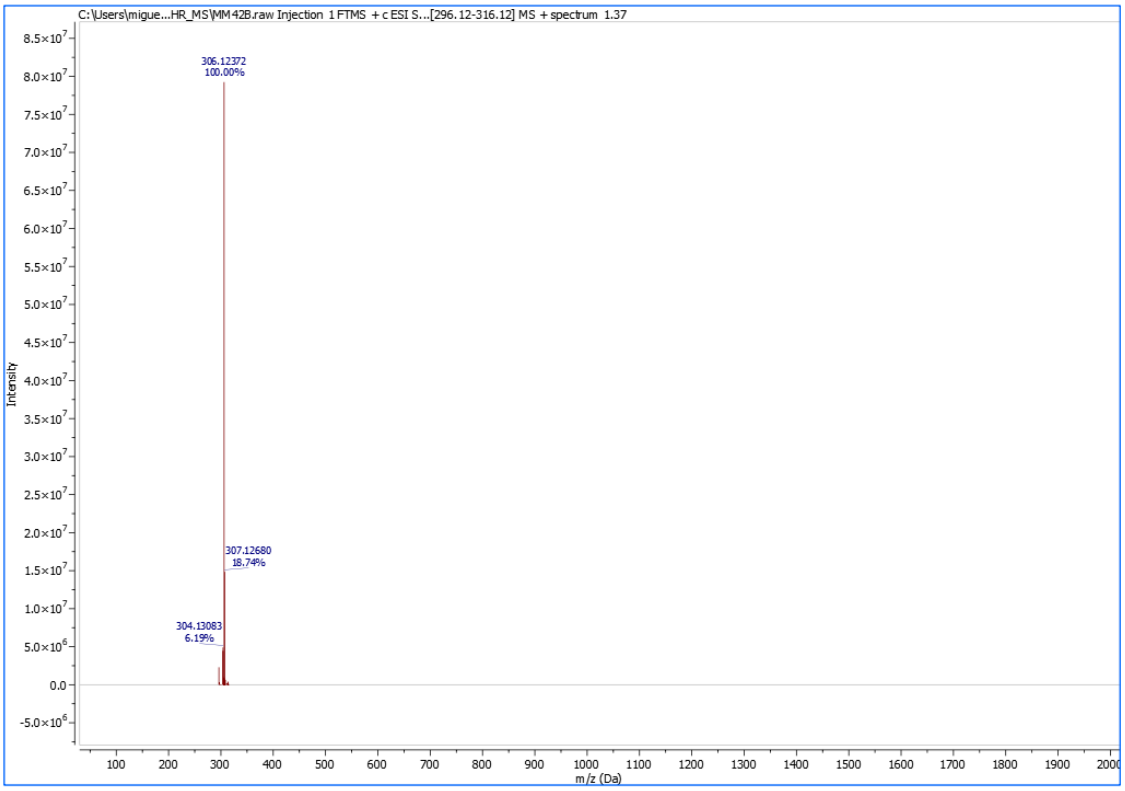

Meas. m/z	Formula	Adduct	Predicted m/z	Error [ppm]
306.1237	$C_{18}H_{15}N_3O_2$	H^+	306.1237	0.049

Figure 72. Electrospray ESI data for compound **MM42B**.

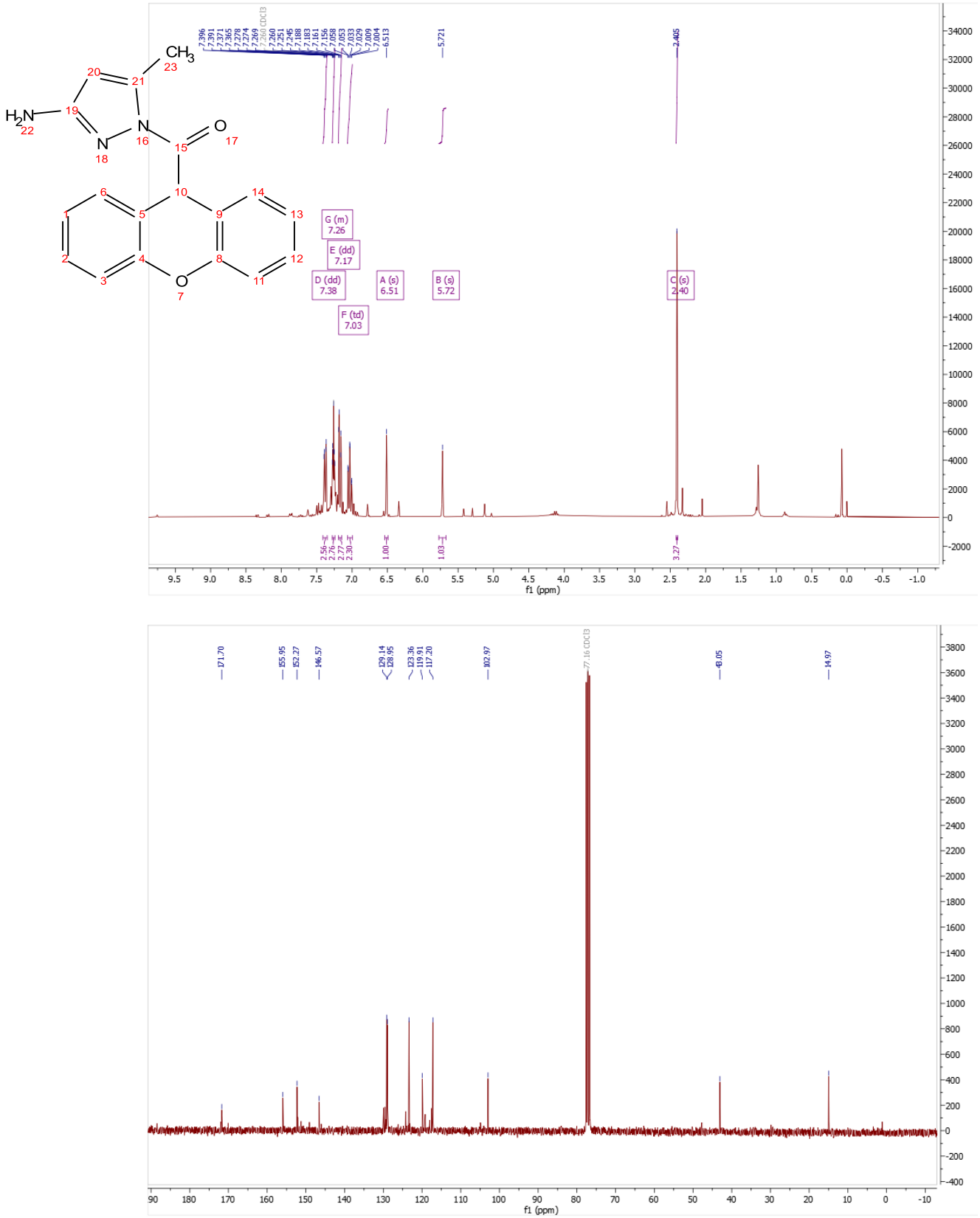

Figure 73. ^{1}H NMR (top, 300.13 MHz, $CDCl_3$) and ^{13}C NMR (bottom, 75.48 MHz, $CDCl_3$) for compound **MM42C**.

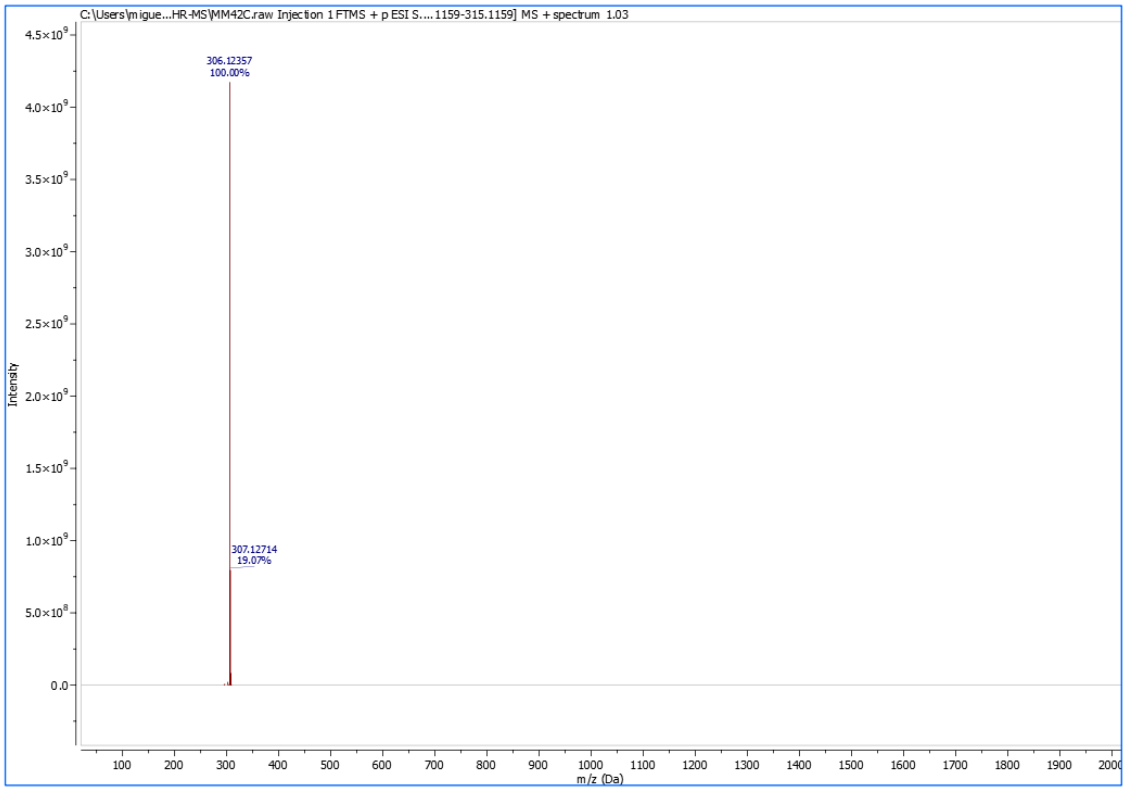

Meas. m/z	Formula	Adduct	Predicted m/z	Error [ppm]
306.1236	$C_{18}H_{15}N_3O_2$	H^+	306.1237	-0.136

Figure 74. Electrospray ESI data for compound **MM42C**.

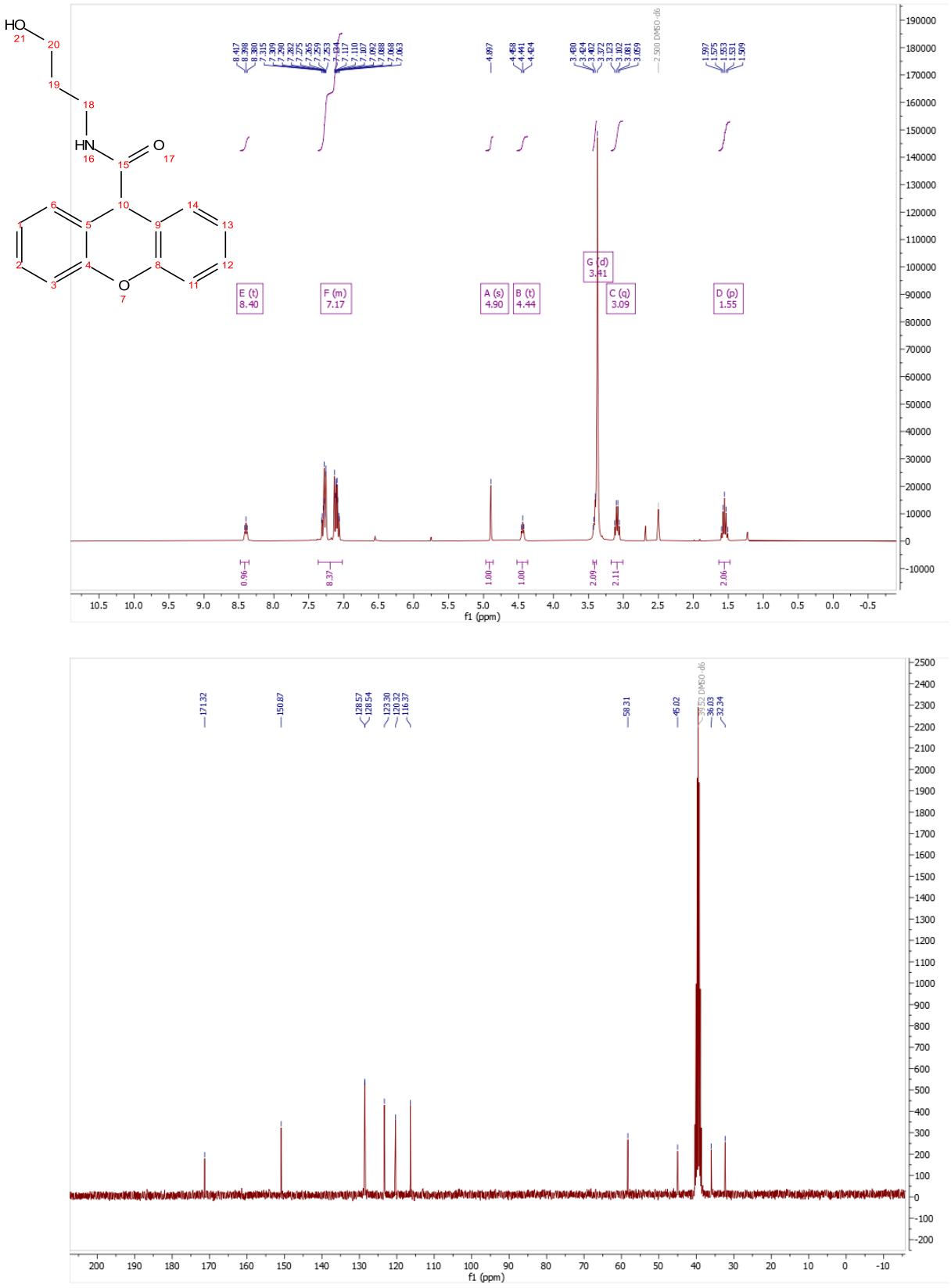

Figure 75. ^{1}H NMR (top, 300.13 MHz, DMSO-d_6) and ^{13}C NMR (bottom, 75.48 MHz, DMSO-d_6) for compound **MM43**.

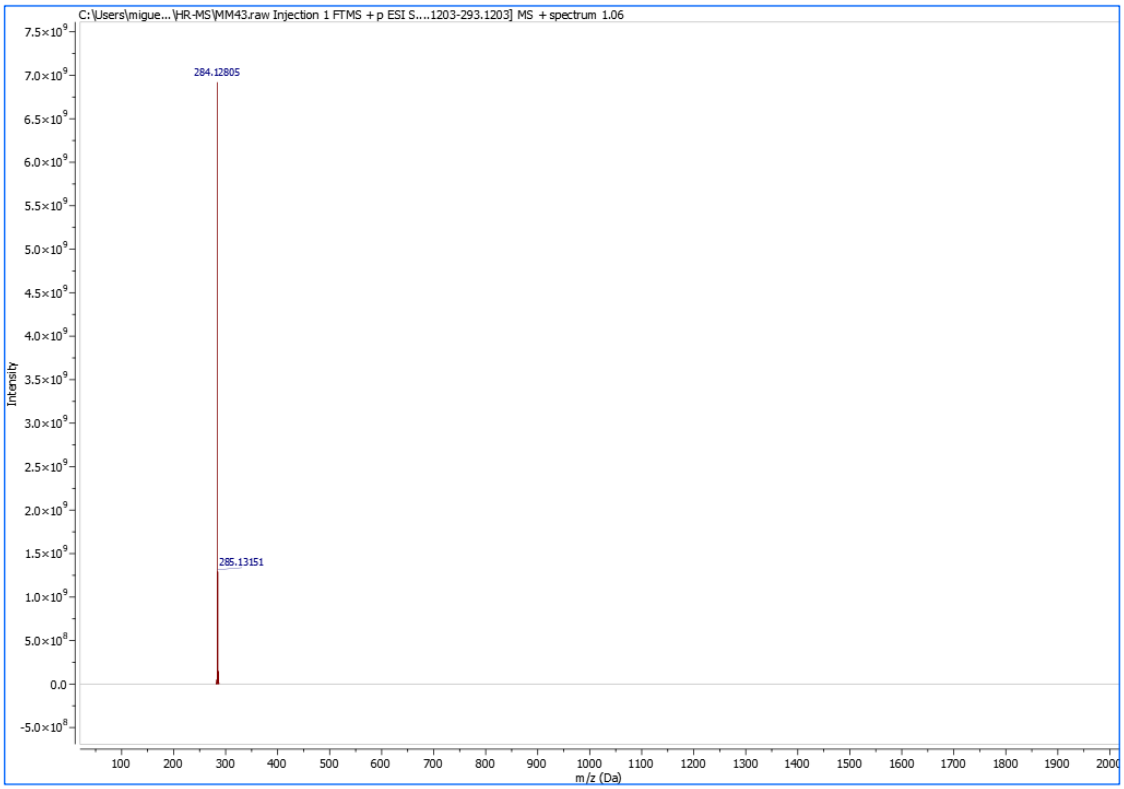

Meas. m/z	Formula	Adduct	Predicted m/z	Error [ppm]
284.1281	$C_{17}H_{17}NO_3$	H^+	284.1281	-0.071

Figure 76. Electrospray ESI data for compound **MM43**.

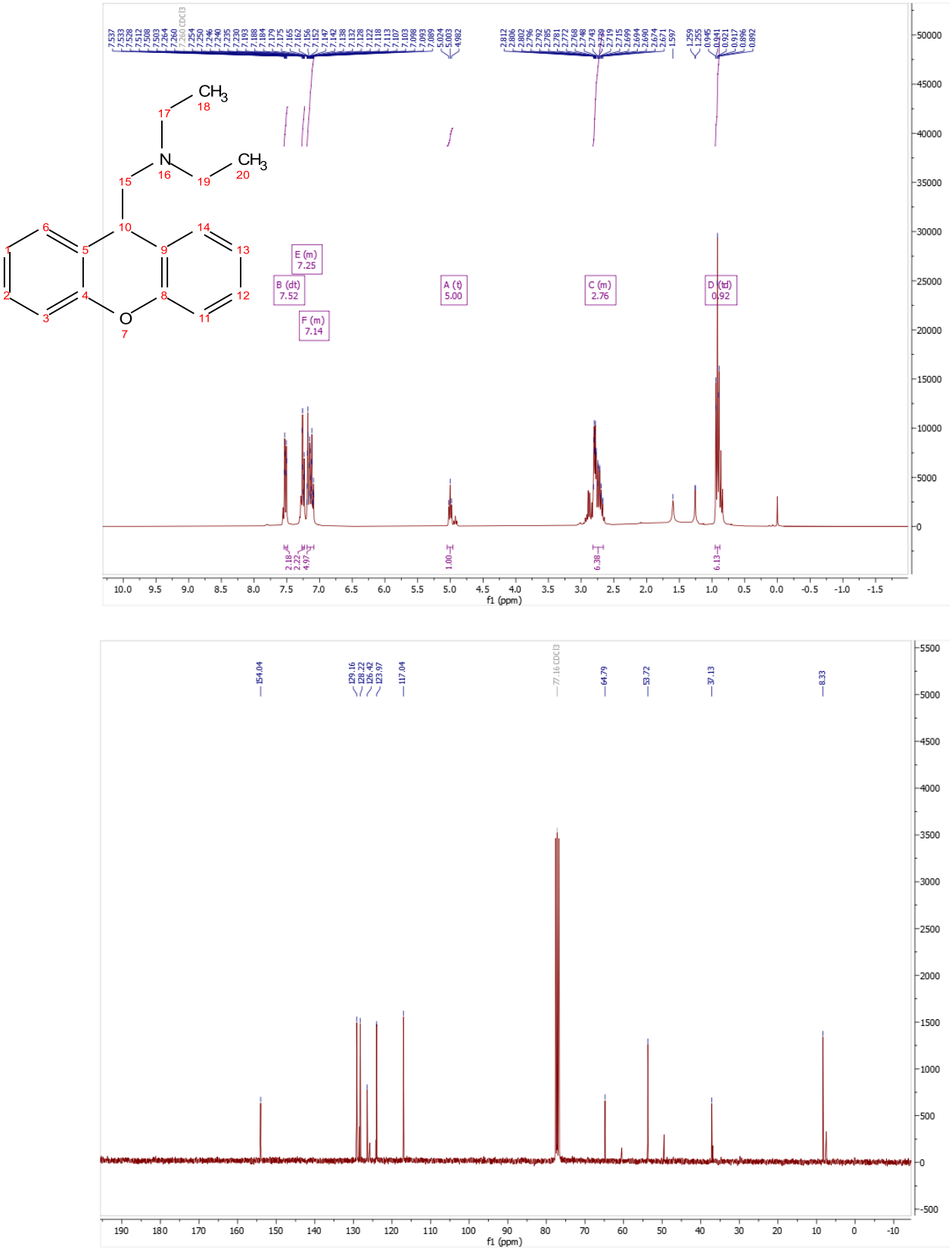

Figure 77. ^{1}H NMR (top, 300.13 MHz, $CDCl_3$) and ^{13}C NMR (bottom, 75.48 MHz, $CDCl_3$) for compound **MM46**.

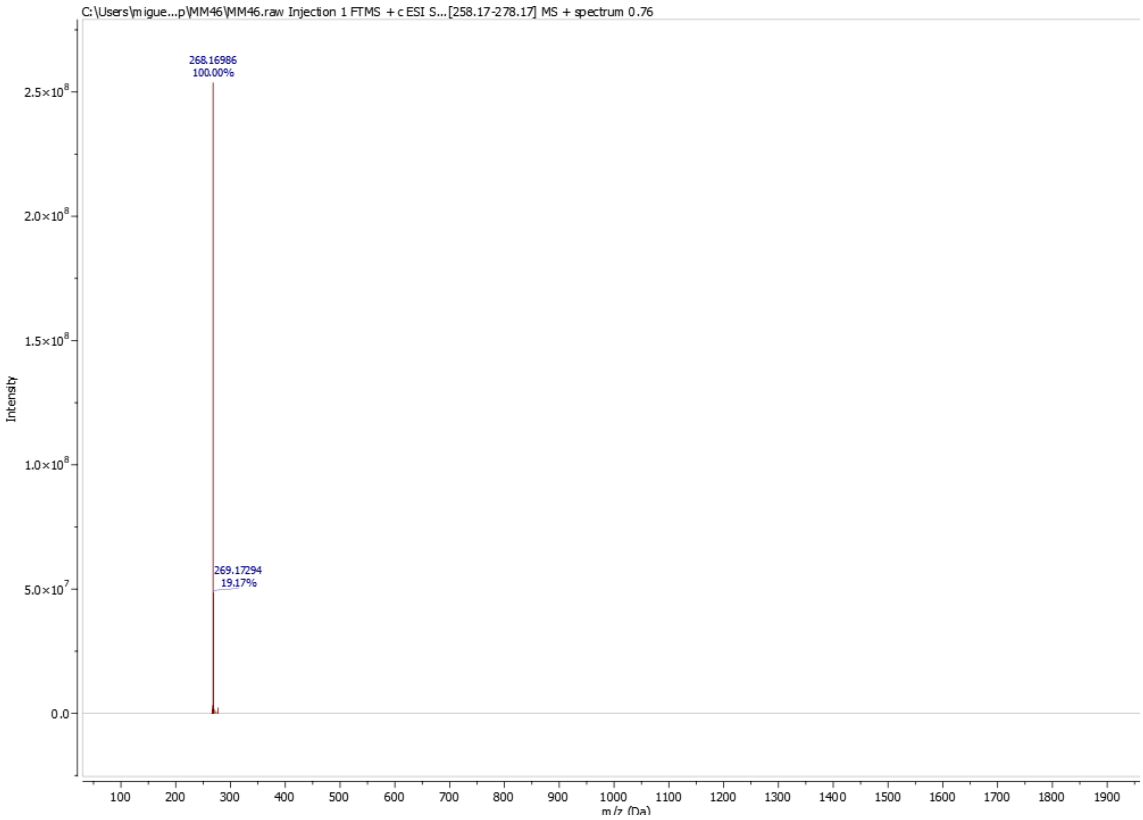

Meas. m/z	Formula	Adduct	Predicted m/z	Error [ppm]
268.1699	$C_{18}H_{21}NO$	H^+	268.1696	1.007

Figure 78. Electrospray ESI data for compound **MM46**.

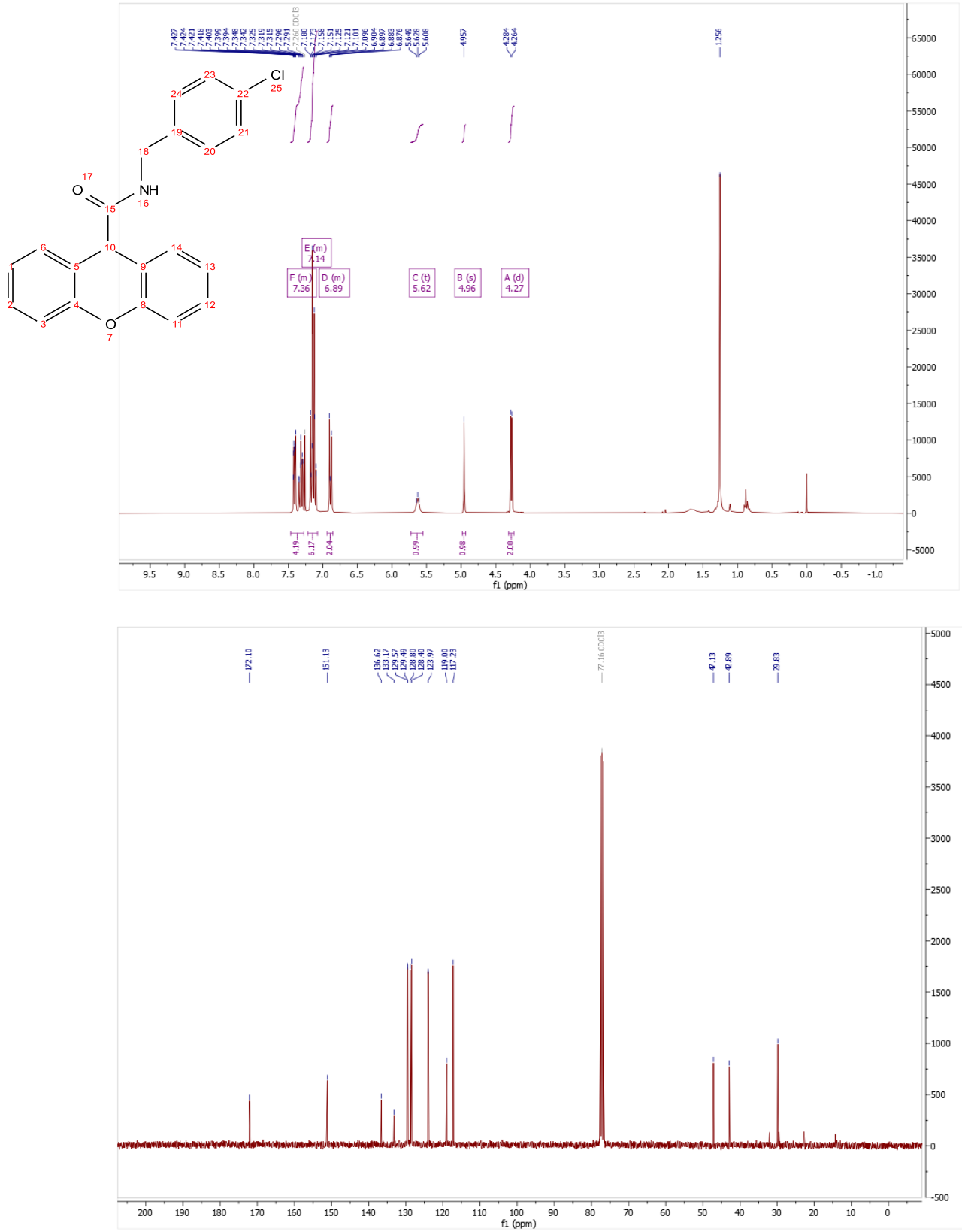

Figure 79. ^{1}H NMR (top, 300.13 MHz, $CDCl_3$) and ^{13}C NMR (bottom, 75.48 MHz, $CDCl_3$) for compound **MM48A**.

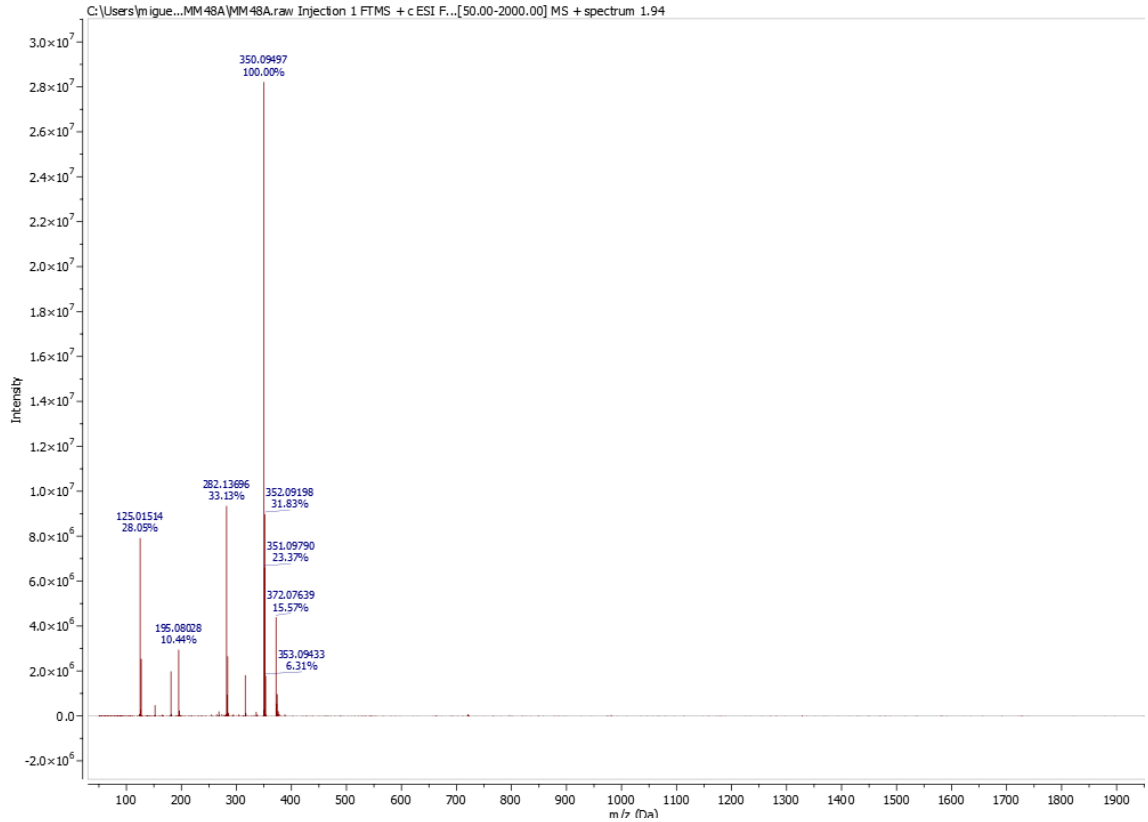

Meas. m/z	Formula	Adduct	Predicted m/z	Error [ppm]
350.0950	$C_{21}H_{16}ClNO_2$	H^+	350.0942	-2.10

Figure 80. Electrospray ESI data for compound **MM48A**.

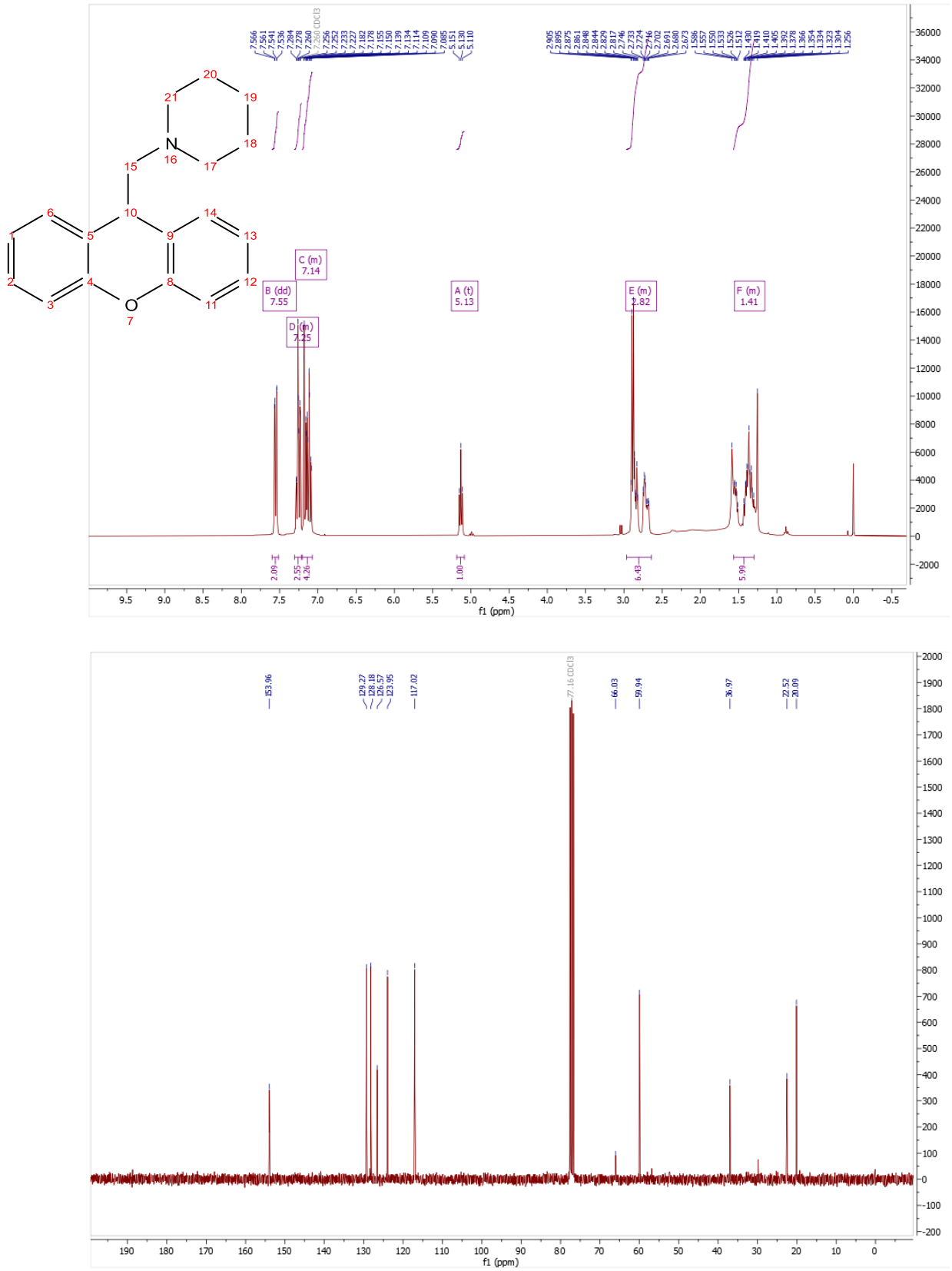

Figure 81. ^{1}H NMR (top, 300.13 MHz, $CDCl_3$) and ^{13}C NMR (bottom, 75.48 MHz, $CDCl_3$) for compound **MM50**.

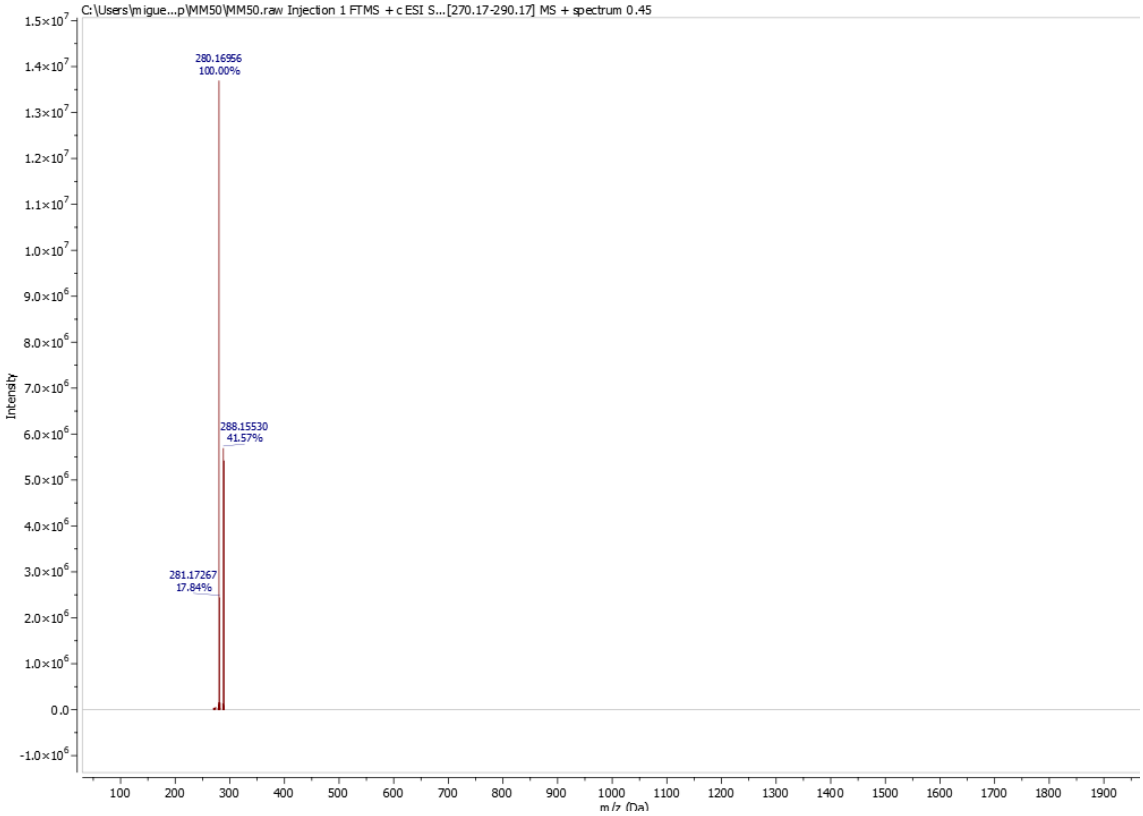

Meas. m/z	Formula	Adduct	Predicted m/z	Error [ppm]
280.1696	$C_{19}H_{21}NO$	H^+	280.1696	0.11

Figure 82. Electrospray ESI data for compound **MM50**.

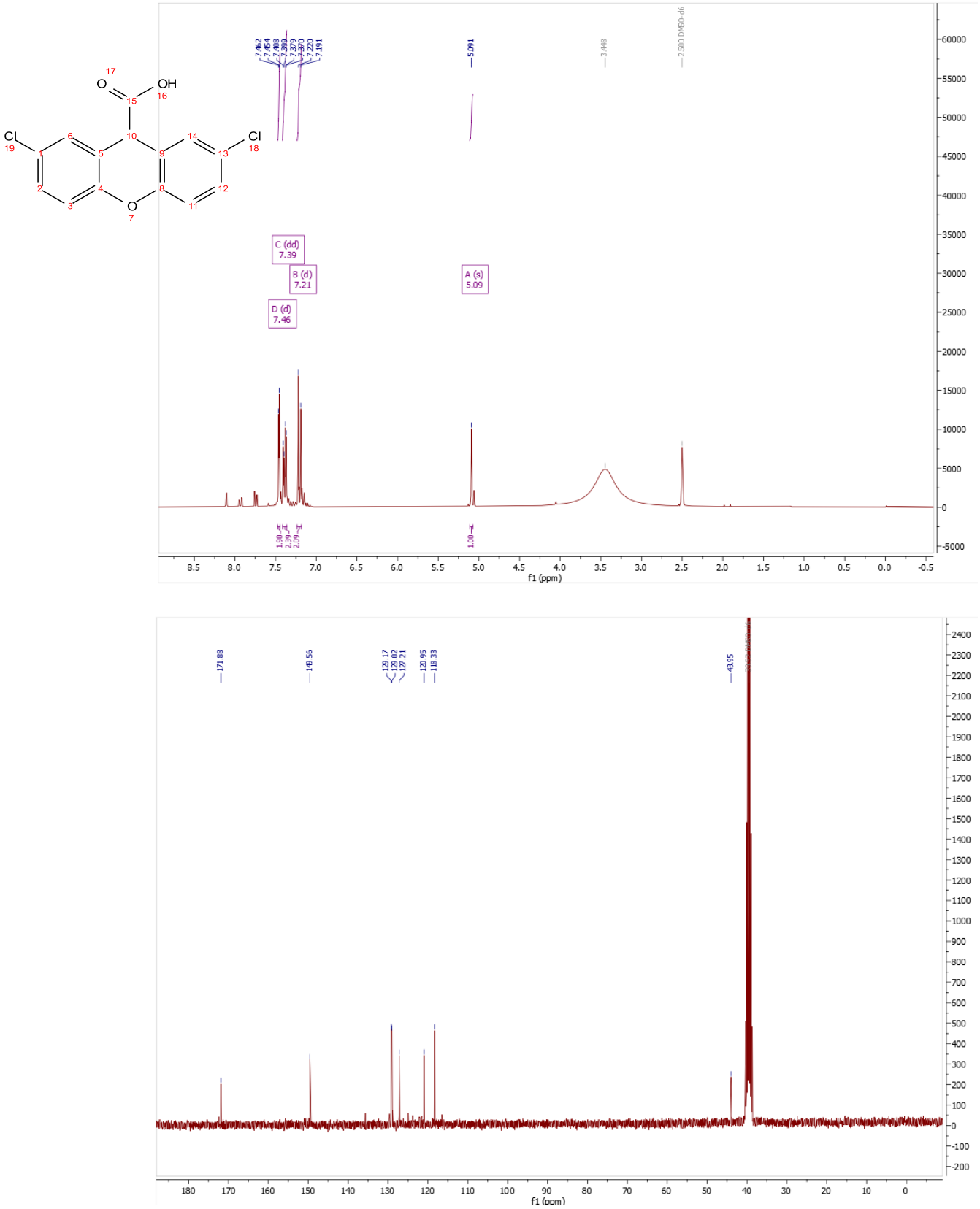

Figure 83. ^{1}H NMR (top, 300.13 MHz, DMSO-d_6) and ^{13}C NMR (bottom, 75.48 MHz, DMSO-d_6) for compound **MM52**.

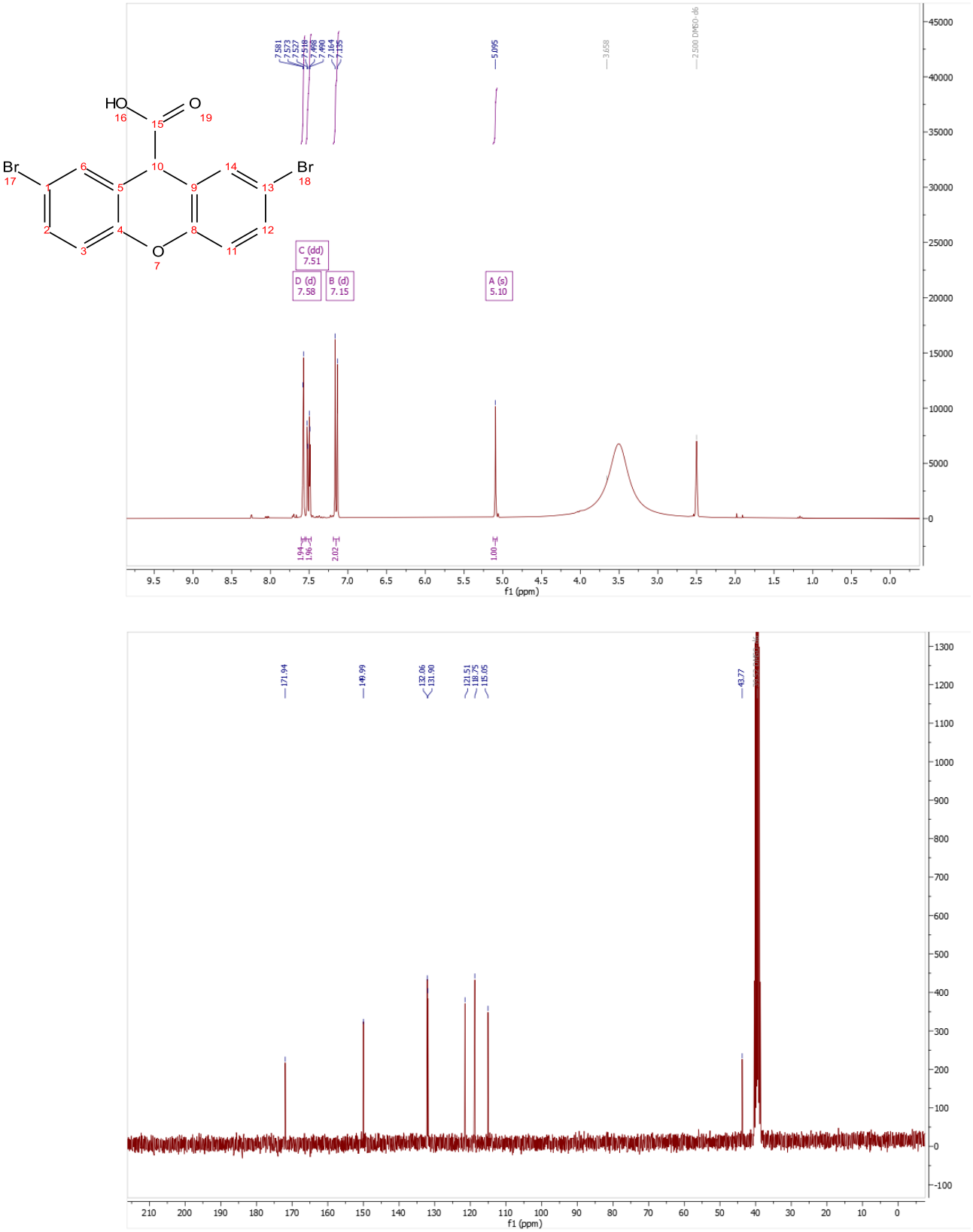

Figure 84. ^{1}H NMR (top, 300.13 MHz, DMSO-d_6) and ^{13}C NMR (bottom, 75.48 MHz, DMSO-d_6) for compound **MM54**.

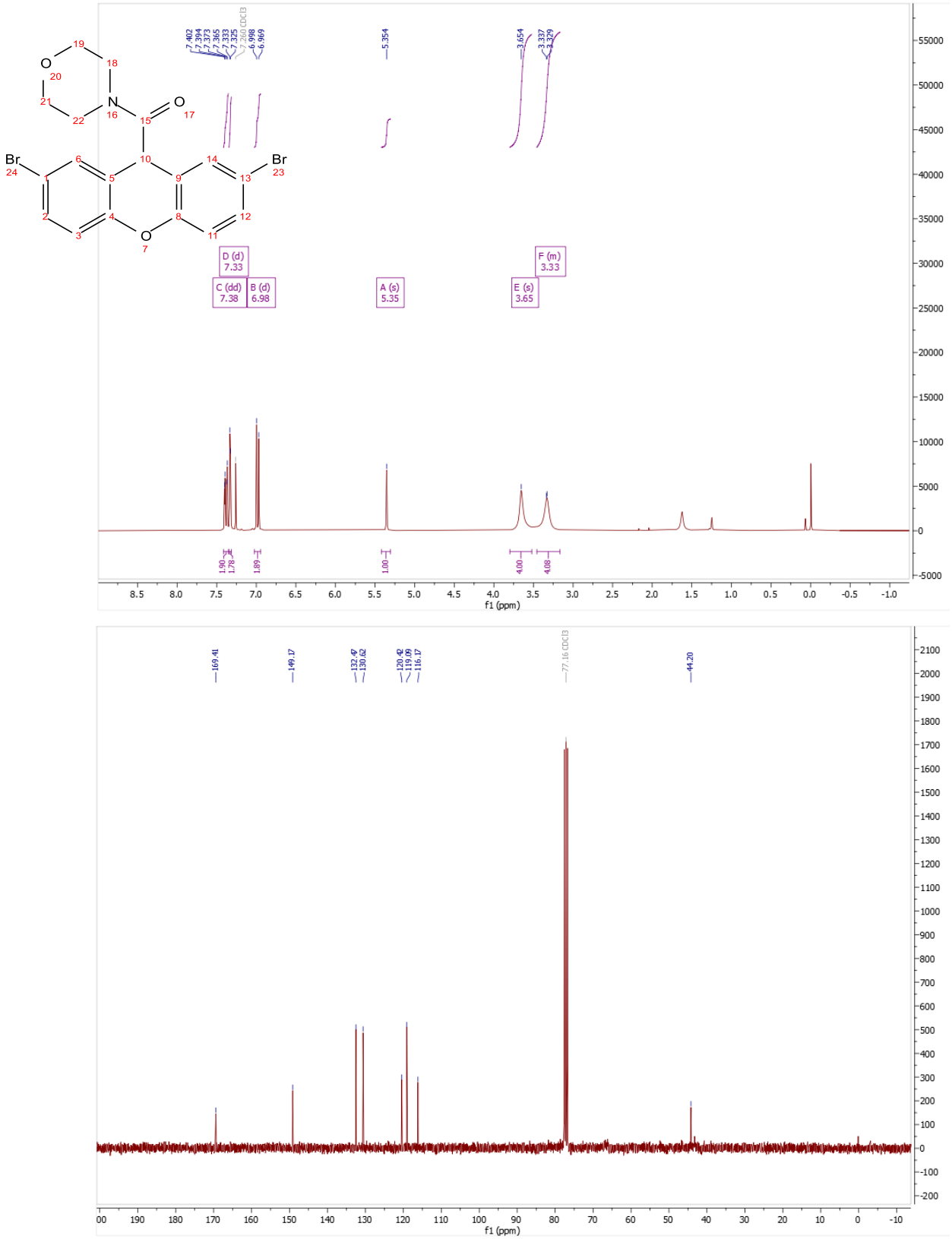

Figure 85. ^{1}H NMR (top, 300.13 MHz, $CDCl_3$) and ^{13}C NMR (bottom, 75.48 MHz, $CDCl_3$) for compound **MM56**.

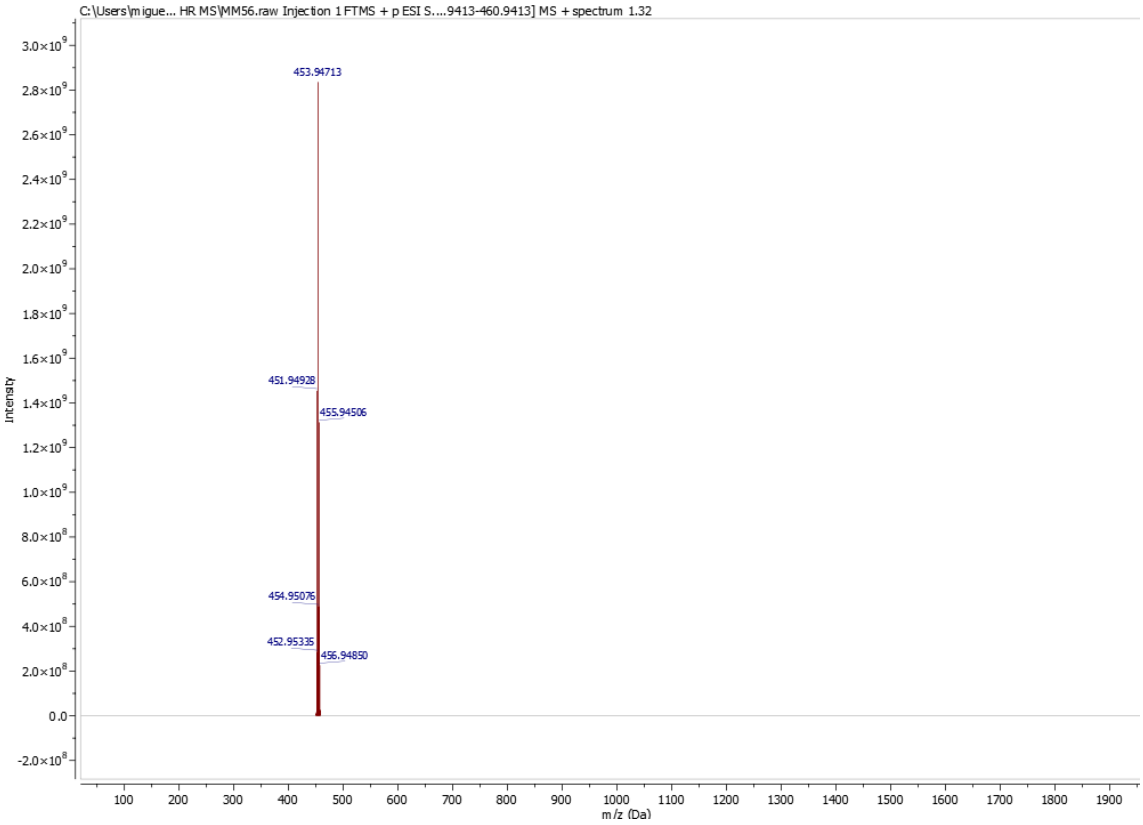

Meas. m/z	Formula	Adduct	Predicted m/z	Error [ppm]
451.94928	$C_{18}H_{15}Br_2NO_3$	H^+	451.94915	0.132

Figure 86. Electrospray ESI data for compound **MM56**.

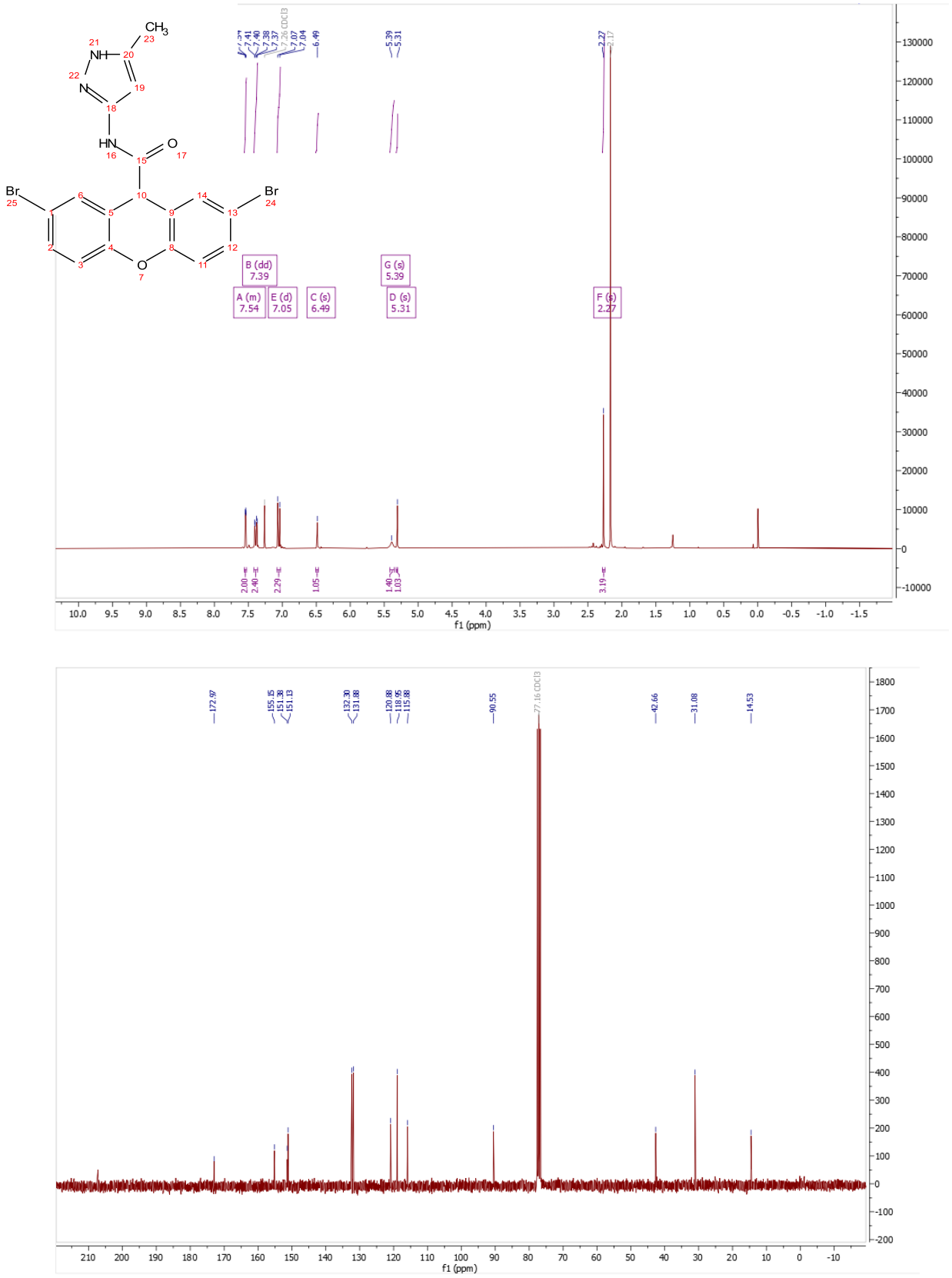

Figure 87. ^{1}H NMR (top, 300.13 MHz, $CDCl_3$) and ^{13}C NMR (bottom, 75.48 MHz, $CDCl_3$) for compound **MM57A**.

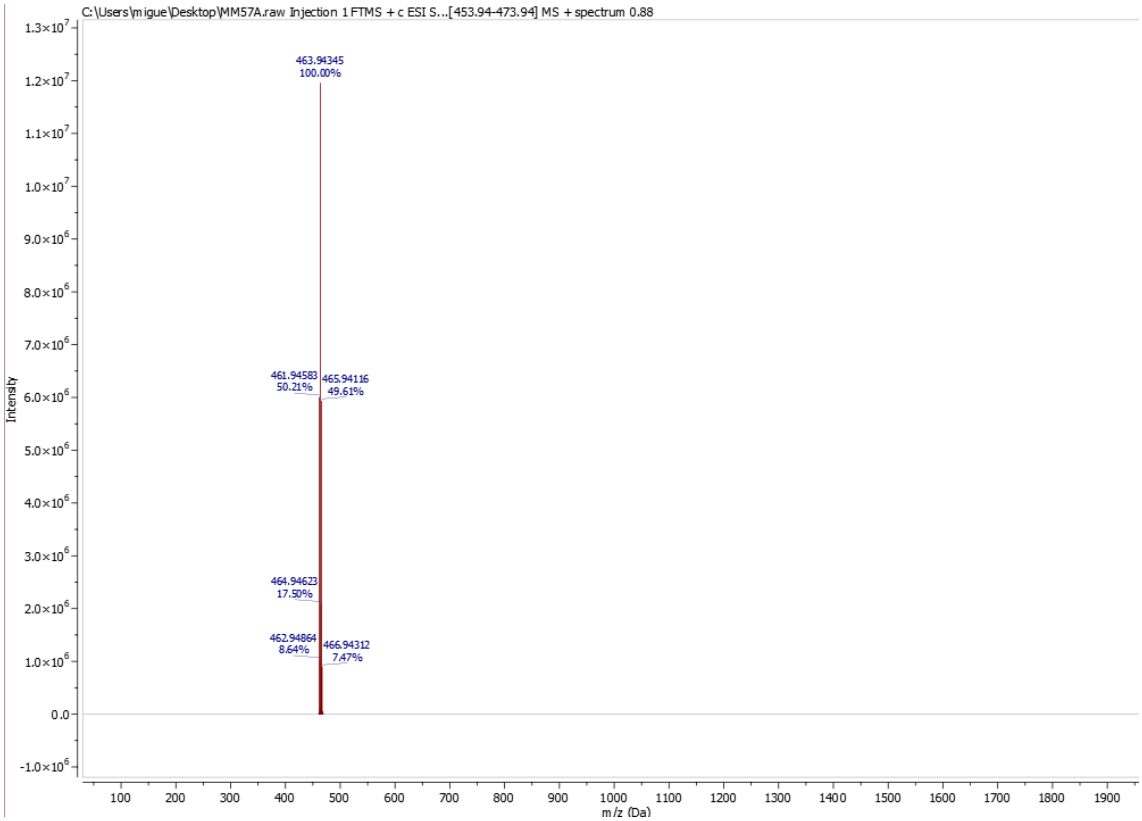

Meas. m/z	Formula	Adduct	Predicted m/z	Error [ppm]
461.9458	$C_{18}H_{13}Br_2N_3O_2$	H^+	461.9447	2.388

Figure 88. Electrospray ESI data for compound **MM57A**.

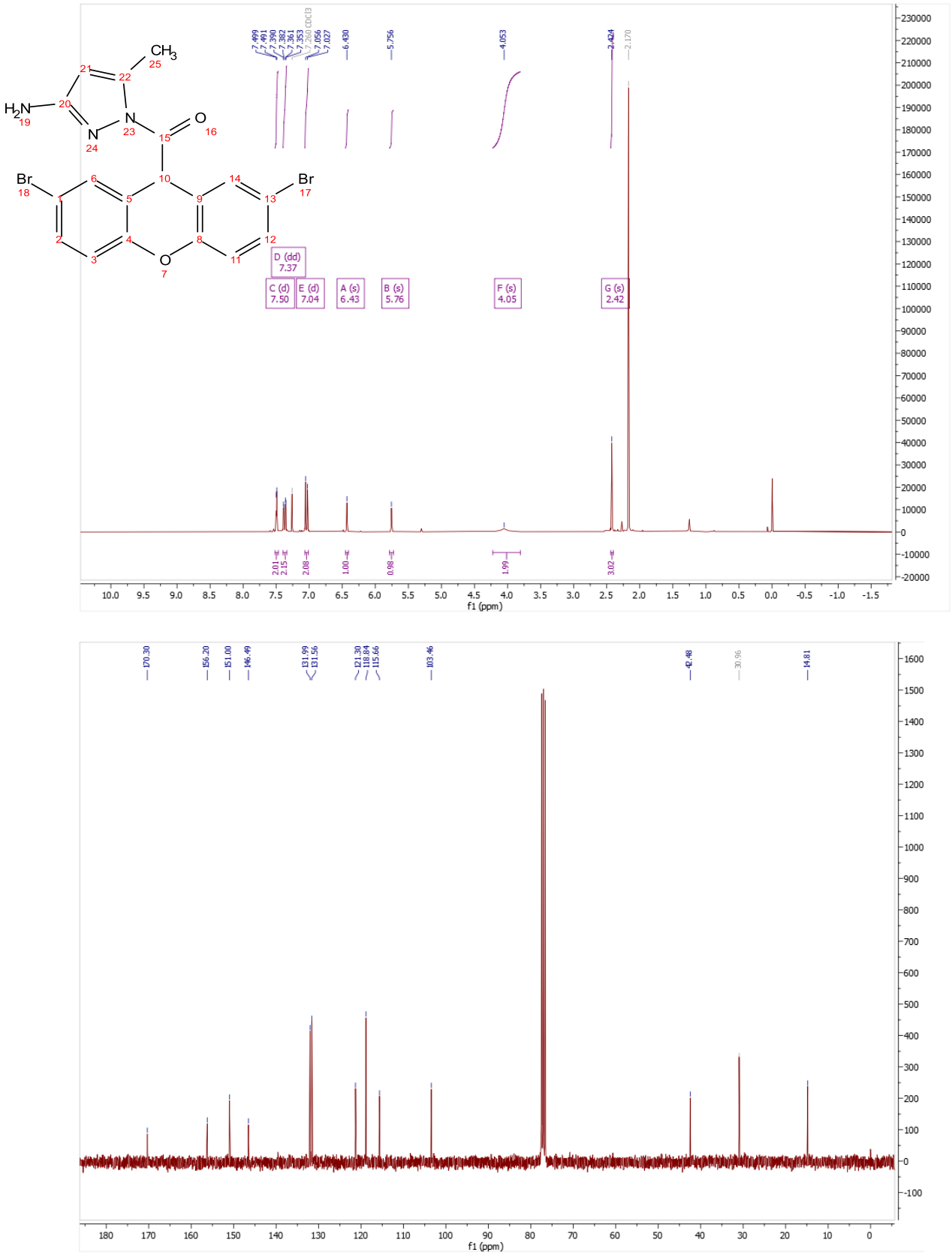

Figure 89. ^{1}H NMR (top, 300.13 MHz, $CDCl_3$) and ^{13}C NMR (bottom, 75.48 MHz, $CDCl_3$) for compound **MM57B**.

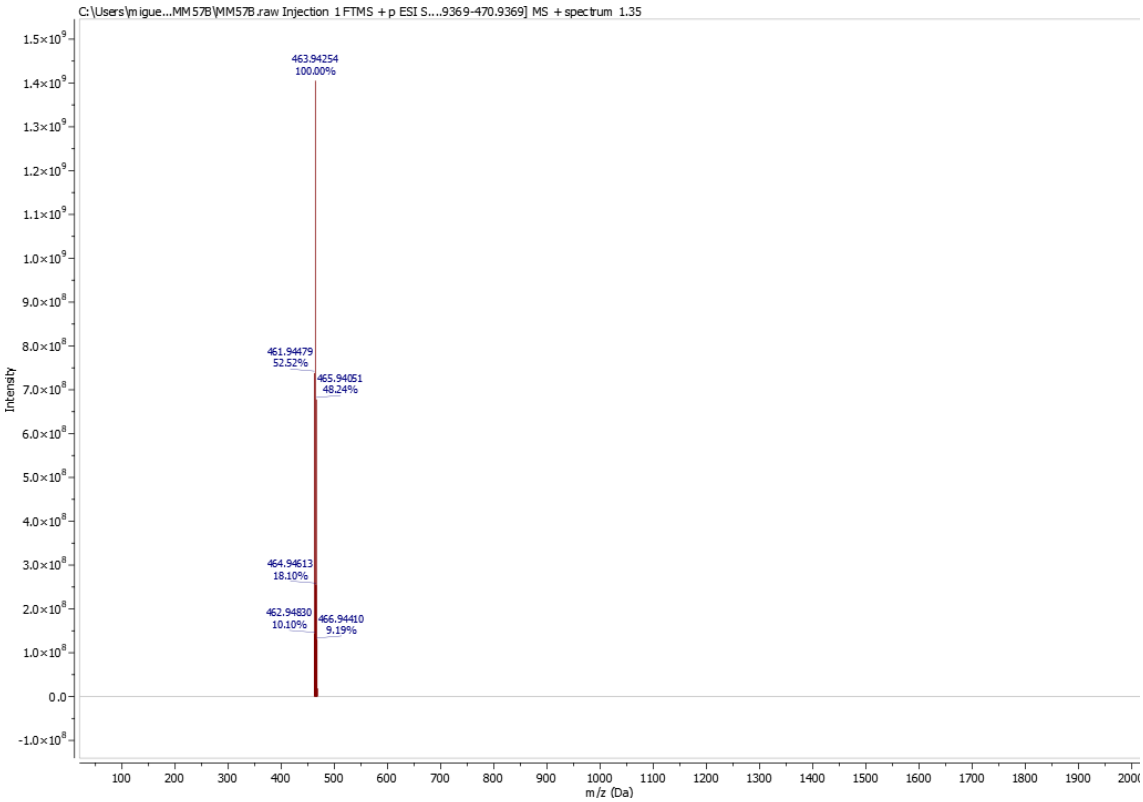

Meas. m/z	Formula	Adduct	Predicted m/z	Error [ppm]
461.94479	$C_{18}H_{13}Br_2N_3O_2$	H^+	461.94473	0.139

Figure 90. Electrospray ESI data for compound **MM57B**.

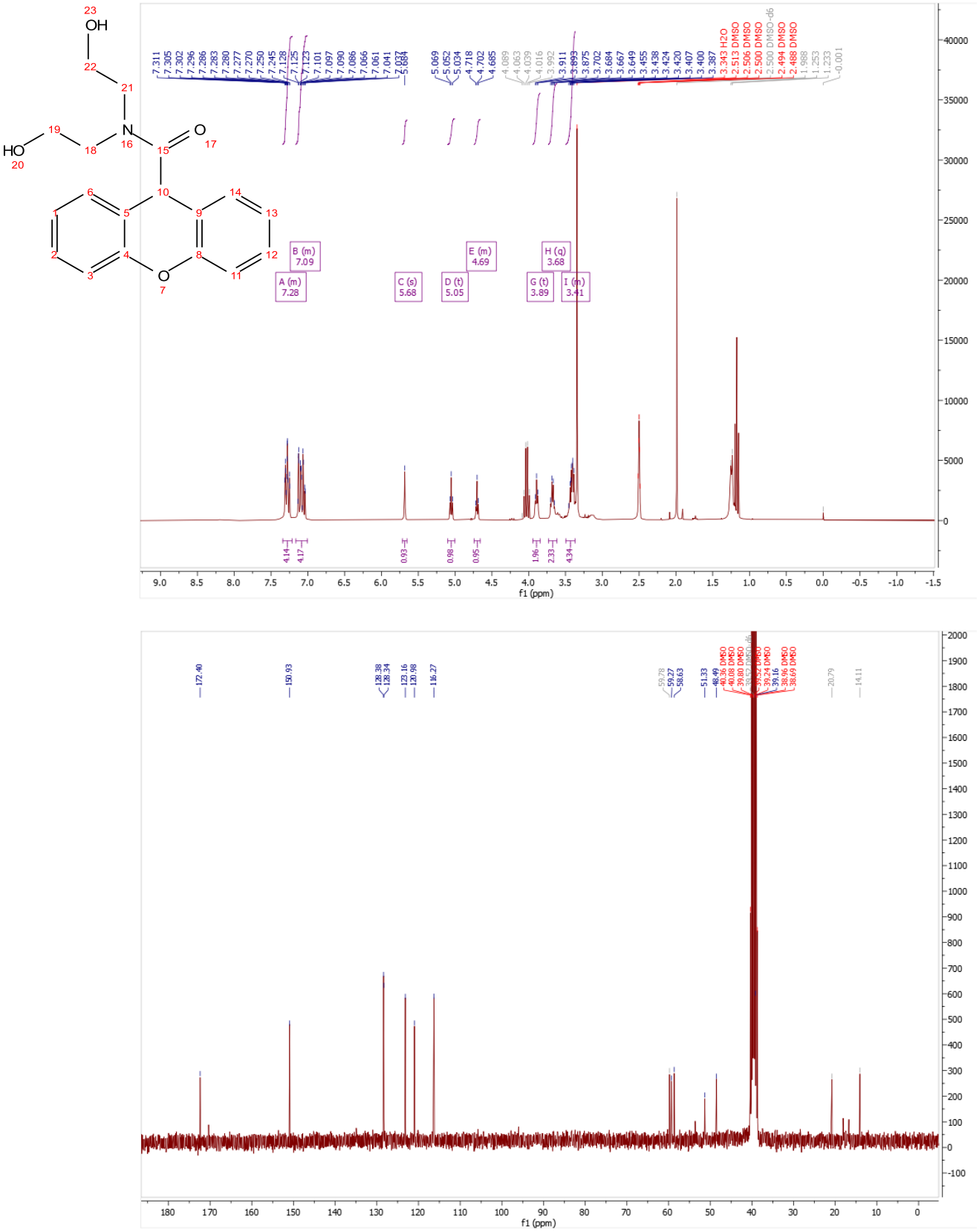

Figure 91. ^{1}H NMR (top, 300.13 MHz, DMSO-d_6) and ^{13}C NMR (bottom, 75.48 MHz, DMSO-d_6) for compound **MM59B3**.

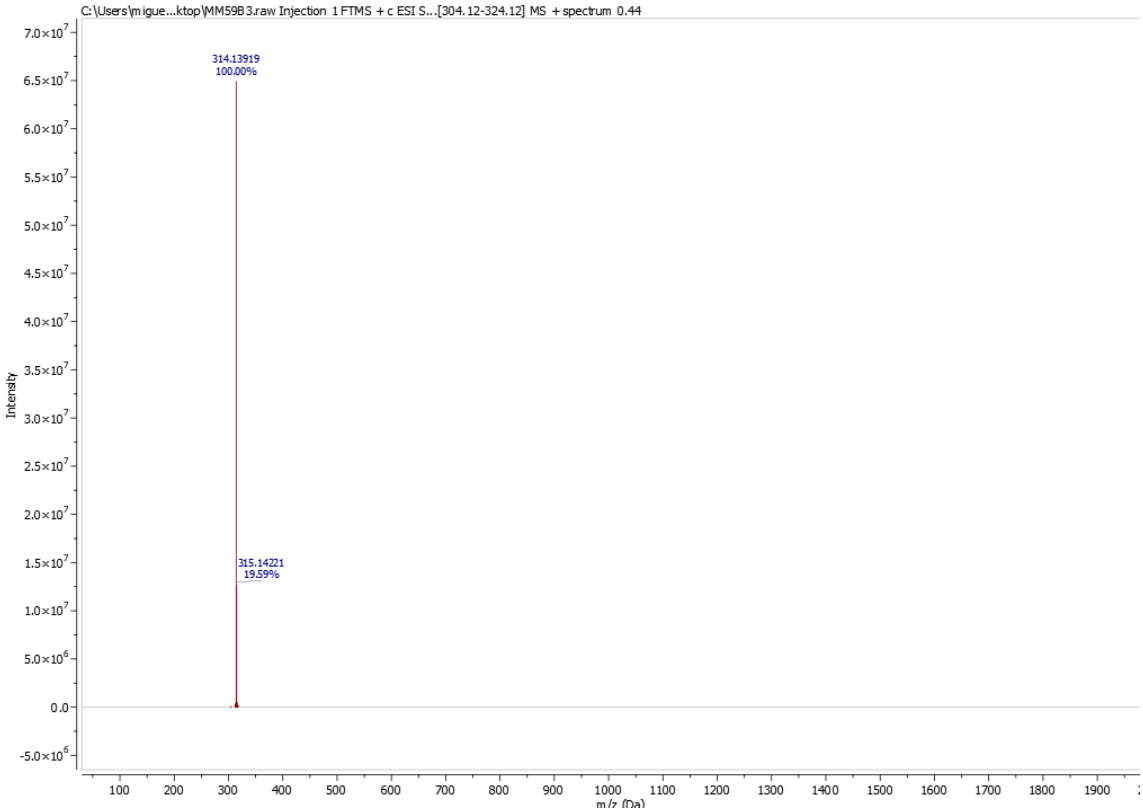

Meas. m/z	Formula	Adduct	Predicted m/z	Error [ppm]
314.1392	$C_{18}H_{19}NO_4$	H^+	314.1387	1.611

Figure 92. Electrospray ESI data for compound **MM59B3**.

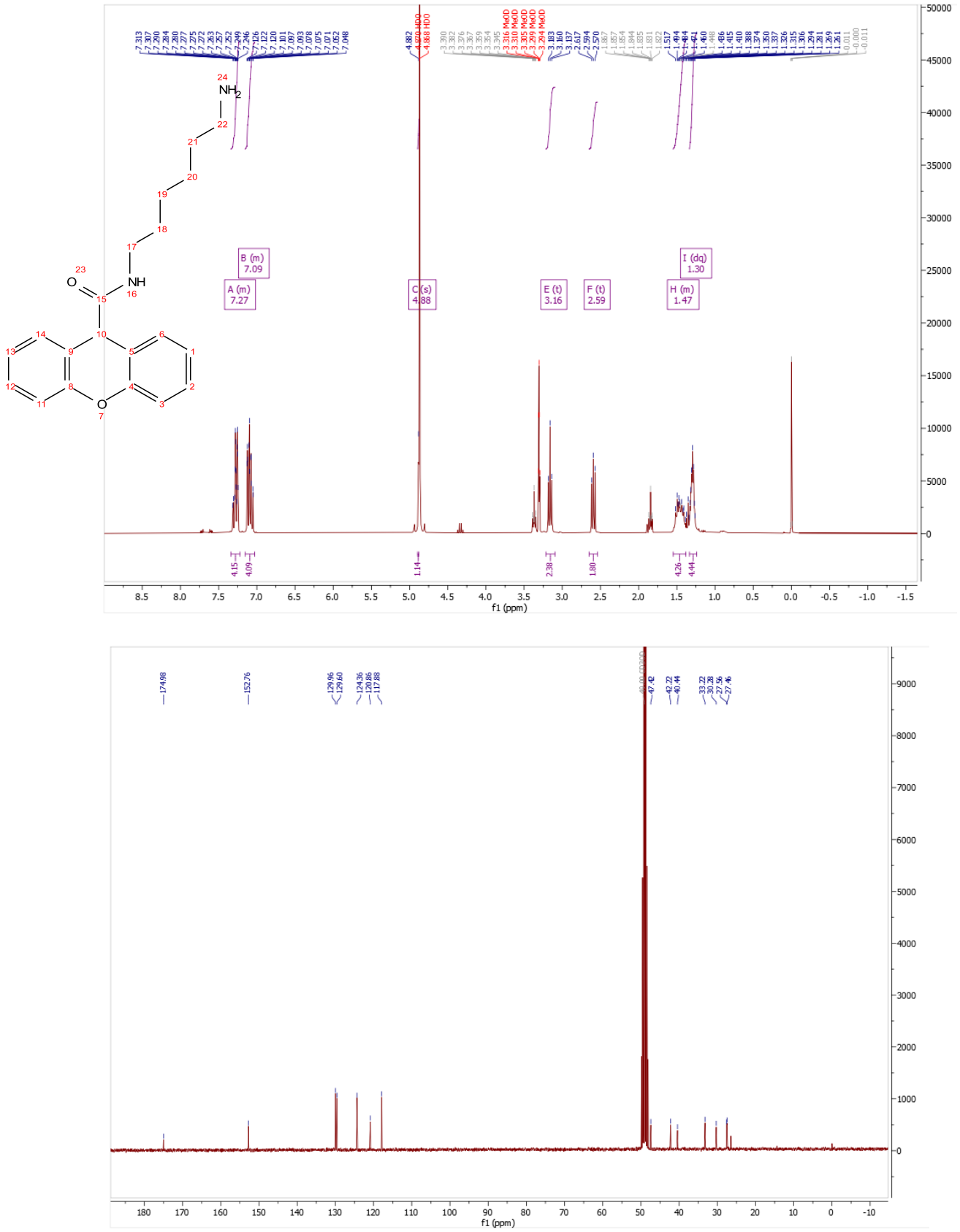

Figure 93.^{1}H NMR (top, 300.13 MHz, Methanol-d_4) and ^{13}C NMR (bottom, 75.48 MHz, Methanol-d_4) for compound **MM63B**.

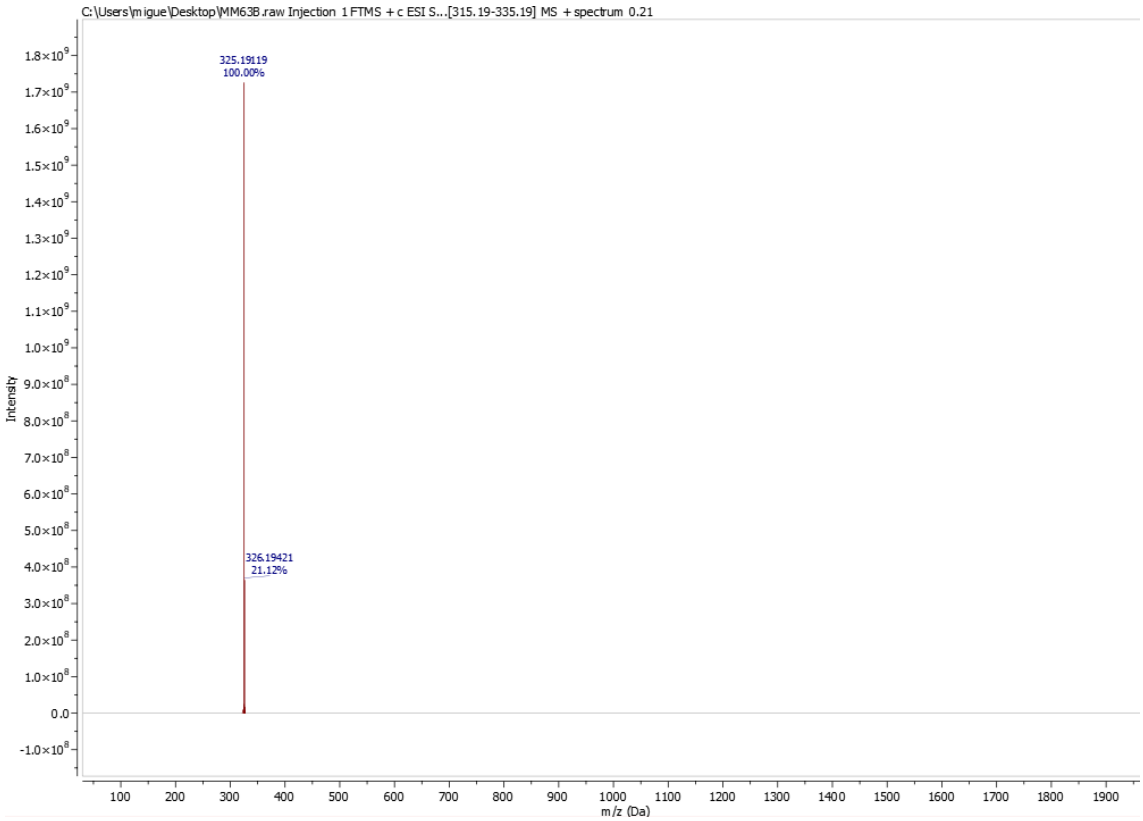

Meas. m/z	Formula	Adduct	Predicted m/z	Error [ppm]
325.19119	$C_{20}H_{21}N_2O_2$	H^+	325.19105	0.425

Figure 94. Electrospray ESI data for compound **MM63B**.

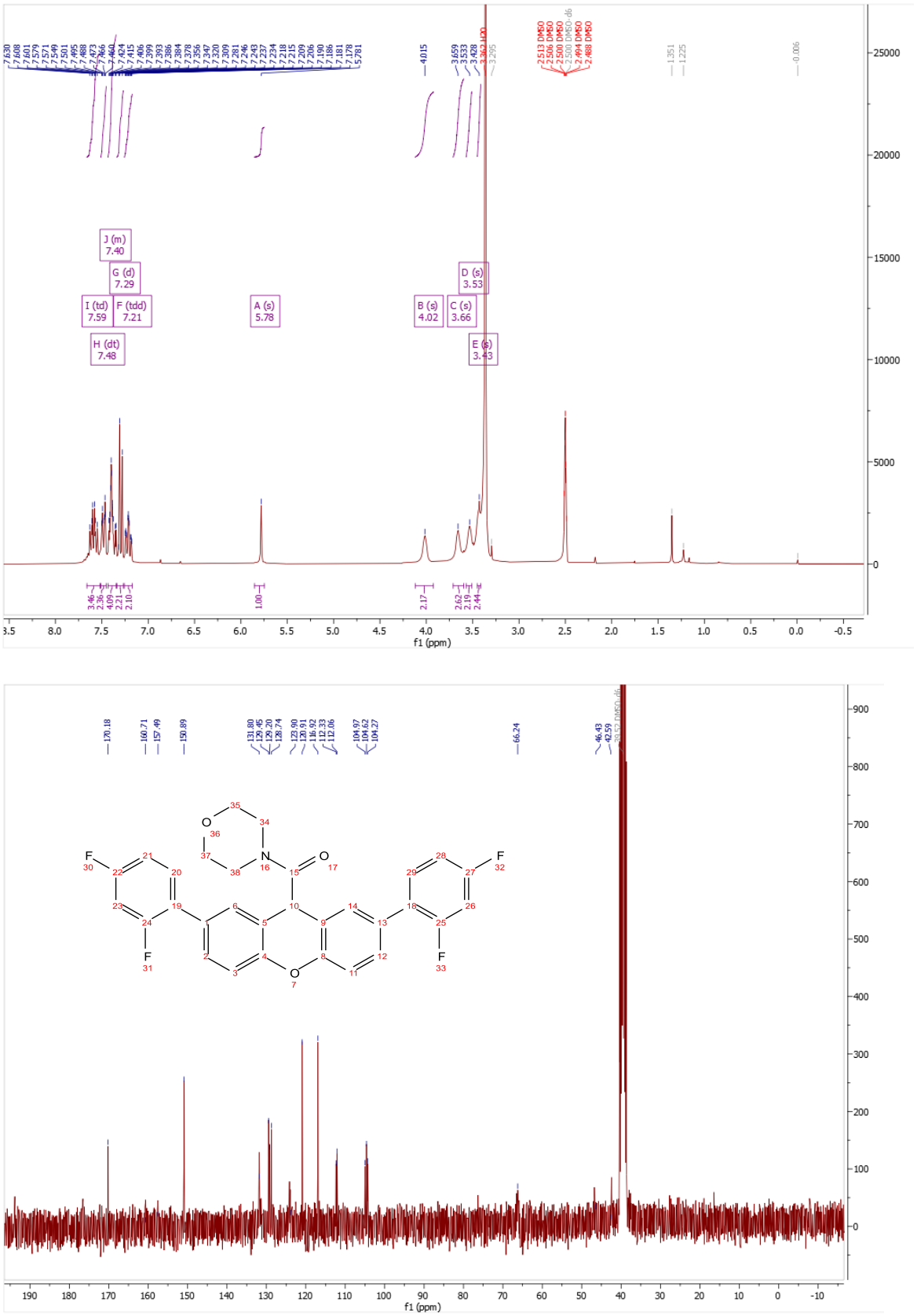

Figure 95. ^{1}H NMR (top, 300.13 MHz, DMSO-d_6) and ^{13}C NMR (bottom, 75.48 MHz, DMSO-d_6) for compound **MM68**.

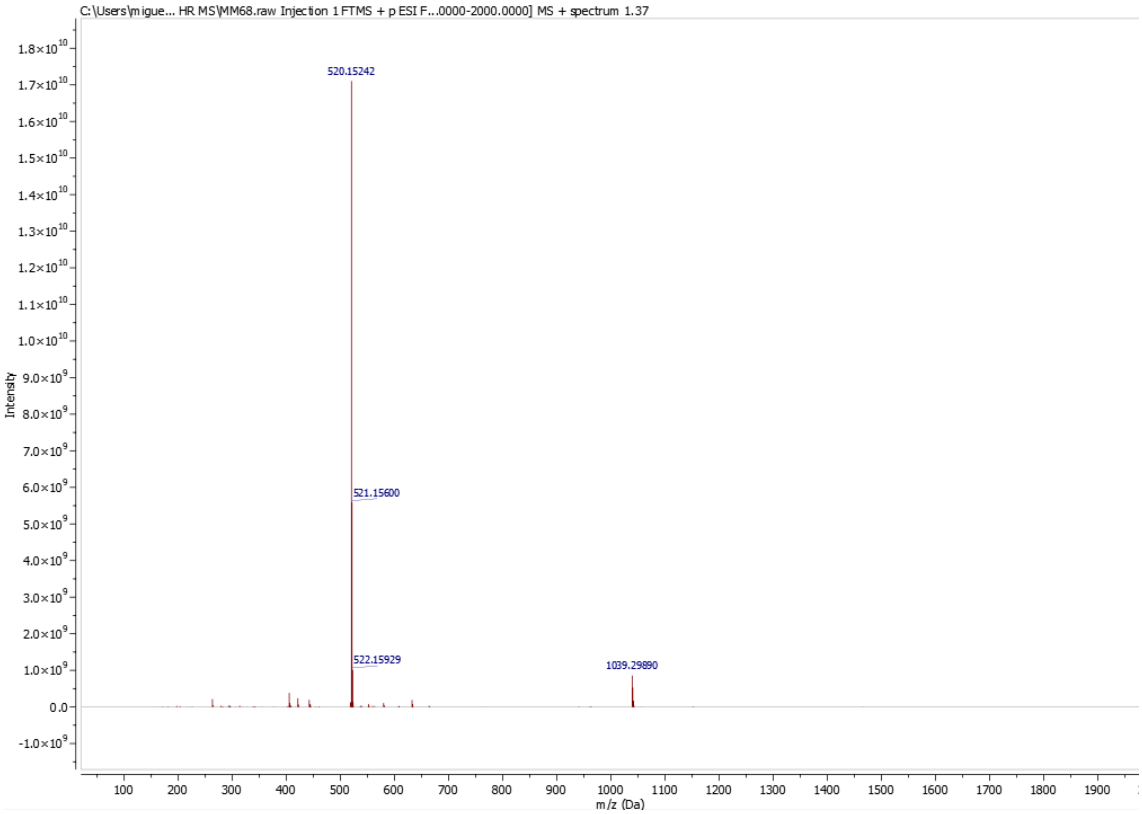

Meas. m/z	Formula	Adduct	Predicted m/z	Error [ppm]
520.15242	$C_{30}H_{21}F_4NO_3$	H^+	520.15303	-1.169

Figure 96. Electrospray ESI data for compound **MM68**.

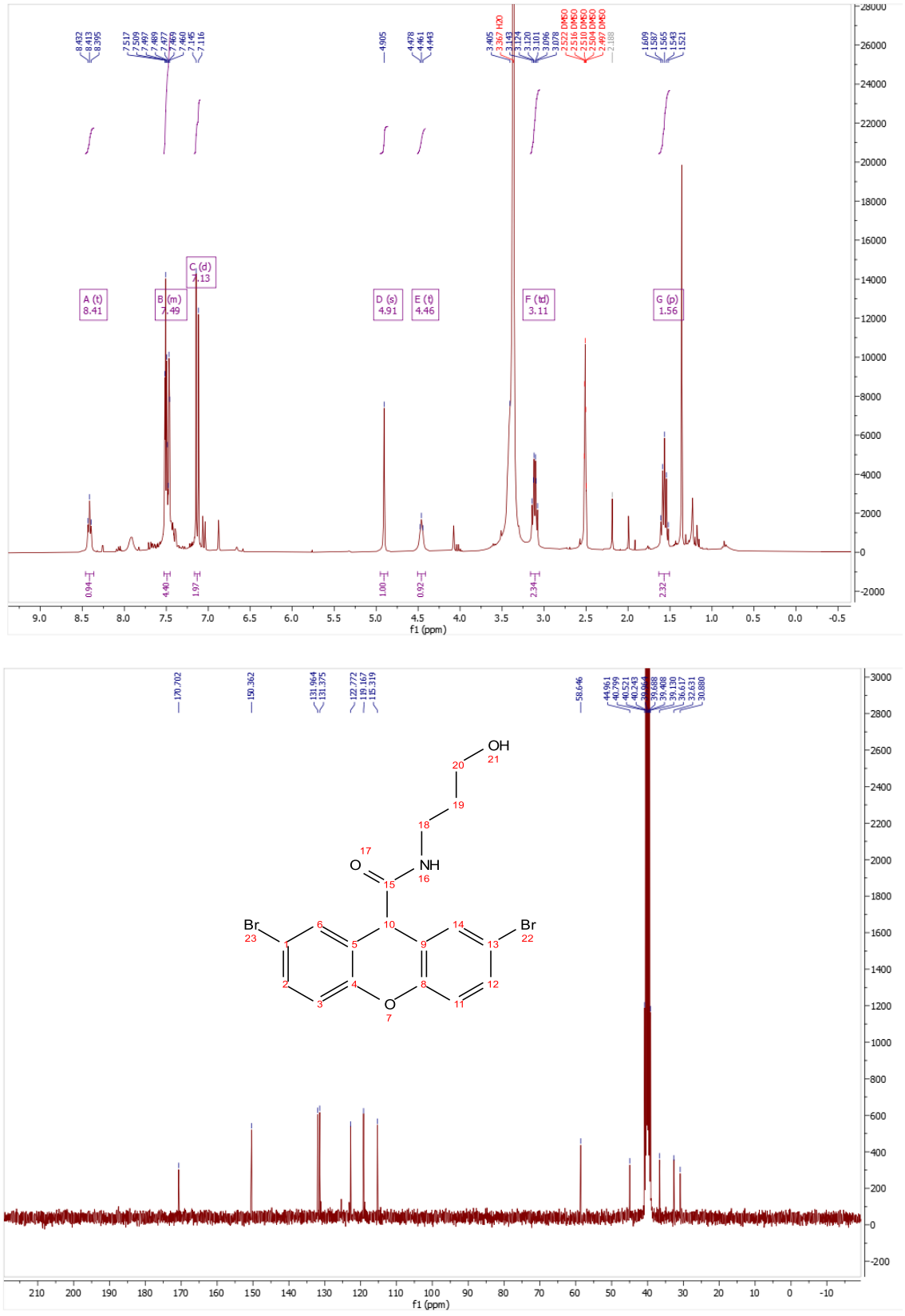

Figure 97. ^{1}H NMR (top, 300.13 MHz, DMSO-d_6) and ^{13}C NMR (bottom, 75.48 MHz, DMSO-d_6) for compound **MM73**.

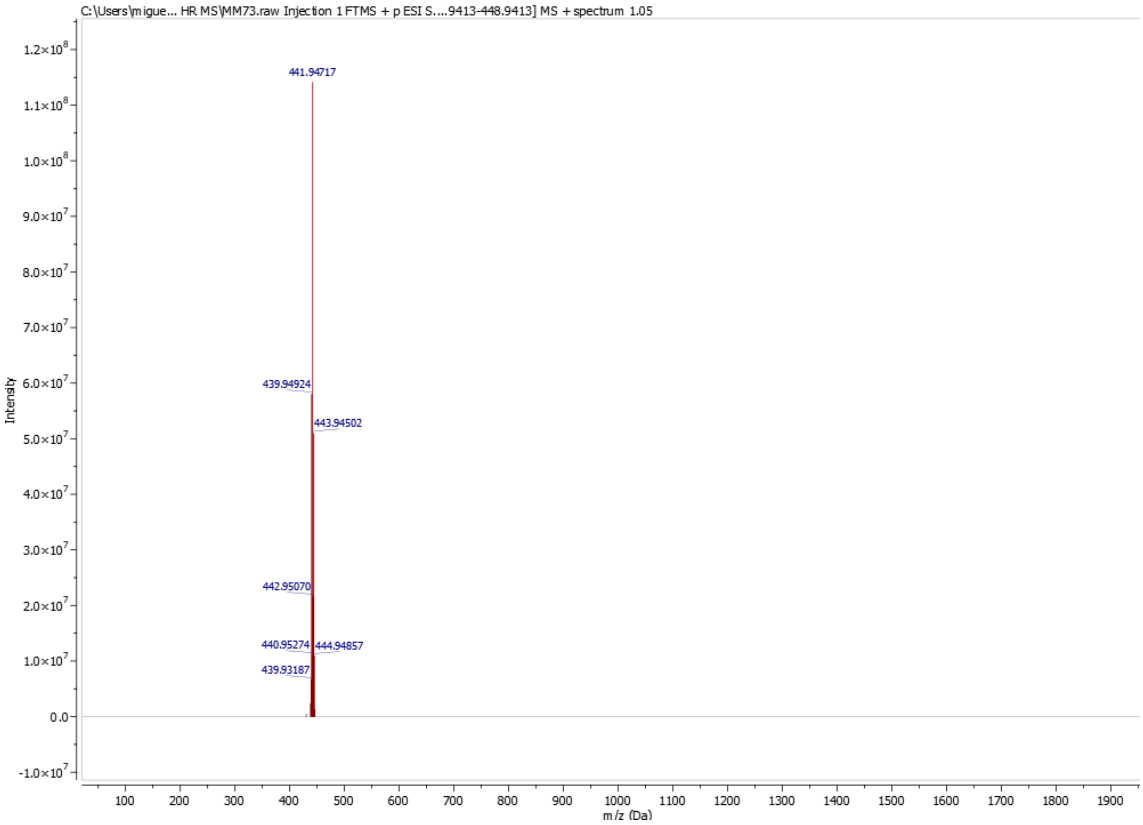

Meas. m/z	Formula	Adduct	Predicted m/z	Error [ppm]
439.94924	$C_{17}H_{15}Br_2NO_3$	H^+	439.94924	0.205

Figure 98. Electrospray ESI data for compound **MM73**.

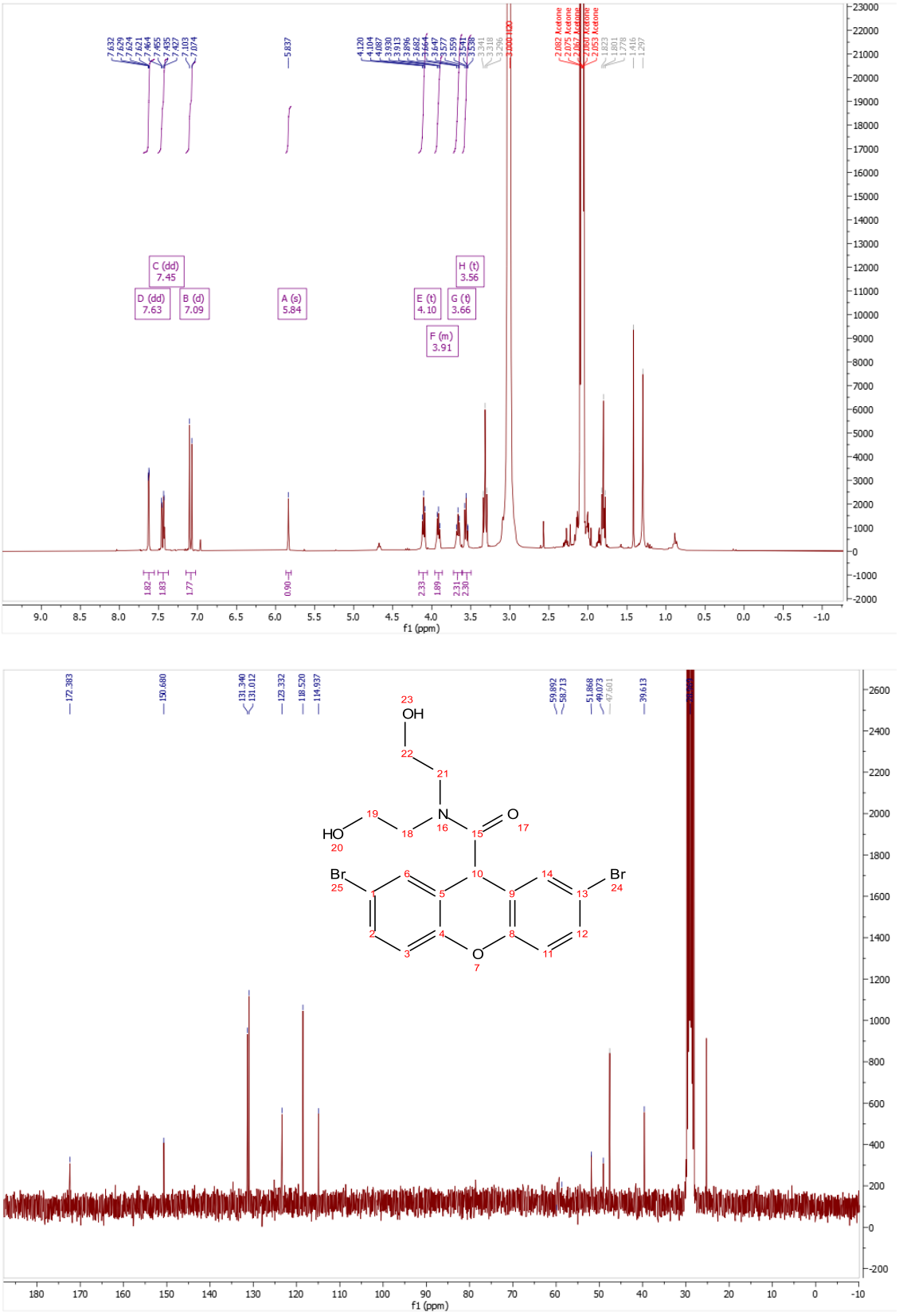

Figure 99. ^{1}H NMR (top, 300.13 MHz, Acetone-d_6) and ^{13}C NMR (bottom, 75.48 MHz, Acetone-d_6) for compound **MM74**.

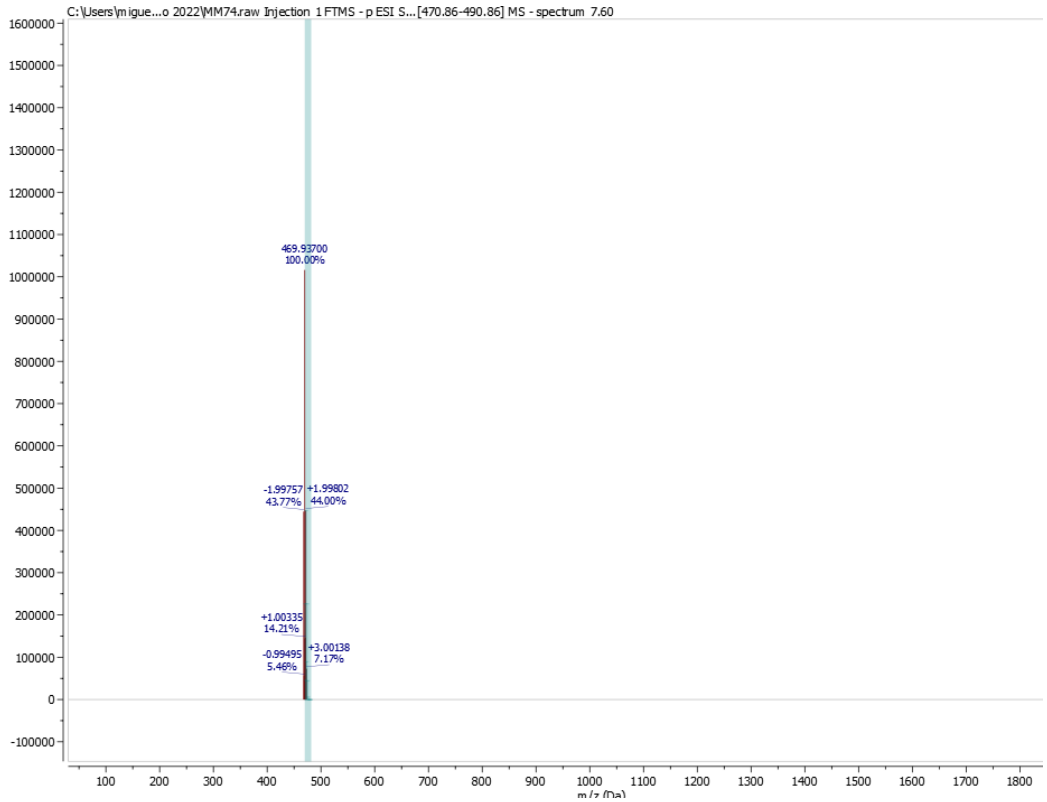

Meas. m/z	Formula	Adduct	Predicted m/z	Error [ppm]
469.93700	$C_{18}H_{17}Br_2NO_4$	H^+	469.95579	48.32

Figure 100. Electrospray ESI data for compound **MM74**.

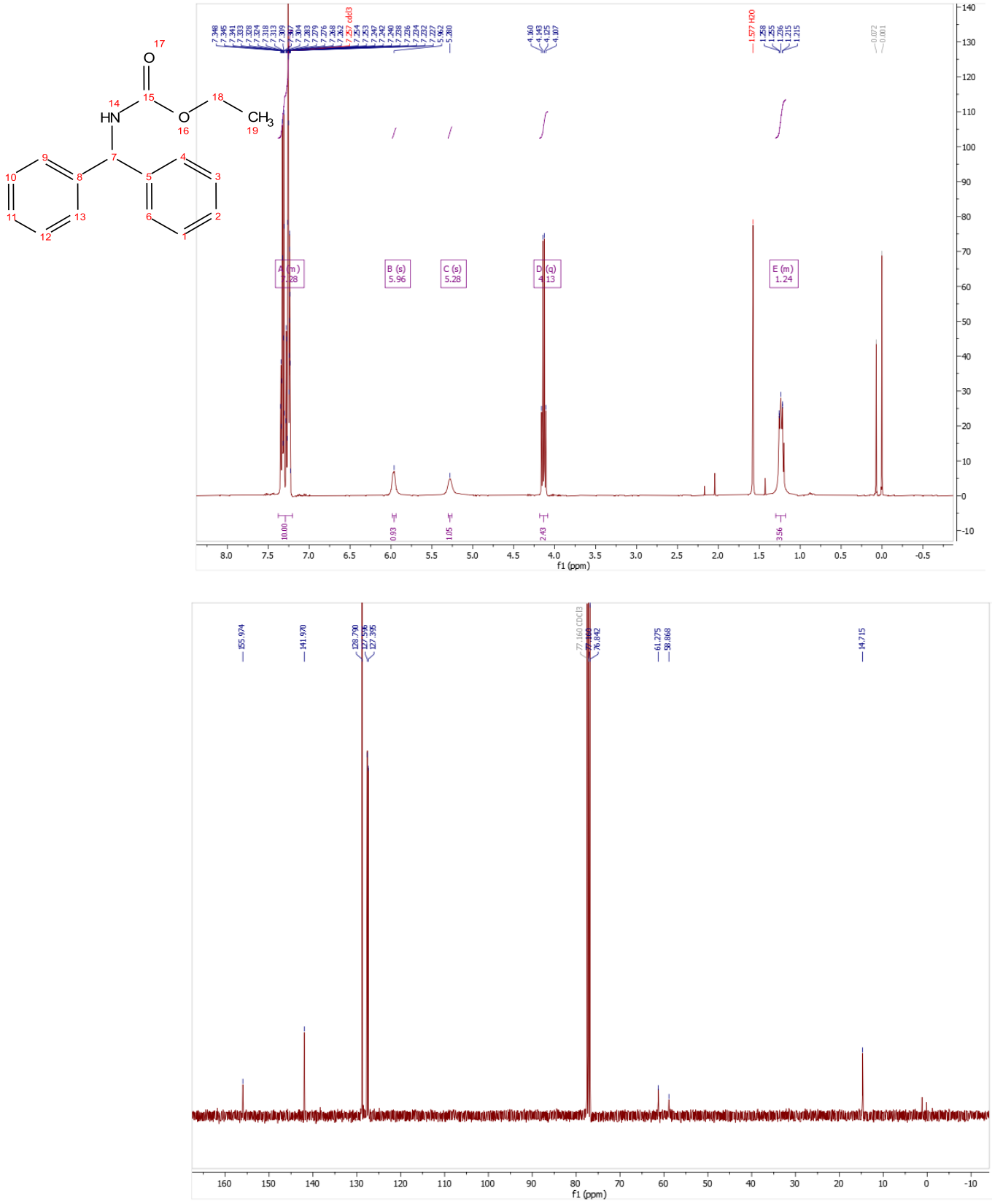

Figure 101. ^{1}H NMR (top, 400 MHz, $CDCl_3$) and ^{13}C NMR (bottom, 101 MHz, $CDCl_3$) for compound **MM81**.

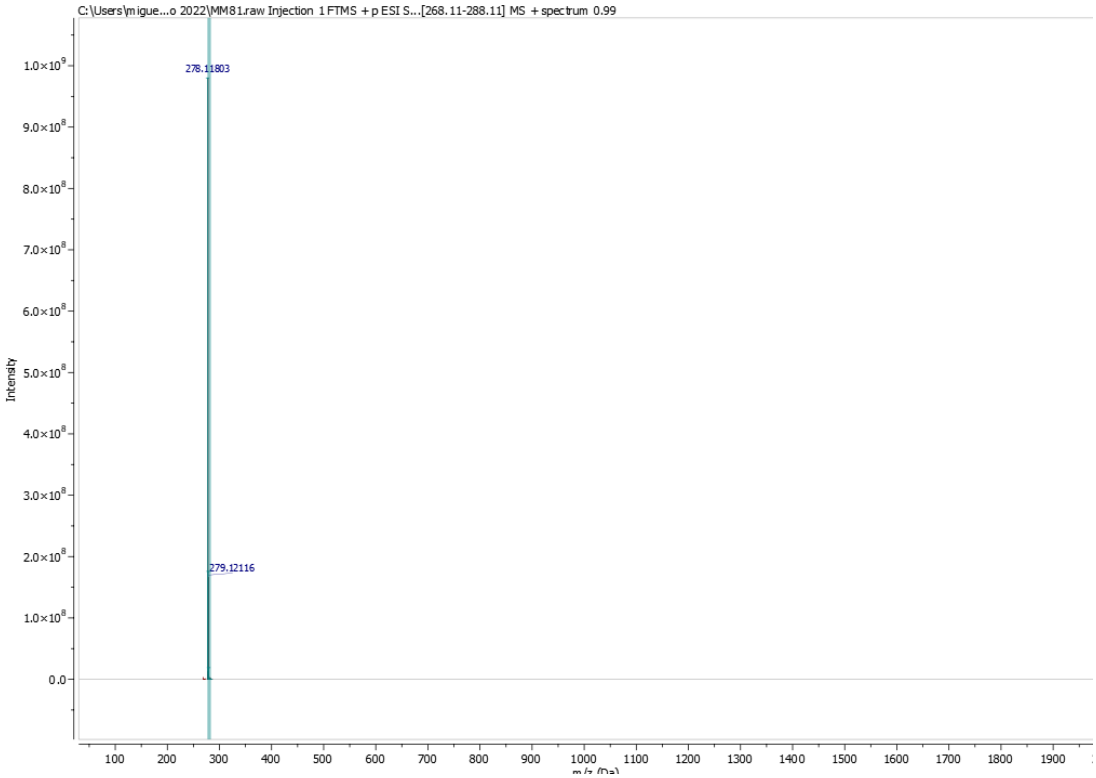

Meas. m/z	Formula	Adduct	Predicted m/z	Error [ppm]
278.1180.	$C_{16}H_{17}NO_2$	Na^+	278.11515	10.36

Figure 102. Electrospray ESI data for compound **MM81**.

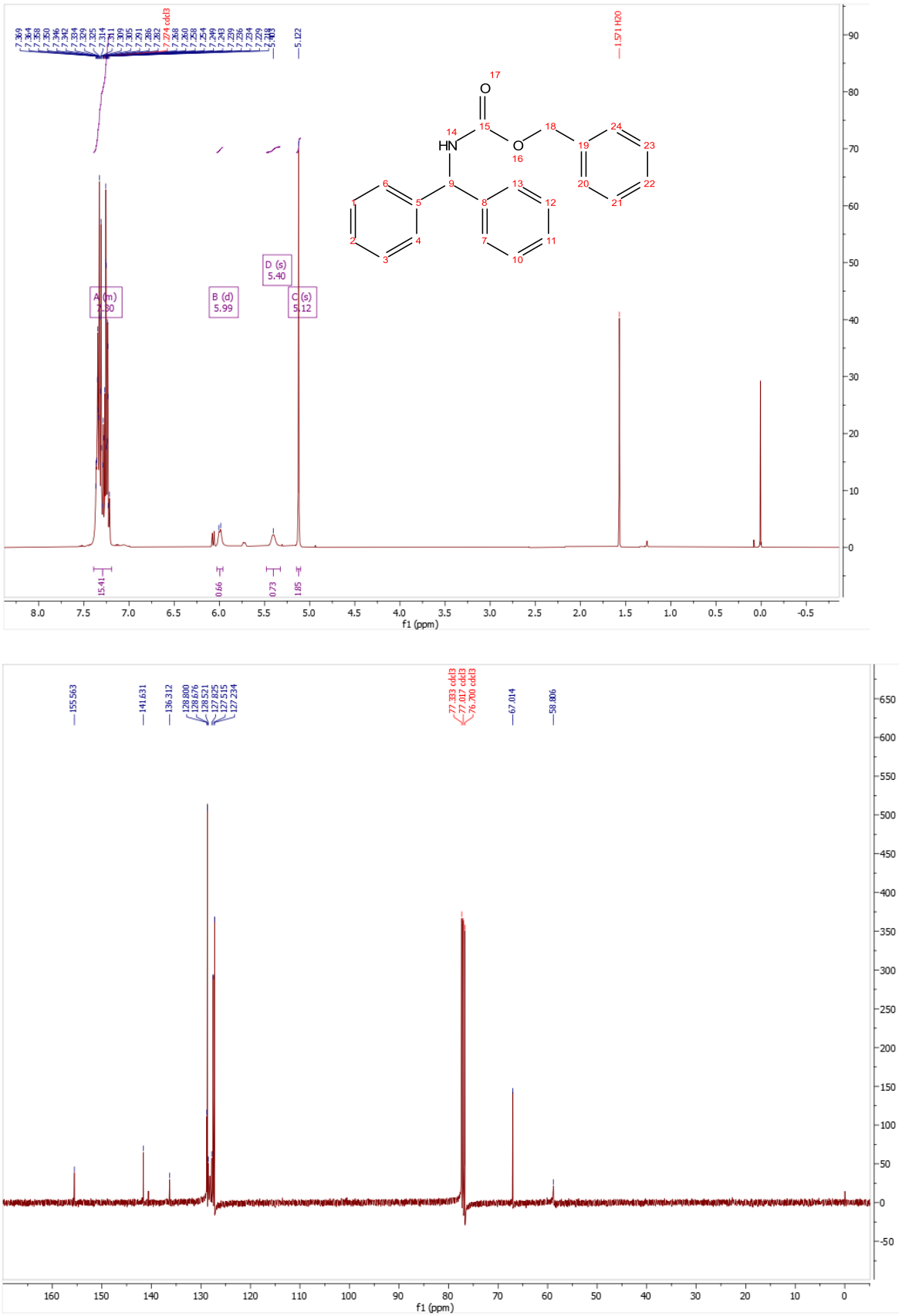

Figure 103. ^{1}H NMR (top, 400 MHz, $CDCl_3$) and ^{13}C NMR (bottom, 101 MHz, $CDCl_3$) for compound **MM85**.

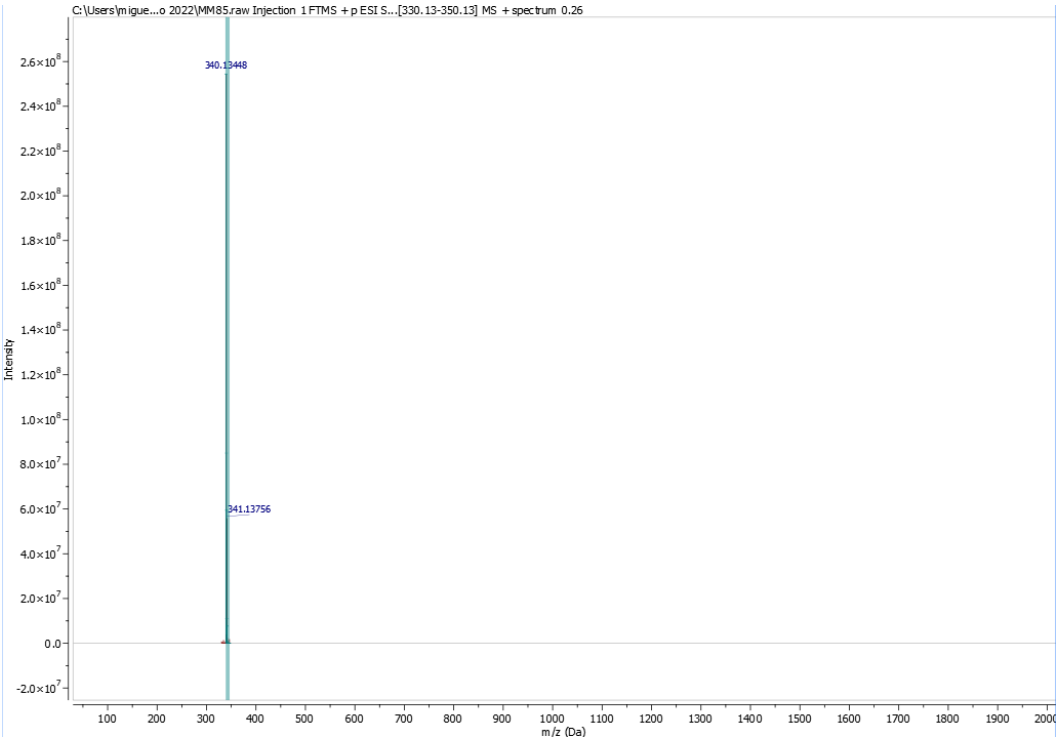

Meas. m/z	Formula	Adduct	Predicted m/z	Error [ppm]
340.13448	$C_{21}H_{19}NO_2$	Na^+	340.13080	10.82

Figure 104. Electrospray ESI data for compound **MM85**.

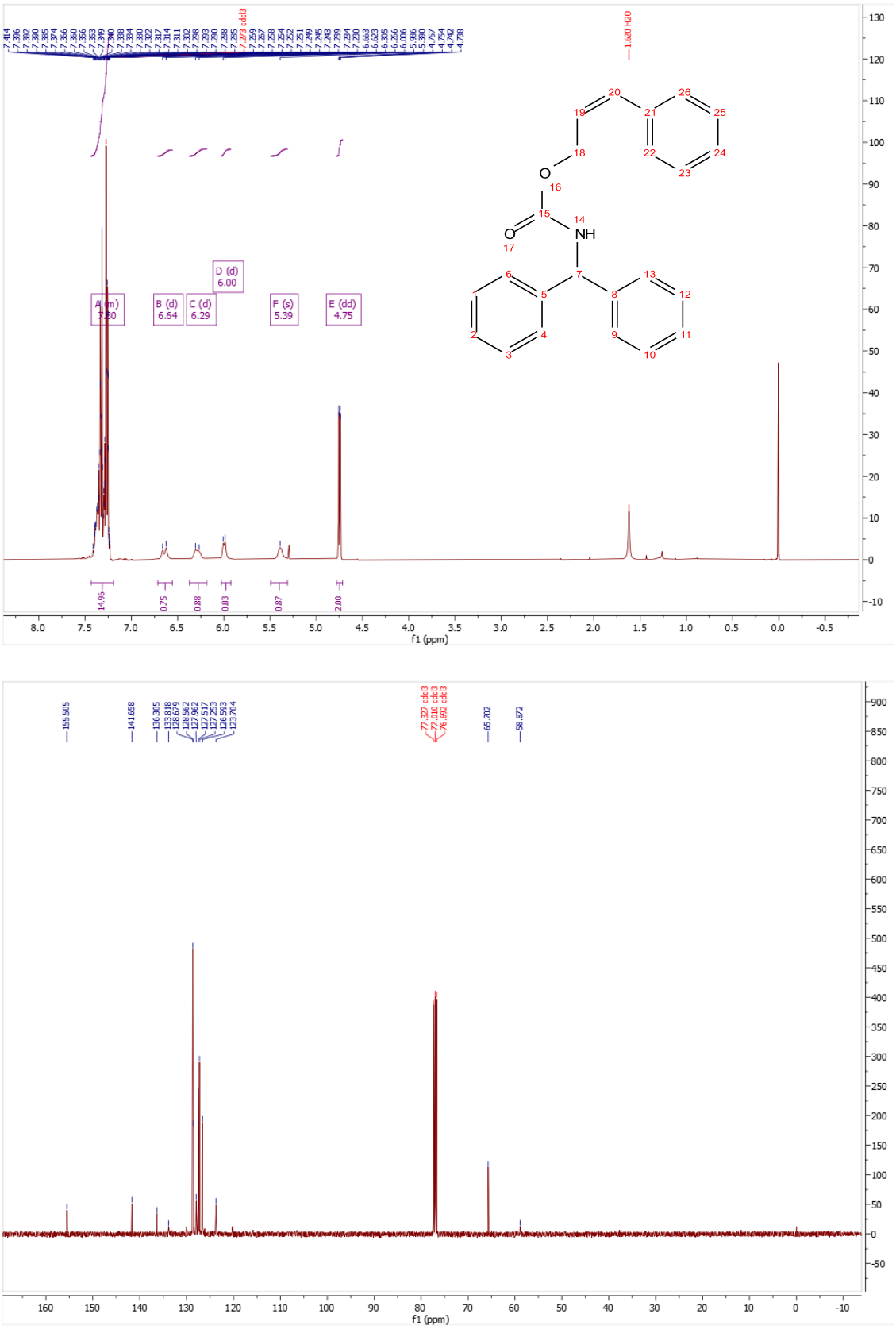

Figure 105. ^{1}H NMR (top, 400 MHz, $CDCl_3$) and ^{13}C NMR (bottom, 101 MHz, $CDCl_3$) for compound **MM88**.

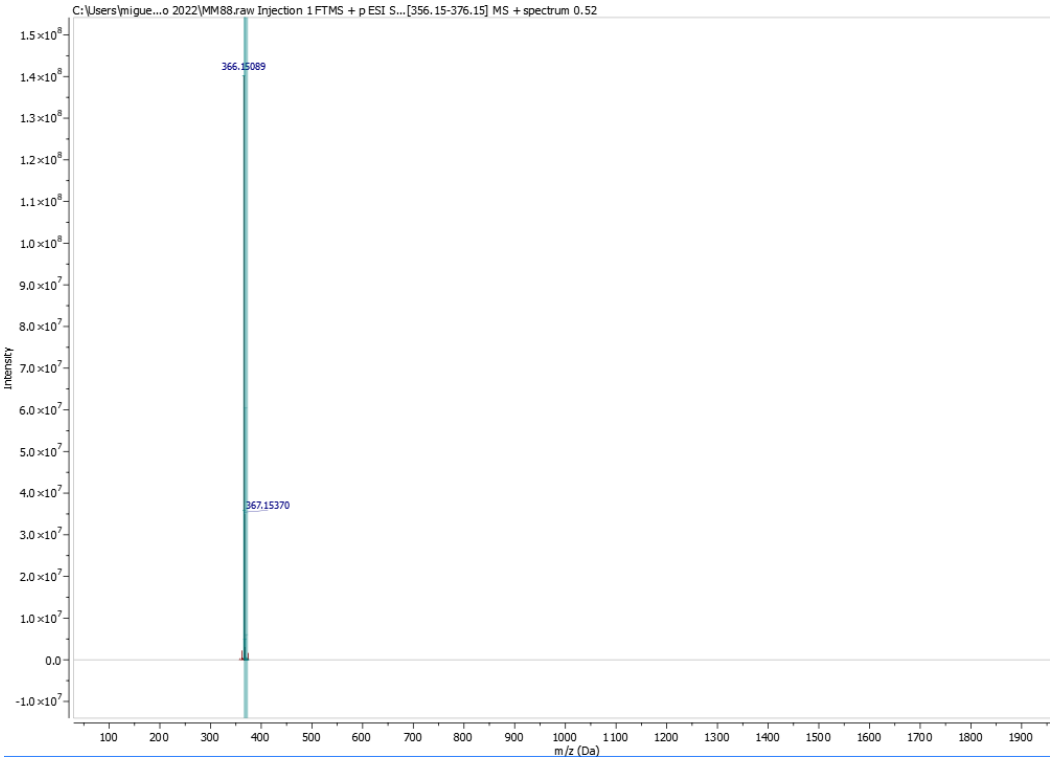

Meas. m/z	Formula	Adduct	Predicted m/z	Error [ppm]
366.15081	$C_{23}H_{21}NO_2$	Na^+	366.14645	11.91

Figure 106. Electrospray ESI data for compound **MM88**.

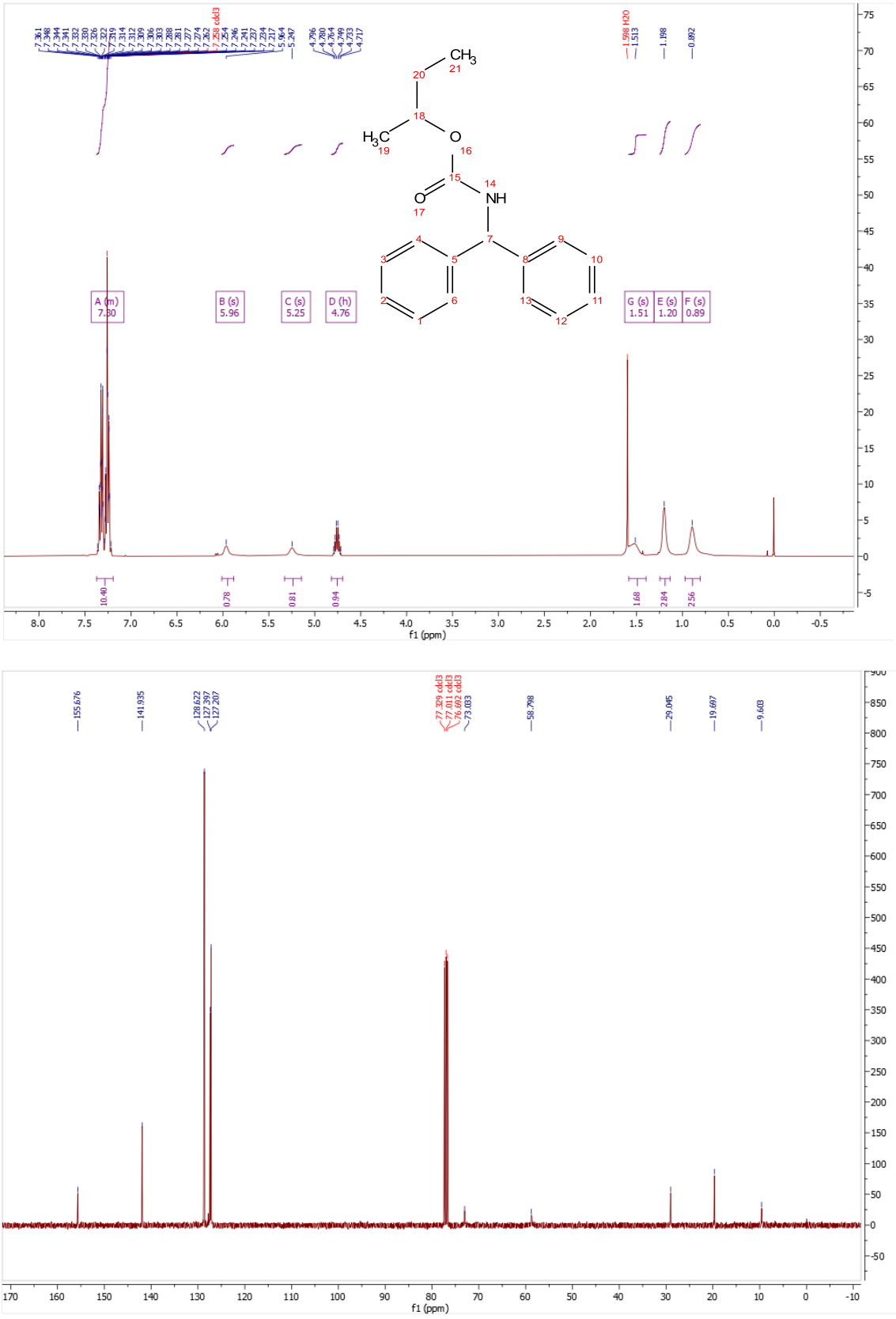

Figure 107. ^{1}H NMR (top, 400 MHz, $CDCl_3$) and ^{13}C NMR (bottom, 101 MHz, $CDCl_3$) for compound **MM90**.

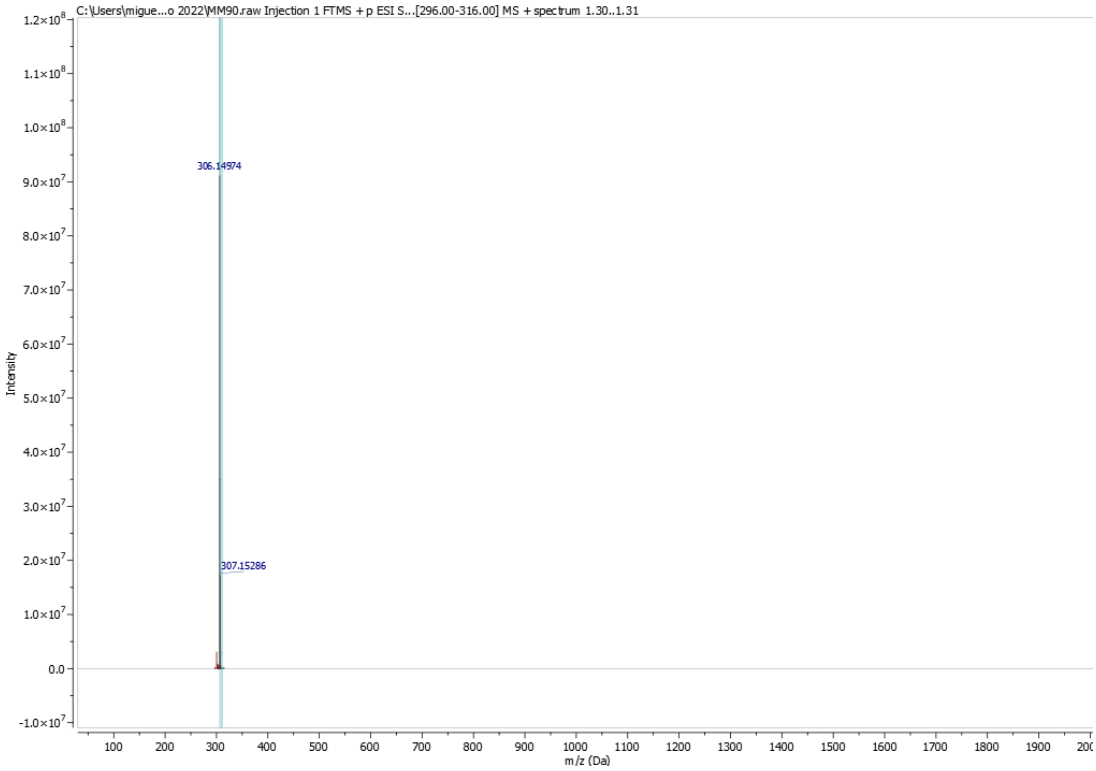

Meas. m/z	Formula	Adduct	Predicted m/z	Error [ppm]
306.14974	$C_{18}H_{21}NO_2$	Na^+	306.14645	10.75

Figure 108. Electrospray ESI data for compound **MM90**.

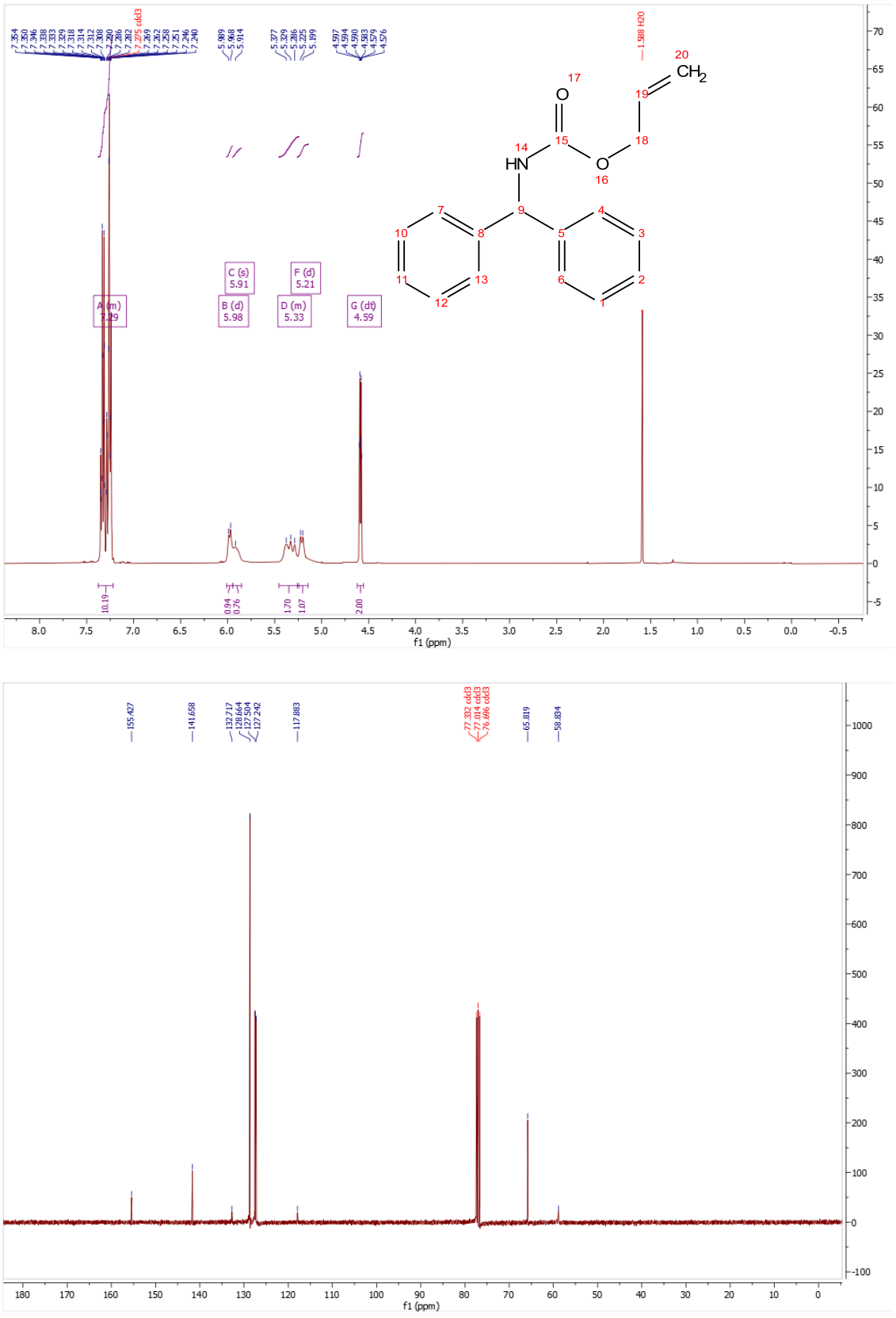

Figure 109. ^{1}H NMR (top, 400 MHz, $CDCl_3$) and ^{13}C NMR (bottom, 101 MHz, $CDCl_3$) for compound **MM91**.

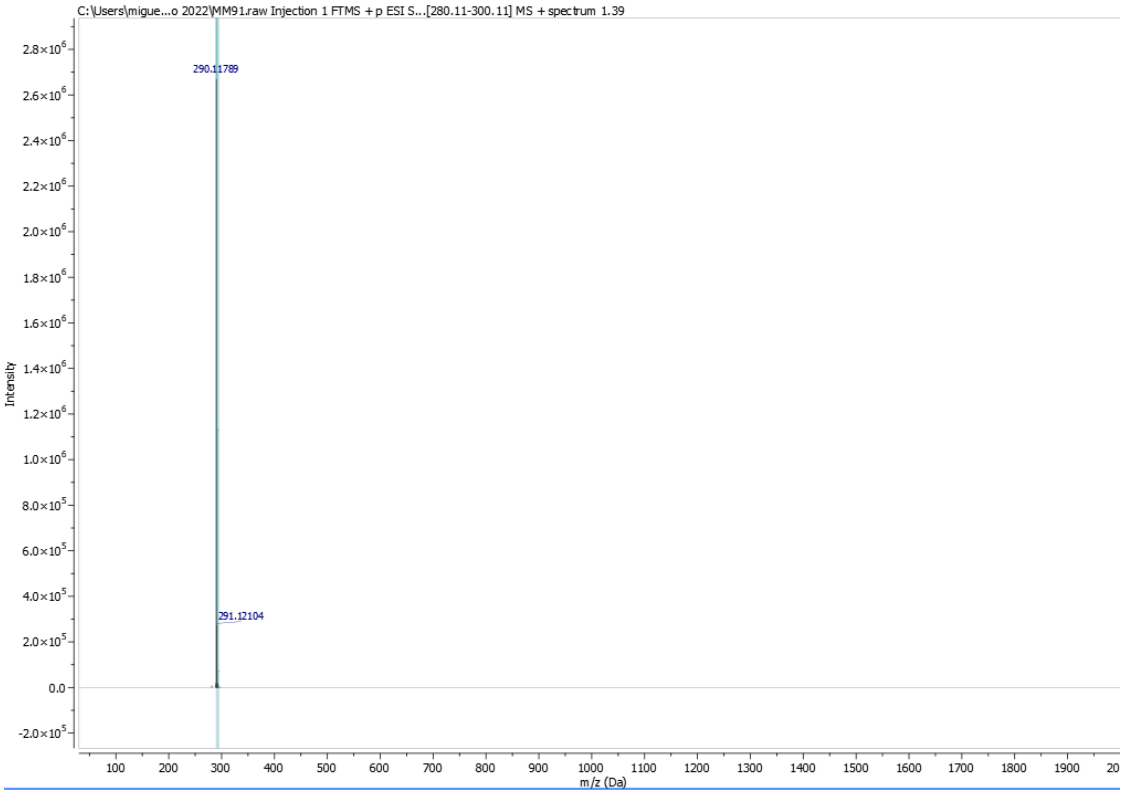

Meas. m/z	Formula	Adduct	Predicted m/z	Error [ppm]
290.11789	$C_{17}H_{17}NO_2$	Na^+	290.11515	9.45

Figure 110. Electrospray ESI data for compound **MM91**.

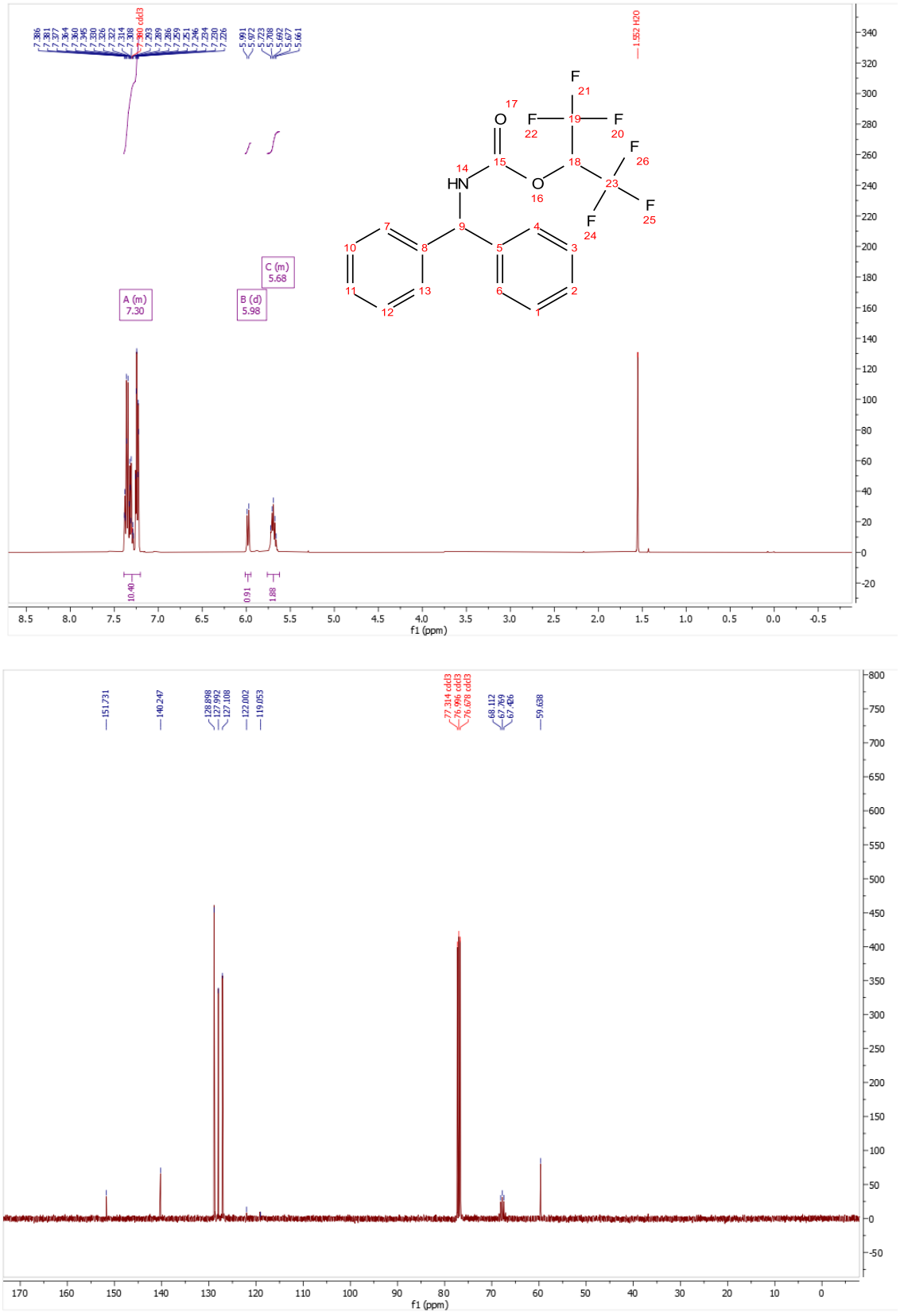

Figure 111. ^{1}H NMR (top, 400 MHz, $CDCl_3$) and ^{13}C NMR (bottom, 101 MHz, $CDCl_3$) for compound **MM92**.

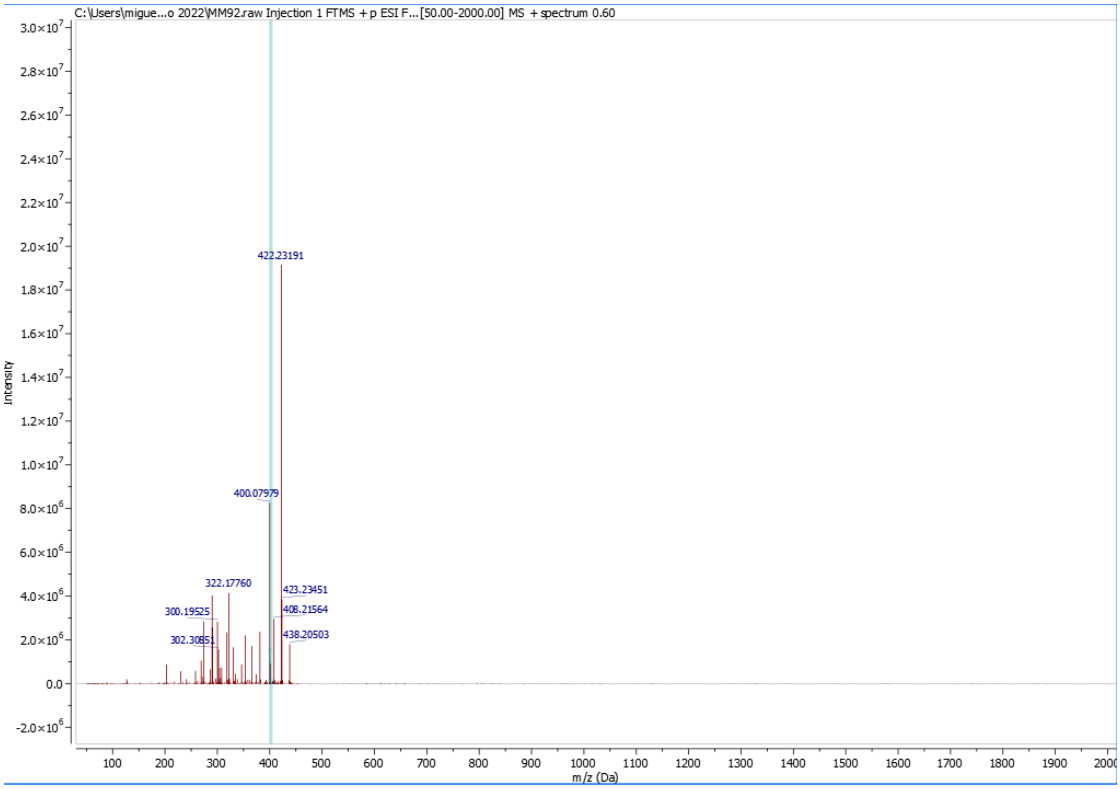

Meas. m/z	Formula	Adduct	Predicted m/z	Error [ppm]
400.07979	$C_{17}H_{13}F_6NO_2$	Na^+	400.07427	13.80

Figure 112. Electrospray ESI data for compound **MM92**.

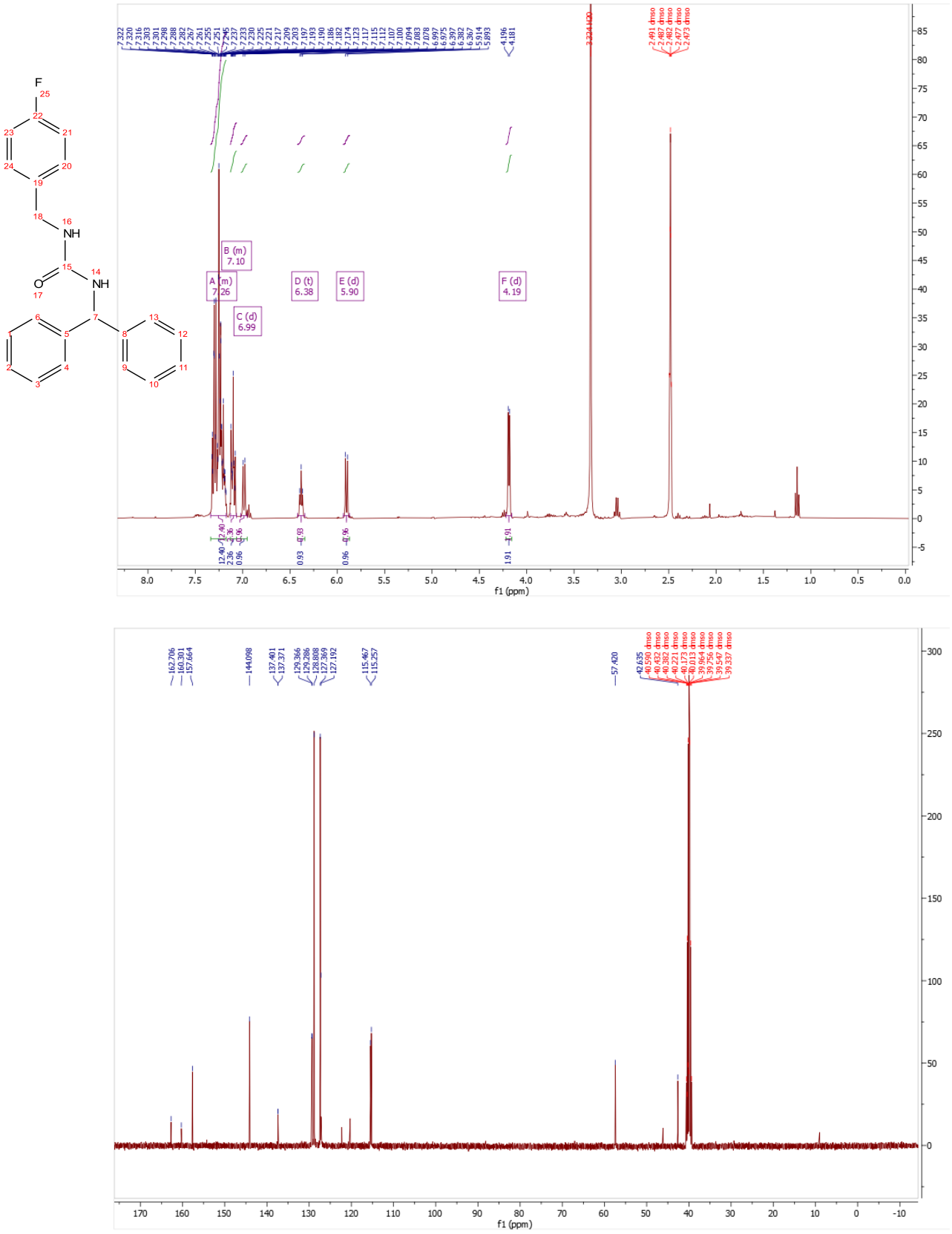

Figure 113. ^{1}H NMR (top, 400 MHz, DMSO-d_6) and ^{13}C NMR (bottom, 101 MHz, DMSO-d_6) for compound **MM94**.

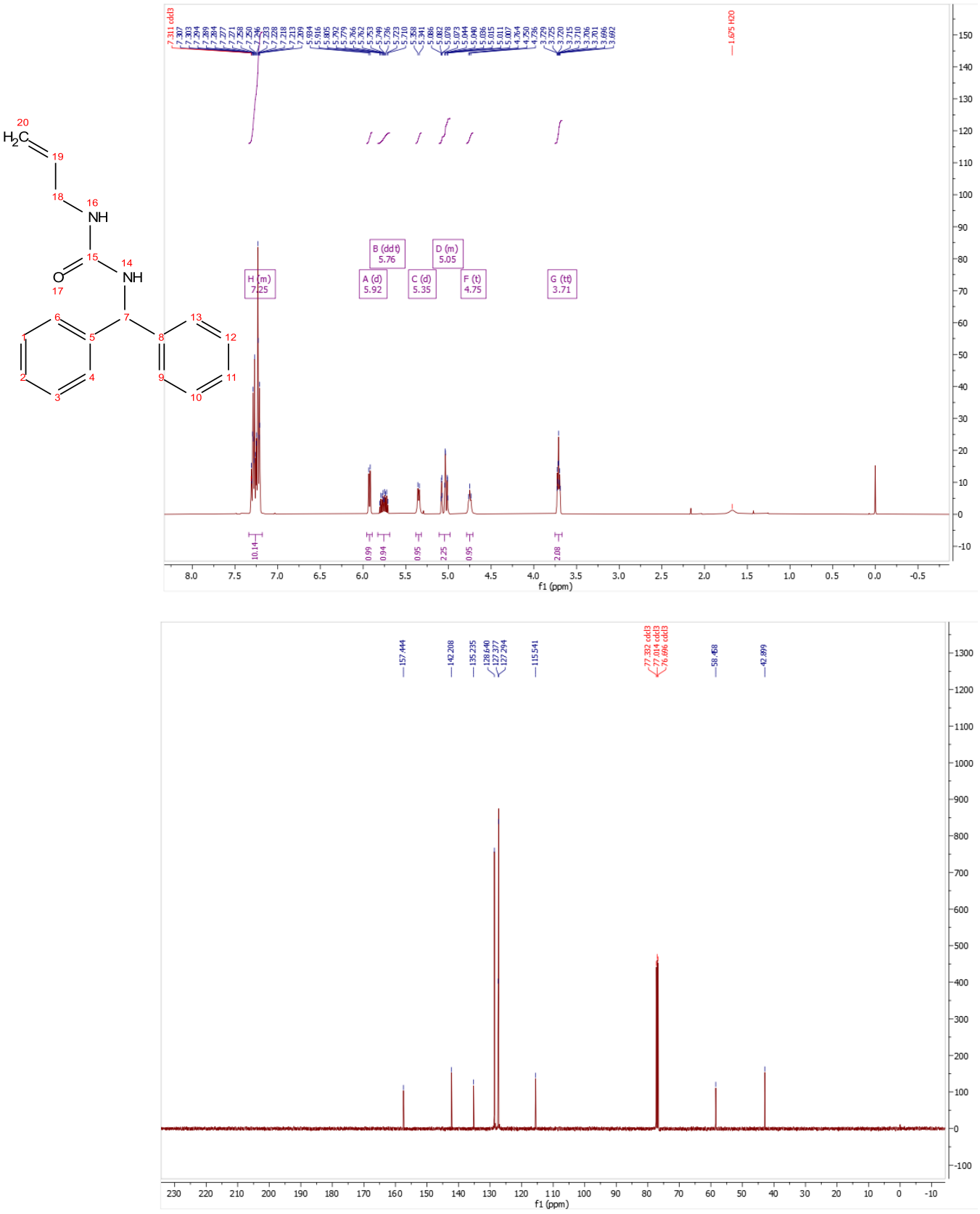

Figure 114. ^{1}H NMR (top, 400 MHz, $CDCl_3$) and ^{13}C NMR (bottom, 101 MHz, $CDCl_3$) for compound **MM95**.

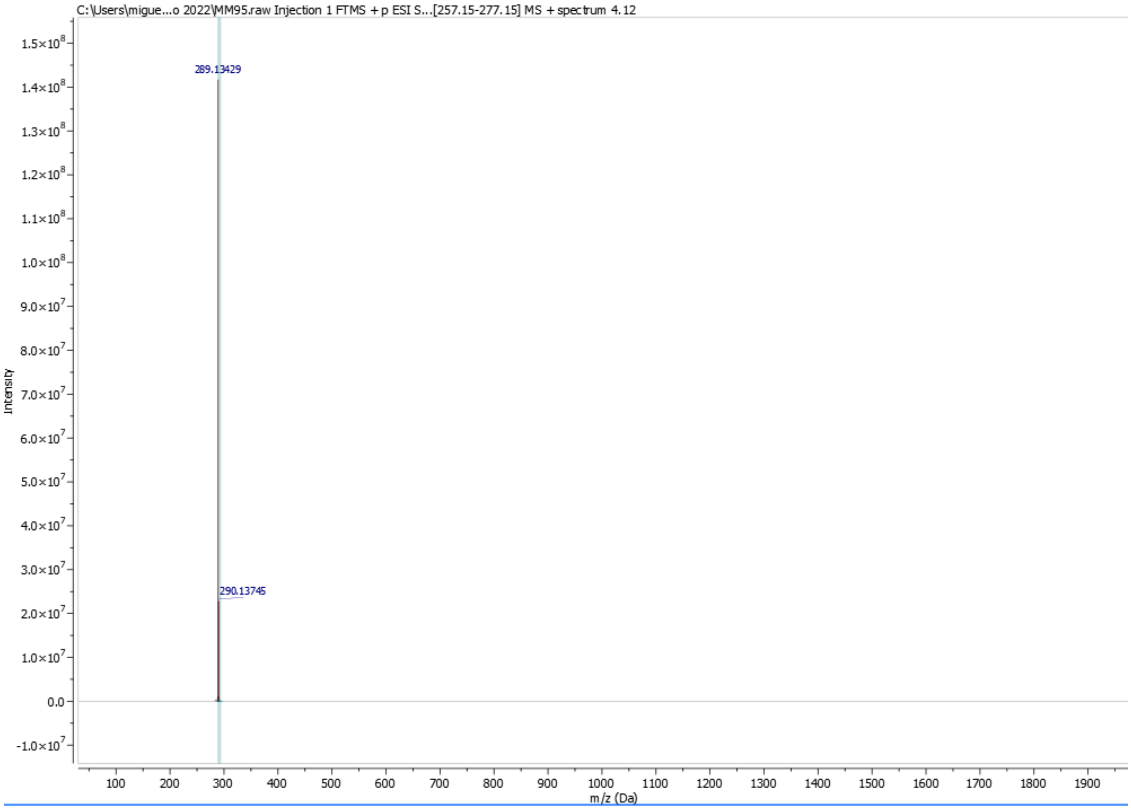

Meas. m/z	Formula	Adduct	Predicted m/z	Error [ppm]
289.13429	$C_{17}H_{18}N_2O$	Na^+	289.13113	10.92

Figure 115. Electrospray ESI data for compound **MM95**.

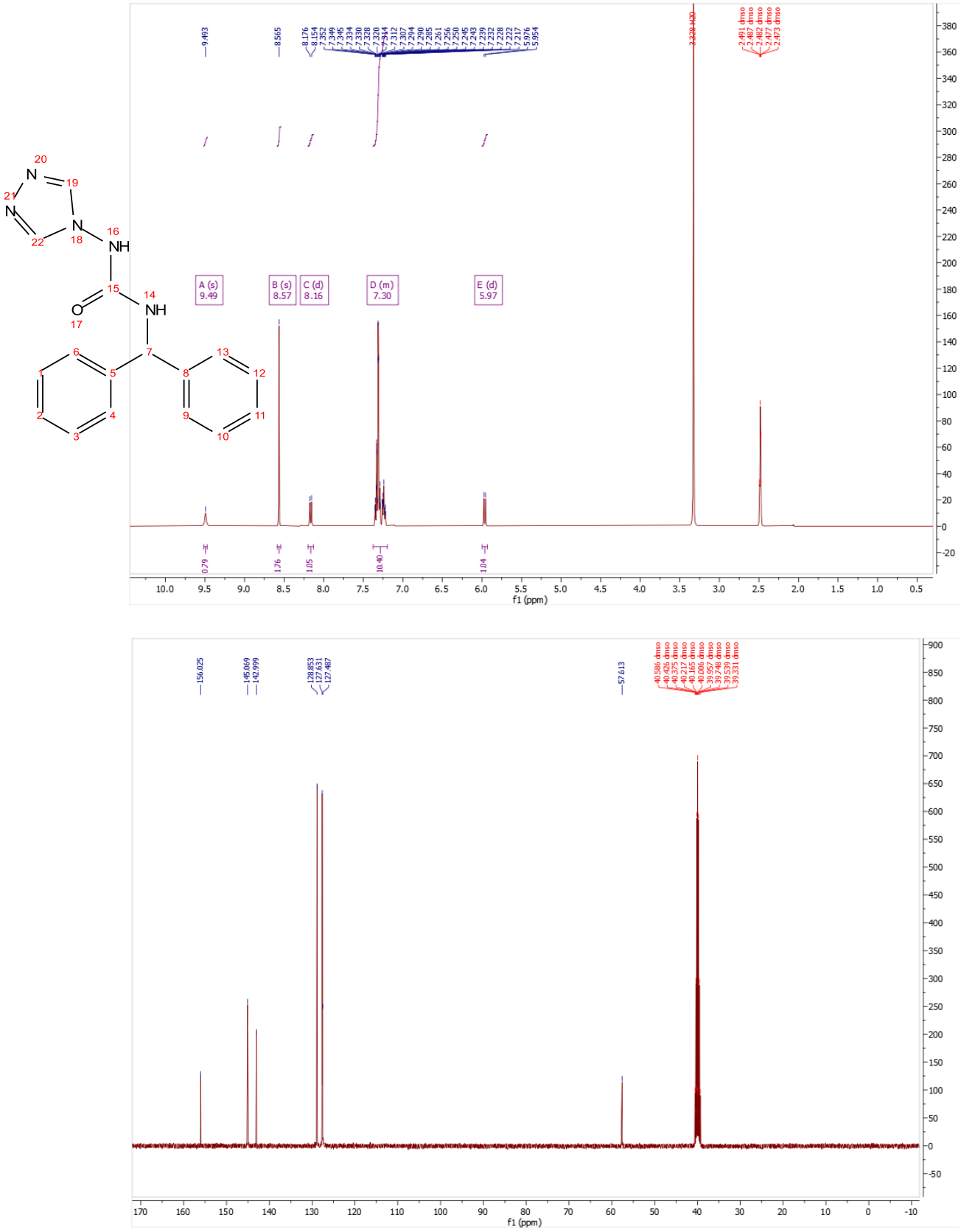

Figure 116. ^{1}H NMR (top, 400 MHz, DMSO-d_6) and ^{13}C NMR (bottom, 101 MHz, DMSO-d_6) for compound **MM96**.

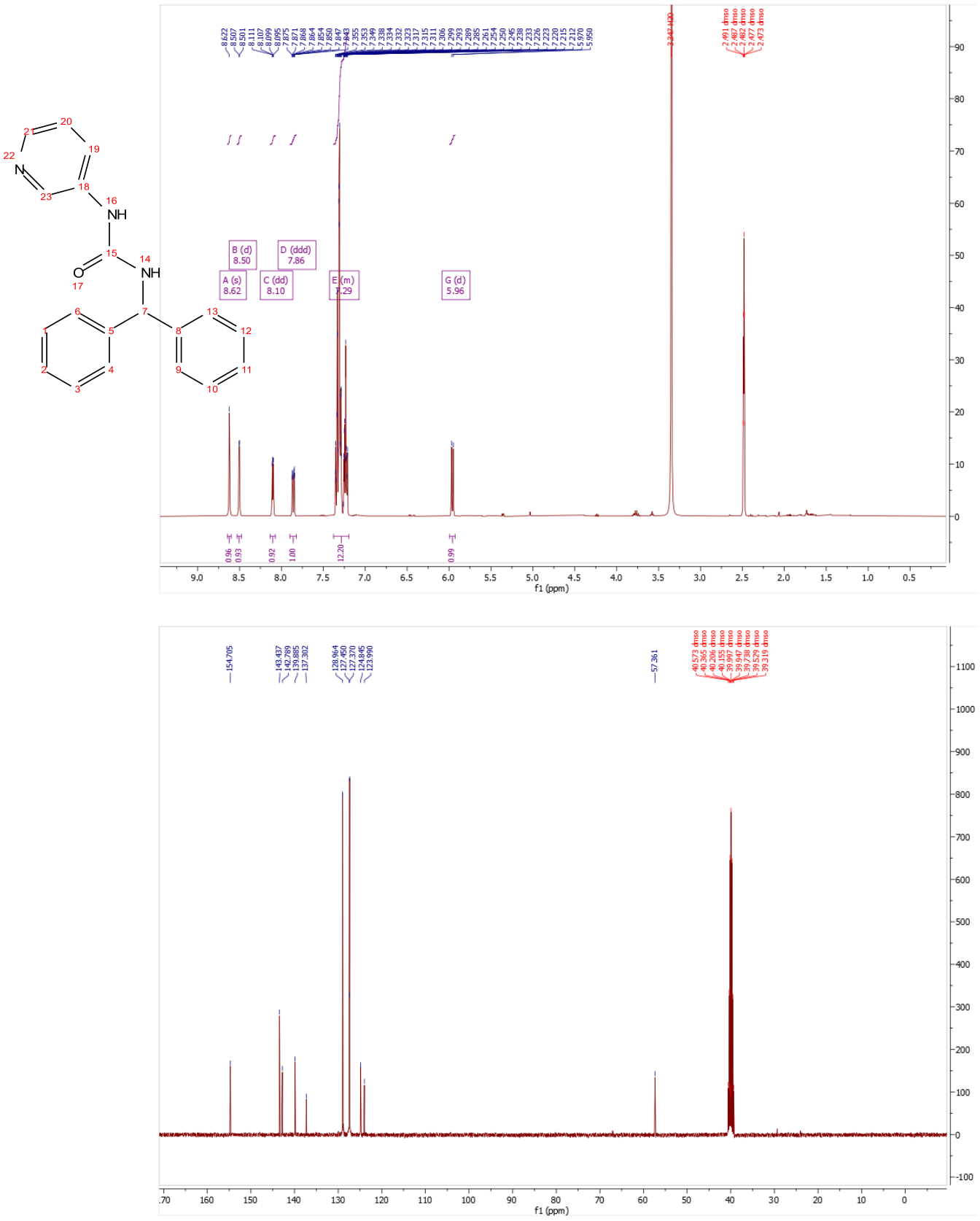

Figure 117. ^{1}H NMR (top, 400 MHz, DMSO-d_6) and ^{13}C NMR (bottom, 101 MHz, DMSO-d_6) for compound **MM97**.

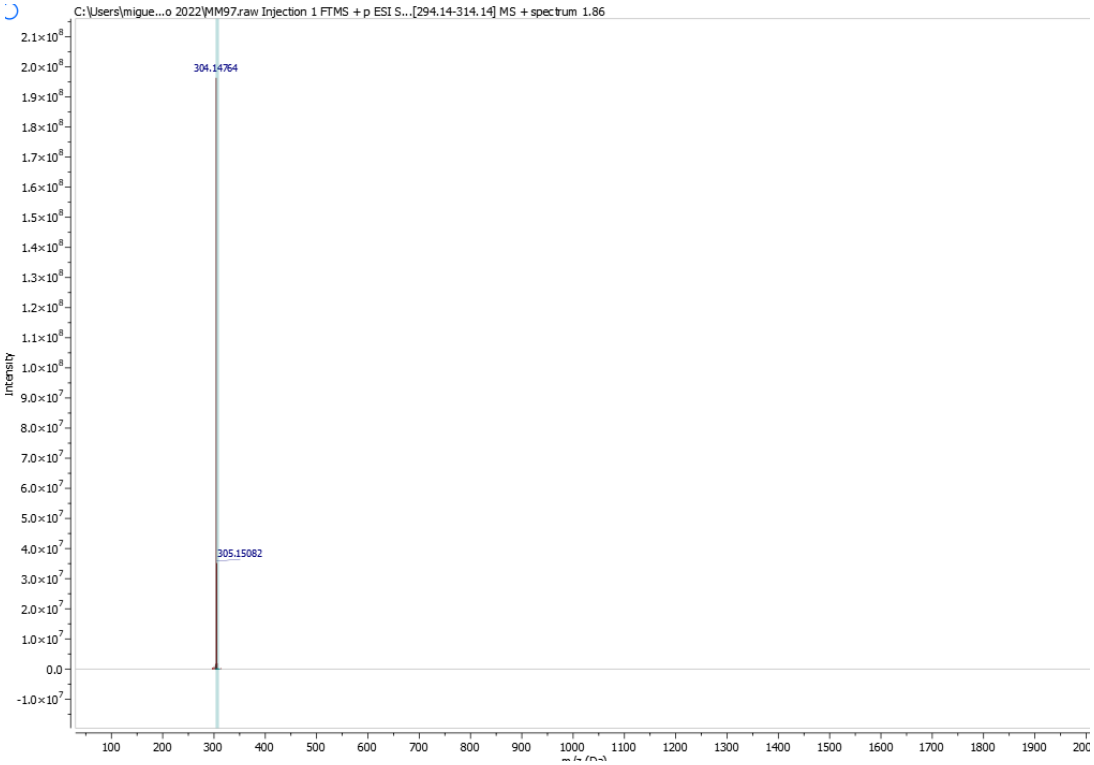

Meas. m/z	Formula	Adduct	Predicted m/z	Error [ppm]
304.14764	$C_{19}H_{17}N_3O$	H^+	304.14444	10.53

Figure 118. Electrospray ESI data for compound **MM97**.

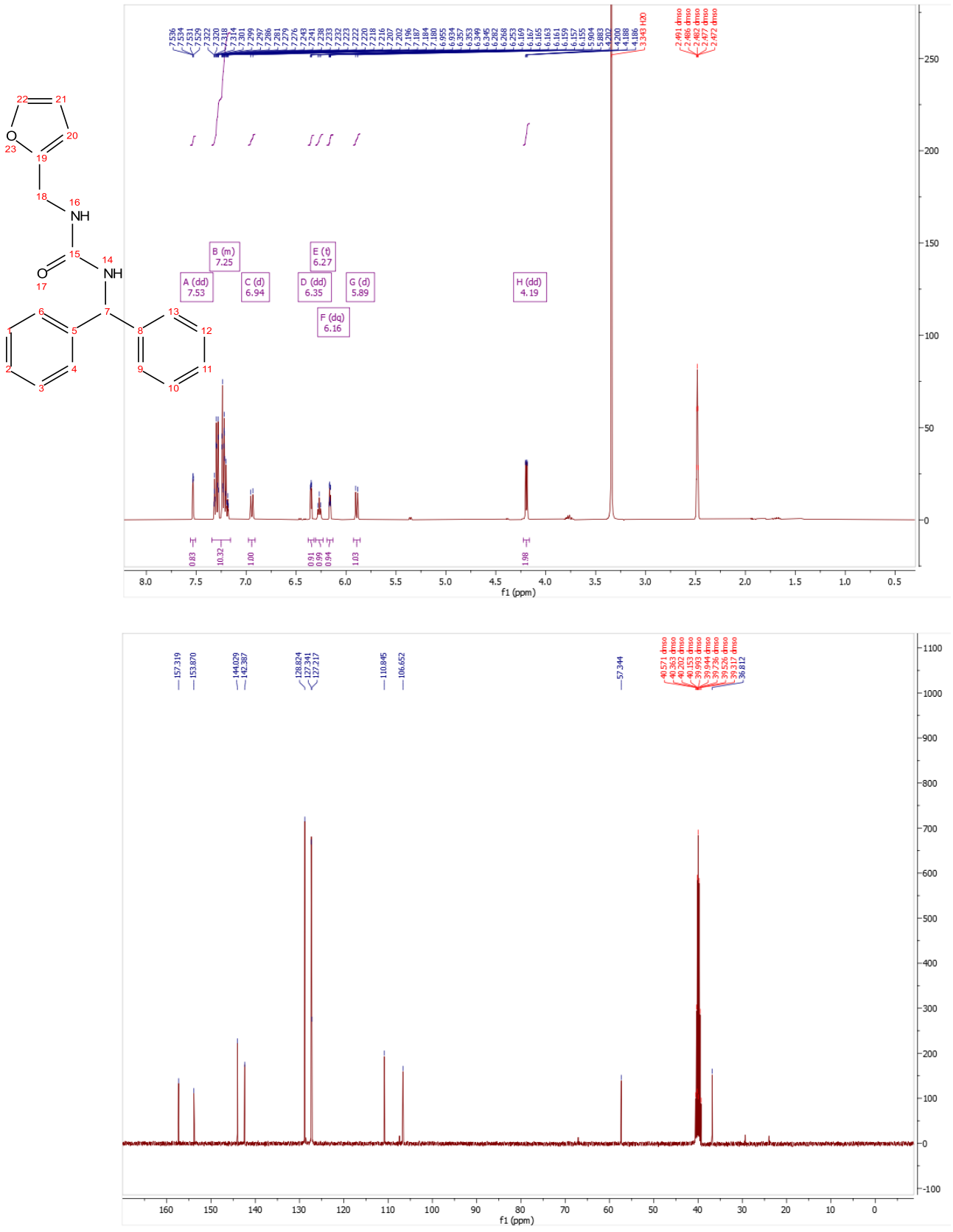

Figure 119. ^{1}H NMR (top, 400 MHz, DMSO-d_6) and ^{13}C NMR (bottom, 101 MHz, DMSO-d_6) for compound **MM98**.

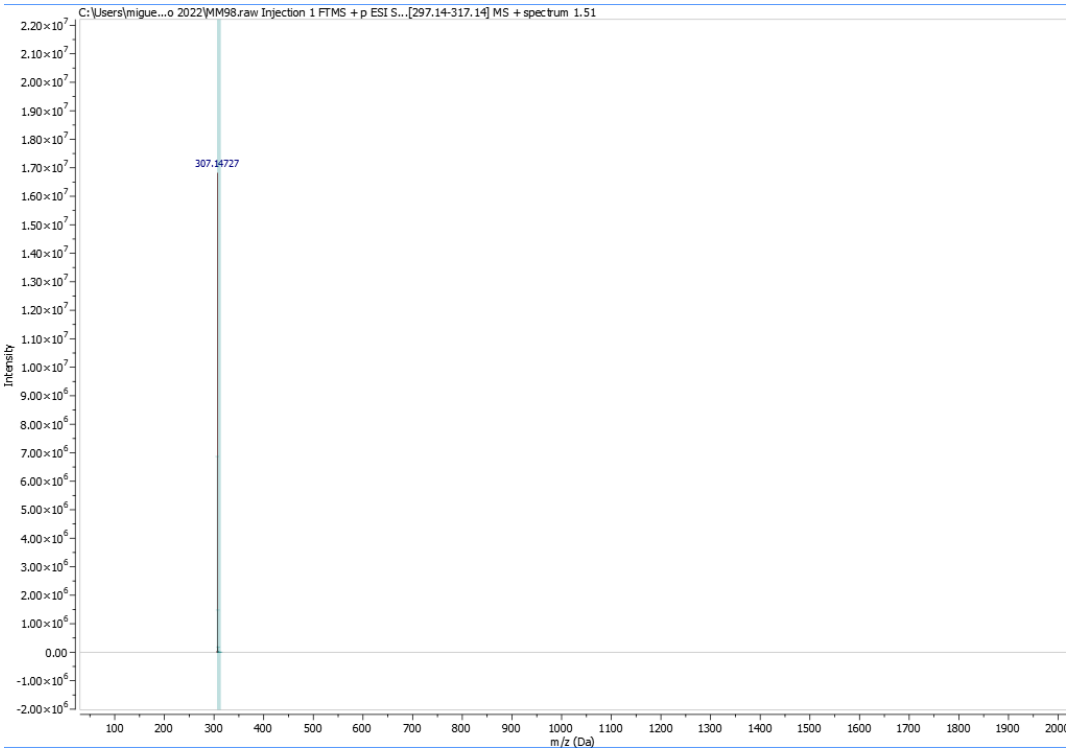

Meas. m/z	Formula	Adduct	Predicted m/z	Error [ppm]
307.14727	$C_{19}H_{18}N_2O_2$	H^+	307.14410	10.31

Figure 120. Electrospray ESI data for compound **MM98**.

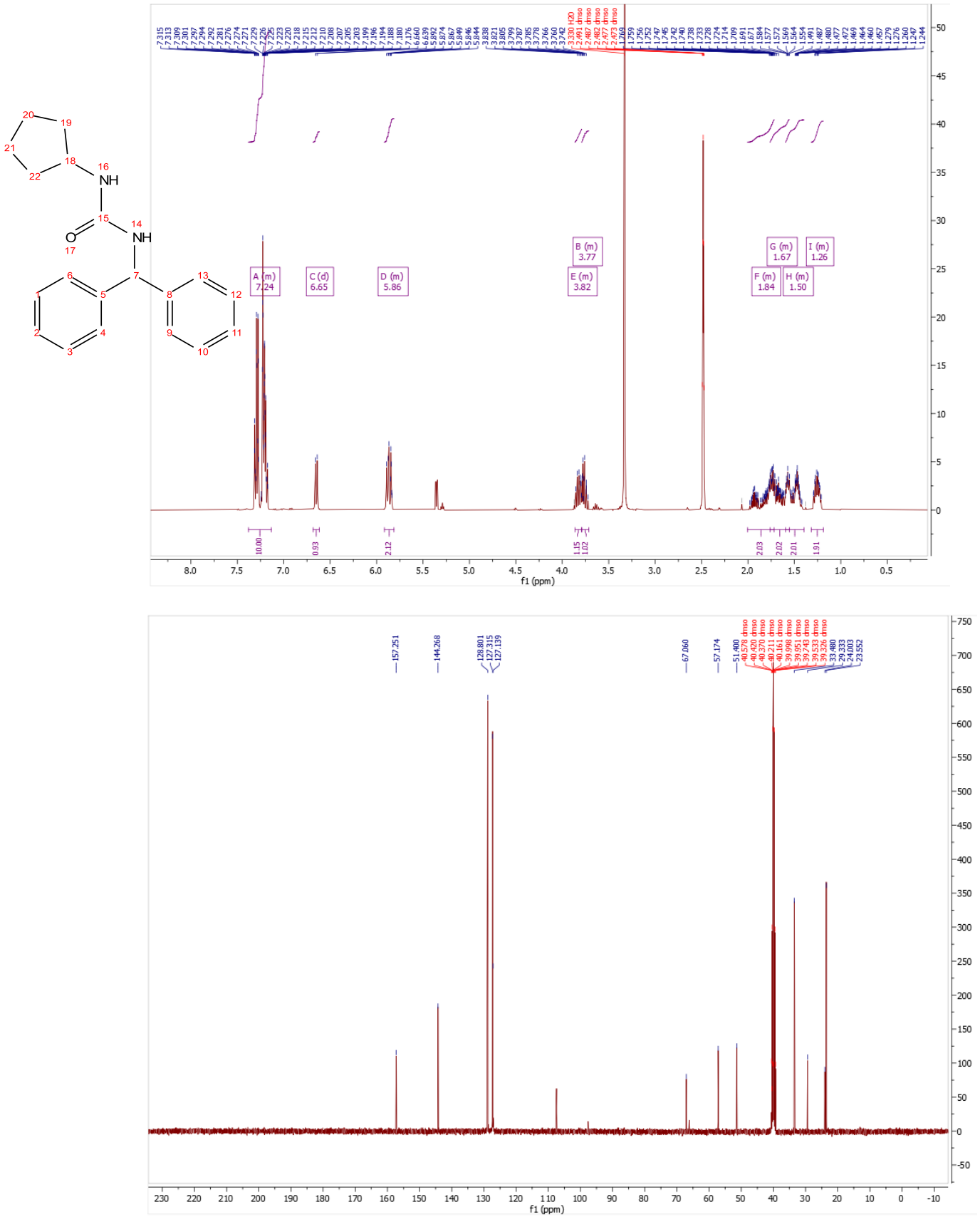

Figure 121. ^{1}H NMR (top, 400 MHz, DMSO-d_6) and ^{13}C NMR (bottom, 101 MHz, DMSO-d_6) for compound **MM99**.

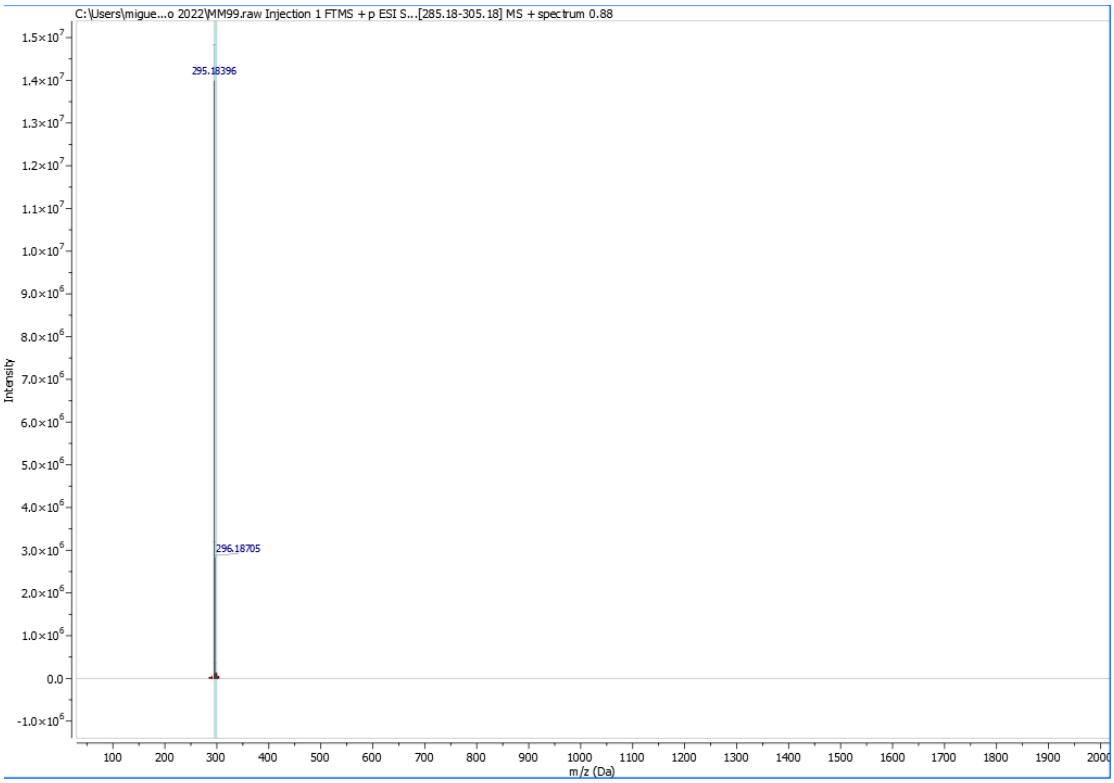

Meas. m/z	Formula	Adduct	Predicted m/z	Error [ppm]
295.18396	$C_{19}H_{22}N_2O$	H^+	295.18049	11.76

Figure 122. Electrospray ESI data for compound **MM99**.

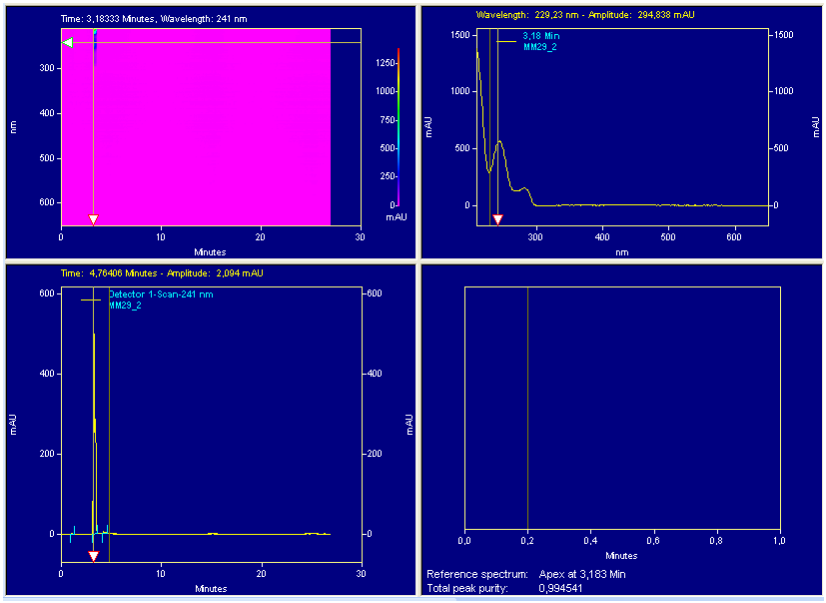

Figure 123. Chromatogram (HPLC) of compound **MM29**. Purity (% a/a): 98.7%.

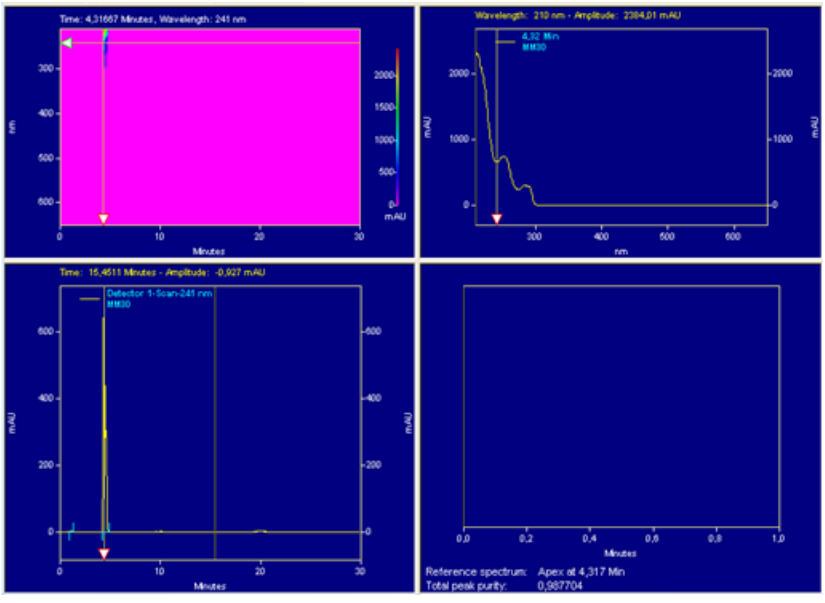

Figure 124. Chromatogram (HPLC) of compound **MM30**. Purity (% a/a): 98.7%.

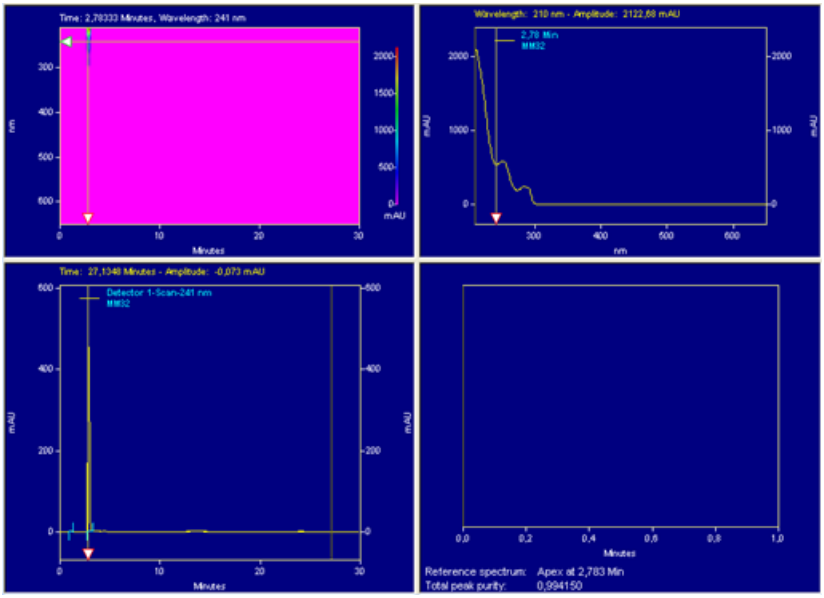

Figure 125. Chromatogram (HPLC) of compound **MM32**. Purity (% a/a): 99.7%.

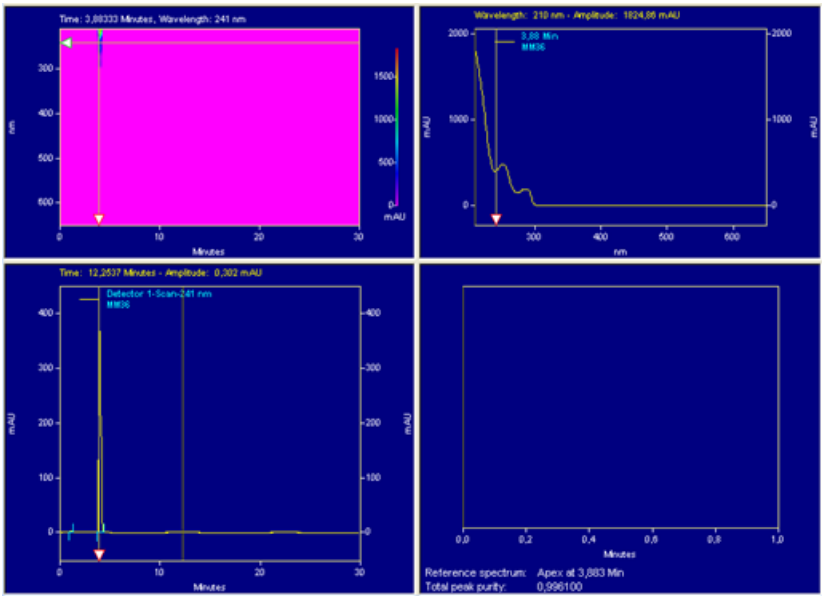

Figure 126. Chromatogram (HPLC) of compound **MM36**. Purity (% a/a): 99.5%.

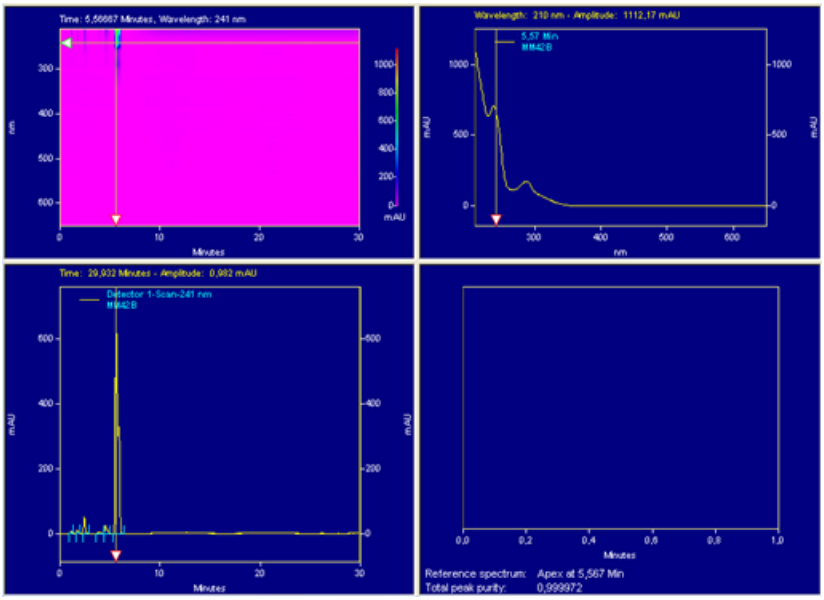

Figure 127. Chromatogram (HPLC) of compound **MM42B**. Purity (% a/a): 91.8%.

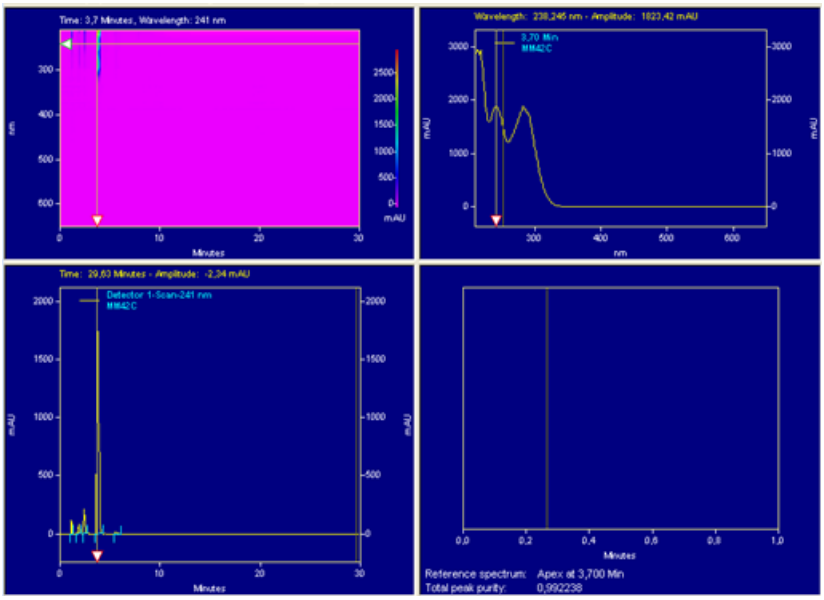

Figure 128. Chromatogram (HPLC) of compound **MM42C**. Purity (% a/a): 87.6%.

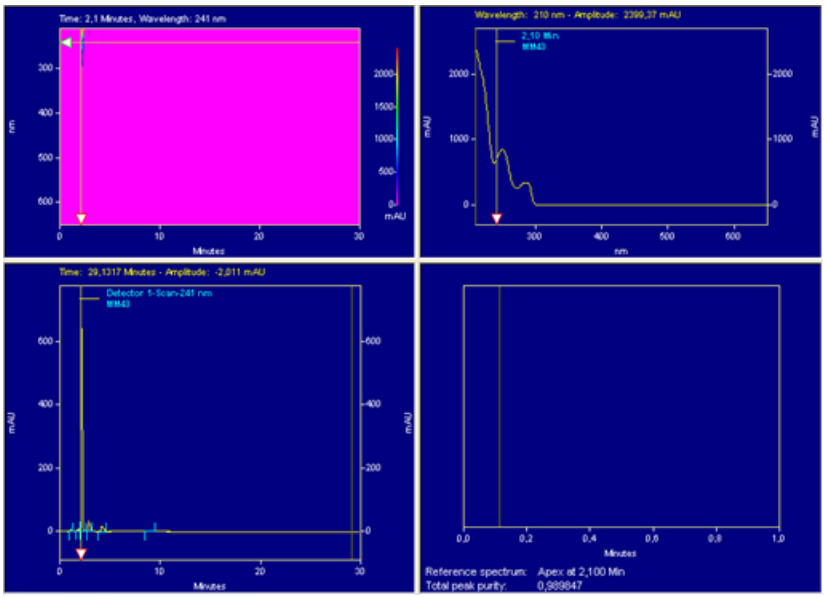

Figure 129. Chromatogram (HPLC) of compound **MM43**. Purity (% a/a): 87.6%.

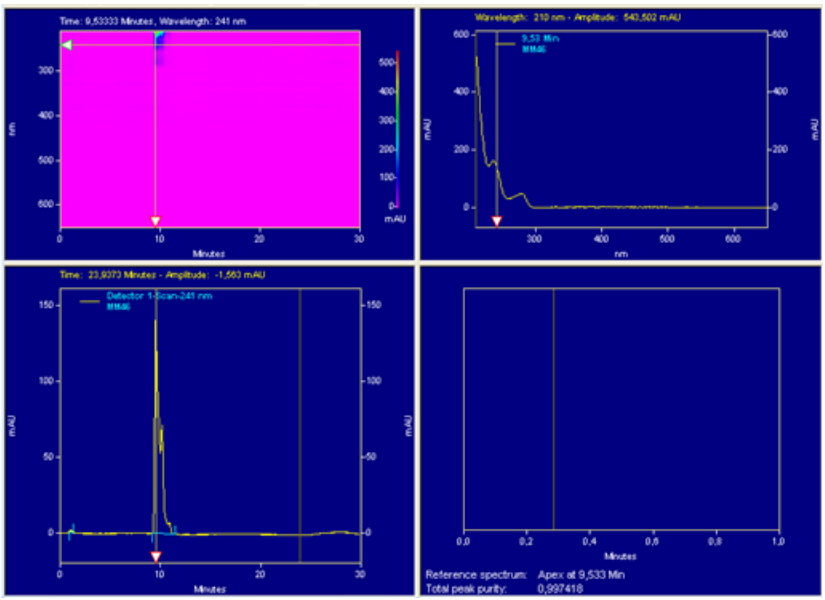

Figure 130. Chromatogram (HPLC) of compound **MM46**. Purity (% a/a): 99.7%.

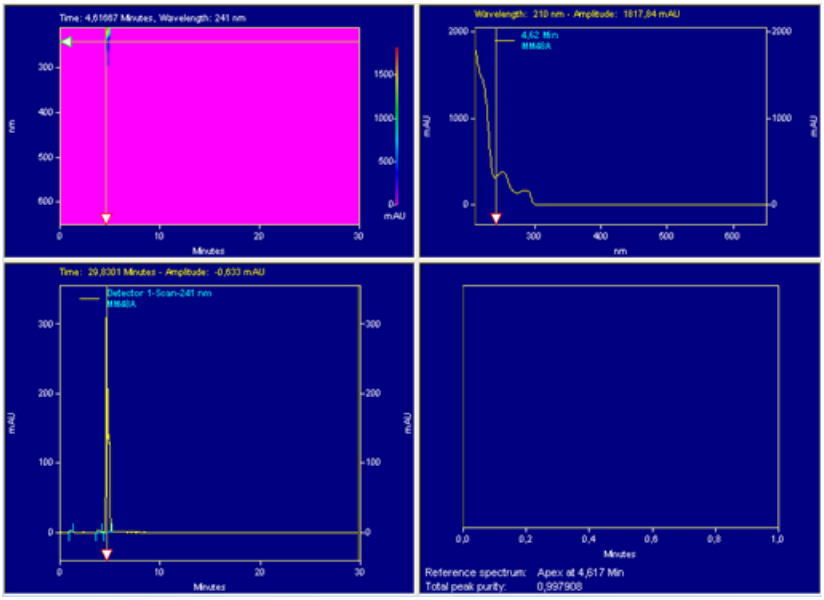

Figure 131. Chromatogram (HPLC) of compound **MM48A**. Purity (% a/a): 98.6%.

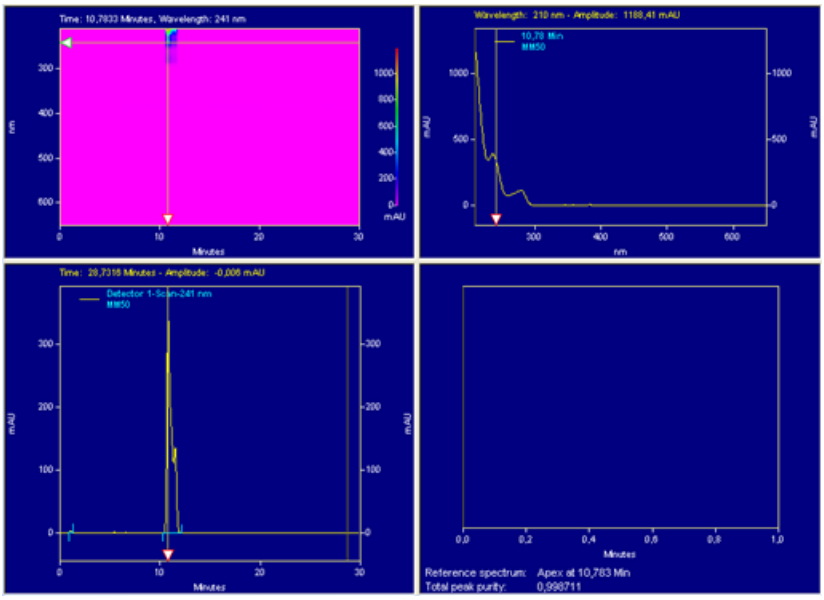

Figure 132. Chromatogram (HPLC) of compound **MM50**. Purity (% a/a): 99.9%.

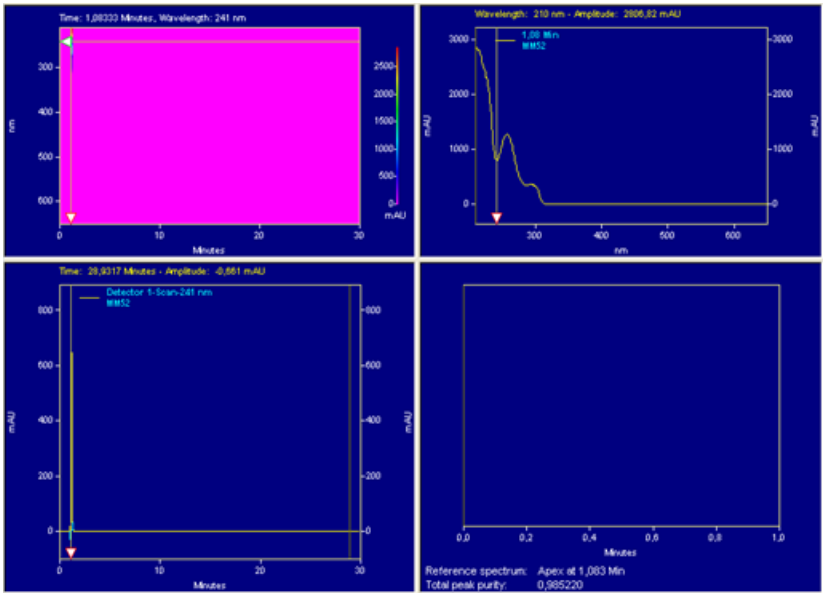

Figure 133. Chromatogram (HPLC) of compound **MM52**. Purity (% a/a): 100.0%.

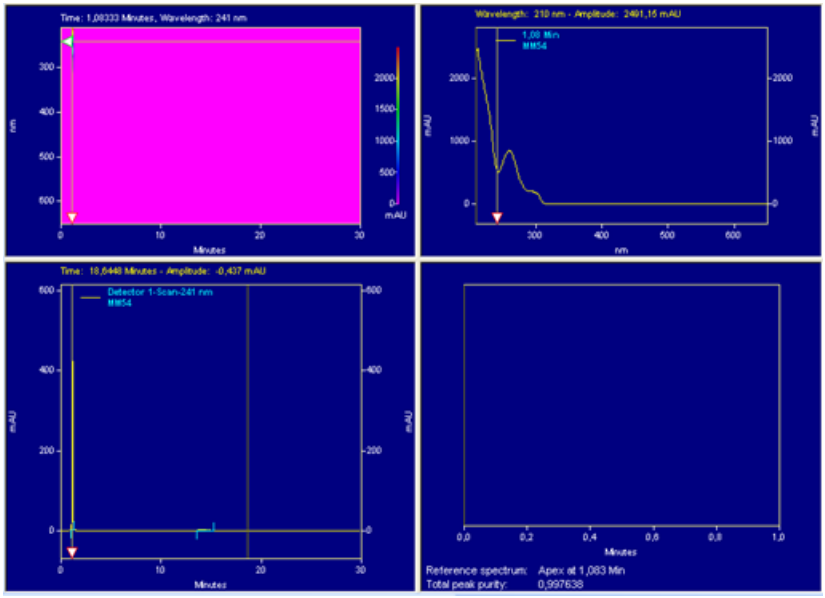

Figure 134. Chromatogram (HPLC) of compound **MM54**. Purity (% a/a): 97.0%.

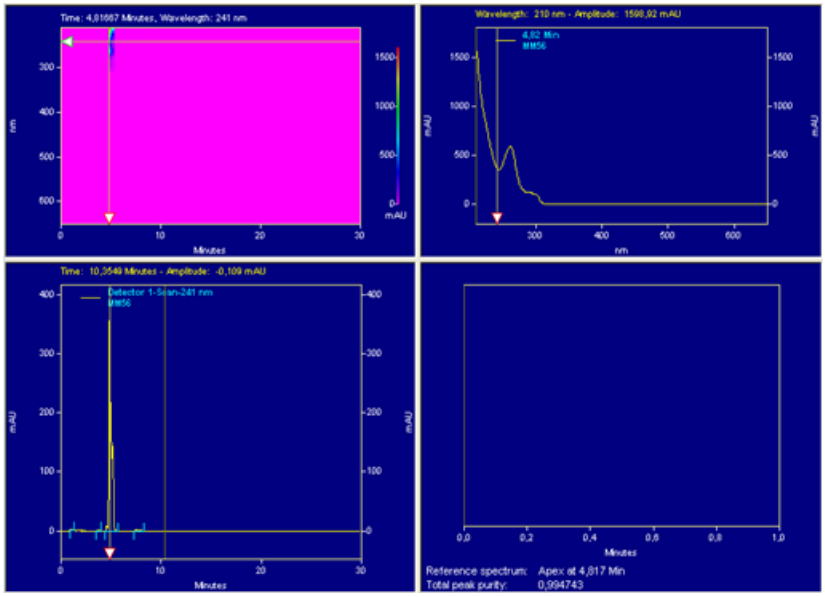

Figure 135. Chromatogram (HPLC) of compound **MM56**. Purity (% a/a): 98.5%.

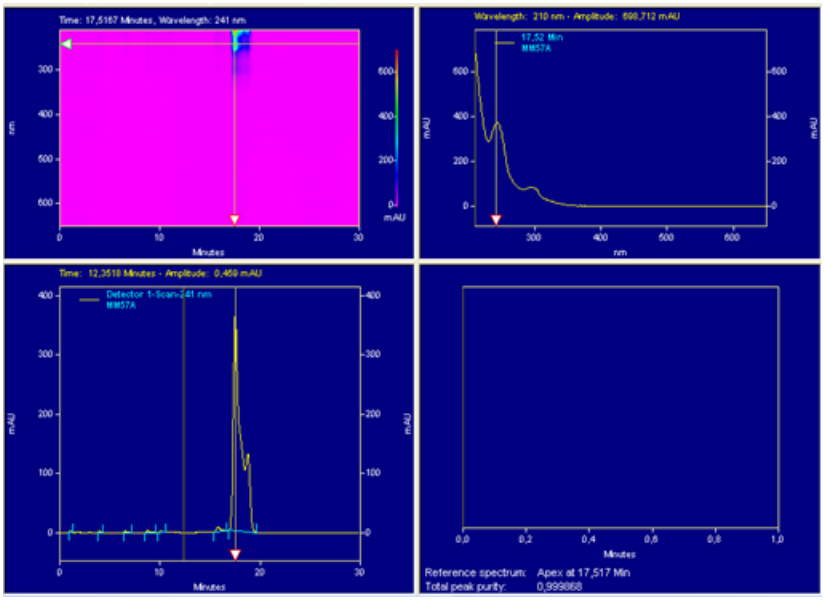

Figure 136. Chromatogram (HPLC) of compound **MM57A**. Purity (% a/a): 97.2%.

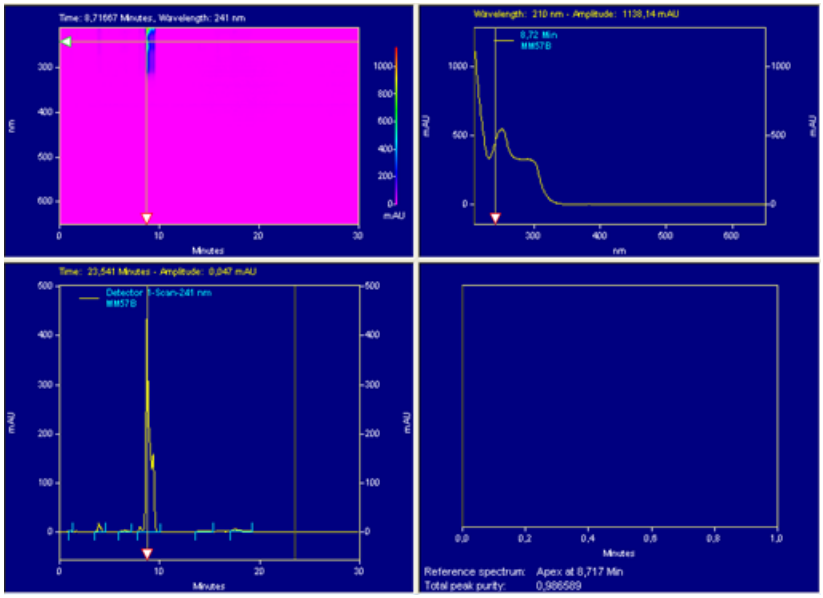

Figure 137. Chromatogram (HPLC) of compound **MM57B**. Purity (% a/a): 94.3%.

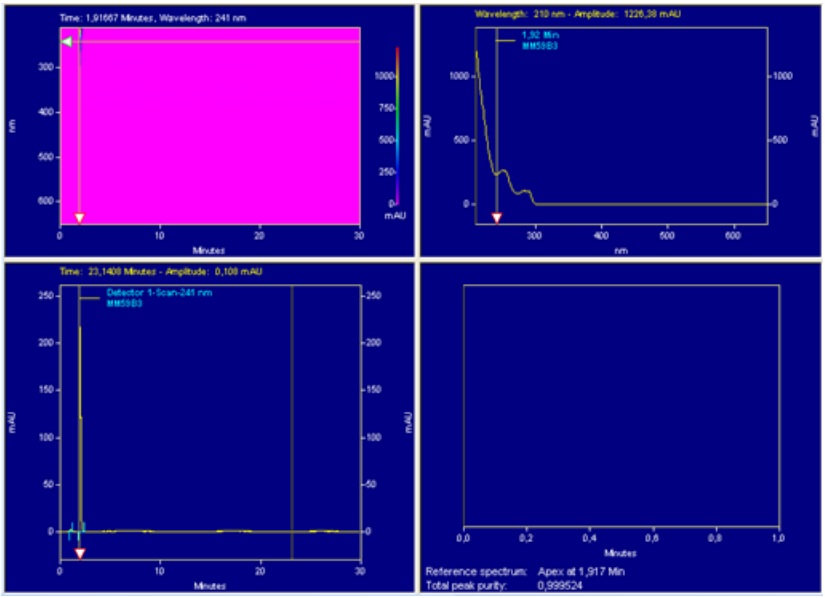

Figure 138. Chromatogram (HPLC) of compound **MM59B3**. Purity (% a/a): 99.1%.

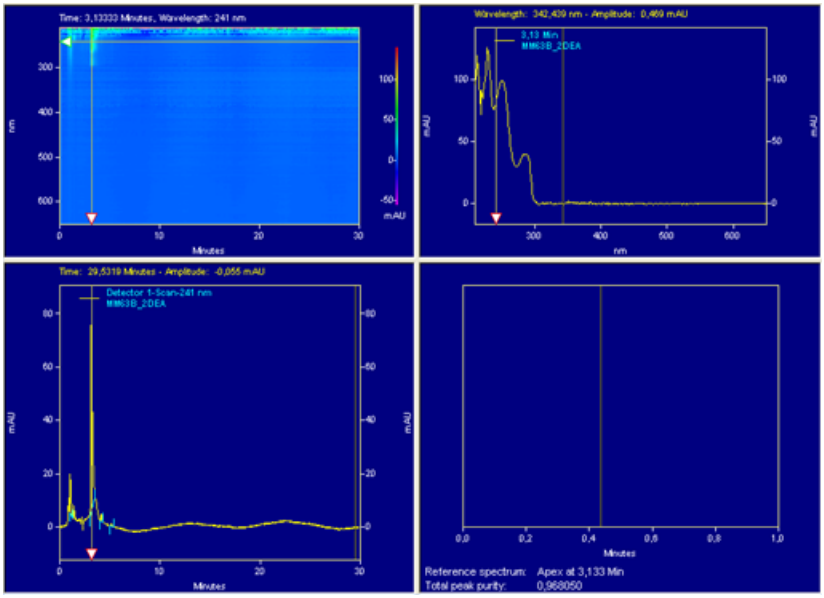

Figure 139. Chromatogram (HPLC) of compound **MM63B**. Purity (% a/a): 84.2%.

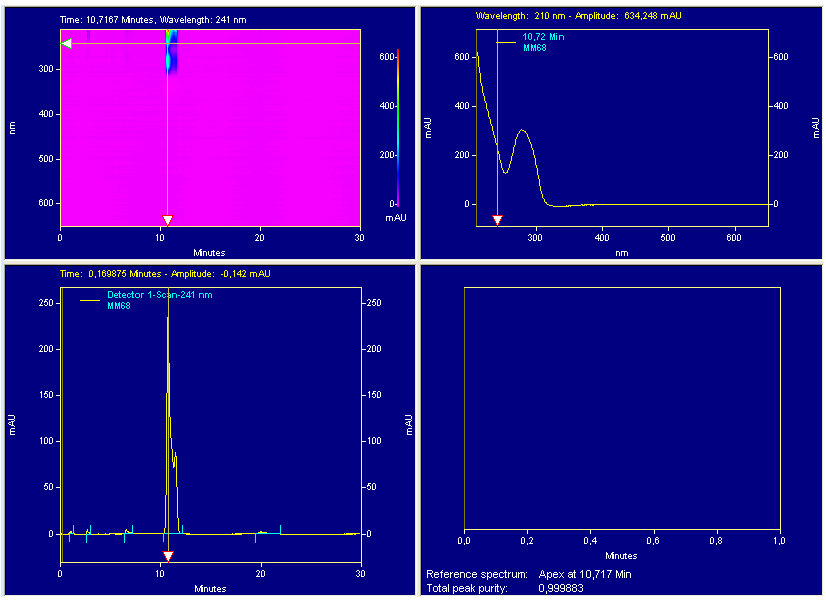

Figure 140. Chromatogram (HPLC) of compound **MM68**. Purity (% a/a): 96.7%.

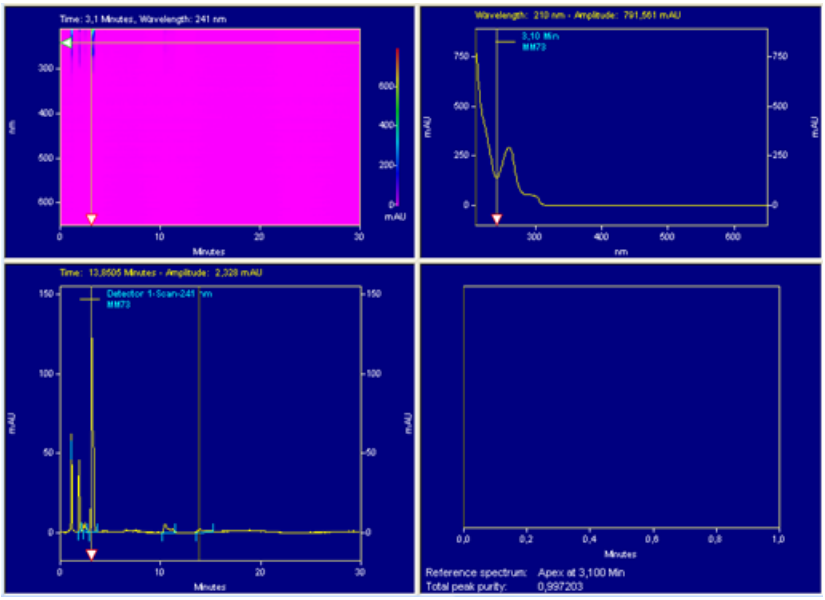

Figure 141. Chromatogram (HPLC) of compound **MM73**. Purity (% a/a): 69.12%.

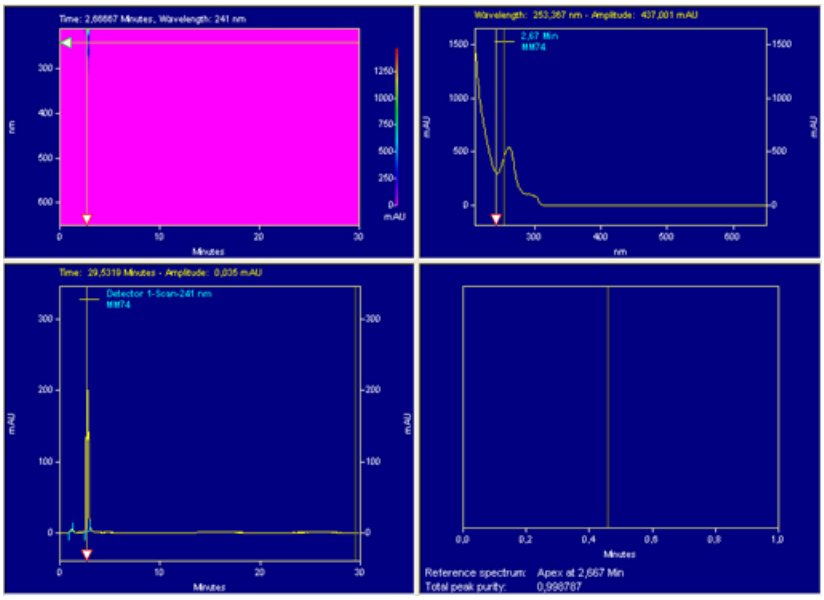

Figure 142. Chromatogram (HPLC) of compound **MM74**. Purity (% a/a): 98.8%.

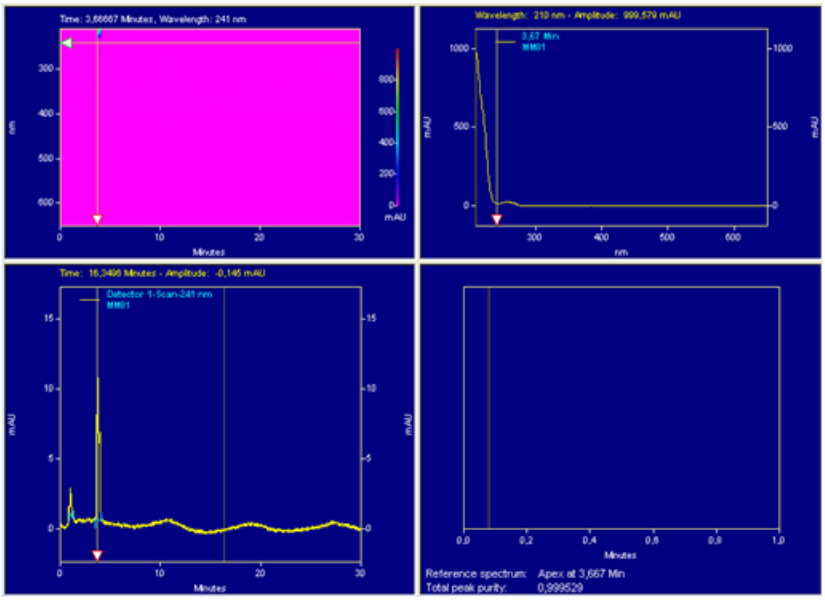

Figure 143. Chromatogram (HPLC) of compound **MM81**. Purity (% a/a): 90.9%. Peak purity index: 99.9 %.

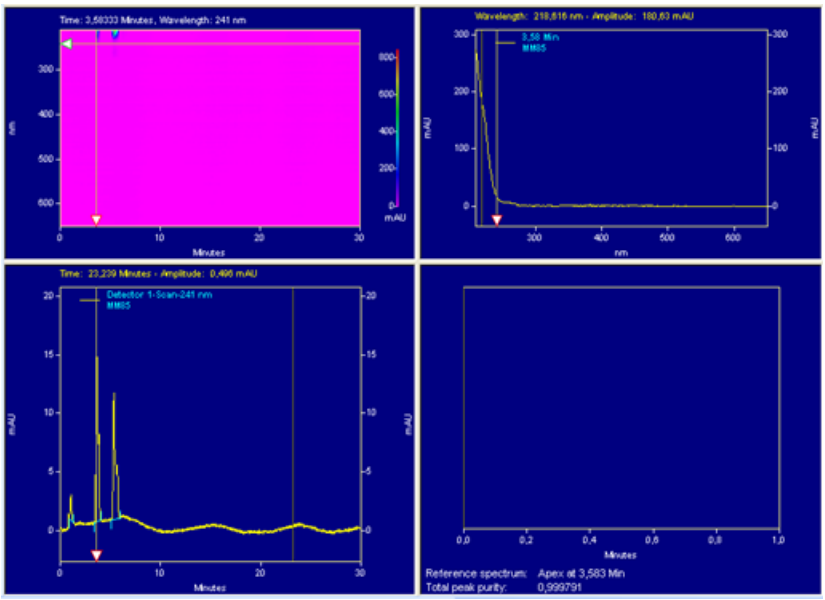

Figure 144. Chromatogram (HPLC) of compound **MM85**. Purity (% a/a): 49.5% (degradation occurred under HPLC procedure). Peak purity index: 99,9.

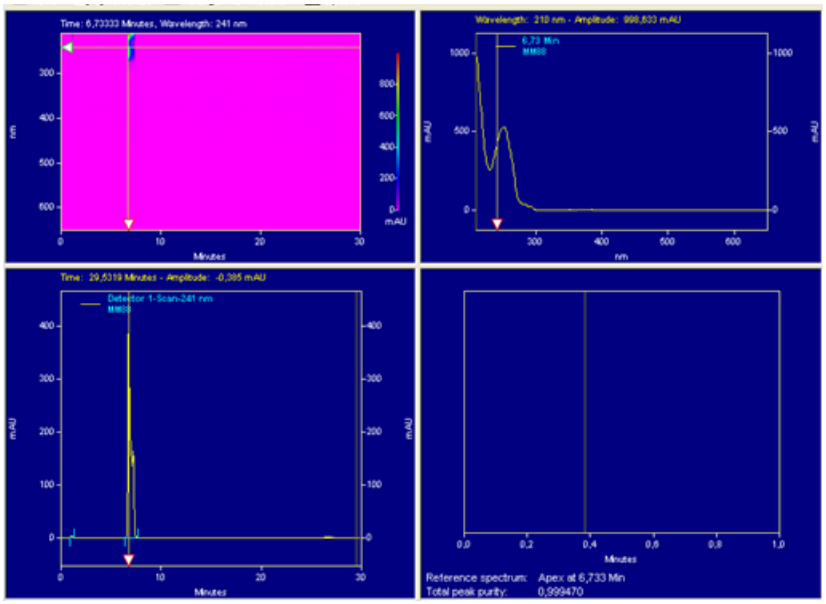

Figure 145. Chromatogram (HPLC) of compound **MM88**. Purity (% a/a): 99.7%. Peak purity index: 99.9 %.

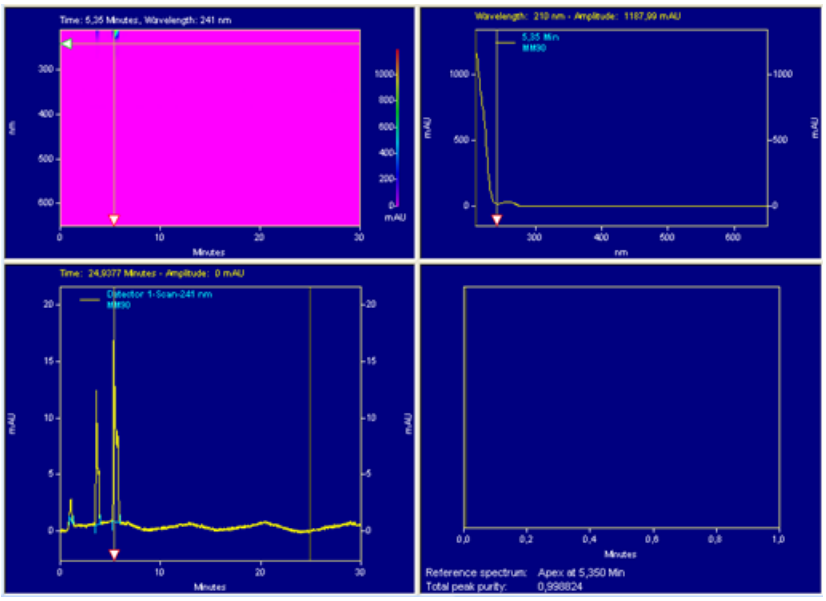

Figure 146. Chromatogram (HPLC) of compound **MM90**. Purity (% a/a): 66.9% (degradation occurred under HPLC procedure). Peak purity index: 99.8 %.

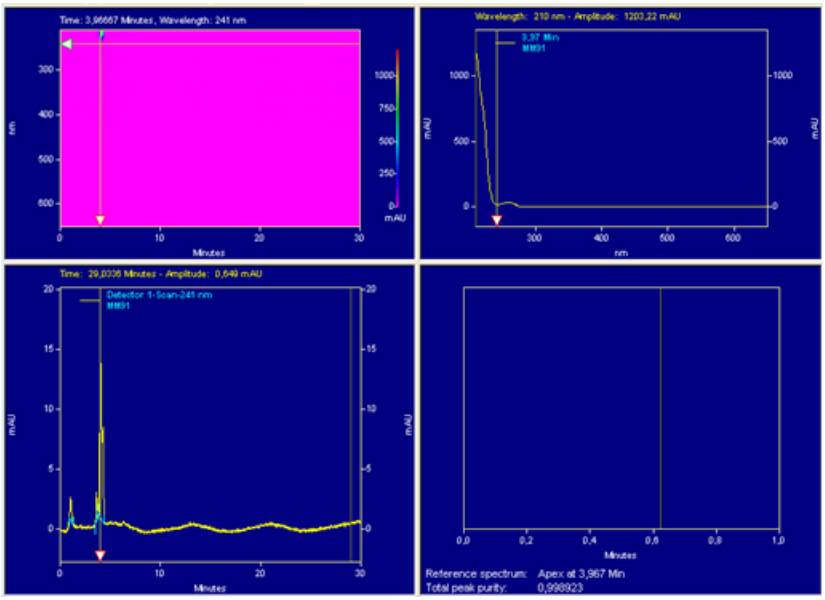

Figure 147. Chromatogram (HPLC) of compound **MM91**. Purity (% a/a): 85.9% (degradation occurred under HPLC procedure). Peak purity index: 99.8 %.

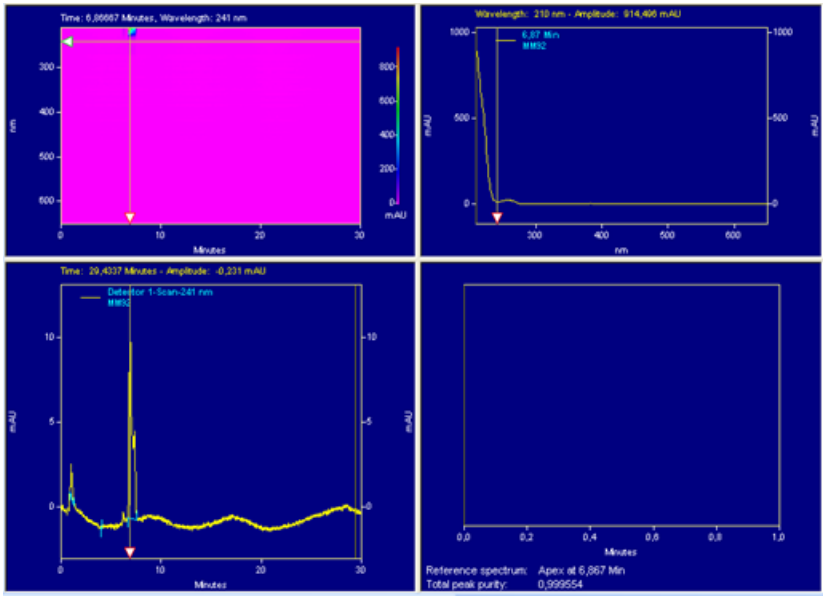

Figure 148. Chromatogram (HPLC) of compound **MM92**. Purity (% a/a): 94.1%. Peak purity index: 99.9 %.

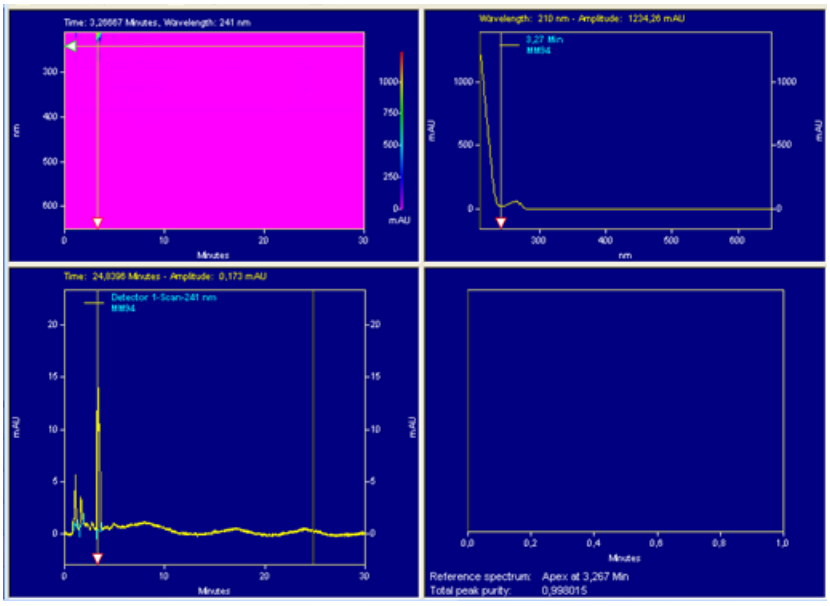

Figure 149. Chromatogram (HPLC) of compound **MM94**. Purity (% a/a): 80.8%. Peak purity index: 99.8 %.

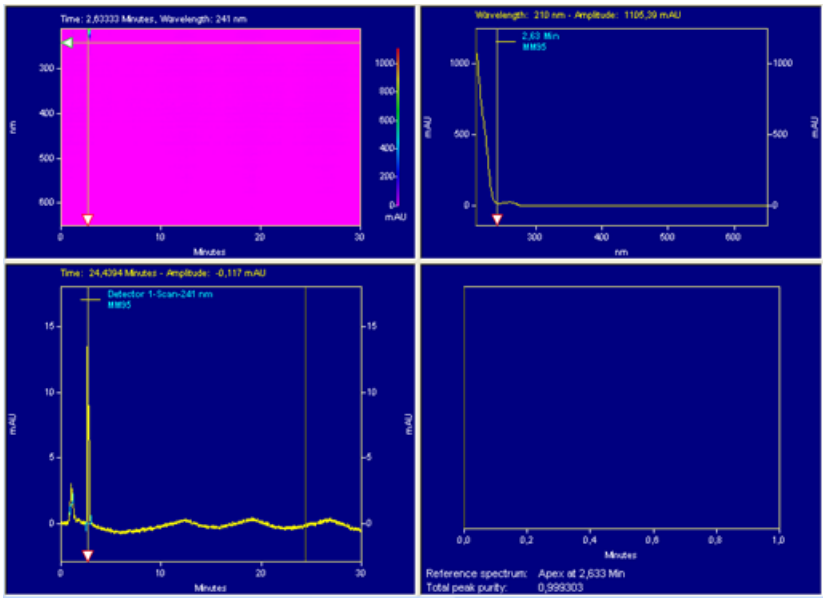

Figure 150. Chromatogram (HPLC) of compound **MM95**. Purity (% a/a): 92.8%. Peak purity index: 99.9 %.

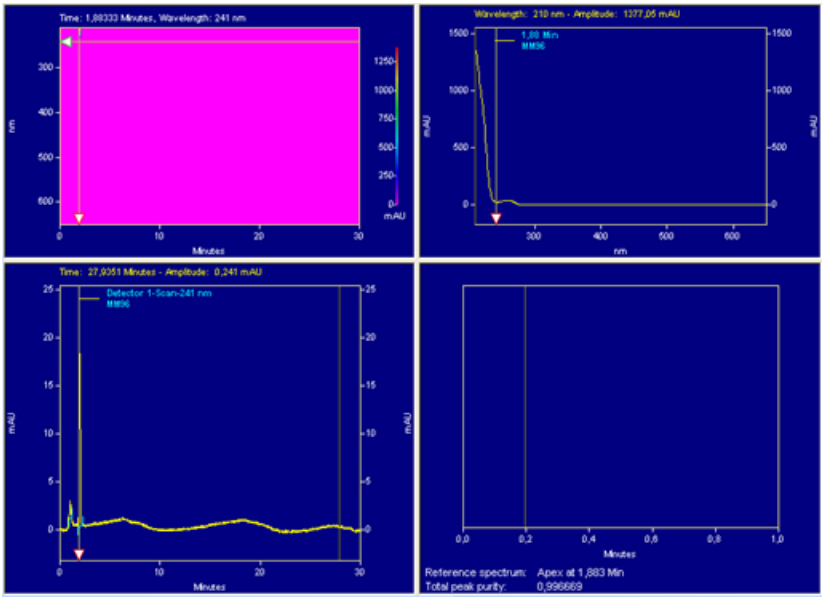

Figure 151. Chromatogram (HPLC) of compound **MM96**. Purity (% a/a): 99.6%. Peak purity index: 93.01 %.

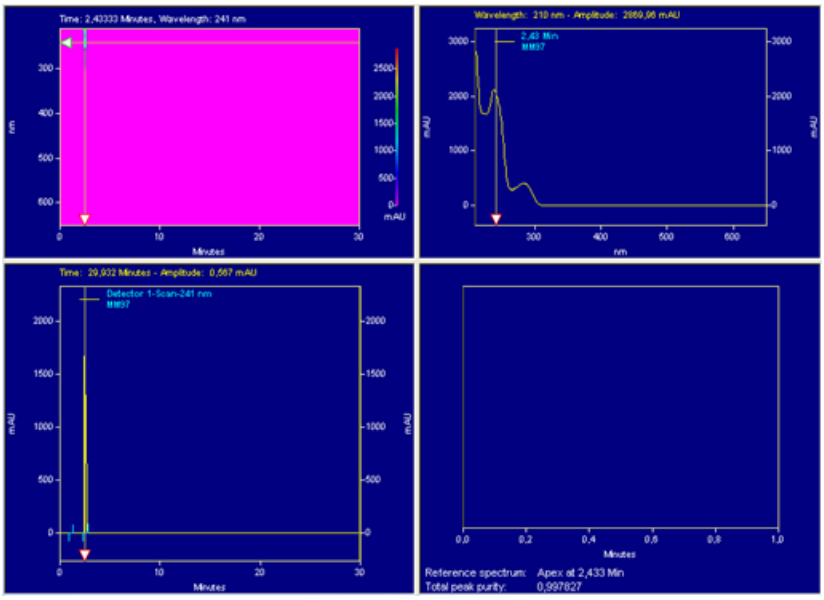

Figure 152. Chromatogram (HPLC) of compound **MM97**. Purity (% a/a): 99.8%. Peak purity index: 99.7 %.

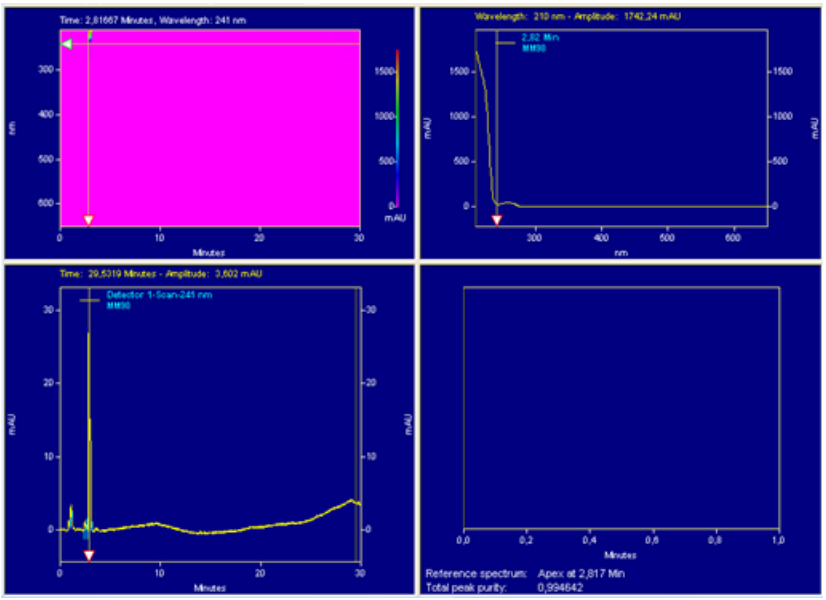

Figure 153. Chromatogram (HPLC) of compound **MM98**. Purity (% a/a): 92.9%. Peak purity index: 99.x4 %.

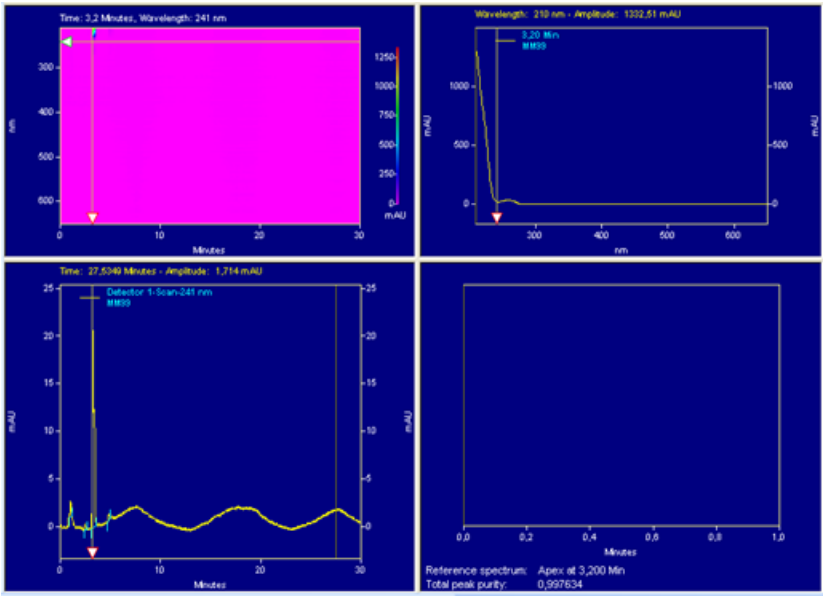

Figure 154. Chromatogram (HPLC) of compound **MM99**. Purity (% a/a): 91.3%. Peak purity index: 99.7 %.

Annex II - Chemical structures of the investigated compounds

Structure	Compound name	Chapter		
		2	3	4
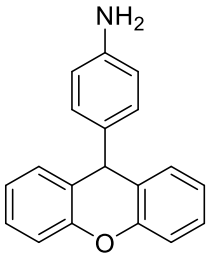 4-(9*H*-xanthen-9-yl)aniline Chemical Formula: $C_{19}H_{15}NO$ Molecular Weight: 273,34	**MM7**	X	X	X
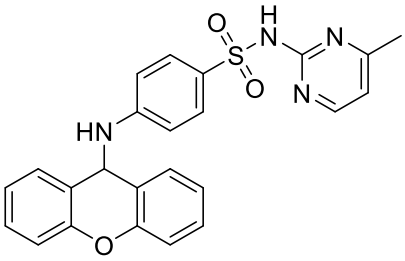 4-((9*H*-xanthen-9-yl)amino)-*N*-(4-methylpyrimidin-2-yl)benzenesulfonamide Chemical Formula: $C_{24}H_{20}N_4O_3S$ Molecular Weight: 444,51	**MM16**	X		
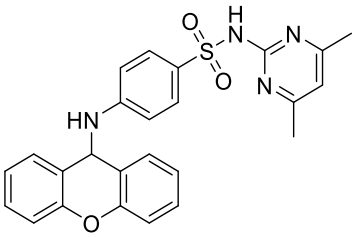 4-((9*H*-xanthen-9-yl)amino)-*N*-(4,6-dimethylpyrimidin-2-yl)benzenesulfonamide Chemical Formula: $C_{25}H_{22}N_4O_3S$ Molecular Weight: 458,54	**MM17**	X		

Structure	Compound name	Chapter		
		2	3	4
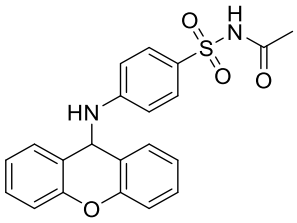 *N*-((4-((9*H*-xanthen-9-yl)amino)phenyl)sulfonyl)acetamide Chemical Formula: $C_{21}H_{18}N_2O_4S$ Molecular Weight: 394,45	**MM18**	X		
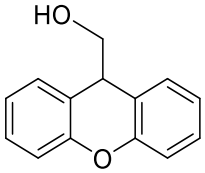 (9*H*-xanthen-9-yl)methanol Chemical Formula: $C_{14}H_{12}O_2$ Molecular Weight: 212,25	**MM29**		X	X
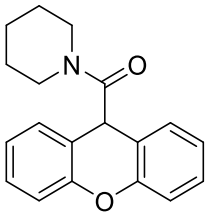 piperidin-1-yl(9*H*-xanthen-9-yl)methanone Chemical Formula: $C_{19}H_{19}NO_2$ Molecular Weight: 293,37	**MM30**		X	X

Structure	Compound name	Chapter		
		2	3	4
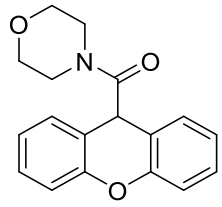 morpholino(9*H*-xanthen-9-yl)methanone Chemical Formula: $C_{18}H_{17}NO_3$ Molecular Weight: 295,34	**MM32**		x	X
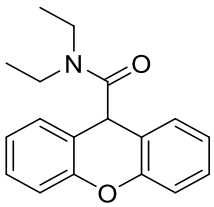 *N*,*N*-diethyl-9*H*-xanthene-9-carboxamide Chemical Formula: $C_{18}H_{19}NO_2$ Molecular Weight: 281,36	**MM36**		X	X
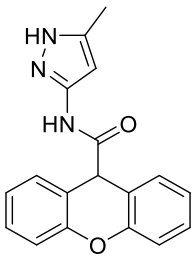 *N*-(5-methyl-1*H*-pyrazol-3-yl)-9*H*-xanthene-9-carboxamide Chemical Formula: $C_{18}H_{15}N_3O_2$ Molecular Weight: 305,34	**MM42B**		X	X

Structure	Compound name	Chapter		
		2	3	4
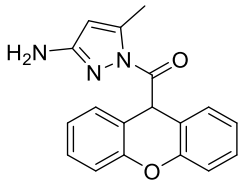 (3-amino-5-methyl-1*H*-pyrazol-1-yl)(9*H*-xanthen-9-yl)methanone Chemical Formula: $C_{18}H_{15}N_3O_2$ Molecular Weight: 305,34	**MM42C**		X	X
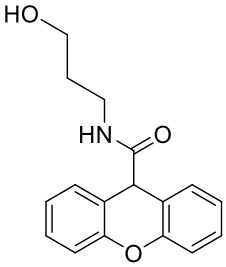 *N*-(3-hydroxypropyl)-9*H*-xanthene-9-carboxamide Chemical Formula: $C_{17}H_{17}NO_3$ Molecular Weight: 283,33	**MM43**		X	X
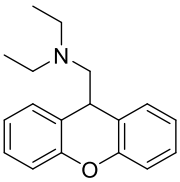 *N*-((9*H*-xanthen-9-yl)methyl)-*N*-ethylethanamine Chemical Formula: $C_{18}H_{21}NO$ Molecular Weight: 267,37	**MM46**		X	X

Structure	Compound name	Chapter		
		2	3	4
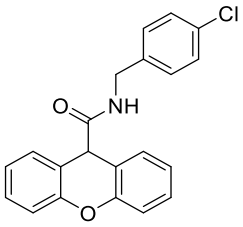 *N*-(4-chlorobenzyl)-9*H*-xanthene-9-carboxamide Chemical Formula: $C_{21}H_{16}ClNO_2$ Molecular Weight: 349,81	**MM48A**		X	X
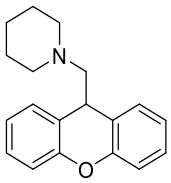 1-((9*H*-xanthen-9-yl)methyl)piperidine Chemical Formula: $C_{19}H_{21}NO$ Molecular Weight: 279,38	**MM50**		X	X
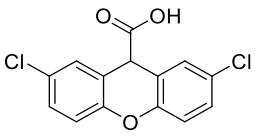 2,7-dichloro-9*H*-xanthene-9-carboxylic acid Chemical Formula: $C_{14}H_8Cl_2O_3$ Molecular Weight: 295,12	**MM52**		X	X

Structure	Compound name	Chapter		
		2	3	4
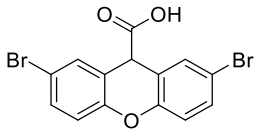 2,7-dibromo-9*H*-xanthene-9-carboxylic acid Chemical Formula: $C_{14}H_8Br_2O_3$ Molecular Weight: 384,02	**MM54**		X	X
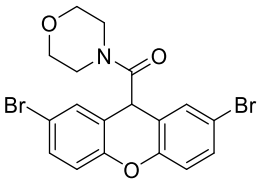 (2,7-dibromo-9*H*-xanthen-9-yl)(morpholino)methanone Chemical Formula: $C_{18}H_{15}Br_2NO_3$ Molecular Weight: 453,13	**MM56B**		X	X
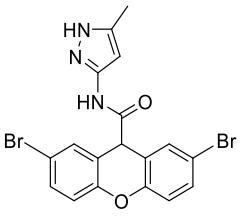 2,7-dibromo-*N*-(5-methyl-1*H*-pyrazol-3-yl)-9*H*-xanthene-9-carboxamide Chemical Formula: $C_{18}H_{13}Br_2N_3O_2$ Molecular Weight: 463,13	**MM57A**		X	X

Structure	Compound name	Chapter		
		2	3	4
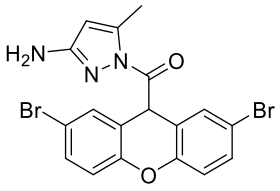 (3-amino-5-methyl-1*H*-pyrazol-1-yl)(2,7-dibromo-9*H*-xanthen-9-yl)methanone Chemical Formula: $C_{18}H_{13}Br_2N_3O_2$ Molecular Weight: 463,13	**MM57B**		X	X
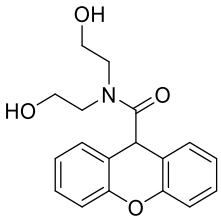 *N*,*N*-bis(2-hydroxyethyl)-9*H*-xanthene-9-carboxamide Chemical Formula: $C_{18}H_{19}NO_4$ Molecular Weight: 313,35	**MM59B3**		X	X
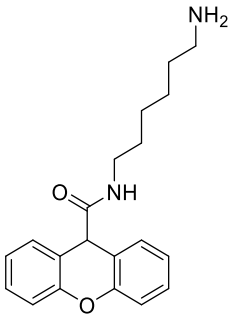 *N*-(6-aminohexyl)-9*H*-xanthene-9-carboxamide Chemical Formula: $C_{20}H_{24}N_2O_2$ Molecular Weight: 324,42	**MM63B**		X	X

Structure	Compound name	Chapter		
		2	3	4
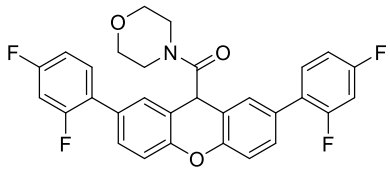 (2,7-bis(2,4-difluorophenyl)-9*H*-xanthen-9-yl)(morpholino)methanone Chemical Formula: $C_{30}H_{21}F_4NO_3$ Molecular Weight: 519,50	**MM68**		X	X
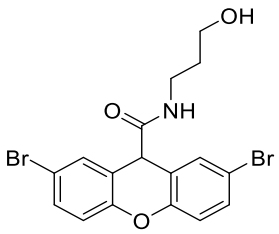 2,7-dibromo-*N*-(3-hydroxypropyl)-9*H*-xanthene-9-carboxamide Chemical Formula: $C_{17}H_{15}Br_2NO_3$ Molecular Weight: 441,12	**MM73**		X	X
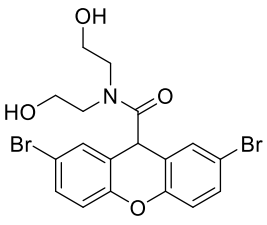 2,7-dibromo-*N*,*N*-bis(2-hydroxyethyl)-9*H*-xanthene-9-carboxamide Chemical Formula: $C_{18}H_{17}Br_2NO_4$ Molecular Weight: 471,15	**MM74**		X	X

Structure	Compound name	Chapter		
		2	3	4
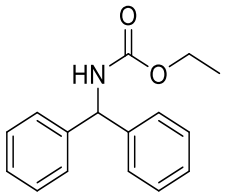 ethyl benzhydrylcarbamate Chemical Formula: $C_{16}H_{17}NO_2$ Molecular Weight: 255,32	**MM81**			X
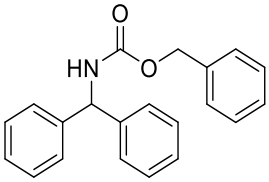 benzyl benzhydrylcarbamate Chemical Formula: $C_{21}H_{19}NO_2$ Molecular Weight: 317,39	**MM85**			X
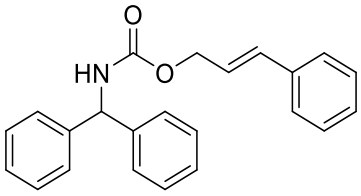 cinnamyl benzhydrylcarbamate Chemical Formula: $C_{23}H_{21}NO_2$ Molecular Weight: 343,43	**MM88**			X

Structure	Compound name	Chapter		
		2	3	4
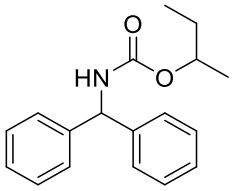 *sec*-butyl benzhydrylcarbamate Chemical Formula: $C_{18}H_{21}NO_2$ Molecular Weight: 283,37	**MM90**			X
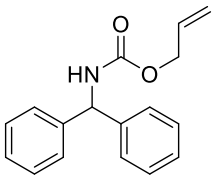 allyl benzhydrylcarbamate Chemical Formula: $C_{17}H_{17}NO_2$ Molecular Weight: 267,33	**MM91**			X
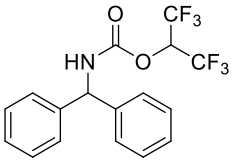 1,1,1,3,3,3-hexafluoropropan-2-yl benzhydrylcarbamate Chemical Formula: $C_{17}H_{13}F_6NO_2$ Molecular Weight: 377,29	**MM92**			X

Structure	Compound name	Chapter		
		2	3	4
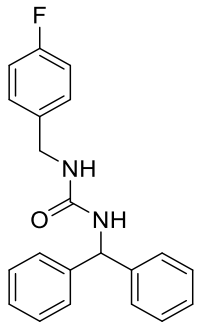 1-benzhydryl-3-(4-fluorobenzyl)urea Chemical Formula: $C_{21}H_{19}FN_2O$ Molecular Weight: 334,39	**MM94**			X
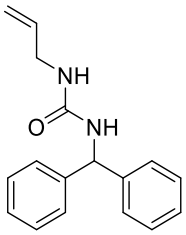 1-allyl-3-benzhydrylurea Chemical Formula: $C_{17}H_{18}N_2O$ Molecular Weight: 266,34	**MM95**			X
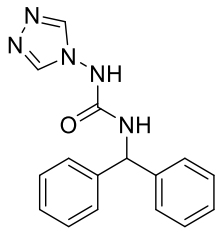 1-benzhydryl-3-(4*H*-1,2,4-triazol-4-yl)urea Chemical Formula: $C_{16}H_{15}N_5O$ Molecular Weight: 293,33	**MM96**			X

Structure	Compound name	Chapter		
		2	3	4
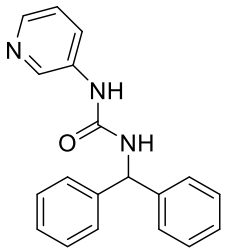 1-benzhydryl-3-(pyridin-3-yl)urea Chemical Formula: $C_{19}H_{17}N_3O$ Molecular Weight: 303,37	**MM97**			X
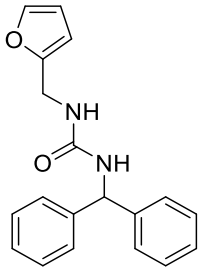 1-benzhydryl-3-(furan-2-ylmethyl)urea Chemical Formula: $C_{19}H_{18}N_2O_2$ Molecular Weight: 306,37	**MM98**			X
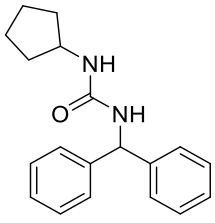 1-benzhydryl-3-cyclopentylurea Chemical Formula: $C_{19}H_{22}N_2O$ Molecular Weight: 294,40	**MM99**			X